CONODONT TAXONOMY, QUANTITATIVE BIOCHRONOLOGY AND EVOLUTION IN THE IMMEDIATE AFTERMATH OF THE PERMIAN-TRIASSIC BOUNDARY

Dissertation

zur

Erlangung der naturwissenschaftlichen Doktorwürde
(Dr. sc. nat.)

vorgelegt der

Mathematisch-naturwissenschaftlichen Fakultät

der

Universität Zürich

von

Morgane Brosse

aus

Frankreich

Promotionskommission

Pr. Dr. Hugo Bucher (Vertreter der Universität Zürich)
Dr. Nicolas Goudemand (Leitung der Dissertation; IGFL, France)
Pr. Dr. Marcelo Sánchez (Universität Zürich)
Pr. Dr. Christoph Zollikofer (Universität Zürich)

Zürich, 2017

Abstract

The most lethal mass-extinction of the history of life occurred at the Permian-Triassic boundary (PTB), about 252 million years ago. It resulted in the decimation of about 90% of marine taxa and led to the replacement of typical Palaeozoic by typical modern marine communities. During the aftermath of the mass-extinction, the biotic recovery is traditionally characterized as delayed, due to protracted hostile environmental conditions (climate warming, global anoxia…).

Establishing the time frame of the mechanisms of the biotic recovery profoundly relies on biostratigraphical data. Pelagic organisms like conodonts and ammonoids quickly recovered after the mass-extinction, reaching diversity level comparable to that of before the crisis in less than a million year. Conodonts were cosmopolitan and had unmatched evolutionary rates, making them major biostratigraphical fossils from the early Palaeozoic to the end of the Triassic. They are of particular importance across the Permian-Triassic boundary and are the cornerstone of all Changhsingian -Griesbachian (latest Permian to earliest Triassic) biostratigraphical scales.

This thesis provides biochronological framework to the interval encompassing the end-Permian mass-extinction and to the basal Triassic (namely, the Griesbachian and the early Dienerian). Our model particularly focused on South China (equatorial realm) and Kashmir (tropical realm) and is reproducible within the Tethyan realm. This dissertation is supplemented on one side by an exploratory study on the taxonomy of the genus *Neogondolella* based on empirical analyses and on the other side by a review of the biotic recovery during the Griesbachian time interval.

The first goal of this thesis is to explore and re-assess the taxonomy of conodonts across the latest Permian and the earliest Triassic. We describe a new shallow-water section in the Nanpanjiang Basin (South China) with an exceptional conodont record of basal Triassic age.

These results are combined with synchronous conodont records of five other sections in South China (Equatorial realm) with various depositional environments. We conducted unitary association analyses, based on maximal associations of species rather than on single first occurrences and generated a quantitative biochronological model. The new robust zones extend across the PTB and are laterally reproducible within the Nanpanjiang Basin.

This publication was the target of a Comment (Appendix C) by Jiang et al. (2016). We reacted to the Comment with a Reply explaining the advantages of the unitary association methods over the traditional interval zones method.

In a next step, we extended our investigations to the Tropical realm and the base of the Dienerian. We conducted a high resolution sampling and reassessed the conodont biochronology and isotopic records of the Member E of Guryul Ravine section. We precisely constrain the Griesbachian-Dienerian boundary at Guryul Ravine and show that it is marked by a perturbation in the carbon cycle and a turnover of the conodont faunas. Both events are probably linked to a major climate change during this interval.

The diversity and the abundance of the conodonts of the Guryul ravine section brought the opportunity to test the possibility to quantify the morphological variability of conodonts thanks to empirical classifications. We conducted cluster analyses on the population of conodonts from Guryul Ravine supplemented with holotypes of conodonts typical from the studied time interval. We show

that even non-statistical groups can still distribute the holotypes and produce homogeneous clusters.

Finally, we studied an exceptional fossil assemblage of Griesbachian age from the Batain Plain of Oman. The faunas retrieved from the Asselah boulder include pelagic and benthic communities which thrived in a well-oxygenated environment in carbonate-saturated water that did not undergo the harsh environmental conditions that prevailed on the continental shelves. We provide a review of the Griesbachian and suggest that the impact of the end-Permian mass-extinction has been over-estimated.

Keywords: Conodonts, taxonomy, quantitative biochronology, Permian-Triassic boundary, Griesbachian-Dienerian boundary, paleoenvironment.

Das grösste Massenaussterben der Erdgeschichte trat an der Perm-Trias Grenze (PTG) vor etwa 252 Millionen Jahren auf. Daraus resultierte eine Dezimierung der marinen Taxa um etwa 90% und führte zur Ablösung von typisch paläozoischen durch moderne maritime Vergesellschaftungen. Nach dem Massenaussterben wird die biotische Erholung traditionell aufgrund lebensfeindlicher Umweltbedingungen (Klimaerwärmung, globaler Sauerstoffmangel ...) als verzögert charakterisiert.

Der Zeitrahmen der Mechanismen der biotischen Erholung wird aufgrund von biostratigraphischen Daten festgelegt. Pelagische Organismen wie Conodonten und Ammoniten erholten sich rasch nach dem Massenaussterben und erreichten in weniger als einer Million Jahre ein Diversitätsniveau, vergleichbar mit dem der vor der Krise. Conodonten waren kosmopolitisch und hatten extrem hohe Evolutionsraten, was sie zu bedeutenden biostratigraphischen Fossilien für das frühe Paläozoikum bis zum Ende der Trias macht. Sie sind von besonderer Bedeutung für die Perm-Trias-Grenze und sind die Eckpfeiler aller biostratigraphischen Skalen des Changhsingium-Griesbachium (spätestes Perm bis früheste Trias).

Diese Arbeit liefert die biochronologischen Rahmenbedingungen für das Zeitintervall, welches das end-permische Massenaussterben und die basale Trias (d.h. das Griesbachium und das frühe Dienerium) umfasst. Unser Modell konzentriert sich besonders auf Südchina (äquatorialer Bereich) und Kaschmir (tropischer Bereich) und ist innerhalb des Tethys Meeres reproduzierbar. Ergänzt wird diese Dissertation einerseits durch eine explorative Studie zur Taxonomie der Gattung *Neogondolella* auf der Grundlage empirischer Analysen und andererseits durch eine Überprüfung der biotischen Erholung während des griesbachschen Zeitintervalls.

Ein erstes Ziel dieser Arbeit war die Erforschung und Neubewertung der Taxonomie von Conodonten aus dem letzten Perm und der frühesten Trias. Wir beschreiben einen neuen Flachwasserabschnitt im Nanpanjiang Becken (Südchina) mit einer außergewöhnlich gut dokumentierten Conodonten-Fauna von basalem triassischem Alter.

Diese Ergebnisse werden kombiniert mit synchronen Conodonten-Aufzeichnungen von fünf weiteren Profilen in Südchina (Äquatorialbereich) welche verschiedene Ablagerungsmilieus aufweisen. Wir führten einheitliche Assoziationsanalysen durch, welche auf maximalen Assoziationen von Arten und nicht auf einzelnen ersten Auftreten basieren, und erzeugten daraus ein quantitatives biochronologisches Modell. Die neuen robusten Zonen erstrecken sich über die PTB und sind im Nanpanjiang-Becken lateral reproduzierbar.

Dieser Publikation ging der Kommentar (Anhang C) von Jiang et al. (2016) voran. Wir reagierten auf diesen Kommentar mit einer Antwort, in der die Vorteile der einheitlichen Assoziationsmethoden gegenüber der traditionellen Intervallzonenmethode erläutert werde.

In einem nächsten Schritt erweiterten wir unsere Erforschungen auf den tropischen Bereich und die Basis des Dieneriums (die Unterstufe nach dem Griesbachium). Wir führten eine hochauflösende Probeentnahme durch und bewerteten die Conodonten Biochronologie und isotopischen Daten der Sektion E aus Guryul Ravine neu. Wir konnten die Griesbachium-Dienerium Grenze in Guryul Ravine genau einschränken und zeigen, dass sie durch eine Störung im Kohlenstoffkreislauf und einem Wechsel der Conodonten Faunen gekennzeichnet ist. Beide Ereignisse sind wahrscheinlich mit einem großen Klimawandel während dieses Intervall verbunden.

Die Vielfalt und die Fülle der Conodonten der Guryul-Ravine Sektion ermöglicht es, die morphologische Variabilität von Conodonten durch empirische Klassifikationen zu quantifizieren. Wir führten Clusteranalysen aus Conodonten-Population von Guryul Ravine durch und ergänzten diese durch die Holotypen, welche typisch sind aus dem untersuchten Zeitintervall. Die Größe der Kohorte (N = 183) erlaubt keine statistische Aufteilung in mehr als fünf Gruppen. Jedoch können wir zeigen, dass nicht-statistische Gruppen immer noch in der Lage sind, die Holotypen voneinander zu unterteilen und homogene Cluster zu erzeugen.

Schließlich untersuchten wir eine außergewöhnliche Ansammlung von Fossilien des Griesbachium Alters aus der Batain Ebene von Oman. Die Faunen welche aus dem Asselah Felsen gewonnen wurden, umfassen pelagische und benthische Gemeinschaften, die in einer sauerstoffreichen Umgebung und Karbonat-gesättigtem Wasser gediehen und nicht den harten Umweltbedingungen ausgesetzt waren, die auf dem Kontinentalschelf herrschten. Wir bieten einen Überblick über das Griesbachium und zeigen, dass die Auswirkung des End-permischen-Massenaussterbens überschätzt worden ist.

Schlüsselwörter: Conodonten, Perm-Trias-Grenze, Griesbachium-Dienerium-Grenze, Taxonomie, quantitative Biochronologie, Klima, paläologische Umwelt.

All chapters of this thesis are the outcome of collaborations and are presented as multi-authors publications. In the following, I detail the contribution of each collaborator for every chapter.

Chapter I: Conodonts from the Early Triassic microbialite of Guangxi (South China): implications for the definition of the base of the Triassic System. Palaeontology 2015, 58(3), 563-584.

Authors: Morgane Brosse, Aymon Baud, Borhan Bagherpour, Åsa M. Frisk, Kuang Guodun, Hugo Bucher and Nicolas Goudemand

Contribution: HB organized the field expedition. AF, KG, BB and HB helped me to collect the data on the field. I prepared and analysed the conodont samples. I wrote the manuscript and NG and HB participated in discussing and drafting the final version.

Chapter IIA: Quantitative biochronology of the Permian-Triassic boundary in South China based on conodont Unitary Associations. Earth-Science Reviews 2016, 155, 153–171

Authors: Morgane Brosse, Hugo Bucher and Nicolas Goudemand

Contribution: I conducted all unitary association analyses. I wrote the manuscript and NG and HB participated in discussing and drafting the final version.

Chapter IIB: Reply to the Comment on "Quantitative biochronology of the Permian-Triassic boundary in South China based on conodont Unitary Associations". Accepted in Earth-Science Reviews

Authors: Morgane Brosse, Hugo Bucher and Nicolas Goudemand

Contribution: I wrote the manuscript with NG and HB.

Chapter III: Conodont-based Griesbachian biochronology of the Guryul Ravine section (Induan, Early Triassic, Kashmir, India). Formatted for Geobios

Authors: Morgane Brosse, Marc Leu, Aymon Baud, Ghulam Mohmmad Bhat, Torsten Vennemann and Nicolas Goudemand

Contribution: GB helped me to organize the field expedition. GB, AB and ML helped me to collect the samples on the field. I prepared and analysed the conodont samples. TV processed the carbon isotope samples. AB provided help for the geological setting part. I conducted the unitary association analyses and wrote the manuscript and NG participated in discussing and drafting the final version.

Chapter IV: Untangling the taxonomy of Neogondolella (Conodonta): Cluster analyses vs. typological taxonomy. The case of Griesbachian conodonts from Guryul Ravine, Kashmir.

Authors: Morgane Brosse and Louise Souquet

Contribution: I supplied and studied the population of conodonts, built the dataset and wrote the manuscript. LS conducted all analyses in R software.

Chapter V: New data on the biotic recovery in the aftermath of the end-Permian mass-extinction: The Griesbachian of Oman. Formatted for Palaeogeography, Palaeoclimatology, Palaeoecology

Authors: Morgane Brosse, Hugo Bucher, Aymon Baud, Hans Hagdorn, Alexander Nützel, David Ware, Åsa M. Frisk and Nicolas Goudemand

Contribution: AF funded this project and organized the field expedition. AB discovered the outcrop. AF, NG and AB collected the data on the field. AB helped analysing the microfacies. AN helped analysing the population of gastropods and provided the two gastropods plates. HH helped analysing the population of crinoids. DW helped analysing the population of ammonoids. I analysed the population of conodonts. I wrote the manuscript and HB participated in discussing and drafting the final version.

INTRODUCTION

“Life will find a way.”

Michael Crichton, Jurassic Park

Palaeontological settings

Life history has been marked by five major biodiversity crisis of a global scale (arrows 1-5 in Fig. 1). Mass extinctions are defined as short intervals of time during which the extinction rates increased and the originations decreased (Sepkoski, 1984). The most severe mass-extinction of all (arrow n°3 in Fig. 1) marks the Paleozoic-Mesozoic boundary and has been precisely dated between 251.941±0.037 and 251.880±0.031 Ma (Burgess et al., 2016) and calculated at 251.956 ± 0.033 Ma (Baresel et al., 2016). About 90% of all marine species on Earth disappeared during this event (Raup, 1979) and typical Palaeozoic faunas were substituted by typical Mesozoic-Cenozoic communities (Sepkoski, 1984). Plant communities also underwent a major ecological turnover (Hochuli et al., 2010; Retallack, 1995; Schneebeli-Hermann, 2012; Schneebeli-Hermann et al., 2013).

At the end of the Palaeozoic, the continents were accreted into the supercontinent Pangea.

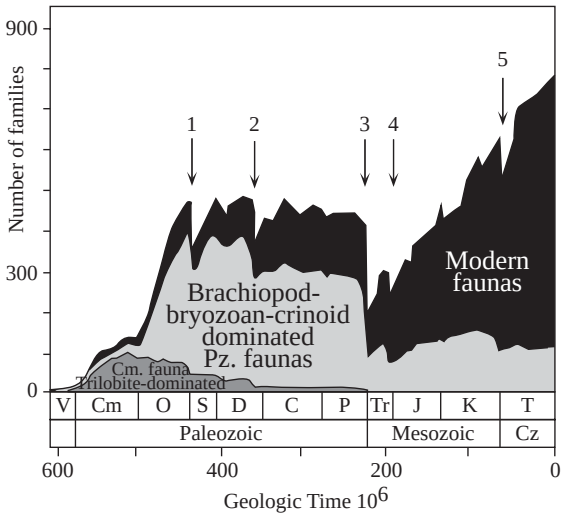

Figure 1: The Phanerozoic history of the taxonomic diversity of marine animal families. The arrows represent the five mass-extinctions, (1) End-Ordovician, (2) Late Devonian, (3) End-Permian, (4) End-Triassic and (5) End-Cretaceous. Modified after Sepkoski (1984).

Its southern half, including India, Australia, Africa and Antarctica formed the Gondwana continent (Fig. 2; Scotese, 2014). The Figure 2 highlights the locations studied for this dissertation and indicates in which chapter they are treated.

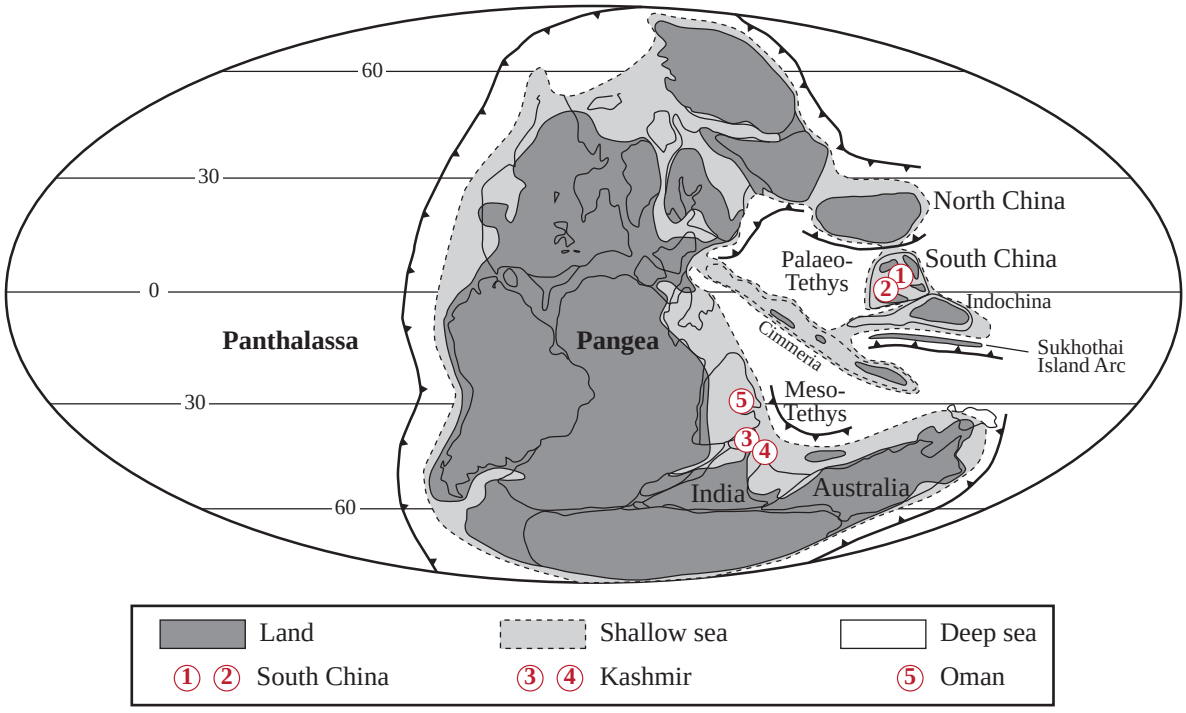

Figure 2: Palaeogeographical map of the Permian-Triassic interval (modified after Metcalfe, 2013). The red number represents the chapters of this dissertation.

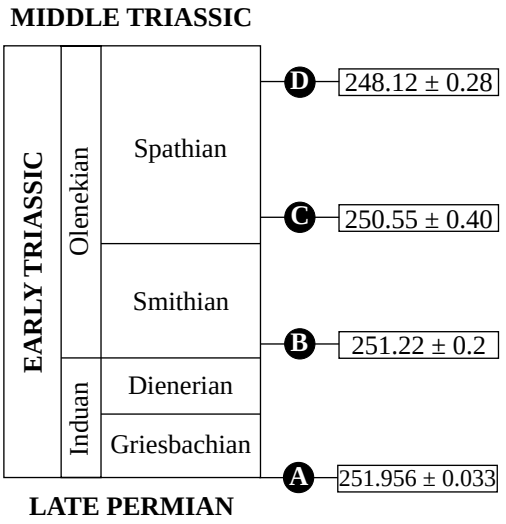

Figure 3: Early Triassic stage subdivision (after Gradstein et al., 2012 and Tozer, 1967) calibrated with published radiometric ages (A) Baresel et al. (2016); (B), (C) and (D) Galfetti et al. (2007).

The Early Triassic is subdivided into two stages (Induan and Olenekian; Gradstein et al., 2012), and four substages (Griesbachian, Dienerian, Smithian and Spathian; Tozer, 1967). The 2-fold division is the one officially recognized by the Sub-Commission on Triassic Stratigraphy (1992), but Early Triassic workers frequently use the 4-fold division. The duration of each subdivision is very unequal, and the Griesbachian + Dienerian was much shorter than 1 Myr while the Smithian + Spathian was more than 3 Myr in duration (Fig. 3).

Traditional view

The traditional view of the aftermath of the Permian-Triassic boundary is that of a delayed biotic recovery (Fig. 4; Benton and Twitchett, 2003; Erwin, 2001). Marine communities throughout the Early Triassic are classically described as low-diversity assemblages of opportunistic, cosmopolitan taxa (e.g. Erwin, 2001; Rodland and Bottjer, 2001; Schubert et al., 1992). Many marine taxa, such as gastropods, are assumed to be affected by a size reduction in the aftermath of the mass extinction (Fraiser and Bottjer, 2004; Fraiser et al., 2005; Payne, 2005; Twitchett, 2007), called the Lilliput effect (Urbanek, 1993). Other benthics, like crinoids, presumably undergo a dramatic extinction at the PTB bottleneck (Paul, 1988; Benton and Twitchett, 2003) and were thought until recently to not reappear in the fossil record until the Smithian (Salamon et al., 2015). The orders *Isocrinida* and *Encrinida* finally reach full diversity level during the Middle Triassic (Schubert et al., 1992; Hagdorn, 2011).

In this apocalyptic view of devastated ecosystems and delayed biotic recovery, the entire Griesbachian interval (Fig. 3; earliest

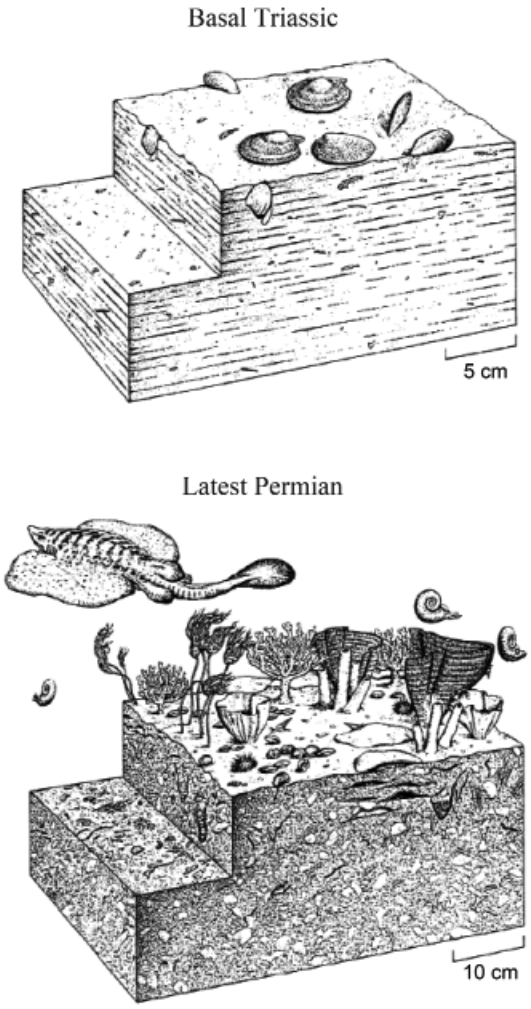

Figure 4: Traditional reconstitution of ancient seabed in southern China immediately before and after the Permian-Triassic mass-extinction. From Benton and Twitchett (2003).

Triassic) in the immediate aftermath of the Permian-Triassic mass extinction was considered as a period of very low diversity and devastated environment (Benton and Twitchett, 2003). In the Nanpanjiang Basin (China), the Griesbachian is indeed characterized by the emergence of microbial limestones, customarily interpreted as devastated environments and ecological and diversity collapses (Awramik, 1990; Schubert and Bottjer, 1992; Schubert and Bottjer, 1995). In support of the classical view of a delayed recovery, palaeoequatorial microbialites of Griesbachian age were traditionally interpreted as representing an anachronistic facies (Baud et al. 1997, 2002, 2007; Kershaw et al. 1999, 2007; Erwin 2006; Pruss et al. 2006). The hypothetical causes for this delayed recovery are an Early Triassic global anoxia explained by a transgression (Hallam, 1991; Isozaki, 1997), Griesbachian prevailing hot temperatures (Sun et al., 2012) or a combination of both (Song et al., 2014) .

Modern view

Recent studies on benthic foraminifers (Song et al., 2009a, b, 2011), trace fossils (e.g. Hofmann et al., 2011), bivalves (Krystyn et al., 2003; Hautmann et al., 2011), and metazoan reefs (Brayard et al., 2011) evidenced that the recovery of benthic communities was more rapid than previously thought. The Early Triassic Lilliput effect hypothesis was also challenged with the discovery of gastropods faunas from Utah, USA (Brayard et al., 2010).

Calcarenitic lenses intercalated within the microbialite domes in South China yielded abundant and diverse assemblages of Griesbachian age. These coquinas yielded pelagic faunas with conodonts and ammonoids (Brühwiler et al., 2008; Brosse et al., 2015; Hautmann et al., 2015) but also benthics such as bivalves and gastropods, supplemented by echinoderm ossicles, ostracods and rare brachiopods (Kaim et al., 2010; Forel et al., 2015; Hautmann et al., 2015).

Similarly surprisingly diverse Griesbachian assemblages have also been documented from Oman. The exceptional case of the so-called "Wadi Wasit block", found in the Hawasina Basin, Oman (Krystyn et al., 2003), yields substantial evidence for a very fast biotic recovery in the aftermath of the PTB. The Wadi Wasit bock yields a very diverse Griesbachian-Dienerian assemblage including bivalves, gastropods, conodonts and ammonoids, indicating a well-oxygenated environment. Krystyn et al. (2003) thus concluded that the Wadi Wasit block was a shelter for marine organisms during the Early Triassic harsh environmental conditions. Another case of Oman Griesbachian 'refugium' is also discussed in Chapter 5 of this dissertation. This new outcrop from the Batain Plain (eastern Oman) is very similar to the Wadi Wasit block, but in addition is mainly constituted of crinoid ossicles attributed to holocrinids, an order that was unknown until the Middle Triassic (Hagdorn, 2011).

Conodonts

Conodonts and ammonoids remained comparatively unscathed and abundant through the Permian-Triassic boundary (PTB) (Orchard 2007; Brayard et al. 2010). The relative abundance, the wide spatial distribution, and the high evolutionary rates of conodonts have made them one of the main biochronological tools for this critical interval. Hence, high-resolution biostratigraphical correlations are frequently based on conodont elements.

Conodonts are extinct eel-shaped marine vertebrates (Donoghue et al. 2000) which are mostly known in the fossil record for their phosphatic teeth elements (Fig. 5). Within the

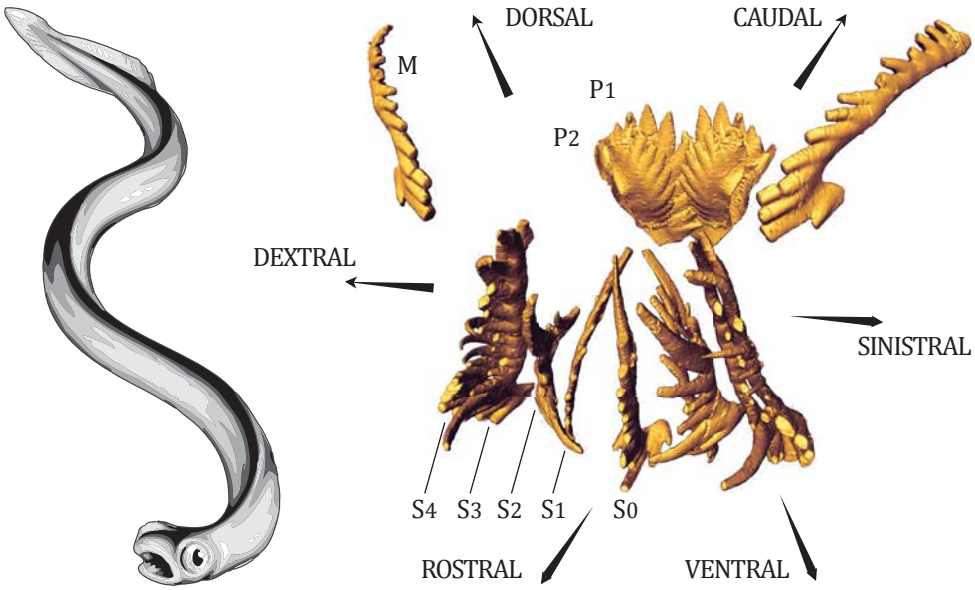

Figure 5: Reconstitution of the conodont animal and position of each phosphatic element within the feeding apparatus (after the reconstruction of Goudemand et al., 2011).

conodont feeding apparatus, the P_1 elements underwent the highest evolutionary rate and are the most commonly found in Griesbachian deposits. As we focus mostly on the PTB and its immediate aftermath, this thesis exclusively addresses P_1 elements.

Goals of the Ph.D

Understanding the mechanisms and the timing of these events has been a major project of the Zurich team for more than a decade. A main asset has been the calibration of the Early Triassic time scale by means of new U-Pb zircon ages measured from volcanic ash layers discovered in South China (Ovtcharova et al., 2006; Galfetti et al., 2007; Baresel et al., 2016; see Fig. 3). Radio-isotopic time calibrations combined with cutting edge biochronological data allow calculating real rates of origination and extinction and is of paramount importance when studying the Early Triassic biotic recovery.

The initial goal of this thesis was to revise the taxonomy on Changhsingian (latest Permian) conodonts from the Nanpanjiang Basin (South China) that occupied an equatorial position at that time. The next phase was to construct a conodont-based, high-resolution time frame for the Changhsingian by using quantitative biochronology methods such as the unitary associations (Fig. 6).

The radio-isotopic analyses of our ash samples were conducted in a separated SNF-funded project with Björn Baresel and Urs Schaltegger, University of Geneva (Baresel et al. 2016a, 2016b; see also Appendix A: collaboration with other projects). Ultimately, our objective was to construct a high resolution multidisciplinary model of the end-Permian mass-extinction.

The scarcity of conodonts during the latest Permian and a first unsuccessful field campaign in Guangxi in 2012 led to the emendation of my Ph.D project. Since 2013, I have shifted my investigations from the latest Permian to the immediate aftermath of the PTB (Griesbachian) of South China. Particularly, we focused on the shallow water microbialite, which have been thoroughly studied by the Zurich team for its coquinas yielding diversified benthic

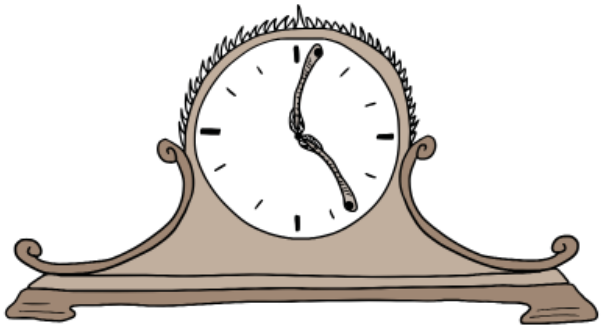

Figure 6: The Conodont clock. This cartoon has been drawn by Dr. Dave Jones during my presentation about conodont-based biochronology at the 59th Annual Meeting of the Palaeontological Association, Cardiff, UK. The artist perfectly captured the initial goal of my Ph.D. http://www.ratbotcomics.com

faunas and for its palaoenvironmental changes (Hautmann et al., 2015; Bagherpour et al., accepted in Gondwana Research; see Appendix A: collaboration with other projects).

Chapter I of this thesis addresses the Griesbachian conodont record of the Wuzhuan microbialite-bearing section and has been published in *Palaeontology* (Brosse et al., 2015). We show that the sequence of anchignathodontid conodonts corresponds to the best supported phylogenetical model (Jiang et al., 2011), indicating that the conodont record at Wuzhuan within the microbialite is closest to the 'true' evolutionary sequence of anchignathodontids. Comparing the First Occurrence (FO) of *Hindeodus parvus* (the species for the base of the Triassic; Yin et al., 1996) at Wuzhuan with it correspondent at Meishan (the GSSP of the PTB), we suggest that the FO of *Hindeodus parvus* at Meishan does not correspond to its first appearance datum, as it was assumed.

For the Chapter II.A, published in *Earth Science Review* (Brosse et al., 2016), we included the conodont record of five other sections from China with various palaeoenvironmental settings, from shallow-water microbialite to deep-water lower slope settings. We produced a conodont biochronological scale based on Unitary Associations zones (UAZs). UAZs correspond to the reunions of maximal associations of fossils (Guex, 1991) and are much more accurate, and devoid of internal contradiction in comparison with the traditional interval zones (based on first occurrences of single species). We eventually stabilized 6 UAZs encompassing the PTB, 2 of a Permian age and 4 of Griesbachian age, which are reproducible within the whole Nanpanjiang Basin.

The paper by Brosse et al. (2016) was commented on by Jiang et al. (2016; Appendix C), mostly based on the fact that our unitary association model was not as precise as the interval zones published by their team (Chen et al., 2015). In our Reply to the Comment in Chapter II.B, we explain the advantages of the unitary association method.

The Chapter III will be submitted to *Geobios* and represents a geographical, palaeoenvironmental and time interval extension of my Ph.D project, as it includes the Tethyan tropical realm, deep water settings and the basal Dienerian. We conducted a high resolution sampling and reassessed the conodont biochronology and isotopic records of the Member E of the Guryul Ravine section (Kashmir). We constructed 10 Unitary Association zones combining the conodont record from China (Chapter II.A) and from Guryul Ravine: 2 UAZs are Permian, 6 are Griesbachian and 2 are Dienerian. The new zones are reproducible within the entire Tethys. The basal Dienerian is marked by a perturbation of the carbon cycle recognized within the entire Tethyan realm. The Griesbachian-Dienerian transition is also characterized by the replacement of cold-water segminiplanate by warm-water segminate

forms (Joachimski et al., 2012). We suggest that the conodont faunal turnover was caused by a climate transition from a cool and dry to a hot and humid climate (Hochuli et al., 2016). This environmental change could be the trigger of the migration of segminiplanate conodonts towards the high latitude, and of the radiation of segminate conodonts during the Dienerian.

The Chapter IV is an exploratory work on the population of the genus *Neogondolella* from Guryul Ravine. This work is included within the Ph.D project of L. Souquet (IGFL, ENS Lyon, France), whole goal is to quantify the morphological variability of conodonts on the basis of empirical (as opposed to conceptual) classifications. We conducted cluster analyses on the population of conodonts from Guryul Ravine, supplemented with holotypes of typical species frequently encountered during this time interval. The size of the cohort (N=183) does not allow a statistical partitioning into more than five groups, but we nevertheless show that non-statistical groups can still distribute the holotypes and produce rather homogeneous clusters.

In the last chapter, which will be submitted to *Palaeogeography, Palaeoclimatology, Palaeoecology*, we focus on offshore localities that escaped the continental clastic input and the anoxia prevailing during the Griesbachian. The new outcrops from the Batain Plain (Oman) yielded a much more diverse fossil assemblage than was expected from the Griesbachian, with diverse pelagic and benthic faunas including conodonts, ammonoids, gastropods and crinoids. We compare our fossil record from Oman with the other occurrences of Griesbachian communities worldwide and suggest that marine communities were (1) not affected by a delayed recovery; (2) the recovery was synchronous at low and high latitudes; (3) the Griesbachian diversity is partially due to the presence of Permian survivors and (4) the Griesbachian fossil gap is likely due to preservation bias. To summarize, we suggest that the effect of the end-Permian mass-extinction has been over-estimated, especially in comparison with subsequent Early Triassic additional extinctions.

The palaeogeographical positions of each studied localities is shown in Figure 2.

Thesis outline

This thesis presents all chapters either as fully-formatted article as published in the respective journal (Chapter I and IIA), as accepted manuscript (Chapter II.B) or in manuscript form (Chapters III, IV and V). I detail the contribution of each authors of the chapter in part: Contribution if each collaborator. Supplementary material is provided at the end of each chapter.

References

Awramik, S. M., 1990. Stromatolites. 336–341. In Briggs, D. E. and Crowther, P. R. Palaeobiology: a synthesis. Blackwell Scientific Publications, London.

Baresel, B., Bucher, H., Brosse, M., Cordey, F., Guodun, K., and Schaltegger, U., 2016. Precise age for the Permian-Triassic boundary in South China from high precision U-Pb geochronology and Bayesian age-depth modelling, Solid Earth Discuss., doi:10.5194/se-2016-145, in review.

Baresel B., Bucher H., Bagherpour B., Brosse M., Guodun K. and Schaltegger U. Timing of global regression and microbial bloom marking the Permo-Triassic mass extinction. in review in Scientific Report.

Baud, A., Cirilli , S. and Marcoux, J., 1997. Biotic response to mass extinction: the Lowermost Triassic microbialites. Facies, 36, 238–242.

Baud, A., Richoz, S., Cirilli , S. and Marcoux, J,. 2002. Basal Triassic carbonate of the Tethys: a microbialite world. 16th International Sedimentological Congress, Johannesburg, Abstract Volume, 24-25.

Baud, A., Richoz, S., and Pruss S., 2007. The lower Triassic anachronistic carbonate facies in space and time. Global and Planetary Change, 55(1), 81–89.

Benton, M. J., and Twitchett, R. J., 2003. How to kill (almost) all life: the end-Permian extinction event: Trends in Ecology and Evolution, 18(7), 358-365.

Brayard, A., Escarguel, G., Bucher, H., Monnet, C., Brühwiler, T., Goudemand, N., Galfetti, T., and Guex, J., 2010. Good genes and good luck: ammonoid diversity and the end-Permian mass extinction: Science, 325(5944), 1118-1121.

Brayard, A., Vennin, E., Olivier, N., Bylund, K. G., Jenks, J., Stephen, D. A., Bucher, H., Hofmann, R., Goudemand, N., and Escarguel, G., 2011. Transient metazoan reefs in the aftermath of the end-Permian mass extinction: Nature Geoscience, 4(10), p. 693-697, doi:10.1038/ngeo1264.

Brosse, M., Bucher, H., Bagherpour, B., Baud, A., Frisk, Å. M., Guodun, K., and Goudemand, N., 2015. Conodonts from the Early Triassic microbialite of Guangxi (South China): implications for the definition of the base of the Triassic System. Palaeontology, *58*(3), 563-584.

Brosse, M., Bucher, H., and Goudemand, N., 2016. Quantitative biochronology of the Permian–Triassic boundary in South China based on conodont unitary associations. Earth-Science Reviews, 155, 153-171.

Burgess, S. D., Bowring, S., & Shen, S. Z., 2014. High-precision timeline for Earth's most severe extinction. Proceedings of the National Academy of Sciences, 111(9), 3316-3321.

Brühwiler, T., Brayard, A., Bucher, H., and Guodun, K., 2008. Griesbachian and Dienerian (Early Triassic) ammonoid faunas from northwestern Guangxi and southern Guizhou (south China). Palaeontology, 51(5), 1151-1180.

Chen, Z. Q., Yang, H., Luo, M., Benton, M. J., Kaiho, K., Zhao, L., Huang, Y., Zhang, K., Fang, Y., Jiang, H., Qiu, H., Li, Y., Tu, C., Shi, L., Zhang, L., Feng, X., and Chen, L., 2015. Complete biotic and sedimentary records of the Permian–Triassic transition from Meishan section, South China: Ecologically assessing mass extinction and its aftermath. Earth-Science Reviews, 149, 67-107.

Donoghue, P. C., Forey, P. L., & Aldridge, R. J., 2000. Conodont affinity and chordate phylogeny. Biological Reviews of the Cambridge Philosophical Society, 75(02), 191-251.

Erwin, D. H. 2001. Lessons from the past: biotic recoveries from mass extinctions. Proceedings of the National Academy of Sciences, 98 (10), 5399–5403.

Erwin, D. H., 2006. Extinction: how life on Earth nearly ended 250 million years ago. Princeton University Press, 1-230.

Forel, M. B., 2015. Heterochronic growth of ostracods (Crustacea) from microbial deposits in the aftermath of the end-Permian extinction. Journal of Systematic Palaeontology, 13(4), 315-349.

Fraiser, M. L., and Bottjer, D. J., 2004. The non-actualistic Early Triassic gastropod fauna: a case study of the Lower Triassic SinbadLimestone member: Palaios, 19(3), p. 259-275.

Fraiser, M. L., Twitchett, R. J., and Bottjer, D. J., 2005. Unique microgastropod biofacies in the Early Triassic: indicator of long-term biotic stress and the pattern of biotic recovery after the end-Permian mass extinction: Comptes Rendus Palevol, 4(6), 543-552.

Galfetti, T., Bucher, H., Ovtcharova, M., Schaltegger, U., Brayard, A., Brühwiler, T., Goudemand, N., Weissert, H., Hochuli, P., Corday, F., and Guodun, K., 2007. Timing of the Early Triassic carbon cycle perturbations inferred from new U–Pb ages and ammonoid biochronozones. Earth and Planetary Science Letters, 258(3), 593-604.

Goudemand, N., Orchard, M. J., Urdy, S., Bucher, H., & Tafforeau, P., 2011. Synchrotron-aided reconstruction of the conodont feeding apparatus and implications for the mouth of the first vertebrates. Proceedings of the National Academy of Sciences, 108(21), 8720-8724.

Gradstein, F. M., Ogg, J. G., Schmitz, M. D., and Ogg, G., 2012. The geologic time scale 2012, 2.

Guex, J., 1991. Biochronological correlations. Springer Verlag.

Hallam, A., 1991. Why was there a delayed radiation after the end-Palaeozoic extinctions?. *Historical Biology*, *5*(2-4), 257-262.

Hagdorn, H., 2011. Triassic: the crucial period of post-Palaeozoic crinoid diversification: Swiss Journal of Palaeontology, 130(1), 91-112.

Hautmann, M., Bucher, H., Brühwiler, T., Goudemand, N., Kaim, A., and Nützel, A., 2011., An unusually diverse mollusc fauna from the earliest Triassic of South China and its implications for benthic recovery after the end-Permian biotic crisis: Geobios, 44(1), 71-85.

Hautmann, M., et al., 2015. Competition in slow motion: the unusual case of benthic marine communities in the wake of the end-Permian mass extinction: Palaeontology, 58(5), 871-901.

Hochuli, P. A., Hermann, E., Vigran, J. O., Bucher, H., and Weissert, H., 2010. Rapid demise and recovery of plant ecosystems across the end-Permian extinction event: Global and Planetary Change, 74(3), 144-155.

Hochuli, P.A., Sanson-Barrera, A., Schneebeli-Hermann, E., and Bucher, H. 2016. Severest crisis overlooked—Worst disruption of terrestrial environments postdates the Permian-Triassic mass extinction. Scientific Reports, 6, pp. 1-7.

Hofmann, R., Goudemand, N., Wasmer, M., Bucher, H., and Hautmann, M., 2011. New trace fossil evidence for an early recovery signal in the aftermath of the

end-Permian mass extinction: Palaeogeography, Palaeoclimatology, Palaeoecology, 310(3), p. 216-226.

Isozaki, Y., 1997. Permo-Triassic boundary superanoxia and stratified superocean: records from lost deep sea. Science, 276(5310), 235-238.

Jiang, H., Aldridge, R.J., Lai, X., Yan, C., and Sun, Y., 2011b. Phylogeny of the conodont genera Hindeodus and Isarcicella across the Permian–Triassic boundary. Lethaia, 44(4), pp. 374-382.

Joachimski, M. M., Lai, X., Shen, S., Jiang, H., Luo, G., Chen, B., Chen, J., and Sun, Y., 2012, Climate warming in the latest Permian and the Permian–Triassic mass extinction: Geology, v. 40, no. 3, p. 195-198.

Kaim, A., Nützel, A., Bucher, H., Brühwiler, T., and Goudemand, N., 2010. Early Triassic (Late Griesbachian) gastropods from South China (Shanggan, Guangxi): Swiss Journal of Geosciences, 101(1), 121-128.

Kershaw, S., Zhang, T. and Lan, G., 1999. A ?microbialite carbonate crust at the Permian–Triassic boundary in South China, and its palaeoenvironmental significance. Palaeogeography, Palaeoclimatology, Palaeoecology, 146(1), 1–18.

Kershaw, S., Li, Y., Crasquin-Soleau, S., Feng, Q., Mu, X., Collin, P. Y., Reynolds and Guo, L., 2007. Earliest Triassic microbialites in the South China block and other areas: controls on their growth and distribution. Facies, 53(3), 409-425.

Krystyn, L., Richoz, S., Baud, A., and Twitchett, R. J., 2003. A unique Permian–Triassic boundary section from the neotethyan Hawasina basin, Central Oman Mountains. Palaeogeography, Palaeoclimatology, Palaeoecology, 191(3).

Metcalfe, I., 2013. Gondwana dispersion and Asian accretion: tectonic and palaeogeographic evolution of eastern Tethys. *Journal of Asian Earth Sciences*, *66*, 1-33.

Orchard, M. J., 2007. Conodont diversity and evolution through the latest Permian and Early Triassic upheavals. Palaeogeography, Palaeoclimatology, Palaeoecology, *252*(1), 93-117.

Ovtcharova, M., Bucher, H., Schaltegger, U., Galfetti, T., Brayard, A., and Guex, J., 2006. New Early to Middle Triassic U–Pb ages from South China: calibration with ammonoid biochronozones and implications for the timing of the Triassic biotic recovery. Earth and Planetary Science Letters, 243(3), 463-475.

Paul, C. R. C., 1988. Extinction and survival in the echinoderms, in Extinction and Survival in the Fossil Record, Systematics Association Special Volume, ed. Larwood G. P., Oxford, UK, v. 34, p. 155-170.

Payne, J. L., 2005. Evolutionary dynamics of gastropod size across the end-Permian extinction and through the Triassic recovery interval: Paleobiology, 31(2), 269-290.

Pruss, S. B., Bottjer, D. J., Corsetti , F. A. and Baud, A., 2006. A global marine sedimentary response to the end-Permian mass extinction: examples from southern Turkey and the western United States. Earth-Science Reviews, 78(3), 193-206.

Raup, D. M., 1979. Size of the Permo-Triassic bottleneck and its evolutionary implications. Science, 206 (4415).

Retallack, G. J., 1995. Permian-Triassic life crisis on land: Science, 267(5194), 77-80.

Rodland, D. L., and Bottjer, D. J., 2001. Biotic recovery from the end-Permian mass extinction: behavior of the inarticulate brachiopod Lingula as a disaster taxon: Palaios, 16(1), 95-101.

Salamon, M. A., Gorzelak, P., Hanken, N., Riise, H. E., and Ferré, B., 2015. Crinoids from Svalbard in the aftermath of the end-Permian mass extinction. Polish Polar Research, 36(3), 225-238.

Schneebeli-Hermann, E., 2012. Extinguishing a Permian world: Geology, 40(3), 287.

Schneebeli-Hermann, E., Kürschner, W. M., Kerp, H., Bomfleur, B., Hochuli, P. A., Bucher, H., Ware, D., and Roohi, G., 2013. Vegetation history across the Permian–Triassic boundary in Pakistan (Amb section, Salt Range): Gondwana Research, 27.

Schubert, J. K. and Bottjer, D. J., 1995. Aftermath of the Permian–Triassic mass extinction event: paleoecology of Lower Triassic carbonates in the western USA. Palaeogeography,

Schubert, J. K., and Bottjer, D. J., 1992. Early Triassic stromatolites as post-mass extinction disaster forms: Geology, 20(10), 883-886.

Schubert, J. K., Bottjer, D. J., and Simms, M. J., 1992. Paleobiology of the oldest known articulate crinoid. Lethaia, 25(1), 97-110.

Scotese, C.R., 2014. Atlas of Middle and Late Permian and Triassic Paleogeographic maps, maps 43-48 from volume 3 of the PALEOMAP Atlas for ArcGIS (Jurassic and Triassic) and maps 49-52 from volume 4 of the PALEOMAP PaleoAtlas for ArcGIS (Late Paleozoic). Mollweide Projection, PALEOMAP Project, Evanston.

Sepkoski, J. J. 1984. A kinetic model of Phanerozoic taxonomic diversity. III. Post-Paleozoic families and mass extinctions. Paleobiology, 10(02), 246-267.

Song, H., et al., 2011. Recovery tempo and pattern of marine ecosystems after the end-Permian mass extinction: Geology, 39(8), 739-742

Song, H., Tong, J., and Chen, Z. Q, 2009a. Two episodes of foraminiferal extinction near the Permian–Triassic boundary at the Meishan section, South China:

Australian Journal of Earth Sciences, 56(6), 765-773.

Song, H., Tong, J., Chen, Z. Q., Yang, H. A. O., and Wang, Y., 2009b. End-Permian mass extinction of foraminifers in the Nanpanjiang Basin, South China: Journal of Paleontology, 83(05), 718-738.

Song, H., Wignall, P. B., Chu, D., Tong, J., Sun, Y., Song, H., He, W., and Tian, L. (2014). Anoxia/high temperature double whammy during the Permian-Triassic marine crisis and its aftermath. Scientific reports, 4.

Sun, Y., Joachimski, M. M., Wignall, P. B., Yan, C., Chen, Y., Jiang, H., Wang, L., and Lai, X., 2012. Lethally hot temperatures during the Early Triassic greenhouse. Science, 338(6105), pp. 366-370.

Tozer, E.T., 1967. A standard for Triassic time. Department of Energy, Mines and Resources. Geological Survey of Canada Bulletin, 156(1967), 1-103.

Twitchett, R. J., 2007. The Lilliput effect in the aftermath of the end-Permian extinction event: Palaeogeography, Palaeoclimatology, Palaeoecology, 252(1), 132-144.

Twitchett, R. J., Krystyn, L., Baud, A., Wheeley, J. R., and Richoz, S., 2004. Rapid marine recovery after the end-Permian mass-extinction event in the absence of marine anoxia: Geology, 32(9), 805-808.

Urbanek, A., 1993. Biotic crises in the history of Upper Silurian graptoloids: a palaeobiological model: Historical Biology, 7(1), 29-50.

Yin, H.F., Wu, S.B., Ding, M.H., Zhang, K.X., Tong, J.N., Yang, F.Q., and Lai, X.L., 1996. The Meishan section, candidate of the global stratotype section and point of Permian-Triassic boundary. The Paleozoic-Mesozoic Boundary Candidates of the Global Stratotype Section and Point of the Permian-Triassic Boundary, pp. 31-48.

Chapter I

Conodonts from the Early Triassic microbialite of Guangxi (South China): implications for the definition of the base of the Triassic System

Morgane Brosse, Aymon Baud, Borhan Bagherpour, Åsa M. Frisk, Kuang Guodun, Hugo Bucher and Nicolas Goudemand

Palaeontology, 58(3), 563-584
doi: 10.1111/pala.12162

“A riddle wrapped in a mystery inside an enigma”.

Stephen Jay Gould about conodonts
borrowed from Winston Churchill

Palaeontology The Palaeontological Association www.palass.org

[Palaeontology, 2015, pp. 1–22]

CONODONTS FROM THE EARLY TRIASSIC MICROBIALITE OF GUANGXI (SOUTH CHINA): IMPLICATIONS FOR THE DEFINITION OF THE BASE OF THE TRIASSIC SYSTEM

by MORGANE BROSSE[1], HUGO BUCHER[1], BORHAN BAGHERPOUR[1], AYMON BAUD[3], ÅSA M. FRISK[1,4], KUANG GUODUN[2] *and* NICOLAS GOUDEMAND[1]

[1]Paläontologisches Institut der Universität Zürich, Karl Schmid-Strasse 4, 8006, Zürich, Switzerland; e-mail: morgane.brosse@pim.uzh.ch
[2]Guangxi Bureau of Geology and Mineral Resources, Jiangzheng Road 1, 530023, Nanning, China
[3]Geological Museum, Lausanne University, Quartier UNIL-Dorigny, Bâtiment Anthropole, CH-1015, Lausanne, Switzerland
[4]Palaeobiology, Department of Earth Sciences, Uppsala University, Villavägen 16, 753 36, Uppsala, Sweden

Typescript received 3 December 2014; accepted in revised form 20 February 2015

Abstract: We describe a new Early Triassic (Griesbachian) succession of conodont faunas from a high-resolution sampling of the basal Early Triassic microbial limestone and the base of the overlying unit at the Wuzhuan section (Nanpanjiang Basin, Guangxi, South China). The microbial limestone records the earliest phase of the Early Triassic biotic recovery after the end-Permian mass extinction. For the first time, rich conodont faunas are reported from within the microbialite. The faunas from Wuzhuan are largely dominated by anchignathodontids, including several *Isarcicella* species, which were previously documented only from strata above the microbialite. A total of 14 conodont species assigned to three genera is recorded from the Wuzhuan section. Starting from the base of the microbialite upwards, several species are sequentially added to the conodont assemblage. The alpha diversity peaks at the top of the microbialite. The conodont record in the considered microbialite interval at Wuzhuan is presumably unaffected by local ecological changes. It therefore more likely represents an evolutionary rather than an ecological pattern. We compare the Wuzhuan's conodont record with a well-supported phylogenetic model and suggest that the sequence of first occurrences at Wuzhuan is the closest to the 'true' sequence of evolutionary events that took place during this Griesbachian radiation of anchignathodontids. Based on comparisons with the GSSP section at Meishan, we suggest further that the first occurrence of *Hindeodus parvus* in Meishan does not correspond to its first appearance datum.

Key words: Permian–Triassic boundary, Nanpanjiang Basin, microbial limestone, calcarenite lenses, anchignathodontids.

THE end-Permian mass extinction (between 251.941 ± 0.037 and 251.880 ± 0.031 Ma, see Burgess *et al.* 2014) is known to be the largest biodiversity crisis in the history of life and was marked by the disappearance of many typical Palaeozoic organisms (e.g. trilobites, rugose and tabulate corals, fusulinid foraminifers). About 90% of all marine species on Earth disappeared during this event (Raup 1979), and major changes in plant communities have been documented (Retallack 1995; Hermann *et al.* 2011; Schneebeli-Hermann 2012; Schneebeli-Hermann *et al.* 2015). It has been argued that the end-Permian mass extinction was followed by a delayed biotic recovery (Erwin 2001). Marine communities throughout the Early Triassic are classically described as low-diversity assemblages typified by opportunistic, cosmopolitan taxa (Schubert and Bottjer 1992; Erwin 2001; Rodland and Bottjer 2001). Yet, more recent studies on benthic foraminifers (Song *et al.* 2009*a*, *b*, 2011), trace fossils (Hofmann *et al.* 2011), bivalves (Krystyn *et al.* 2003; Hautmann *et al.* 2011) and metazoan reefs (Brayard *et al.* 2011) have suggested that the recovery of benthic communities was more rapid than previously thought. The recovery of nekto-pelagic clades such as ammonoids and conodonts also was much faster than previously assumed (Orchard 2007; Brayard *et al.* 2009), with a succession of several extinction-recovery cycles. The brief resurgence of microbial limestone has been customarily interpreted as devastated environments and ecological and diversity collapses (Awramik 1990; Schubert and Bottjer 1992; Schubert and Bottjer 1995). In support of the classical view of a delayed

recovery, palaeoequatorial microbialites of basal Triassic age were traditionally interpreted as representing an anachronistic facies (Baud *et al.* 1997, 2002, 2007; Kershaw *et al.* 1999, 2007; Erwin 2006; Pruss *et al.* 2006). However, this apocalyptic view needs to be revised: in several South Chinese sections, lenses with abundant and diverse benthic macrofaunas were discovered in shell coquinas that are trapped in-between domes of microbial limestone, such as in Shanggan, Guangxi (Kaim *et al.* 2010; Hautmann *et al.* 2011). Shell coquinas are also present in Wuzhuan, and their corresponding conodont faunas are here described in detail.

Owing to their abundance and high evolutionary rates, conodonts are of great importance for dating Early Triassic rocks. Although many marine organisms were decimated during the end-Permian mass extinction, conodonts remain comparatively unscathed and abundant through the Permian–Triassic boundary (PTB; Orchard 2007). Hence, high-resolution biostratigraphical correlations frequently utilize conodont elements. Yet, the conodont record from the earliest Triassic microbialite is poorly known, which has hitherto precluded high-resolution correlations between regions where the microbialite occurs and those with non-microbial basal Early Triassic rocks. Either the few available range charts lack descriptions and illustrations of conodonts (Ezaki *et al.* 2003, 2008), or only a few specimens of the index species (e.g. *Hindeodus parvus*) from very few samples are illustrated (Kershaw *et al.* 2002). In other cases, the quality of the illustrations is too poor for unambiguous verification of the determinations (Qi and Liao 2007). When illustrations and occurrences are adequately documented, most of the reported occurrences are restricted to beds located below or above the microbial limestone (Jiang *et al.* 2014); conodont occurrences within the microbialite are very scarce (Chen *et al.* 2008*a*). In this respect, the Wuzhuan section is remarkable because abundant conodont faunas were found within the microbial limestone itself. Hence, our study on the Wuzhuan section represents the first documentation of a detailed, high-resolution succession of diversified Griesbachian conodont faunas from the microbial limestone of South China. Abundant and diversified benthic macrofaunas of Permian and Triassic affinities were also discovered in the microbialite at neighbouring sections (Hautmann *et al.* 2011). In this study, we focus on the taxonomy of these conodonts. Their implications for basinwide correlations and comparisons between shallow-water and deeper-water settings will be addressed in a separate study.

GEOLOGICAL SETTING

The Nanpanjiang Basin in South China is of Palaeozoic to Early Mesozoic age, which extends across central and western Guangxi, southern Guizhou and eastern Yunnan

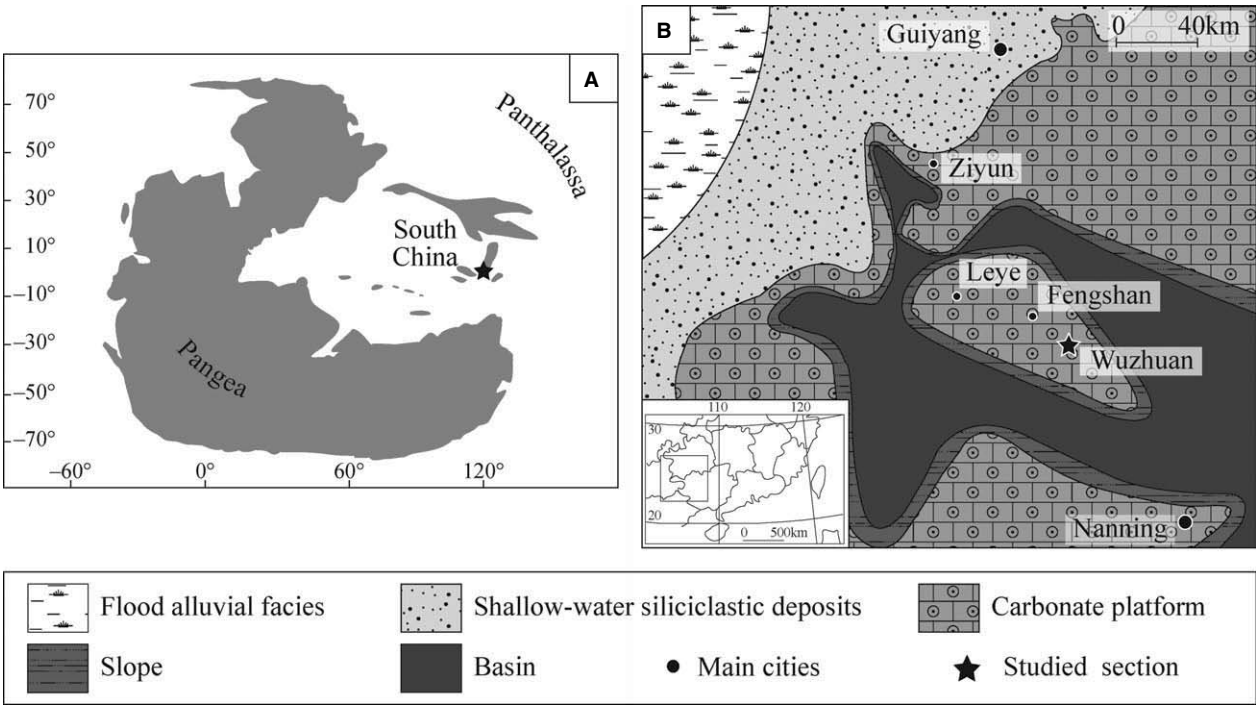

FIG. 1. A, palaeogeographical map of the studied area during Early Triassic. B, locality map indicating the position of Wuzhuan section in the Nanpanjiang Basin (modified from Fan *et al.* 2014).

provinces (Fig. 1). Differential subsidence controlled by block faulting initiated at the beginning of the Late Permian and persisted until the Early–Middle Triassic boundary (HB unpub. data). Where not blanketed by Middle Triassic flysch deposits, isolated shallow-water carbonate platforms persisted until the early Carnian. In shallow-water settings, the Late Permian is represented by the Heshan Formation and displays thick-bedded limestone with chert nodules containing abundant Permian faunas (predominantly represented by foraminifera, bryozoans, corals, brachiopods and bivalves) and locally intercalated with numerous ash layers.

Unconformably overlying the Heshan Formation, the Luolou Formation is of Early Triassic age. Its base records a microbial event of Griesbachian age (Kershaw *et al.* 1999, 2007; Lehrmann 1999; Lehrmann *et al.* 2001; Wang *et al.* 2005; Galfetti *et al.* 2008).

The Wuzhuan section (24°21′44.6″N; 107°20′02.00″E) is exposed along a road cut in the western Donglan County, northern Guangxi (Fig. 1). The PTB is well exposed in this section. The upper 12 m of the Permian medium grey, moderately thick-to-thick limestone is rich in diagenetic chert nodules. Typical Late Permian benthic communities including bryozoans, brachiopods, bivalves, crinoids, algae and foraminifera are well represented, however, conodonts and ammonoids are rare. Numerous ash layers are locally intercalated with the upper part of the Heshan Formation. An ash layer caps the top of the formation in a majority of sections and is the closest layer in time with the main extinction event (HB unpub. data). All following references to sample position refer to metres above the bottom level (0 m) at the top of the ash layer, that is, at the boundary between the Heshan and Luolou formations. The Luolou Formation at Wuzhuan is divided into two units as established by Galfetti *et al.* (2008). It is further subdivided here into six new subunits, as shown in Figure 2. The lowermost unit corresponds roughly to the microbialite.

The terminology of Shapiro (2000) is adopted here for the description of the microfacies of the microbialite. Subunit 1a consists of two thin fossiliferous calcarenites enclosing one layer of microbial limestone with clotted facies thrombolite and small isolated domes with a dendrolitic fabric; it is about 40 cm thick. In the calcarenites, we found Late Permian foraminifers. Their remarkable concentration and the grainstone fabric of their matrix suggest latest Permian or earliest Triassic reworking. Hence, the PTB at Wuzhuan is likely to lie within this 40-cm interval, above the last ash layer of the Heshan Formation. The lower part (Subunit 1b, 5 m) of the microbialite displays predominantly thrombolite in clotted facies, while the upper part of the microbialite (Subunit 1c, 4.5 m) displays dome-shaped dendrolites with the intercalation of coarse calcarenitic lenses. These calcarenitic lenses are fossiliferous and yield rich benthic faunas including bivalves, gastropods and brachiopods. Similar lenses have been reported in other sections of the Nanpanjiang Basin. These yielded abundant and diversified bivalves (Hautmann *et al.* 2011), gastropods (Kaim *et al.* 2010) and occasionally ammonoids (Brühwiler *et al.* 2008).

The top of the microbialite is capped by a 20-cm-thick bioclastic wackestone (Subunit 1d) containing a very abundant conodont fauna, overlain by a greywacke (Subunit 2a) and in turn followed by a succession of laminated, dark mudstones and silts with intercalated thin-bedded limestone beds (Subunit 2b). Table 1 shows the positions of these subunits with respect to the lithostratigraphical schemes of Ezaki *et al.* (2008) and Galfetti *et al.* (2008).

MATERIAL AND METHODS

A total of 27 carbonate samples, each weighing between 1 and 6 kg, were collected from units 1 and 2 (Table 1). In addition to samples from each of the nine coquinoid lenses from Subunit 1c, samples were collected at 50 cm spacing on average throughout the microbialite (Unit 1). Another sample was collected from the bioclastic wackestone lying directly on top of the microbialite (Subunit 1d), and uppermost samples were from the thin-bedded limestone beds at the top of the section (Subunit 2b).

The samples were dissolved with a ~10% buffered acetic acid solution following the procedure of Jeppsson *et al.* (1999). The insoluble residues were concentrated by heavy liquid separation using sodium polytungstate (Jeppsson and Anehus 1999). Concentrated residues were sieved with a 0.075-mm mesh, and handpicked and studied under a binocular microscope.

RESULTS

Of the 27 samples from the Luolou Formation that were processed, 15 yielded conodont elements. The Heshan Formation was also sampled but turned out to be barren.

FIG. 2. Detailed stratigraphical log of the Wuzhuan section showing the distribution of conodont taxa throughout the Griesbachian Luolou Formation (left), and corresponding phylogenetic tree (right; modified after Jiang *et al.* 2010, using the ranges in the left part). The boundary between the Heshan and the Luolou formations is the base of the scale. Black circles correspond to confirmed occurrences and white circles correspond to undetermined species. Only beds yielding conodont elements have been numbered. The thick line in the phylogenetic tree represents the estimated range of *H. parvus* as recorded in Meishan. At Wuzhuan, the FO of *H. parvus* appears older. *H*, *Hindeodus*; *N*, *Neogondolella*; *I*, *Isarcicella*.

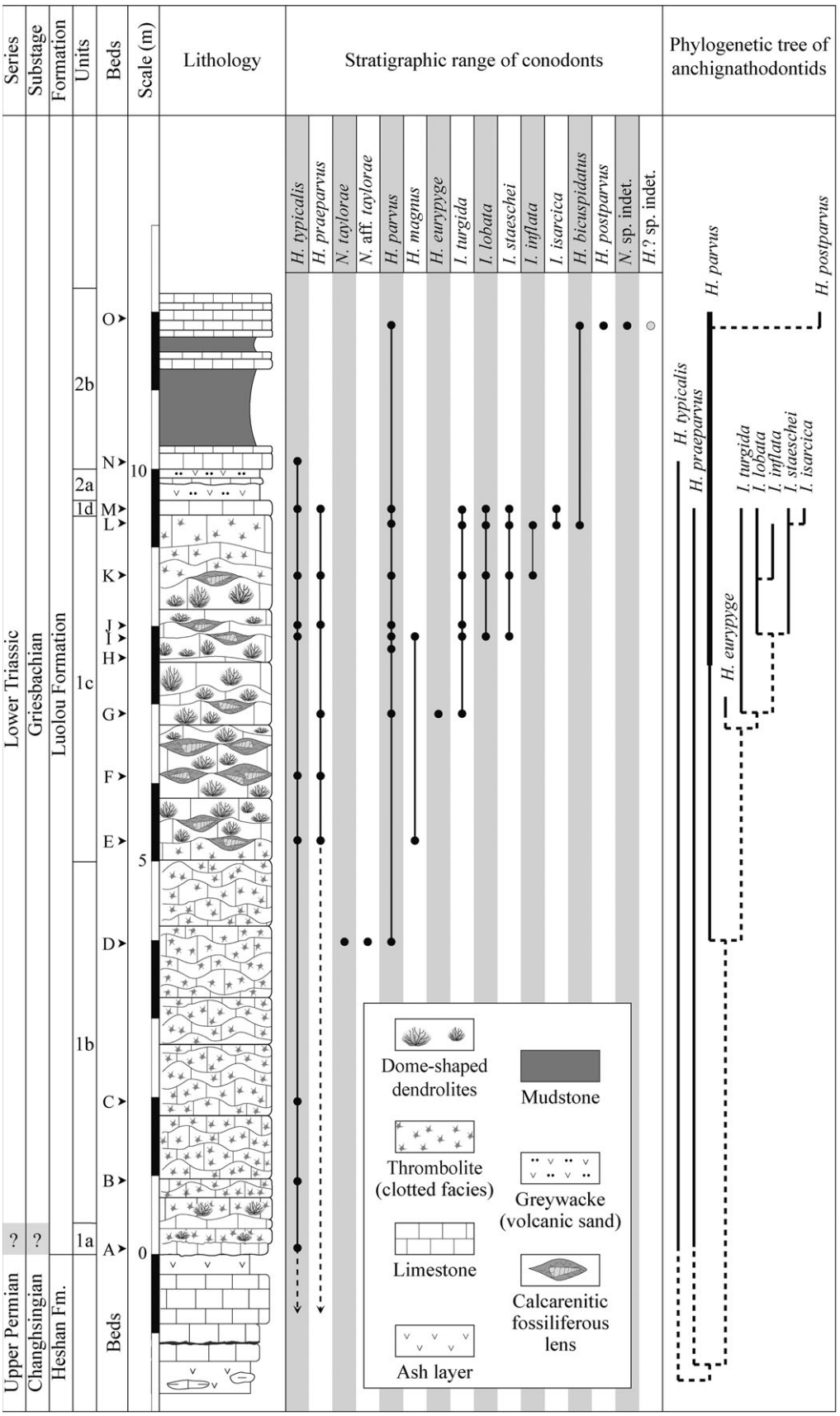
Series
Substage
Formation
Units
Beds
Scale (m)
Lithology
Stratigraphic range of conodonts
Phylogenetic tree of anchignathodontids
Lower Triassic
Upper Permian
Griesbachian
Changhsingian
Luolou Formation
Heshan Fm.
? ?
1a
1b
1c
1d
2a
2b
A
B
C
D
E
F
G
H
I
J
K
L
M
N
O
0
5
10
H. typicalis
H. praeparvus
N. taylorae
N. aff. taylorae
H. parvus
H. magnus
H. eurypyge
I. turgida
I. lobata
I. staeschei
I. inflata
I. isarcica
H. bicuspidatus
H. postparvus
N. sp. indet.
H.? sp. indet.
Dome-shaped dendrolites
Thrombolite (clotted facies)
Limestone
Ash layer
Mudstone
Greywacke (volcanic sand)
Calcarenitic fossiliferous lens

TABLE. 1. Occurrence of conodont species in the Luolou Formation at the Wuzhuan section.

Elevation (m) from base of Luolou Formation	Sample names	Lithological units (displayed in Fig. 2)	Corresponding units in Galfetti *et al.* (2008)	Corresponding units in Ezaki *et al.* (2008)	Quantity dissolved (kg)	*H. typicalis*	*H. parvus*	*N. taylorae*	*N.* aff. *taylorae*	*H. praeparvus*	*H. magnus*	*H. eurypyge*	*I. turgida*	*I. lobata*	*I. staeschei*	*I. inflata*	*I. isarcica*	*H. bicuspidatus*	*H. postparvus*	*N. sp. indet*	*H.?* sp. indet
11.8	WUZ.O	2b	2	3	5		9						1?	1?				4	33	1	1
10.1	WUZ.N	2a	2	3	1	4															
9.5	WUZ.M	1d	1	3	7	4	58			2			1	15	40		12				
9.3	WUZ.L	1c	1	2	4		42						1	9	21	1	9	6			
8.7	WUZ.K	1c	1	2	6	7	49			3			17	12	2	1					
8	WUZ.J	1c	1	2	4	5	10			2			2								
7.9	WUZ.I	1c	1	2	1	4	4			1	1		5	2	1						
7.6	WUZ.H	1c	1	2	3		2														
6.9	WUZ.G	1c	1	2	1		12			4		1	2								
6.1	WUZ.F	1c	1	2	13	2				2											
5.3	WUZ.E	1c	1	2	3	2				3	1										
4	WUZ.D	1b	1	2	9		2	1	1												
1.9	WUZ.C	1b	1	2	3	1															
1	WUZ.B	1b	1	2	4	2															
0.1	WUZ.A	1a	1	2	6	1															

The sample elevation is given as distance from the base of Luolou Formation.
H, *Hindeodus*; *N*, *Neogondolella; I*, *Isarcicella.*

Within the microbialite, the coquinoid lenses were not significantly richer in conodont elements than the rest of the unit, and several calcarenitic lenses did not contain conodonts.

Fourteen species assigned to three genera were identified from about 1000 P_1 and 600 ramiform elements (Table 1). Most of these elements are assigned to anchignathodontids (*Hindeodus* and *Isarcicella* in order of decreasing abundance), and only a few specimens to *Neogondolella*. The general preservation is moderate to good, but numerous fragmentary elements could not be determined at the species level. For this reason, we do not provide a table of relative abundances. The colour of the elements is black (CAI = 5). The illustrated specimens are presented in Figures 3–8.

Conodont occurrences are presented in Figure 2. Ranging almost throughout the entire section, the basal Triassic index species *H. parvus* (Fig. 4) first occurs 4 m above the formational boundary, where it is associated with a single P_1 element of *Neogondolella taylorae* (Fig. 7J). The first occurrence (FO) of *Isarcicella* species is in Subunit 1c, 7–8 m above the base of the microbialite. *Isarcicella* is reported for the first time within the microbialite. A very different assemblage dominated by *Hindeodus postparvus* occurs in Subunit 2b, 2–3 m above the top of the microbialite unit.

The conodonts collected from the Wuzhuan section (Fig. 2) also document an evolutionary radiation, with a taxonomic diversity peak at the top of the microbialite (sample L, top of Subunit 1c). Starting from the base of Unit 1 (microbialite), several species are sequentially added upwards to the conodont assemblage and only *N. taylorae, H. magnus* and *H. eurypyge* disappear before the top of the Unit 1. Only one specimen of *N. taylorae* is found in the entire section, and its exclusion from most samples (as for other neogondolellids) is attributed to ecological constraints as neogondolellids likely preferred colder environments (and hence, at the equator, deeper-water settings) than anchignathodontids (Joachimski *et al.* 2012). Indeed, in other sections (e.g. Dajiang section, Jiang *et al.* 2014), *N. taylorae*, *H. magnus* is known to occur also above the FO of *Isarcicella isarcica*.

DISCUSSION

Conodont elements are known from within the microbialite only in a few sections. Up to now, the best documented sections were as follows: Dongwan, Sichuan (Ezaki *et al.* 2003); Langpai, Guizhou (Ezaki *et al.* 2008); Dawen, Guizhou (Chen *et al.* 2008*a*); and Dajiang section, Guizhou (Jiang *et al.* 2014). Yet, none of these

sections records a high-resolution sequence of abundant conodonts that compares with that of Wuzhuan.

The fossil record is always discontinuous, locally incomplete due to depositional gaps, and affected by taphonomic biases and selective preservation. Hence, a sequence of FOs does not necessarily reflect the true chronology of phylogenetic events and one may ask to what extent the evolutionary radiation of anchignathodontids recorded at Wuzhuan reflects a true evolutionary radiation. In the case of this study, however, invariance of microfacies and sedimentological features and virtually constant $\delta^{13}C_{carb}$ values throughout the upper half of Unit 1 (pers. obs.) indicate stable environmental conditions. Hence, the conodont record in this interval at Wuzhuan is unaffected by local ecological changes and is more likely to represent an evolutionary rather than an ecological pattern. The sequence of FOs of anchignathodontids (species of genera *Hindeodus* and *Isarcicella*, see Fig. 2) is indeed remarkably consistent with the phylogenetic hypothesis proposed by Jiang *et al.* (2010, fig. 4). Jiang *et al.* (2010) used the ranges of conodont taxa in the Meishan section (Sichuan, China), the most intensively documented PTB section, to calibrate a cladogram based on the analysis of 25 P_1 element characters for 22 species of anchignathodontids. Hence, Jiang *et al.*'s phylogeny is considered to be the best available model for conodonts around the PTB. It is also largely in agreement with the phylogenetic scheme proposed by Perri and Farabegoli (2003, fig. 7, p. 291). The most notable difference between Jiang *et al.*'s model and our phylogenetic tree (modified from Jiang *et al.* 2010, using the ranges of taxa in Wuzhuan, see Fig. 2) is that we can possibly resolve some of their ghost lineages: in Wuzhuan, *I. turgida* occurs already below the FOs of *I. lobata*, *I. inflata*, *I. staeschei* and *I. isarcica*, in agreement with the phylogenetic model; and *H. parvus* occurs also below the FO of *H. eurypyge* and *I. turgida*, which, if confirmed, would shorten the longest ghost lineage of Jiang *et al.* (2010). This suggests that the conodont record at Wuzhuan is the closest to the 'true' sequence of evolutionary events that took place during this Griesbachian radiation of anchignathodontids.

In particular, the FO of *H. parvus* in Wuzhuan is found about 3 m below the FOs of *H. eurypyge* and *I. turgida*, which, assuming a maximum of 0.4 mm/year growth rate of recent stromatolites (Chivas *et al.* 1990), suggests the age of origination of *H. parvus* is at least 7.5 kyr older than the ages of *H. eurypyge* and *I. turgida.* This would also imply that the FO of *H. parvus* is older in Wuzhuan than its supposed first appearance datum (FAD) in Meishan: indeed, based on the Meishan's record, it appears that the origination of *H. parvus* would have taken place anytime between the origination of *I. turgida* and the origination of *I. lobata* (Jiang *et al.* 2010, fig. 4; Fig. 2, the bold line in the stratigraphical range of *H. parvus*), markedly after the origination of *H. eurypyge*. In other words, the FO of *H. parvus* in Meishan does not correspond to its FAD.

CONCLUSION

We document the first high-resolution sequence of abundant and diverse conodonts from the microbialite unit at the base of the Luolou Formation in South China including the FOs of index species such as *I. lobata*, *I. staeschei* and *I. isarcica*. The conodont record at Wuzhuan supports the cladistics-based phylogeny of Jiang *et al.* (2010) and seems to better approximate the evolutionary radiation of anchignathodontids than other sections, including the GSSP section at Meishan. Comparisons with the latter suggest that the FO of *H. parvus* in Meishan is younger than the FO of *H. parvus* in Wuzhuan and thus does not correspond to its FAD.

SYSTEMATIC PALAEONTOLOGY (Brosse and Goudemand)

The descriptions of species are exclusively based on P_1 elements. Synonymies are limited to key citations and are not intended to be exhaustive lists. All illustrated specimens are shown at the same scale. Figured elements are stored in PIMUZ, Paleontological Institute and Museum of the University of Zurich, Karl Schmid-Strasse 4, 8006 Zurich, Switzerland.

The terminology for the orientation of the element is the traditional one based on the orientation and curvature of the cusp; it refers to the element only, not to its natural orientation within the animal (Purnell *et al.* 2000). 'Lower' refers to the side of the element from which the basal cavity opens. 'Upper' refers to the opposite side. The

FIG. 3. A, *Hindeodus eurypyge* Nicoll *et al.*, 2002; bed WUZ.G, PIMUZ 30988. B–E, F?, *Hindeodus bicuspidatus* Kozur, 2004; B, bed WUZ.L, PIMUZ 31054; C, bed WUZ.O, PIMUZ 30989; D, bed WUZ.O, PIMUZ 31002; E, bed WUZ.L, PIMUZ 31045; F, (mirrored) bed WUZ.L, PIMUZ 31017. G, *Hindeodus*? sp. indet. (mirrored) bed WUZ.O, PIMUZ 31018. H–N, *Hindeodus postparvus* Kozur, 1989; H, (mirrored, juvenile) bed WUZ.O, PIMUZ 31004; I, (mirrored) bed WUZ.O, PIMUZ 31019; J, (mirrored) WUZ.O, PIMUZ 31020; K, (mirrored) bed WUZ.O, PIMUZ 31022; L, bed WUZ.O, PIMUZ 31023; M, (mirrored) bed WUZ.O, PIMUZ 31024; N, (mirrored) bed WUZ.O, PIMUZ 31021. Respectively, 'lateral' and 'upper' views, for some specimens additionally 'lower' and 'posterior' views. Scale bar represents 400 μm.

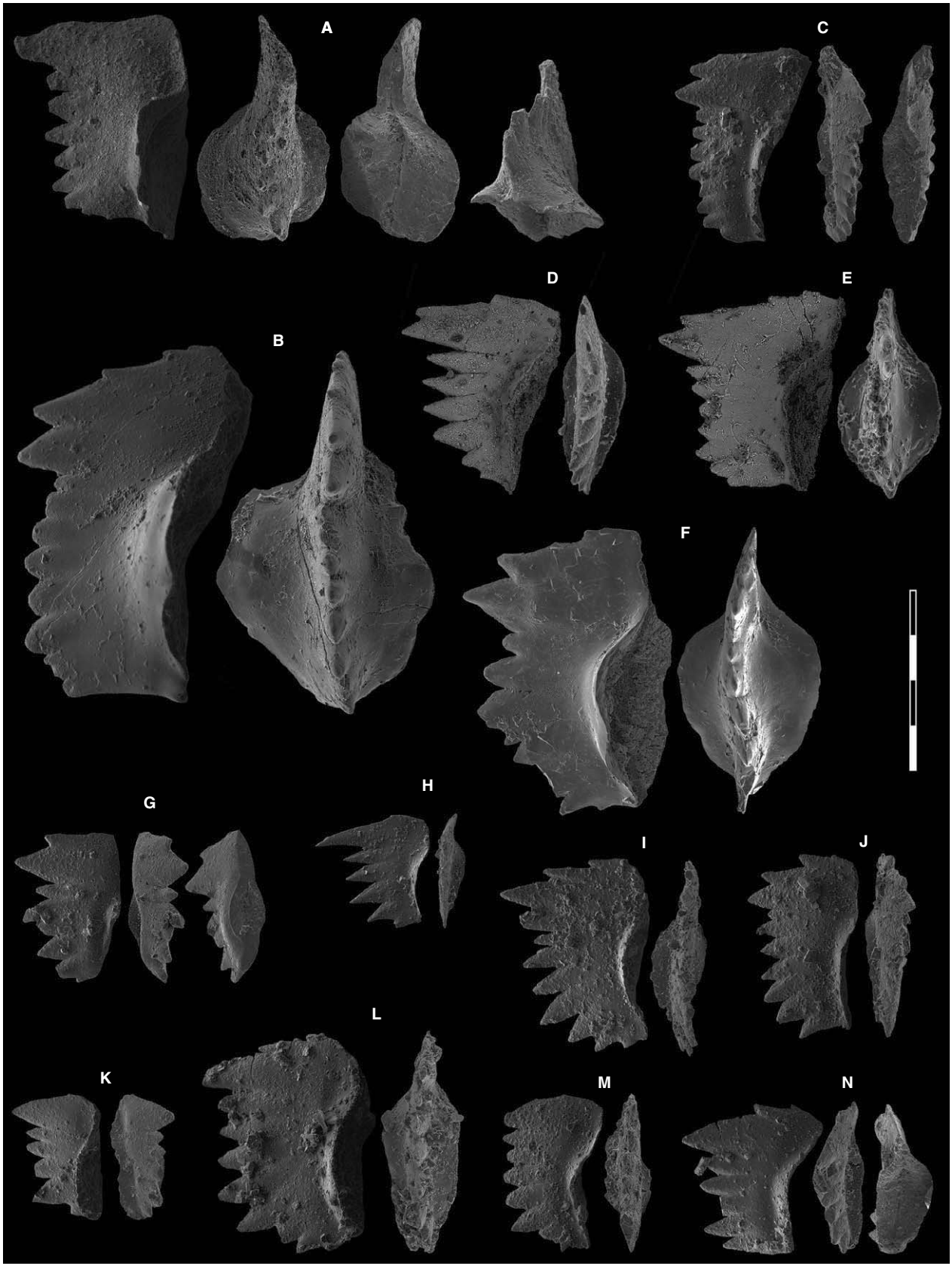
A
C
D
E
B
F
G
H
I
J
L
K
M
N

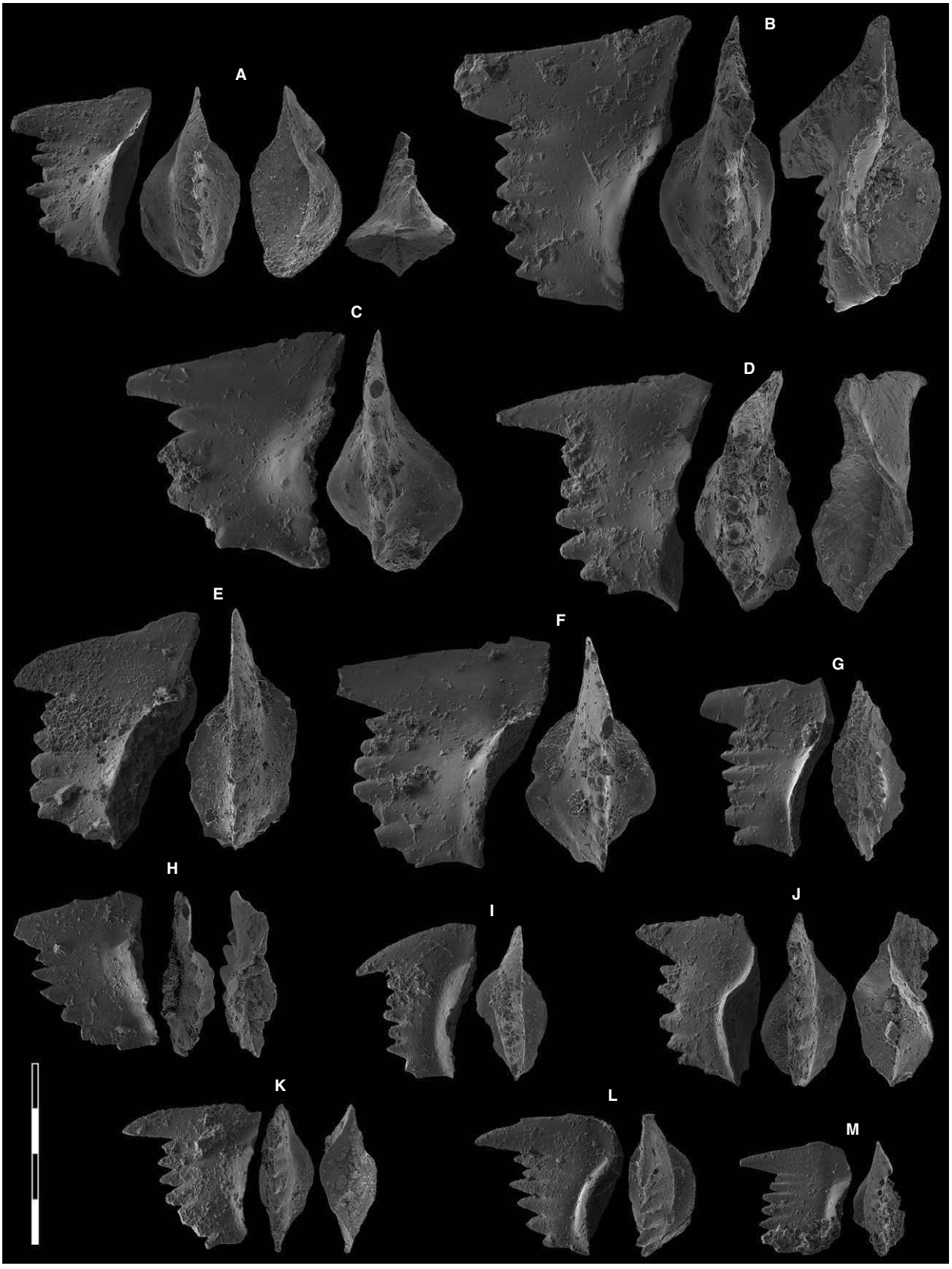
A
B
C
D
E
F
G
H
I
J
K
L
M

term 'cusp' refers only to the cusp *sensu stricto*. It represents the structure above the apex of the basal cavity (Klapper *et al.* 1973) and is homologous in distinct conodont elements. The cusp is often larger than the other denticles, but not necessarily. The big denticle that is found on the 'anterior' of carminiscaphate elements of anchignathodontids is appropriately termed 'distal denticle' (as in Agematsu *et al.* 2014).

Genus HINDEODUS Rexroad and Furnish, 1964

Type species. *Hindeodus cristulus* Youngquist and Miller, 1949.

Hindeodus bicuspidatus Kozur, 2004
Figure 3B–E, ?F

1991 *Hindeodus* n. sp.; Schönlaub, p. 88, pl. 1, fig. 6 (only).
*2004 *Hindeodus bicuspidatus* Kozur, p. 50, pl. 2, fig. 4.
2011 *Hindeodus anterodentatus* Dai and Tian; Jiang *et al.*, pl. 1, figs 3, 5.
2014 *Hindeodus bicuspidatus* Kozur; Zhang *et al.*, fig. 4: 22–24.

Diagnosis. Two large denticles of similar height instead of one single 'distal denticle' in the anterior part of the P_1 element.

Description. The most distal denticle is slightly smaller than the adjacent one, although both are considerably higher and larger than the other denticles. They can be inclined anteriorly and posteriorly. A few microdenticles are sometimes found on the anterior margin of the blade. Five to eight thickened denticles grow on the posterior part of the blade. The upper view of *H. bicuspidatus* is illustrated for the first time here, in Figure 3B, E. The basal cavity is large and asymmetrical. In upper view, the denticle line is discontinuous between the anteriormost denticles of the blade and the posterior denticles above the basal cavity.

Remarks. H. bicuspidatus differs from *H. anterodentatus* in the size of the anteriormost denticle, which is much bigger in *H. bicuspidatus*.

The two 'distal denticles' in *H. bicuspidatus* can be either inclined anteriorly (Kozur 2004, pl. 2, fig. 4, holotype; Zhang *et al.* 2014, fig. 4: 23; Schönlaub 1991, pl. 1, fig. 6) or posteriorly (Zhang *et al.* 2014, fig. 4: 22, 24; Jiang *et al.* 2011, pl. 5, fig. 3; Fig. 3B–E). The specimen illustrated in Figure 3F has an irregular denticulation reminiscent of *H. postparvus* or *H. sosioensis,* but its wide, deeply excavated and asymmetrical basal cavity is more typical of *H. bicuspidatus*.

Occurrence. Iran: Kuh-e-Hambast, section V, bed Aba V-3, lower *Clarkina meishanensis* – *Hindeodus praeparvus* Zone (Kozur 2004). China: Feixianguan Formation, Shangsi section, Sichuan, beds 28c, 30c, *H. parvus*, *I. lobata* and *I. isarcica* zones (Jiang *et al.* 2011); Zhongzhai section, Guizhou, bed 28 (Zhang *et al.* 2014); Luolou Formation, Wuzhuan section, Guangxi, beds WUZ.L and WUZ.O.

Hindeodus eurypyge Nicoll *et al.*, 2002
Figure 3A

1989 *Anchignathodus parvus* Kozur and Pjatakova; Dai and Zhang, pl. 39, figs 16, 17, pl. 45, figs 22–24.
*2002 *Hindeodus eurypyge* Nicoll *et al.*, pp. 616–620, figs 4, 5, 7–9.
2007 *Hindeodus eurypyge* Nicoll *et al.*; Metcalfe and Nicoll, pl. 1, figs 2–6.

Diagnosis. P_1 with a tall erect 'distal denticle' and 3–10 posterior blade denticles. Basal margin ovate with rounded posterior margin and basal margin flare. Basal cavity extending posteriorly of the 'distal denticle' with an ovate outline, deeply excavated with a groove extending anteriorly under the 'distal denticle'. Base of the basal cavity narrowed posteriorly to a rounded margin. Posterior end of the element high and rounded.

Description. P_1 with a rectangular lateral profile. In upper view, the blade of the specimen in Figure 3A is clearly S-shaped. The 'distal denticle' is higher than the adjacent denticles, erect and triangular. Like the holotype, the anterior margin of the 'distal denticle' is smooth. The denticles are triangular anteriorly until the mid-carina and become slightly chisel-like in the posterior half of the carina. They have an ovate section. The basal margin is very narrow anteriorly, but extends at the posterior edge of the 'distal denticle' in a wide and ovate outline with basal margin flare.

Occurrence. Meishan D, Zhejiang, discontinuous from bed 27a to bed D/C-2 in the Yinkeng Formation (Nicoll *et al.* 2002);

FIG. 4. *Hindeodus parvus* Kozur and Pjatakova, 1976. A, bed WUZ.D, PIMUZ 30990. B, (mirrored) bed WUZ.J, PIMUZ 30993. C, bed WUZ.L, PIMUZ 30995. D, bed WUZ.K, PIMUZ 30994. E, (mirrored) bed WUZ.J, PIMUZ 30992. F, (mirrored) bed WUZ.M, PIMUZ 30991. G, bed WUZ.I, PIMUZ 31001. H, bed WUZ.J, PIMUZ 31007. I, (mirrored) bed WUZ.K, PIMUZ 30996. J, bed WUZ.G, PIMUZ 31000. K, (mirrored) bed WUZ.G, PIMUZ 30999. L, (mirrored) bed WUZ.O, PIMUZ 30998. M, (mirrored) bed WUZ.J, PIMUZ 31003. Respectively, 'lateral' and 'upper' views, for some specimens additionally 'lower' and 'posterior' views. Scale bar represents 400 μm.

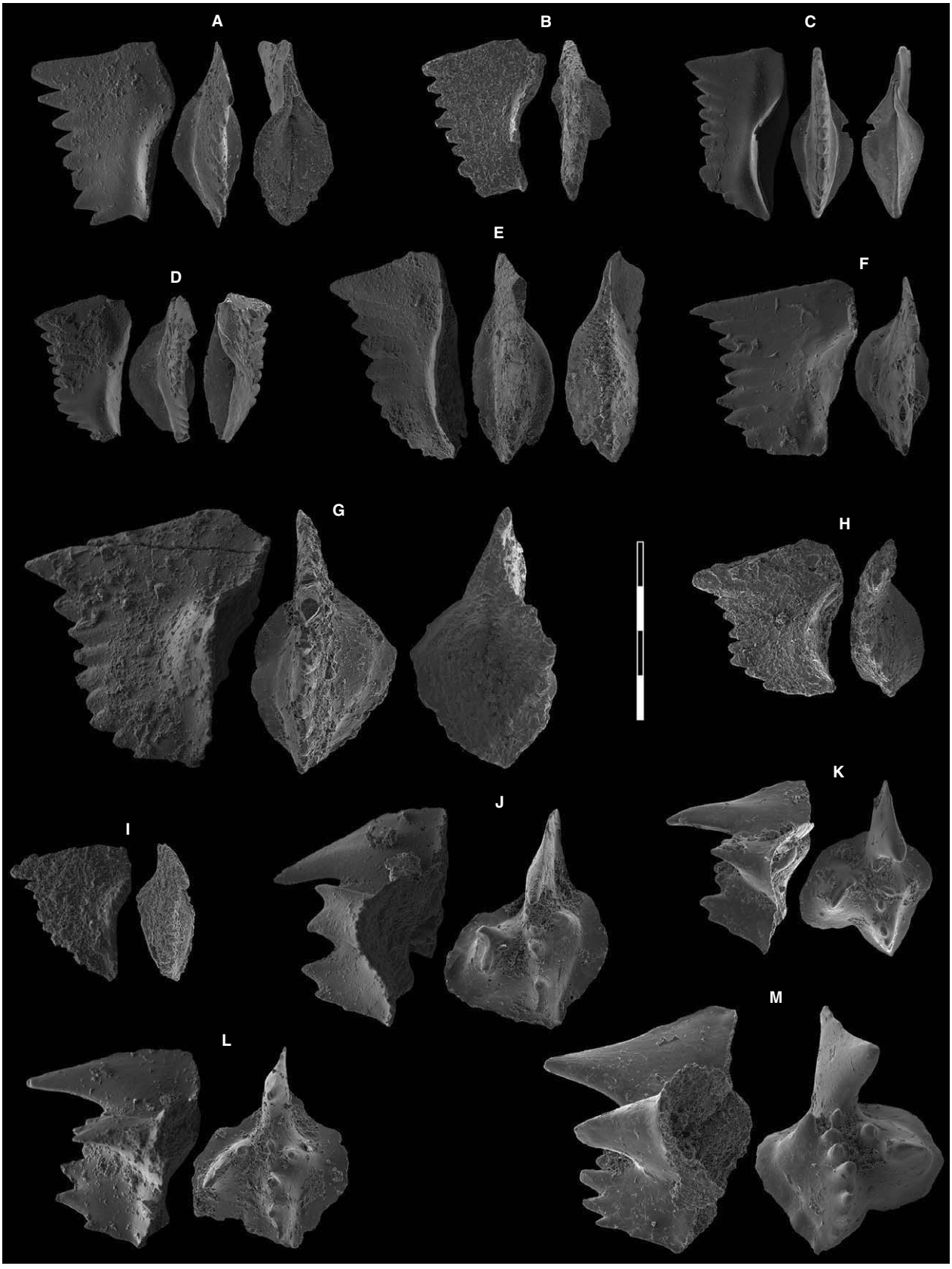
A
B
C
D
E
F
G
H
I
J
K
L
M

Shangsi, Sichuan, bed 6405548, *Merrillina ultima – Stepanovites? mostleri* Zone (Metcalfe and Nicoll 2007); Luolou Formation, Wuzhuan, Guangxi, bed WUZ. G.

Hindeodus magnus Kozur, 2004
Figure 7F–H

1993 *Hindeodus parvus* Kozur and Pjatakova; Tian, pl. 6, fig. 15 (only).
?1995 *Hindeodus latidentatus* Kozur *et al.*; Zhang *et al.*, pl. 2, fig. 12.
*2004 *Hindeodus magnus* Kozur, pl.1, fig. 14.

Diagnosis. Large P_1 element, with very large, broad 'distal denticle'. Carina with 8–9 rather large and broad denticles. Cup broad, symmetrical, rounded at posterior end.

Description. 'Distal denticle' broad and erect, posteriorly followed by 7–10 more or less fused denticles with pointed-to-rounded tips.

Remarks. Kozur (2004) noted that the P_1 element in *H. magnus* is much larger that than in *H. parvus*, and its 'distal denticle' is comparatively broader than for *H. parvus*. Also, the denticles in *H. magnus* are broader and relatively shorter than those in *H. parvus*. *H. magnus* bears also some resemblance to *H. latidentatus*, notably in the shape of the posteriormost denticles, which are more discrete and less fused than the anterior ones. However, *H. magnus* does not display the U-shaped space between the denticles that is characteristic of *H. latidentatus*, and has a relatively broader 'distal denticle'. In comparison with *H. magnus*, *H. praeparvus* has more discrete posterior denticles and a smaller 'distal denticle'.

The specimen shown in Figure 7H is not typical in having a wide, symmetrical and subtrapezoidal basal cavity that expands under the entire element, is tapered under the blade and is rounded and flared at the posterior margin.

Occurrence. China: Luolou Formation, Wuzhuan, Guangxi, bed WUZ. E; Zhejiang, Meishan C, Bed 25. Iran: lowermost Elikah Formation, Abadeh and Zal sections.

Hindeodus parvus Kozur and Pjatakova, 1976
Figure 4

*1976 *Anchignathodus parvus* Kozur and Pjatakova, pp. 123–125, fig. 1a, b, e, h.
1981 *Hindeodus parvus* Kozur and Pjatakova; Matsuda, pp. 91–93, pl. 5, figs 1–3.
1981 *Hindeodus minutus* Ellison; Matsuda, pp. 78–84, pl. 1, figs 8–12 (only).
1996 *Hindeodus parvus* Kozur and Pjatakova; Koike, pp. 342–344, fig. 3: 3–15.
1996 *Hindeodus parvus* Kozur and Pjatakova; Mei, pp. 145–146, pl. 18.2, figs 2–4, 14.
1998 *Hindeodus parvus* Kozur and Pjatakova; Orchard and Krystyn, pl. 6, figs 9, 16, 17, 20.
2002 *Hindeodus parvus* Kozur and Pjatakova; Nicoll *et al.*, p. 628, fig. 15: 1–4, fig. 16: 1–3.
2007 *Hindeodus parvus* Kozur and Pjatakova; Jiang *et al.*, pl. 5, figs 1–7.
2008*a* *Hindeodus parvus* Kozur and Pjatakova; Chen *et al.*, fig. 10: 1–13.
2008*a* *Hindeodus parvus parvus* Kozur and Pjatakova; Chen *et al.*, pp. 11–12, fig. 10: 14–19, fig. 11: 1–5.
2008*b* *Hindeodus parvus* Kozur and Pjatakova; Chen *et al.*, p. 105, pl. 5, figs 1–5.
2013 *Hindeodus parvus* Kozur and Pjatakova; Yan *et al.*, fig. 5G–L, P, S, U (only).

Diagnosis. P_1 element with a 'distal denticle' whose height is considerably higher than the other denticles. It can be preceded by a small microdenticle. Carina often bearing 4–8 denticles. First denticles posterior to the 'distal denticle' subequal. Posterior denticles often but not always inclined posteriorly.

Description. 'Distal denticle' tall and erect, sometimes inclined posteriorly. Its anterior margin sometimes bears one or even two microdenticles (Fig. 4F, H, J, L). The 'distal denticle' is followed posteriorly by five to seven more or less fused denticles. The denticles are often broader on the posterior half of the carina.

Remarks. Kozur (1989, 1996) and Mei (1996) have established three morphotypes of *H. parvus*. *H. parvus erectus* (morphotype 1) has a subvertical posterior edge; *H. parvus parvus* (morphotype 2), including the holotype, has a steeply inclined posterior blade bearing a few denticles

FIG. 5. A–B, *Hindeodus typicalis* Sweet, 1970*a*, morphotype 1; A, (mirrored) bed WUZ.E, PIMUZ 31025; B, bed WUZ.K, PIMUZ 31026. C?, D?, E, *Hindeodus typicalis* Sweet, 1970*a*, morphotype 2; C, bed WUZ.B, PIMUZ 31027; D, (mirrored) bed WUZ.B, PIMUZ 31028; E, (mirrored) bed WUZ.J, PIMUZ 31029. F–I, *Hindeodus typicalis* Sweet, 1970*a*, morphotype 3; F, (mirrored) bed WUZ.M, PIMUZ 31031; G, bed WUZ.I, PIMUZ 31030; H, bed WUZ.F, PIMUZ 31032; I, bed WUZ.I, PIMUZ 31033. J–M, *Isarcicella isarcica* Huckriede, 1958; J, (mirrored) bed WUZ.M, PIMUZ 31034; K, (mirrored) bed WUZ.L, PIMUZ 31036; L, (mirrored) bed WUZ.M, PIMUZ 31035; M, bed WUZ.L, PIMUZ 31037. Respectively, 'lateral' and 'upper' views, for some specimens additionally 'lower' view. Scale bar represents 400 μm.

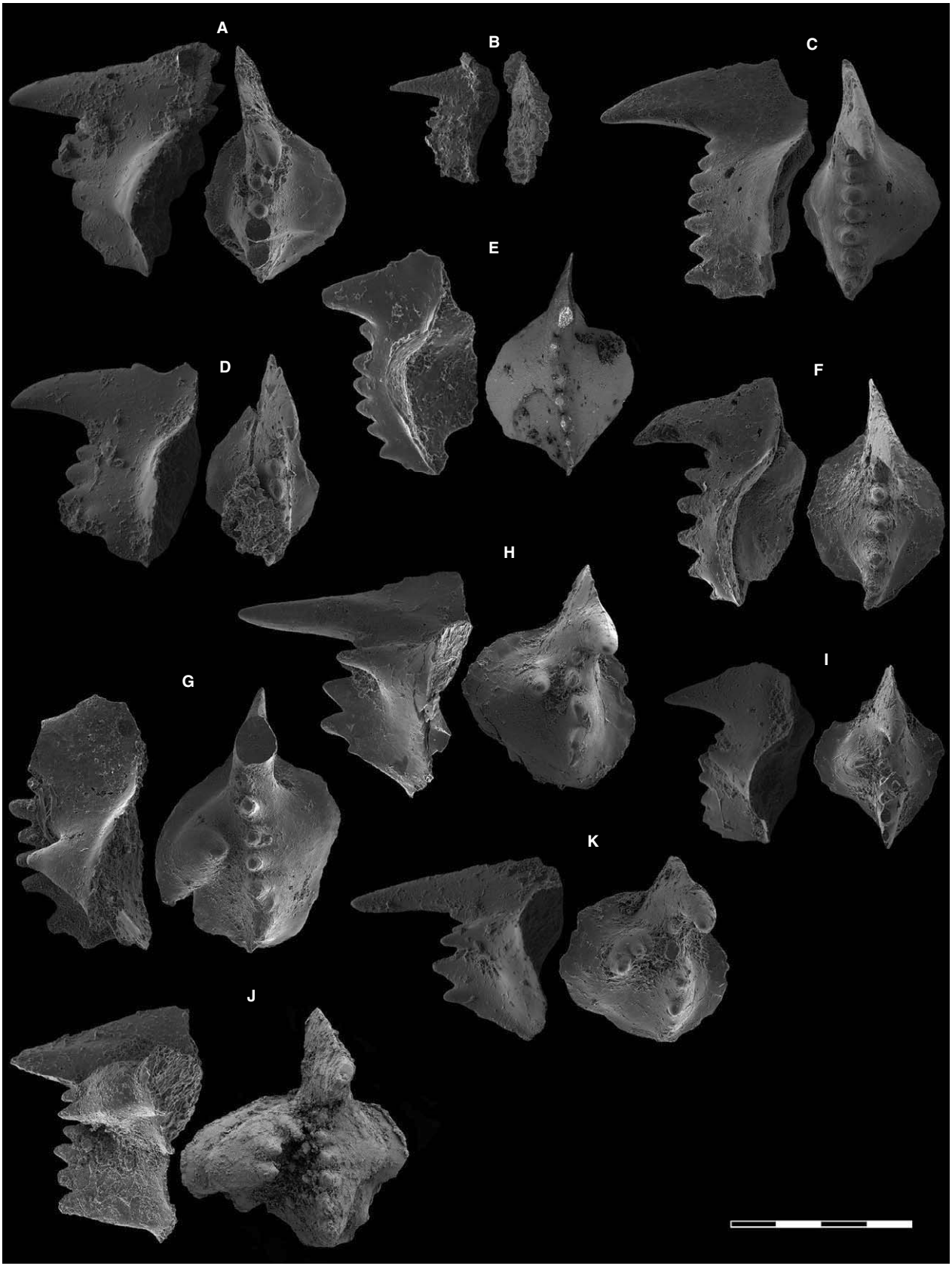
A
B
C
D
E
F
G
H
I
J
K

(Kozur 1989, 1996). A third morphotype, referred to as morphotype 3, was described in Meishan, with a less inclined, denticulate posterior edge (Mei 1996). We retain *H. parvus* for the three forms.

Occurrence. Tibet: *Otoceras latilobatum* Zone, Selong. Spiti: *Otoceras woodwardi* Zone, Guling, Lingti, Lalung. Canadian Arctic: *Otoceras boreale* Zone, Ellesmere Island (Henderson and Baud 1997). China: Meishan, Zhejiang, transition beds 25 (aff.), 27c, 27d (Yin *et al.* 1996); Luolou Formation, Wuzhuan, Guangxi, microbialite and thin-bedded limestone beds above. Kashmir: Khunamuh Formation, Guryul Ravine, beds 56–61 (E2–E3; beds number from Nakazawa *et al.* 1975). Salt Range: Kathwai Dolomite (Sweet 1970*b*). Griesbachian, Early Triassic worldwide.

Hindeodus postparvus Kozur, 1989
Figure 3H–N

1977 *Anchignathodus parvus* Kozur and Pjatakova; Kozur, figs 19, 20.
*1989 *Hindeodus postparvus* Kozur, p. 400.
1996 *Hindeodus postparvus* Kozur; Kozur, pl. 2, figs 9–10.
1998 *Hindeodus postparvus* Kozur; Orchard and Krystyn, pl. 6, fig. 1.
2008*a* *Hindeodus postparvus* Kozur; Chen *et al.*, fig. 11: 6–12.

Diagnosis. Carina with small, erected anterior denticles and strongly divergent posterior denticles. 'Distal denticle' only slightly bigger than other denticles. A small denticle can be present on the anterior edge of the 'distal denticle'. Basal cavity expands under most of the element's length, widest at mid-length.

Description. In lateral view, the element's margin is slightly arched at mid-length where the basal cavity is widest. There can be one or two small denticles on the anterior margin of the biggest elements (Fig. 3I, J, L, N). The blade posteriorly bears large denticles of unequal size which can be strongly divergent at the posterior end.

Remarks. Although displaying typical characteristics of *H. postparvus* (particularly the divergent posteriormost denticles), the specimens from Wuzhuan also bear similarities with *H. sosioensis*, such as small denticles on the anterior margin of the 'distal denticle' and unequally sized denticles. Yet, all lack the strongly unequal denticles of *H. sosioensis.* The specimen of *H. sosioensis* illustrated by Jiang *et al.* (2014, pl. 3, fig. 10) is an intermediate form between one of our specimens (Fig. 3I) and Kozur's holotype of *H. sosioensis.* Note that *H. sosioensis* and *H. postparvus* co-occur both in the floated block of Sicily (Kozur 1996, 1998) and in bed DJ-35 at Dajiang (Jiang *et al.* 2014, pl. 3, figs 10–13).

Occurrence. Southern Alps: Early Triassic of Sicily, floated block (Kozur, 1996); China: Wuzhuan section, Guangxi, bed WUZ.O.

Hindeodus praeparvus Kozur, 1996
Figure 7A–E

1994*a* *Hindeodus latidentatus* Kozur *et al.*; Wang, pl. 1, fig. 9.
1994*b* *Hindeodus latidentatus* Kozur *et al.*; Wang, pl. 2, figs 4, 5.
1996 *Hindeodus parvus erectus* Kozur; Kozur, pl. 4, fig. 7.
*1996 *Hindeodus latidentatus praeparvus* Kozur, pp. 93–94, pl. 2, figs 1–4 (only).
1996 *Hindeodus latidentatus* Kozur *et al.*; Yin *et al.*, pl. 2, fig. 3 (only).
1998 *Hindeodus praeparvus* Kozur; Orchard and Krystyn, p. 352, pl. 6, figs 22–23.
2002 *Hindeodus praeparvus* Kozur; Nicoll *et al.*, fig. 17.
2008*a* *Hindeodus praeparvus* Kozur; Chen *et al.*, fig. 9: 7–14.
2013 *Hindeodus praeparvus* Kozur; Zhao *et al.*, pl. 5, figs V–W.

Diagnosis. P_1 element with a moderately high 'distal denticle'. Anterior denticles slender and closely spaced. Posterior denticles broader and more widely spaced. V-shaped spaces between denticles.

Description. Our material agrees in all observable characters with the description of Kozur (1996).

Remarks. The distinction between the anterior and posterior denticles is shared with *H. latidentatus*, a species of which *H. praeparvus* was first described as a subspecies (Kozur 1996). Orchard and Krystyn (1998) elevated *H. latidentatus praeparvus* to the rank of species and noted that *H. latidentatus* has U-shaped posterior denticles, whereas those of *H. praeparvus* are V-shaped.

FIG. 6. A–D, *Isarcicella lobata* Perri and Farabegoli, 2003; A, bed WUZ.I, PIMUZ 31038; B, (mirrored, juvenile) bed WUZ.O, PIMUZ 31005; C, bed WUZ.K, PIMUZ 31039; D, bed WUZ.M, PIMUZ 31040. E, ?F, *Isarcicella inflata* Perri and Farabegoli, 2003; E, bed WUZ.L, PIMUZ 31053; F, bed WUZ.K, PIMUZ 31057. G–K, *Isarcicella staeschei* Dai and Zhang, 1989; G, (mirrored) bed WUZ.K, PIMUZ 31042; H, (mirrored) bed WUZ.M, PIMUZ 31043; I, (mirrored) bed WUZ.M, PIMUZ 31041; J, (mirrored) bed WUZ.I, PIMUZ 31063; K, (mirrored) bed WUZ.M, PIMUZ 31044. Respectively, 'lateral' and 'upper' views. Scale bar represents 400 μm.

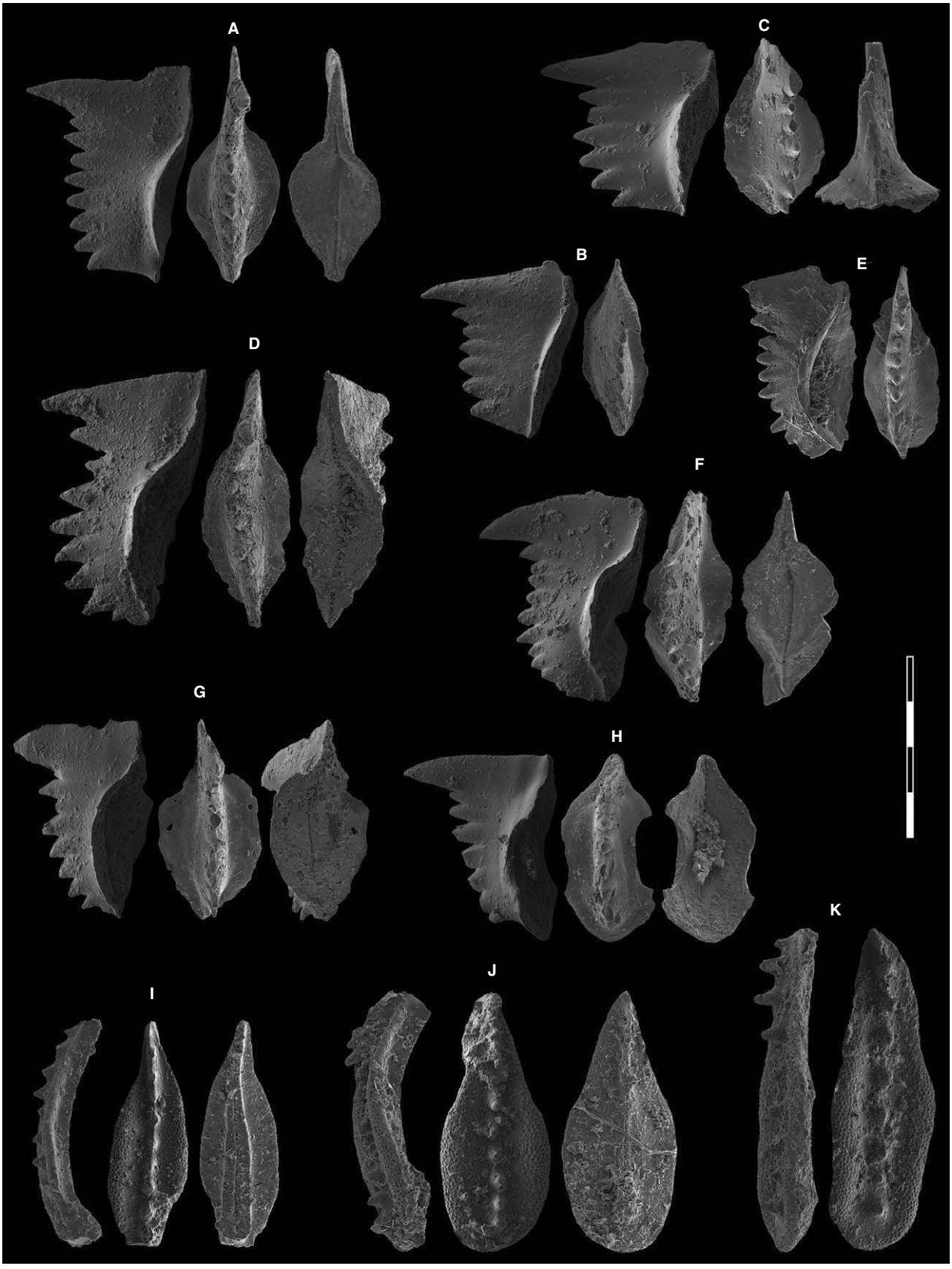
A
C
B
E
D
F
G
H
K
J
I

Occurrence. Spiti: *Otoceras woodwardi* Zone, Guling and Lingti. Kashmir: Khunamuh Formation, E2 (beds number from Nakazawa *et al.* 1975), Guryul Ravine (Bhatt and Arora 1984). China: lower and upper bed 27, Meishan, Zhejiang (Wang 1994*a*, *b*; Yin *et al.* 1996); Wuzhuan, Guangxi. Late Changhsingian and Griesbachian.

Hindeodus? sp. indet.
Figure 3G

Remarks. Owing to its resemblance to coeval forms assigned to *Hindeodus*, this element is retained tentatively within that genus although its P_1 element is carminate and not carminiscaphate. Its basal cavity is reduced and shallow. In lateral view, its unequal denticles remind those of *H. sosioensis* and it occurs in the same sample as *H. postparvus*.

Hindeodus typicalis Sweet, 1970*a*
Figure 5A–B, C?, D?, E–I

*1970*a* *Anchignathodus typicalis* Sweet, pp. 7–8, pl. 1, figs 13, 22.
1981 *Hindeodus minutus* Ellison; Matsuda, pp. 78–84, pl. 1, figs 1–7 (only).
1996 *Hindeodus typicalis* Sweet; Mei, p. 146, pl. 18.2, figs 6, 10, 11 (only).
1998 *Hindeodus typicalis* Sweet; Orchard and Krystyn, p. 354, pl. 6, figs 14, 18, 19, 25, 26.
2013 *Hindeodus typicalis* Sweet; Zhao *et al.*, fig. 5T–U.

Diagnosis. P_1 element with large 'distal denticle', but not very high compared with other denticles. Blade with four to eight subequal denticles. Outline of the blade slightly S-shaped in lateral view. Carina slightly arched posteriorly as a consequence of the monotonic decrease in the height of the denticles towards the posterior end.

Remarks. Sweet (1970*a*) differentiated *H. typicalis* from *H. minutus* (Ellison 1941) on the base of a much lower length:height ratio and a more gradual denticular margin. Specimens from Wuzhuan display a wide intraspecific variation and can be split into three morphotypes: morphotype 1 is short with a straight superior margin decreasing regularly to the posterior end, and it corresponds to *H. typicalis sensu stricto* (Fig. 5A–B); morphotypes 2 and 3 have an S-shaped denticular margin similar to that of *H. minutus*; morphotype 3 is short (length:height ratio is about 1, see Fig. 5F–I), whereas morphotype 2 is the longest of the three morphotypes (length:height ratio is 1.5–2; see Fig. 5C–E). Among the morphotype 2 specimens, those shown in Figure 5C–D are found in the same bed (WUZE B) and resemble *H. changxingensis* in having a straight carina in lateral view. However, the carina is not adenticulate, as it is described for the holotype of *H. changxingensis*.

Occurrence. Tibet: *Otoceras latilobatum* Zone, Selong. Spiti: *O. woodwardi* and *Ophiceras tibeticum* zones, Guling, Lingti, Lalung, Muth. Kashmir: Khunamuh Formation, Guryul Ravine, beds 53, 55–57, 61 (beds number from Nakazawa *et al.* 1975). Late Permian – Early Triassic worldwide.

Genus ISARCICELLA Kozur, 1975

Type species. *Spathognathodus isarcicus* Huckriede, 1958.

Isarcicella inflata Perri and Farabegoli, 2003
Figure 6E, ?F

1981 *Hindeodus parvus* Kozur and Pjatakova; Matsuda, p. 91, pl. 5, fig. 1.
1991 *Isarcicella isarcica* morphotype l; Perri, p. 42, pl. 4, fig. 10, pl. 5, fig. 5.
1991 *Isarcicella isarcica* morphotype 2; Perri, p. 42, pl. 5, fig. 4.
*2003 *Isarcicella inflata* n. sp.; Perri and Farabegoli pl. 4, figs 15–19 (only).
2007 *Isarcicella inflata* Perri and Farabegoli; Jiang, pl. 5, fig. 19.
2011 *Isarcicella inflata* Perri and Farabegoli; Jiang *et al.*, pl. 2, figs 10–12.
2011 *Isarcicella inflata* Perri and Farabegoli; Kolar-Jurkovšek *et al.*, pl. 5, fig. 5.
2014 *Isarcicella lobata* Perri and Farabegoli; Jiang *et al.*, pl. 4, fig. 2 (only).

Diagnosis. P_1 element with a very wide, asymmetrical, lobed, swollen and thickened cup lacking lateral nodes or denticles. 'Distal denticle' high, blade bearing 6–8 denticles.

Description. The 'distal denticle' is considerably higher than the other denticles, straight or arched posteriorward. The denticles

FIG. 7. A–E, *Hindeodus praeparvus* Kozur, 1996; A, bed WUZ.G, PIMUZ 31008; B, bed WUZ.G, PIMUZ 31009; C, bed WUZ.M, PIMUZ 31010; D, bed WUZ.J, PIMUZ 31014; E, bed WUZ.F, PIMUZ 31016. F–H, *Hindeodus magnus* Kozur, 2004; F, bed WUZ.I, PIMUZ 31015; G, bed WUZ.E, PIMUZ 31013; H, bed WUZ.E, PIMUZ 31056. I, *Neogondolella* sp. indet., bed WUZ.O, PIMUZ 31059. J, *Neogondolella taylorae* Orchard *in* Orchard *et al.*, 1994, bed WUZ.D, PIMUZ 31051. K, *Neogondolella* aff. *taylorae*, bed WUZ.D, PIMUZ 31058. Respectively, 'lateral' and 'upper' views, for some specimens additionally 'lower' or 'posterior' views. Scale bar represents 400 μm.

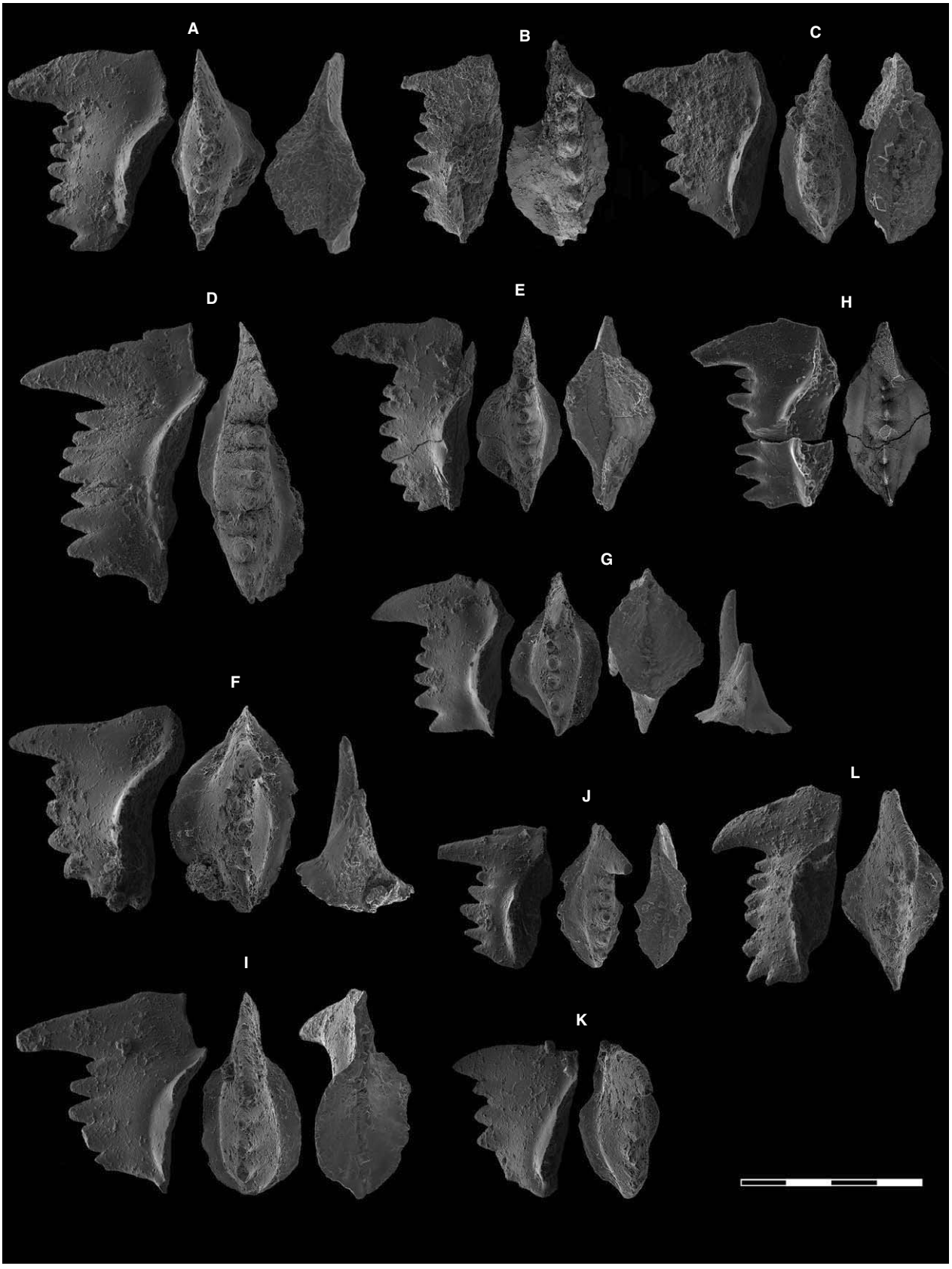
A
B
C
D
E
H
G
F
L
J
I
K

have rounded tips and can be very discrete (Fig. 6F), with a laterally compressed-to-rounded section. The cup is very wide with margin flares.

Remarks. Perri and Farabegoli (2003) differentiated this species from *I. lobata* in having a 'very much wider and inflated cup', whose outer side is 'always greatly expanded'. Perri and Farabegoli suggested that *I. inflata* derived from *I. lobata* and this hypothesis is retained here (see our phylogenetic tree, Fig. 2). The specimens of *I. inflata* from Wuzhuan have a more symmetrical basal cavity than the holotype (Fig. 6F).

Occurrence. Southern Alps: Werfen Formation, Mazzin Member, Bulla section, Tesero section, San Pellegrino Pass section, Agordo-Frassené section. China: Meishan, Zhejiang, beds 29; Shangsi, Sichuan, beds 31a–33; Luolou Formation, Wuzhuan, Guangxi, beds WUZ.K–L.

Isarcicella isarcica Huckriede, 1958
Figure 5J–M

*1958 *Spathognathodus isarcica* n. sp. Huckriede, p. 162, pl. 10, fig. 7a–b, e.
1970*b* *Anchignathodus isarcicus* Huckriede; Sweet, pp. 223–224, pl. 1, figs 18–19.
1975 *Isarcicella isarcicus* Huckriede; Kozur *et al.*, pl. 1, fig. 18.
1991 *Isarcicella isarcica* morphotype 3; Perri, pp. 42–43, pl. 4, fig. l, pl. 6, figs 1–3 (only).
1993 *Isarcicella isarcica* Huckriede; Wang and Cao, p. 254, pl. 55, figs 8–9.
1993 *Isarcicella isarcica* Huckriede; Tian, pl. 6, figs 19, 22 (only).
1994 *Isarcicella isarcica* Huckriede; Orchard *et al.*, pp. 832–833, pl. 2, figs 13–14.
1997 *Isarcicella isarcica* Huckriede; Wang and Wang, p. 165, pl. 2, fig. 1.
1999 *Isarcicella isarcica* Huckriede; Nicora and Perri, pl. 3, fig. 16.
2011 *Isarcicella isarcica* Huckriede; Jiang *et al.*, figs 7–9.

Diagnosis. An *Isarcicella* species in which the P_1 element has two lateral processes bearing nodes or denticles. P_1 element asymmetrical with two lateral node- or denticle-bearing processes, one on each side of the blade.

Description. Our material agrees in all observable characters with the description of Huckriede (1958).

Occurrence. Tibet: Selong. Southern Alps: Werfen Formation, Mazzin Member, Bulla section, Tesero section. China: widespread in the *I. isarcica* interval zone.

Isarcicella lobata Perri and Farabegoli, 2003
Figure 6A–D

1964 *Spathognathodus isarcicus* Huckriede; Staesche, text-fig. 61.
1981 *Hindeodus parvus* Kozur and Pjatakova; Matsuda, pp. 91–93, pl. 5, figs 1, 3 (only).
1991 *Isarcicella isarcica* Huckriede; Perri, pp. 42–43, pl. 3, fig. 7, pl. 4, fig. 8.
1995 *Hindeodus parvus-Isarcicella* transition?; Metcalfe pl. 1, figs 12–13.
1998 *Hindeodus parvus* morphotype 2; Farabegoli and Perri, pl. 4.3.1, fig. 13.
1999 *Hindeodus parvus erectus* Kozur; Nicora and Perri, pl. 3, fig. 7.
1999 *Hindeodus parvus parvus* Kozur and Pjatakova; Nicora and Perri, pl. 3, fig. 14.
*2003 *Isarcicella lobata*; Perri and Farabegoli, pp. 298–298, pl. 2, figs 1–3, pl. 3, figs 18–23 (only).
2004 *Isarcicella lobata* Perri and Farabegoli; Perri *et al.*, p. 475, pl. 1, figs 7, 9.
2007 *Isarcicella lobata* Perri and Farabegoli; Jiang *et al.*, pl. 5, figs 17, 18.
2011 *Isarcicella lobata* Perri and Farabegoli; Jiang *et al.*, pl. 3, figs 2–4 (only).
2014 *Isarcicella lobata* Perri and Farabegoli; Jiang *et al.*, pl. 4, figs 1, 3 (only).

Diagnosis. An *Isarcicella* species in which the P_1 element has no lateral node/denticle. P_1 element with an asymmetrical swollen and thickened cup with a lateral lobe. 'Distal denticle' higher than the other denticles, which are thickened.

Description. The 'distal denticle' is considerably higher than the other denticles, straight or arched posteriorward. The denticles have rounded tips and a rounded section. The cup is asymmetrical and swollen and lacks nodes or denticles. For the best preserved P_1 element (Fig. 6C), the denticles are bigger and more discrete posteriorly.

FIG. 8. A–J, ?K, ?L, *Isarcicella turgida* Kozur *et al.*, 1975; A, bed WUZ.I, PIMUZ 31012; B, bed WUZ.I, PIMUZ 31046; C, bed WUZ.G, PIMUZ 31047; D, bed WUZ.K, PIMUZ 31048; E, (mirrored) bed WUZ.K, PIMUZ 31049; F, (mirrored) bed WUZ.K, PIMUZ 31055; G, (mirrored) bed WUZ.K, PIMUZ 31050; H, bed WUZ.K, PIMUZ 31205; I, bed WUZ.I (element lost); J, (juvenile) bed WUZ.O, PIMUZ 30997; K, (mirrored) bed WUZ.J, PIMUZ 31006; L, bed WUZ.I, PIMUZ 31011. Respectively, 'lateral' and 'upper' views, for some specimens additionally 'lower' or 'posterior' views. Scale bar represents 400 μm.

Remarks. Isarcicella lobata is sometimes confused with *H. parvus* (Matsuda 1981, pl. 5, figs 1, 3), but it differs by the asymmetrical wide basal cavity. It shares with *I. turgida* a swelling of the base of the denticles, but the blade is not as swollen and its basal cavity is asymmetrical and more inflated.

Occurrence. Southern Alps: Werfen Formation, Mazzin Member, Bulla section, Tesero section, San Pellegrino Pass section, Agordo-Frassené section. Kashmir: Khunamuh Formation, Guryul Ravine, beds 56 and 57 (beds number from Nakazawa *et al.* 1975). China: Meishan, Zhejiang, beds 28 and 29; Shangsi, Sichuan, beds 30–33; Luolou Formation, Wuzhuan, Guangxi, beds WUZ.I-M.

Isarcicella staeschei Dai and Zhang, 1989
Figure 6G–K

1964 *Spathognathodus isarcicus* Huckriede; Staesche, p. 288, text-figs 62–63.
1981 *Isarcicella isarcica* Huckriede; Matsuda, pp. 93–94, pl. 5, figs 4–7.
1981 *Isarcicella*? sp.; Matsuda, pp. 94–95, pl. 5, fig. 8.
*1989 *Isarcicella staeschei* Dai and Zhang, pp. 430–431, pl. 45, figs 16–17; pl. 46, figs 4–7, 11–13, 18, 19; pl. 53, figs 13–14.
1996 *Isarcicella isarcica* Huckriede; Kozur, p. 100, pl. 5, figs 6, 9.
1998 *Isarcicella staeschei* Dai and Zhang; Orchard and Krystyn, p. 354, pl. 6, figs 4, 5, 10–12.
2003 *Isarcicella staeschei* Dai and Zhang; Perri and Farabegoli, p. 300, pl. 3, figs 1–14, pl. 4, figs 7–9.
2004 *Isarcicella staeschei* Dai and Zhang; Perri *et al.*, p. 475, pl. 1, figs 1–6, pl. 2, figs 3, 6–14.
2011 *Isarcicella staeschei* Dai and Zhang; Jiang *et al.*, pl. 3, figs 9–12.

Diagnosis. An *Isarcicella* species in which the P_1 element has one lateral process bearing nodes or denticles. P_1 element strongly asymmetrical with one lateral process bearing nodes or denticles. 'Distal denticle' twice as high as other denticles. Carina with 4–6 discrete denticles. Basal cavity expending almost under the entire element.

Description. Our material agrees in all observable characters with the description of Dai and Zhang (1989).

Remarks. Two distinct morphotypes of *I. staeschei* have been described: a 'single lateral denticle' morphotype (Fig. 6G–I) and a 'more than one lateral denticle' morphotype (Fig. 6J, K), the latter including the holotype. According to Kozur (1996), morphotype 2 occurs exclusively in the *I. isarcica* zone, while according to Perri and Farabegoli (2003), it is older than the FO of *I. isarcica* in the Southern Alps. At Wuzhuan, morphotype 2 also occurs before the FO of *I. isarcica*, extending Perri and Farabegoli's observation to Guangxi.

Occurrence. China: Feixianguan Formation, Shangsi, Xiaoba and Xikou, Sichuan; Lower Jinjiling Formation, Meishan, Zhejiang, beds 27d and 28; Luolou Formation, Wuzhuan, Guangxi, beds WUZ.I-M. Southern Alps: Werfen Formation, Mazzin Member, Bulla section, Tesero section, San Pellegrino Pass section, Agordo-Frassené section. Kashmir: Khunamuh Formation, Guryul Ravine, beds 61 and 63 (beds number from Nakazawa *et al.* 1975).

Isarcicella turgida Kozur *et al.*, 1975
Figure 8A–J, ?K, ?L

*1975 *Anchignathodus turgidus* n. sp. Kozur *et al.*, p. 5, pl. 7, figs 11–12.
1995 *Isarcicella*? *turgida* Kozur *et al.*; Kozur, p. 72, pl. 2, figs 5, 8.
1996 *Isarcicella*? *turgida* Kozur *et al.*; Kozur, p. 100, pl. 4, fig. 8.
2003 *Isarcicella turgida* Kozur *et al.*; Perri and Farabegoli, p. 245, pl. 2, figs 13–15.
2003 *Isarcicella lobata* Perri and Farabegoli; Perri and Farabegoli, pp. 298–298, pl. 3, figs 15–17, 24–29 (only).
2004 *Isarcicella turgida* Kozur *et al.*; Perri *et al.*, p. 475, pl. 1, fig. 8.
2011 *Isarcicella turgida* Kozur *et al.*; Jiang *et al.*, pl. 2, figs 3–6.

Diagnosis. P_1 element with a characteristic thickened carina. Basal cavity moderately excavated and slightly asymmetrical, extending over two-thirds of the overall length of the element.

Description. The carina is thickened with a relatively short blade. The broad denticles have a rounded (e.g. Fig. 8A) to marked laterally compressed section (e.g. Fig. 8D). They are sometimes broader and more discrete posteriorly (Fig. 8A, B, G). The basal cavity is moderately excavated and slightly asymmetrical to nearly symmetrical (Fig. 8C, F).

Remarks. In overall shape, *I. turgida* is very similar to *H. parvus*. It differs only by the swollen blade. Specimens from Wuzhuan can be intermediate (Fig. 8C, E). *I. lobata* also shows a swelling of the entire basal cavity, but *I. turgida* has a narrower and subsymmetrical basal cavity.

Occurrence. Iran: Elikah Formation, Unit 64. China: Feixianguan Formation, Shangsi, Sichuan, beds 31a–33; Luolou Formation, Wuzhuan, Guangxi, 7 m above the top of the microbialite (beds WUZ.I–L). Southern Alps: Werfen Formation, Mazzin Member, Bulla section, Tesero section, San Pellegrino Pass section, Agordo-Frassené section.

Genus NEOGONDOLELLA Bender and Stoppel, 1965

Type species. *Gondolella mombergensis* (Tatge, 1956).

Neogondolella taylorae Orchard *in* Orchard *et al.*, 1994
Figure 7J

*1994 *Neogondolella taylorae* n. sp. Orchard *et al.*, p. 833, pl. 3, fig. 15 (only).
1996 *Clarkina* aff. *planata* Clark; Mei, pl. 18.2, fig. 13.
1998 *Neogondolella taylorae* beta morphotype nov.; Orchard and Krystyn, p. 362, pl. 2, figs 5, 9, 13–16.
2013 *Clarkina taylorae* Orchard; Zhao *et al.*, pl. 5, figs J–L.

Diagnosis. P_1 element with an elongated and oval-shaped platform. Platform widest at mid-length, rounded well-developed posterior margin surrounding the cusp. Carina with discrete nodes terminated anteriorly in a blade and posteriorly in a rounded erect cusp.

Remarks. The platform outline bears some resemblance to *N. planata,* but it is less flat. The single specimen from Wuzhuan is similar to *N. nevadensis,* but has a distinct posterior platform margin. Orchard and Krystyn (1998) distinguished three morphotypes. Our specimen is similar to morphotype beta, but has a slightly larger posterior margin.

Occurrence. Tibet: *Otoceras latilobatum* Zone, Selong. Spiti: *Otoceras woodwardi* and *Ophiceras tibeticum* zones, Guling, Lingti, Lalung, Muth. China: Meishan, Zhejiang; Wuzhuan, Guangxi (bed WUZ.D).

Neogondolella aff. *taylorae*
Figure 7K

Description. P_1 element more elongated (length:width ratio is *ca.* 3:1) than *N. taylorae*. Platform symmetrical and widest at mid-length, tapered anteriorly extending to the anterior end. Cusp erect and surrounded by a very large platform margin. Denticles discrete, including the most anterior ones which are erect and taller than the others. Element very straight in lateral profile.

Occurrence. Co-occurs with *N. taylorae*, 4 m above the base of the microbialite at Wuzhuan, Guangxi (bed WUZ.D).

Neogondolella sp. indet.
Figure 7I

Description. P_1 element with asymmetrical, anteriorly tapered platform. It differs from *N. taylorae* in having fused anterior denticles. This specimen could be an element of *N. carinata*, but the broken posterior part prevents any confident determination at the species level.

Occurrence. In the thin-bedded limestone beds above the microbialite in Wuzhuan, 12 m above the PTB (bed WUZ.O).

Acknowledgements. This research is supported by the Swiss NSF project 200021_135446 (to HB). We are deeply grateful to Mike Orchard, Tea Kolar-Jurkovšek and Sally Thomas for reviewing the manuscript and making insightful comments and to Michael Hautmann for editing and critical reading of the manuscript. Lorena Tessitore and Marc Leu are thanked for their help in processing samples. Prof. Rossana Martini and Agathe Martinier (Université de Genève) are thanked for their help with the SEM.

Editor. Michael Hautmann

REFERENCES

AGEMATSU, S., SANO, H. and SASHIDA, K. 2014. Natural assemblages of Hindeodus conodonts from a Permian–Triassic boundary sequence, Japan. *Palaeontology*, **57** (6), 1277–1289.

AWRAMIK, S. M. 1990. Stromatolites. 336–341. *In* BRIGGS, D. E. G. and CROWTHER, P. R. *Palaeobiology: a synthesis*. Blackwell Scientific Publications, London.

BAUD, A., CIRILLI, S. and MARCOUX, J. 1997. Biotic response to mass extinction: the Lowermost Triassic microbialites. *Facies*, **36**, 238–242.

—— RICHOZ, S., CIRILLI, S. and MARCOUX, J. 2002. *Basal Triassic carbonate of the Tethys: a microbialite world*. 16th International Sedimentological Congress, Johannesburg, Abstract Volume, 24–25.

—— —— and PRUSS S. 2007. The lower Triassic anachronistic carbonate facies in space and time. *Global and Planetary Change*, **55** (1), 81–89.

BENDER, H. and STOPPEL, D. 1965. Perm-Conodonten. *Geologisches Jahrbuch der BGR, (Hannover)*, **82** (3), 331–364.

BHATT, D. K. and ARORA, R. K. 1984. Otoceras bed of Himalaya and Permian–Triassic boundary-assessment and elucidation with conodont data. *Journal of the Geological Society of India*, **25** (11), 720–727.

BRAYARD, A., ESCARGUEL, G., BUCHER, H. and BRÜHWILER, T. 2009. Smithian and Spathian (Early Triassic) ammonoid assemblages from terranes: paleoceanographic and paleogeographic implications. *Journal of Asian Earth Sciences*, **36** (6), 420–433.

—— VENNIN, E., OLIVIER, N., BYLUND, K. G., JENKS, J., STEPHEN, D. A., BUCHER, H., HOFMANN, R., GOUDEMAND, N. and ESCARGUEL, G. 2011. Transient metazoan reefs in the aftermath of the end-Permian mass extinction. *Nature Geoscience*, **4** (10), 693–697.

BRÜHWILER, T., BRAYARD, A., BUCHER, H. and GUODUN, K. 2008. Griesbachian and Dienerian (Early Triassic) ammonoid faunas from northwestern Guangxi and southern Guizhou (south China). *Palaeontology*, **51** (5), 1151–1180.

BURGESS, S. D., BOWRING, S. and SHEN, S. Z. 2014. High-precision timeline for Earth's most severe extinction.

Proceedings of the National Academy of Sciences, **111** (9), 3316–3321.

CHEN, J., BEATTY, T. W., HENDERSON, C. M. and ROWE, H. 2008*a*. Conodont biostratigraphy across the Permian–Triassic boundary at the Dawen section, Great Bank of Guizhou, Guizhou Province, South China: implications for the Late Permian extinction and correlation with Meishan. *Journal of Asian Earth Sciences*, **36** (6), 442–458.

—— HENDERSON, C. M. and SHEN, S. Z. 2008*b*. Conodont succession around the Permian–Triassic boundary at the Huangzhishan Section, Zhejiang and its stratigraphic correlation. *Acta Palaeontologica Sinica*, **7** (1), 91–114.

CHIVAS, A. R., TORGERSEN, T. and POLACH, H. A. 1990. Growth rates and Holocene development of stromatolites from Shark Bay, Western Australia. *Australian Journal of Earth Sciences*, **37** (2), 113–121.

DAI, J. and ZHANG, J. 1989. Study on the Permian–Triassic biostratigraphy and event stratigraphy of northern Sichuan and southern Shaanxi. *Ministry of Geology and Mineral Resources, Geological Memoirs, Series*, **2**, 435 pp.

ELLISON, S. 1941. Revision of the Pennsylvanian conodonts. *Journal of Paleontology*, **15** (2), 107–143.

ERWIN, D. H. 2001. Lessons from the past: biotic recoveries from mass extinctions. *Proceedings of the National Academy of Sciences*, **98** (10), 5399–5403.

—— 2006. *Extinction: how life on Earth nearly ended 250 million years ago*. Princeton University Press, 230 pp.

EZAKI, Y., LIU, J. and ADACHI, N. 2003. Earliest Triassic microbialite micro-to megastructures in the Huaying area of Sichuan Province, South China: implications for the nature of oceanic conditions after the end-Permian extinction. *Palaios*, **18** (4–5), 388–402.

—— —— NAGANO, T. and ADACHI, N. 2008. Geobiological aspects of the earliest Triassic microbialites along the southern periphery of the tropical Yangtze Platform: initiation and cessation of a microbial regime. *Palaios*, **23** (6), 356–369.

FAN, G., WANG, Y., KERSHAW, S., LI, G., MENG, Z., LIN, Q. and YUAN, Z. 2014. Recurrent breakdown of Late Permian reef communities in response to episodic volcanic activities: evidence from southern Guizhou in South China. *Facies*, **60** (2), 603–613.

FARABEGOLI, E. and PERRI, M. C. 1998. Permian/Triassic boundary and Early Triassic of the Bulla section (Southern Alps, Italy): lithostratigraphy, facies and conodont biostratigraphy. *Giornale di geologia*, **60** (Special Issue), 292–310.

GALFETTI, T., BUCHER, H., MARTINI, R., HOCHULI, P. A., WEISSERT, H., CRASQUIN-SOLEAU, S., BRAYARD, A., GOUDEMAND, N., BRÜHWILER, T. and GUODUN, K. 2008. Evolution of Early Triassic outer platform paleoenvironments in the Nanpanjiang Basin (South China) and their significance for the biotic recovery. *Sedimentary Geology*, **204** (1), 36–60.

HAUTMANN, M., BUCHER, H., BRÜHWILER, T., GOUDEMAND, N., KAIM, A. and NÜTZEL, A. 2011. An unusually diverse mollusc fauna from the earliest Triassic of South China and its implications for benthic recovery after the end-Permian biotic crisis. *Geobios*, **44** (1), 71–85.

HENDERSON, C. M. and BAUD, A. 1997. Correlation of the Permian–Triassic boundary in Arctic Canada and comparison with Meishan, China. *Stratigraphy*, **11**, 143–152.

HERMANN, E., HOCHULI, P. A., MÉHAY, S., BUCHER, H., BRÜHWILER, T., WARE, D., HAUTMANN, M., ROOHI, G., UR-REHMAN, K. and YASEEN, A. 2011. Organic matter and palaeoenvironmental signals during the Early Triassic biotic recovery: the Salt Range and Surghar Range records. *Sedimentary Geology*, **234** (1), 19–41.

HOFMANN, R., GOUDEMAND, N., WASMER, M., BUCHER, H. and HAUTMANN, M. 2011. New trace fossil evidence for an early recovery signal in the aftermath of the end-Permian mass extinction. *Palaeogeography, Palaeoclimatology, Palaeoecology*, **310** (3), 216–226.

HUCKRIEDE, R. 1958. Die Conodonten der mediterranen Trias und ihr stratigraphischer Wert. *Paläontologische Zeitschrift*, **32** (3–4), 141–175.

JEPPSSON, L. and ANEHUS, R. 1999. A new technique to separate conodont elements from heavier minerals. *Alcheringa*, **23** (1), 57–62.

—— —— and FREDHOLM D. 1999. The optimal acetate buffered acetic acid technique for extracting phosphatic fossils. *Journal of Paleontology*, **73** (5), 964–972.

JIANG, H., LAI, X., LUO, G., ALDRIDGE, R., ZHANG, K. and WIGNALL, P. 2007. Restudy of conodont zonation and evolution across the P/T boundary at Meishan section, Changxing, Zhejiang, China. *Global and Planetary Change*, **55** (1), 39–55.

—— ALDRIDGE, R. J., LAI, X., YAN, C. and SUN, Y. 2010. Phylogeny of the conodont genera *Hindeodus* and *Isarcicella* across the Permian–Triassic boundary. *Lethaia*, **44** (4), 374–382.

—— LAI, X., YAN, C., ALDRIDGE, R. J., WIGNALL, P. and SUN, Y. 2011. Revised conodont zonation and conodont evolution across the Permian–Triassic boundary at the Shangsi section, Guangyuan, Sichuan, South China. *Global and Planetary Change*, **77** (3), 103–115.

—— —— SUN, Y., WIGNALL, P. B., LIU, J. and YAN, C. 2014. Permian–Triassic conodonts from Dajiang (Guizhou, South China) and their implication for the age of microbialite deposition in the aftermath of the End-Permian mass extinction. *Journal of Earth Science*, **25** (3), 413–430.

JOACHIMSKI, M. M., LAI, X., SHEN, S., JIANG, H., LUO, G., CHEN, B., JUN, C. and SUN, Y. 2012. Climate warming in the latest Permian and the Permian–Triassic mass extinction. *Geology*, **40** (3), 195–198.

KAIM, A., NÜTZEL, A., BUCHER, H., BRÜHWILER, T. and GOUDEMAND, N. 2010. Early Triassic (Late Griesbachian) gastropods from South China (Shanggan, Guangxi). *Swiss Journal of Geosciences*, **103** (1), 121–128.

KERSHAW, S., ZHANG, T. and LAN, G. 1999. A ?microbialite carbonate crust at the Permian–Triassic boundary in South China, and its palaeoenvironmental significance. *Palaeogeography, Palaeoclimatology, Palaeoecology*, **146** (1), 1–18.

—— GUO, L., SWIFT, A. and FAN, J. 2002. ?Microbialites in the Permian–Triassic boundary interval in central China: structure, age and distribution. *Facies*, **47** (1), 83–89.

—— LI, Y., CRASQUIN-SOLEAU, S., FENG, Q., MU, X., COLLIN, P. Y., REYNOLDS, A. and GUO, L. 2007.

Earliest Triassic microbialites in the South China block and other areas: controls on their growth and distribution. *Facies*, **53** (3), 409–425.

KLAPPER, G., LINDSTRÖM, M., SWEET, W. C. and ZIEGLER, W. 1973. *In* ZIEGLER, W. (ed.). *Catalogue of Conodonts, 1*. E. Schweizerbart'sche Verlagsbuchhandlung, Stuttgart, 504 pp.

KOIKE, T. 1996. The first occurrence of Griesbachian conodonts in Japan. *Transactions and Proceedings of the Palaeontological Society of Japan*, **181**, 337–346.

KOLAR-JURKOVŠEK, T., JURKOVŠEK, B. and ALJINOVIĆ, D. 2011. Conodont biostratigraphy across the Permian–Triassic boundary at the Lukač section in western Slovenia. *Rivista Italiana di Paleontologia e Stratigrafia*, **117**, 115–133.

KOZUR, H. W. 1975. Beiträge zur Conodontenfauna des Perm. *Geologisch-Paläontologische Mitteilungen Innsbruck*, **5**, 1–44.

—— 1977. Revision der Conodontengattung Anchignathodus und ihrer Typusart. *Zeitschrift für Geologische Wissenschaften*, **5**, 1113–1127.

—— 1989. Significance of events in conodont evolution for the Permian and Triassic stratigraphy. *Courier Forschungsinstitut Senckenberg*, **117**, 385–408.

—— 1995. Permian conodont zonation and its importance for the Permian stratigraphic standard scale. *Geologisch-Paläontologische Mitteilungen Innsbruck*, **20**, 165–205.

—— 1996. The conodonts *Hindeodus*, *Isarcicella* and *Sweetohindeodus* in the uppermost Permian and lowermost Triassic. *Geologia Croatica*, **49** (1), 81–115.

—— 1998. Some aspects of the Permian–Triassic boundary (PTB) and of the possible causes for the biotic crisis around this boundary. *Palaeogeography, Palaeoclimatology, Palaeoecology*, **143** (4), 227–272.

—— 2004. Pelagic uppermost Permian and the Permian–Triassic boundary conodonts of Iran. Part 1: Taxonomy. *Hallesches Jahrbuch für Geowissenschaften, B Geologie, Paläontologie, Mineralogie*, **18**, 29–68.

—— and PJATAKOVA, M. 1976. Die Conodontenart *Anchignathodus parvus* n. sp., eine wichtige Leitform der basalen Trias. *Koninklijke Nederlandse Akademie van Wetenschappen, Amsterdam, Proceedings, Series B*, **79**, 123–128.

—— MOSTLER, H. and RAHIMI-YAZD, A. 1975. Beiträge zur Mikrofauna permotriadischer Schichtfolgen. Teil II: Neue Conodonten aus dem Oberperm und der basalen Trias von Nord-und Zentraliran. *Geologisch-Paläontologische Mitteilungen Innsbruck*, **5** (3), 1–23.

KRYSTYN, L., RICHOZ, S., BAUD, A. and TWITCHETT, R. J. 2003. A unique Permian–Triassic boundary section from the neotethyan Hawasina basin, Central Oman Mountains. *Palaeogeography, Palaeoclimatology, Palaeoecology*, **191** (3), 329–344.

LEHRMANN, D. J. 1999. Early Triassic calcimicrobial mounds and biostromes of the Nanpanjiang basin, South China. *Geology*, **27** (4), 359–362.

—— WAN, Y., WEI, J., YU, Y. and XIAO, J. 2001. Lower Triassic peritidal cyclic limestone: an example of anachronistic carbonate facies from the Great Bank of Guizhou, Nanpanjiang Basin, Guizhou province, South China. *Palaeogeography, Palaeoclimatology, Palaeoecology*, **173** (3), 103–123.

MATSUDA, T. 1981. Appendix to conodonts of Guryul Ravine. *Palaeontologia Indica*, **46**, 187–188.

MEI, S. 1996. Restudy of conodonts from the Permian–Triassic boundary beds at Selong and Meishan and the natural Permian–Triassic boundary. 141–148. *In* WANG, H. and WANG, X. (eds). *Centennial memorial volume of Professor Sun Yunzhu, palaeontology and stratigraphy*. China University of Geosciences Press, Beijing.

METCALFE, I. 1995. Mixed Permo-Triassic boundary conodont assemblages from Gua Sei and Kampong Gua, Pahang, Peninsular Malaysia. *Courier Forschungsinstitut Senckenberg*, **182**, 487–495.

—— and NICOLL, R. S. 2007. Conodont biostratigraphic control on transitional marine to non-marine Permian–Triassic boundary sequences in Yunnan-Guizhou, China. *Palaeogeography, Palaeoclimatology, Palaeoecology*, **252** (1), 56–65.

NAKAZAWA, K., KAPOOR, H. M., ISHII, K. I., BANDO, Y., OKIMURA, Y. and TOKUOKA, T. 1975. The upper Permian and the lower Triassic in Kashmir, India. *Memoirs of the Faculty of Science, Kyoto University, Series of Geology and Mineralogy*, **42**, 1–106.

NICOLL, R. S., METCALFE, I. and CHENG-YUAN, W. 2002. New species of the conodont genus *Hindeodus* and the conodont biostratigraphy of the Permian–Triassic boundary interval. *Journal of Asian Earth Sciences*, **20** (6), 609–631.

NICORA, A. and PERRI, M. C. 1999. The P/T boundary in the Tesero section, western Dolomites (Trento). 3.3. Bio- and chronostratigraphy. Conodonts. *In Stratigraphy and facies of the Permian deposits between Eastern Lombardy and the Western Dolomites*. Field Trip Guidebook, 23–25 September 1999, Earth Science Department, Pavia University, Brescia, Italy.

ORCHARD, M. J. 2007. Conodont diversity and evolution through the latest Permian and Early Triassic upheavals. *Palaeogeography, Palaeoclimatology, Palaeoecology*, **252** (1), 93–117.

—— and KRYSTYN, L. 1998. Conodonts of the lowermost Triassic of Spiti, and new zonation based on *Neogondolella* successions. *Rivista Italiana di Paleontologia e Stratigrafia*, **104** (3), 341–367.

—— NASSICHUK, W. W. and RUI, L. 1994. Conodonts from the lower Griesbachian *Otoceras Latilobatum* bed of Selong, Tibet and the position of the Permian–Triassic boundary. *Canadian Society of Petroleum Geologists, Memoir*, **17**, 823–843.

PERRI, M. C. 1991. Conodont biostratigraphy of the Werfen Formation (Lower Triassic), Southern Alps, Italy. *Bollettino della Società Paleontologica Italiana*, **30** (1), 23–46.

—— and FARABEGOLI, E. 2003. Conodonts across the Permian–Triassic boundary in the Southern Alps. *Courier Forschungsinstitut Senckenberg*, **245**, 281–313.

—— MOLLOY, P. D. and TALENT, J. A. 2004. Earliest Triassic conodonts from Chitral, northernmost Pakistan. *Rivista Italiana di Paleontologia e Stratigrafia*, **110** (2), 467–478.

PRUSS, S. B., BOTTJER, D. J., CORSETTI, F. A. and BAUD, A. 2006. A global marine sedimentary response to the end-Permian mass extinction: examples from southern

Turkey and the western United States. *Earth-Science Reviews*, **78** (3), 193–206.

PURNELL, M. A., DONOGHUE, P. C. and ALDRIDGE, R. J. 2000. Orientation and anatomical notation in conodonts. *Journal of Paleontology*, **74** (1), 113–122.

QI, Y. P. and LIAO, T. P. 2007. Discovery of the latest Permian gondolellid conodonts from the microbialites across the Permian–Triassic boundary in the Tudiya Section, Chongqing, South China and its implications. *Permophiles*, **49**, 28–31.

RAUP, D. M. 1979. Size of the Permo-Triassic bottleneck and its evolutionary implications. *Science*, **206** (4415), 217–218.

RETALLACK, G. J. 1995. Permian–Triassic life crisis on land. *Science*, **267** (5194), 77–80.

REXROAD, C. and FURNISH, W. M. 1964. Conodonts from the Pella Formation (Mississippian), south-central Iowa. *Journal of Paleontology*, **38** (4), 667–676.

RODLAND, D. L. and BOTTJER, D. J. 2001. Biotic recovery from the end-Permian mass extinction: behavior of the inarticulate brachiopod Lingula as a disaster taxon. *Palaios*, **16** (1), 95–101.

SCHNEEBELI-HERMANN, E. 2012. Extinguishing a Permian world. *Geology*, **40** (3), 287–288.

—— KÜRSCHNER, W. M., KERP, H., BOMFLEUR, B., HOCHULI, P. A., BUCHER, H., WARE, D. and ROOHI, G. 2015. Vegetation history across the Permian–Triassic boundary in Pakistan (Amb section, Salt Range). *Gondwana Research*, **27** (3), 911–924. doi:10.1016/j.gr.2013.11.007

SCHÖNLAUB, H. P. 1991. The Permian–Triassic of the Gartnerkofel-1 core (Carnic Alps, Austria): conodont biostratigraphy. *Abhandlungen der Geologischen Bundesanstalt Wien*, **45**, 79–98.

SCHUBERT, J. K. and BOTTJER, D. J. 1992. Early Triassic stromatolites as post-mass extinction disaster forms. *Geology*, **20** (10), 883–886.

—— —— 1995. Aftermath of the Permian–Triassic mass extinction event: paleoecology of Lower Triassic carbonates in the western USA. *Palaeogeography, Palaeoclimatology, Palaeoecology*, **116** (1), 1–39.

SHAPIRO, R. S. 2000. A comment on the systematic confusion of thrombolites. *Palaios*, **15** (2), 166–169.

SONG, H., TONG, J. and CHEN, Z. 2009*a*. Two episodes of foraminiferal extinction near the Permian–Triassic boundary at the Meishan section, South China. *Australian Journal of Earth Sciences*, **56** (6), 765–773.

—— —— —— YANG, H. and WANG, Y. 2009*b*. End-Permian mass extinction of foraminifers in the Nanpanjiang Basin, South China. *Journal of Paleontology*, **83**, 718–738.

—— WIGNALL, P. B., CHEN, Z. Q., TONG, J., BOND, D. P., LAI, X., ZHAO, X., JIANG, H., YAN, C., NIU, Z., CHEN, Z. and WANG, Y. 2011. Recovery tempo and pattern of marine ecosystems after the end-Permian mass extinction. *Geology*, **39** (8), 739–742.

STAESCHE, U. 1964. Conodonten aus dem Skyth von Südtirol. *Neues Jahrbuch für Geologie und Paläontologie, Abhandlungen*, **119** (3), 247–306.

SWEET, W. C. 1970*a*. Permian and Triassic conodonts from a section at Guryul Ravine, Vihi district, Kashmir. *University of Kansas Paleontological Contributions, Paper*, **49**, 1–10.

—— 1970*b*. Uppermost Permian and Lower Triassic conodonts of the Salt Range and Trans-Indus Ranges, West Pakistan. 207–275. *In* KUMMEL, B. and TEICHERT, C. (eds). *Stratigraphic boundary problems: Permian and Triassic of West Pakistan*, Special Publication **4**, University of Kansas.

TATGE, U. 1956. Conodonten aus dem germanischen Muschelkalk. *Paläontologische Zeitschrift*, **30** (3/4), 129–147.

TIAN, S. 1993. Evolution of conodont genera *Neogondolella*, *Hindeodus* and *Isarcicella* in northwestern Hunan, China. *Stratigraphy and Palaeontology of China*, **2**, 173–191.

WANG, C. 1994*a*. A conodont-based high-resolution eventostratigraphy and biostratigraphy for the Permian–Triassic boundaries in South China. *Palaeoworld*, **4**, 234–248.

—— 1994*b*. Conodonts of Permian–Triassic boundary beds and biostratigraphic boundary. *Acta Palaeontologica Sinica*, **34** (2), 129–151.

—— and WANG, S. 1997. Conodonts from Permian–Triassic boundary beds in Jiangxi, China and evolutionary lineage of *Hindeodus–Isarcicella*. *Acta Palaeontologica Sinica*, **36**, 151–178.

WANG, Y., TONG, J., WANG, J. and ZHOU, X. 2005. Calcimicrobialite after end-Permian mass extinction in South China and its palaeoenvironmental significance. *Chinese Science Bulletin*, **50** (7), 665–671.

WANG, Z. and CAO, Y. 1993. *In* WANG, C. 1993. *Conodonts of the Lower Yangtze Valley-an index to biostratigraphy and organic metamorphic maturity*. Science Press, Beijing, 326 pp. [in Chinese with English summary]

YAN, C., WANG, L., JIANG, H., WIGNALL, P., SUN, Y., CHEN, Y. and LAI, X. 2013. Uppermost Permian to Lower Triassic conodonts at Bianyang section, Guihzou province, South China. *Palaios*, **28**, 509–522.

YIN, H., SWEET, W. C., GLENISTER, B. F., KOTLYAR, G., KOZUR, H., NEWELL, N. D., SHENG, J., YANG, Z. and ZAKHAROV, Y. D. 1996. Recommendation of the Meishan section as Global Stratotype Section and Point for basal boundary of Triassic System. *Newsletters on Stratigraphy*, **34** (2), 81–108.

YOUNGQUIST, W. and MILLER, A. 1949. Conodonts from the Late Mississippian Pella Beds of South-Central Iowa. *Journal of Paleontology*, **23** (6), 617–622.

ZHANG, K., LAI, X., DING, M. and LIU, J. 1995. Conodont sequence and its global correlation of Permian–Triassic boundary in Meishan section, Changxing, Zhejiang Province. *Earth Science, Journal of China University of Geosciences*, **20** (6), 669–676. [in Chinese]

ZHANG, Y., ZHANG, K., SHI, G., HE, W., YUAN, D., YUE, M. and YANG, T. 2014. Restudy of conodont biostratigraphy of the Permian–Triassic boundary section in Zhongzhai, southwestern Guizhou Province, South China. *Journal of Asian Earth Sciences*, **80**, 75–83.

ZHAO, L., CHEN, Y., CHEN, Z. Q. and CAO, L. 2013. Uppermost Permian to Lower Triassic conodont zonation from Three Gorges area, South China. *Palaios*, **28** (8), 523–540.

Chapter II.A

Quantitative biochronology of the Permian-Triassic boundary in South China based on conodont Unitary Associations

Morgane Brosse, Hugo Bucher and Nicolas Goudemand

Earth-Science Reviews 155, 153–171
http://dx.doi.org/10.1016/j.earscirev.2016.02.003

“Though this be madness, yet there is method in’t.”

William Shakespeare, Hamlet

Earth-Science Reviews 155 (2016) 153–171

Contents lists available at ScienceDirect

Earth-Science Reviews

journal homepage: www.elsevier.com/locate/earscirev

Quantitative biochronology of the Permian–Triassic boundary in South China based on conodont unitary associations

Morgane Brosse [a,*], Hugo Bucher [a], Nicolas Goudemand [a,b]

[a] Paläontologisches Institut und Museum der Universität Zürich, Karl Schmid-Strasse 4, CH-8006 Zürich, Switzerland
[b] Institut de Génomique Fonctionnelle de Lyon, CNRS UMR 5242, Université de Lyon, Université Claude Bernard Lyon 1, Ecole Normale Supérieure de Lyon, 46 Allée d'Italie, Lyon, 69364, France

ARTICLE INFO

Article history:
Received 12 November 2015
Received in revised form 12 February 2016
Accepted 16 February 2016
Available online 23 February 2016

Keywords:
Permian–Triassic boundary
Unitary associations
Mass extinction
Conodonts
South China

ABSTRACT

The biochronological characterization of the Permian–Triassic boundary (PTB) is here improved by means of conodont unitary associations zones (UAZs). The selected data set comprises the six best documented sections in South China, including the Meishan global stratotype section and point of the PTB. This new biochronological zonation has a much higher accuracy than previous schemes, which were based on continuous interval zones. We show how traditional interval zones around the PTB in South China suffer from diachronous boundaries that cross each other as the result of sampling effort (intensity and density) and of geographical or ecological exclusion of zonal index taxa, inclusive of the first occurrence of the base Triassic index species *Hindeodus parvus*. Our quantitative and robust approach produces a discrete sequence comprising six UAZs. In the closest agreement with the position of the PTB in Meishan, the PTB falls here in the interval of separation between UAZ_2 and UAZ_3. In Meishan, this interval of separation corresponds to the stratigraphic interval above bed 25 and below bed 27, which also includes the formational boundary between the Changhsing and the Yinkeng formations. We provide a new and independent support for this placement by showing that it correlates with the main turnover of conodont species within the analysed time interval. As previously documented, the main extinction interval ranged from bed 25 to bed 28 in Meishan, which are here assigned to UAZ_2 and to UAZ_4, respectively. Therefore, the main extinction episode is not of end-Permian age but straddles the PTB. Previous claims for two distinct extinction pulses bracketing the PTB in South China were based on traditional conodont interval zones and are not supported by the new UA zonation. The oldest Triassic UAZ_3 is identified by the characteristic species *Hindeodus pisai* and by any of the ten characteristic pairs of species *Neogondolella zhejiangensis* or *Neogondolella tulongensis* associated with *Hindeodus changxingensis*, *Hindeodus parvus*, *Neogondolella planata*, *Neogondolella taylorae* or *Isarcicella huckriedei*. Separate analyses of anchignathodontids and neogondolellids sub-data sets show that the base of the Triassic is unambiguously defined by the occurrences of the characteristic species *H. changxingensis*, *Isarcicella prisca*, and *I. huckriedei* in shallow-water settings, and of two characteristic species, *N. planata* and *N. taylorae*, in deep-water settings. Moreover, we document uncoupled diversity trends across the PTB for each of these two clades. A substantial diversification phase of anchignathodontids spans the interval from UAZ_3 to UAZ_5. It is followed by a drastic (50%) reduction of the number of species between UAZ_5 and UAZ_6. On the other hand, neogondolellids show a protracted extinction from UAZ_4 to UAZ_6. In South China, correlations are proposed for the microbialite-bearing sections and deeper-water PTB sections. The UA method also highlights which parts of the conodont record are still insufficiently documented for reliable correlations. Biochronological correlations with Meishan and its U–Pb radio-isotopic ages allow inferring a maximal duration of 61 ± 48 ka for the gap at the base of the Triassic microbial limestone at Dajiang, a time interval that also corresponds to the duration of the main extinction episode in Meishan.

Contents

* Corresponding author.
E-mail address: morgane.brosse@pim.uzh.ch (M. Brosse).

http://dx.doi.org/10.1016/j.earscirev.2016.02.003
0012-8252/

1. Introduction

The end-Permian mass extinction (about 251.9 Ma; see Burgess et al. (2014)) is considered as the mother of all mass extinctions. It is marked by the disappearance of more than 90% of all marine species (Raup, 1979) and by major changes in plant communities (Retallack, 1995; Hochuli et al., 2010). The construction of a high-accuracy and high-resolution biozonation is of paramount importance for defining a synchronous Permian–Triassic boundary (PTB) and for elucidating causes and effects acting during and immediately after the mass extinction. It provides the biochronological time frame for correlating sections across the globe and for reconstructing the global sequence of abiotic and biotic events during that crucial time interval.

Conodont elements are abundant and almost ubiquitous in Permian and Triassic marine sediments. Moreover, their high evolutionary rates make them an ideal dating tool for strata around the PTB, where other age-diagnostic fossils are more prone to selective preservation during diagenesis (e.g. ammonoids). The conodont biostratigraphy around the PTB has been the focus of numerous studies and has been nowhere more intensively studied than in South China, where several Permian–Triassic sections are nearly-continuous and complemented with ash layers. Yet, as exemplified by the synthetic work of Mei et al. (1998), who established a refined biostratigraphy and taxonomy of conodonts for the Meishan section, conodont biozones are usually defined as interval zones. Interval zones are continuous zones that are identified by the first occurrence (FO) of an index species.

The main weakness of interval zones is the time lag that can exist between the true evolutionary origination of a species (i.e. its first appearance datum or FAD) and its first local occurrence, which depends on local ecological conditions, sampling effort and selective preservation (Guex, 1991), thus generally leading to diachronous correlations. The best alternative to avoid these shortcomings is to use unitary association zones (UAZs). These association zones are discrete (discontinuous) zones defined by the occurrence of characteristic species or of characteristic pairs of species. They also provide a laterally constant sequence of zones without any crossings, whatever their resolution. Using interval zones, the identification of a given zone in a particular section depends not only on the occurrence of an index taxon but also on the absence of the taxon defining the next younger zone, which means that the local range of any particular conodont, for instance *Hindeodus parvus*, is not necessarily very informative and accurate in time. The fossil record is incomplete, discontinuous, and also reflects ecological partitioning. Hence, the absence of fossil evidence for a particular species is not the evidence of its absence, either locally or globally. As a consequence, if we find only *H. parvus* in our sample, the absence of, for instance *Isarcicella staeschei*, is no proof that our sample is not from a time interval where *I. staeschei* was indeed living in some other area. On the contrary, UAZs are unambiguously identified by the occurrence of a characteristic species (its entire range being within the UAZ) or pair of species (the overlap of their ranges is entirely included within the UAZ), making the correlations much more robust. It also implies that some fossiliferous stratigraphic intervals without characteristic taxa cannot be assigned to a single UAZ. This means that the age of these samples is bounded by the next overlying and underlying samples containing characteristic species. These so-called intervals of separation are intercalated between UAZs. As subsequent information may become available (e.g. by increasing the sampling effort), the separation intervals will either shrink or will reveal new, previously undetected UAZs. In many ways, a parallel can be drawn between the intervals of separation and the error bars inherent to any physical measurement (e.g. resolution of radio-isotopic ages). The relative superposition of UAZs is invariant with respect to the time axis and their lateral reproducibility can only be improved as additional data will accumulate. Most recent descriptions of the method can be found in Monnet et al. (2015) and Guex et al. (2015).

A previous quantitative biochronological analysis of the Permian–Triassic extinction was performed with CONOP (Shen et al., 2011). CONOP is a n-dimensional extension of the two-dimensional graphic correlation method, n being the number of processed sections. The graphic correlation method starts by composing the two "best" sections and then adds the remaining sections one by one to the last built composite. Because the sequence with which the profiles are composed is not commutable (i.e. every change in the order of composition of the sections yields a different final composite), CONOP has been designed to compose all sections at once, thus circumventing this bias. However, the main flaw of the graphic correlation method is not removed from CONOP. Both methods may generate unnatural associations of species that are not known from the raw data and which cannot be deduced from virtual coexistences (coexistences in time but not in space, see Section 2). Such unnatural associations are generated by the projection of species FOs and LOs onto the line of correlation, which artificially lengthens some species' ranges. These projections lead to wrong overlaps or associations, and hence to overestimated species counts. Last but not least, CONOP does not yield a single solution but a set of equally "optimal" solutions, whatever the quality of the raw data.

As opposed to CONOP, the UA method yields a unique solution provided that the processed raw data set is of good enough quality,

i.e. that the amount of unknown biostratigraphic relations between the species is not disproportionate with respect to the amount of known relations (associations and superpositions). If a data set is too poorly constrained (too many unknown relations), then the UA method will not yield a stable solution and the data set must be improved before attempting any new analysis. A thorough comparison between UA and CONOP methods was performed by Galster et al. (2010), to which the reader is referred for further details.

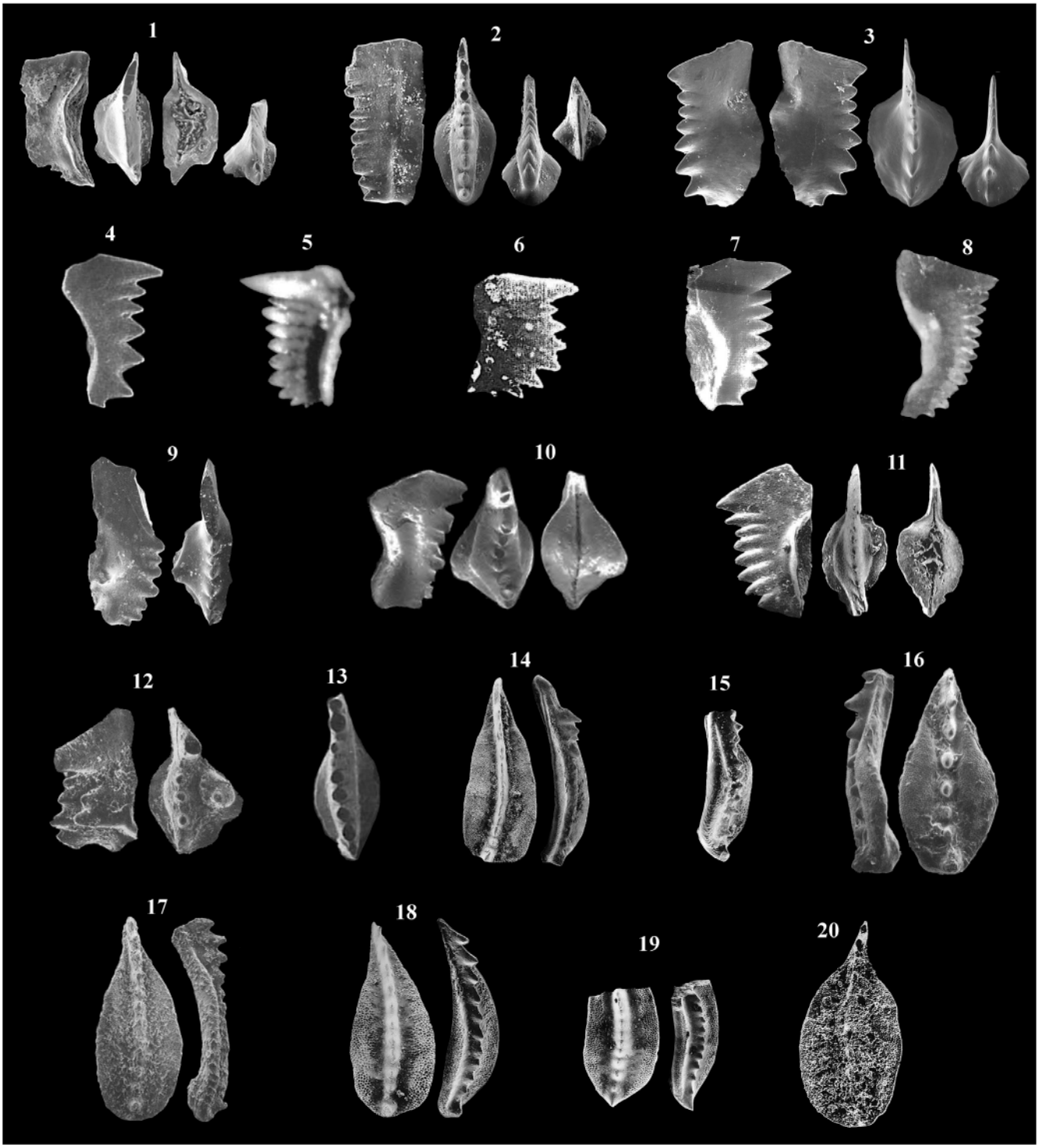

Fig. 1. Some of the key conodont species commonly found around PTB. 1- *Hindeodus changxingensis* Wang, 1994 (Fig. 2A; Metcalfe et al., 2007). Meishan, China. 2- *Hindeodus eurypyge* Nicoll et al., 2002. Meishan, China. 3- *Hindeodus inflatus* Nicoll et al., 2002. Meishan, China. 4- *Hindeodus latidentatus* Kozur et al., 1975. Iran. 5- *Hindeodus parvus* Kozur and Pjatakova, 1976. Bulla section, Dolomites. 6- *Hindeodus postparvus* Kozur, 1989. Achura, Azerbaijan. 7- *Hindeodus praeparvus* Kozur, 1996. Tesero, Southern Alps. 8- *Hindeodus typicalis* Sweet, 1970a (illustrated in pl.1, Fig. 20; Sweet, 1970b), Guryul Ravine, Kashmir. 9- *Isarcicella huckriedei* Jiang et al., 2011. Shangsi, China. 10- *Isarcicella lobata* Perri and Farabegoli, 2003. Tesero section, Southern Alps. 11- *Isarcicella prisca* Kozur, 1995 (illustrated in Perri, 1991). Bulla section, Southern Alps. 12- *Isarcicella staeschei* Dai and Zhang, 1989. China. 13- *Isarcicella turgida* Kozur et al., 1975. Iran. 14- *Neogondolella deflecta* Wang and Wang, 1981 (Fig. III(A); Mei et al., 1998). Meishan, China. 15- *Neogondolella meishanensis* Zhang et al., 1995 (reillustrated in Mei et al., 1998). Meishan, China. 16- *Neogondolella planata* Clark, 1959 (reillustrated in Orchard and Krystyn, 1998). Dinner Springs Canyon, Nevada. 17- *Neogondolella taylorae* Orchard, 1994 in Orchard et al, 1994. Selong, Tibet. 18- *Neogondolella yini* Mei, 1998. Meishan, China. 19- *Neogondolella zhangi* Mei, 1998. Meishan, China. 20- *Neogondolella zhejiangensis* Mei, 1996 (Fig. V(D); Mei et al., 1998). Meishan, China. All are holotypes but 1, 14, and 20.

Here, we exclusively consider conodonts with the aim of building a reliable conodont biozonation for the South Chinese record around the PTB. The newly proposed conodont UAZs are also the best possible time bins for counts of taxonomic richness of other co-occurring clades. Indeed, counts of taxonomic richness based on UAZ time bins were demonstrated to be largely immune to the unknown numerical duration of UAZs (Escarguel and Bucher, 2004).

2. Material and methods

2.1. Taxonomic data sets

Conodonts across the PTB in China have been intensively studied over the last decades and many sections produced conodonts. Fig. 1 displays some of the key conodont species commonly found around PTB. Yet, in order to insure the consistency of the taxonomy of the data set, we selected only those sections for which the conodont record has been adequately documented by means of range charts and illustrations of recovered taxa. This allowed us also to cross-check the reliability of the taxonomic usage and the validity of the reported local ranges of species. This first step leads to select the following sections (Fig. 2): Chaotian, Sichuan (Ji et al., 2007); Meishan, Zhejiang (Jiang et al., 2007; Nicoll et al., 2002); Dawen, Guizhou (Chen et al., 2009); Huangzhishan, Zhejiang (Chen et al., 2008); Shangsi, Sichuan (Jiang et al., 2011a); Yangou, Jiangxi (Sun et al., 2012); Bianyang, Guizhou (Yan et al., 2013); Daxiakou, Hubei (Zhao et al., 2013); Dajiang, Guizhou (Jiang et al., 2014); Zhongzhai, Guizhou (Metcalfe and Nicoll, 2007; Zhang et al., 2014); Wuzhuan, Guangxi (Brosse et al., 2015); Daijiagou, Sichuan (Yuan et al., 2015).

For the studied interval, these sections illustrate three broad categories of depositional environments. (1) Dawen, Dajiang, and Wuzhuan: latest Permian skeletal limestone unconformably overlain by microbial limestone. This type of succession is interpreted as shallow-water carbonate platform settings; (2) Meishan, Huangzhishan, Yangou, Bianyang, Daxiakou, and Dajiagou: from shelf to upper-slope settings, representing intermediate-water depths; (3) Shangsi and Chaotian: siliceous limestones and mudstones deposited in deep-water basinal to lower slope settings. Sections listed in (2) and (3) display conformable formational boundaries.

Among these 12 sections, five (Chaotian, Huangzhishan, Bianyang, Zhongzhai and Daijiagou) have less diverse conodont faunas and include mostly long-ranging taxa in the Changhsingian (latest Permian) and Griesbachian (earliest Induan). For this reason, we did not use them for the construction of the initial biozonation. However, they were added to the data set at a later stage. The Daxiakou section (Zhao et al., 2013) was excluded from the analysis, for its conodont documentation is both incomplete (*Hindeodus changxingensis*, *Hindeodus postparvus*, and *Neogondolella subcarinata* are not illustrated, the range of *Hindeodus praeparvus* is not documented) and uncertain (e.g. poor preservation of *Clarkina* (*Neogondolella*) *meishanensis*). The remaining six best-documented sections (Meishan, Dawen, Shangsi, Yangou, Dajiang, and Wuzhuan) illustrate both shallow-water facies with microbial limestone (Dawen, Dajiang and Wuzhuan) and deeper water facies (Yangou, Shangsi, and Meishan). 13 species are found to occur in only

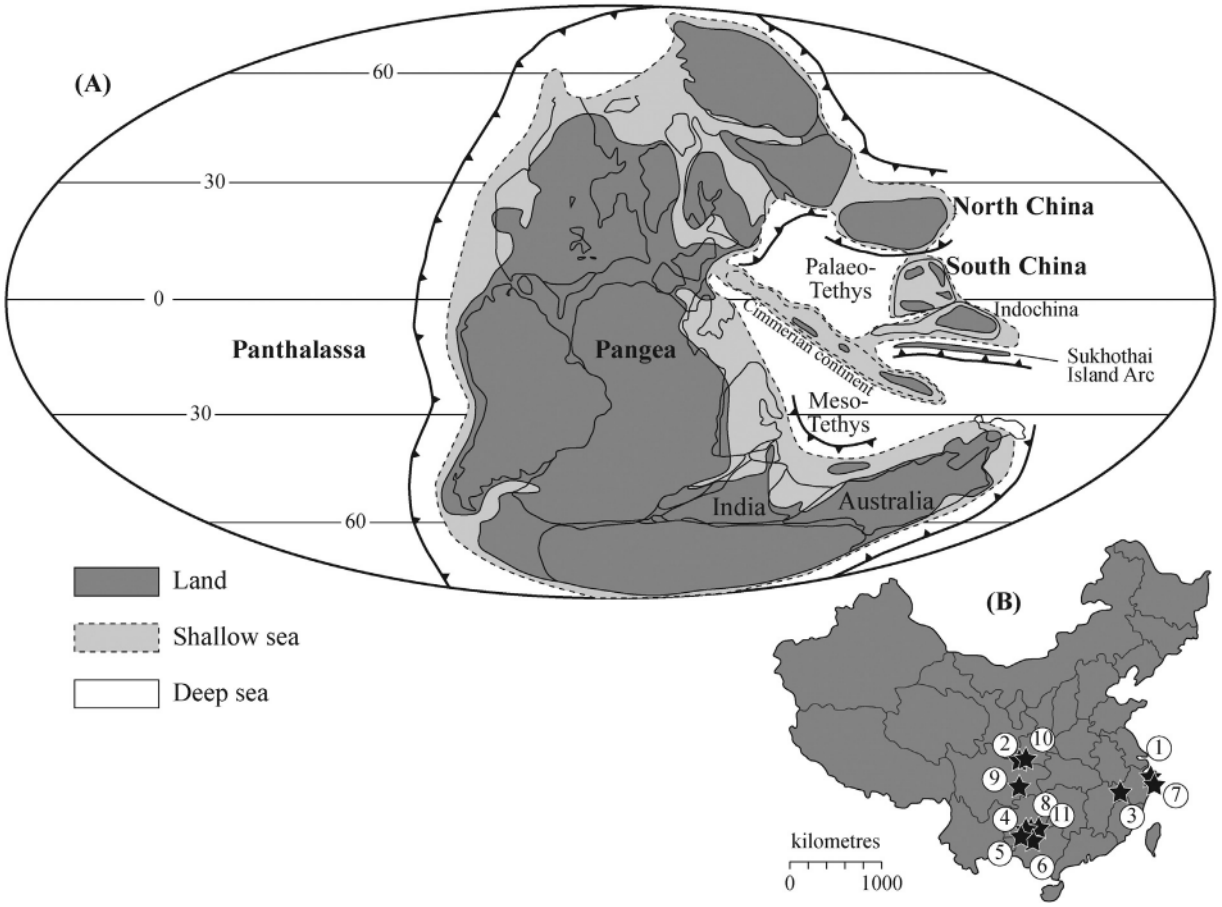

Fig. 2. Location of the studied sections. (A) Paleogeographical map of the Changshingian (modified after Metcalfe (2013)). (B) Geographical location of studied sections: 1—Meishan (Zhejiang); 2—Shangsi (Sichuan); 3—Yangou (Jiangxi); 4—Dawen (Guizhou); 5—Dajiang (Guizhou); 6—Wuzhuan (Guangxi); 7—Huangzhishan (Zhejiang); 8—Bianyang (Guizhou); 9—Dajiagou section (Sichuan); 10—Chaotian (Sichuan); 11—Zhongzhai (Guizhou).

Table 1
Taxonomical revisions used in the present study for standardizing the data set. Data leading to modifications of the local maximal horizons (see Section 2, Appendix A and B) are in bold. *H*: *Hindeodus*, *I*: *Isarcicella*, *N*: *Neogondolella*.

Selected section (paper)	Original determination	Bed number	Our determination
Chaotian (Ji et al. (2007))	***N. orchardi* (pl. 2, Fig. 22, 23)**	**D10**	***N.* sp. indet**
Zhongzhai (Metcalfe and Nicoll (2007))	***N. tulongensis* (pl. 1, Fig. 9)**	**bed 30**	***N.* sp. indet**
Zhongzhai (Zhang et al. (2014))	***H. parvus* (Fig. 5: 1, 2, 7)**	**bed 28**	***H.? praeparvus***
Meishan (Jiang et al. (2007))	*H. praeparvus* (pl. 4, Fig. 12)	24b	*H.? latidentatus*
Meishan (Jiang et al. (2007))	***H. pisai* (pl. 4, Fig. 25, 27)**	**27d**	**Dubious or broken**
Meishan (Jiang et al. (2007))	***I. staeschei* (pl. 5, Figs. 8, 9, 11–13)**	**27d**	***I. huckriedei* (see Jiang et al. 2011b)**
Meishan (Jiang et al. (2007))	***I. peculiaris* (pl. V, Figs. 29–31)**	**28**	***I. prisca***
Dawen (Chen et al. (2009))	*H. latidentatus* (pl. 9, Fig. 1; pl. 9, Fig. 2, 3)	12; 16	*H. praeparvus*
Huangzhishan (Chen et al.,(2008))	***H. latidentatus* (pl. 6, Fig. 9)**	**C18-3**	***H.* sp. indet**
Shangsi (Jiang et al. (2011a))	***H. anterodentatus* (pl. 1, Fig. 3, 5)**	**31a, 33**	***H. bicuspidatus***
Shangsi (Jiang et al. (2011a))	***H. inflatus* (pl. 1, Fig. 14, 15)**	**29d, 33**	***H.* sp. indet**
Shangsi (Jiang et al. (2011a))	*I. prisca* (pl. 2, Fig. 1, 2)	29d, 31a	*H.* sp. indet
Shangsi (Jiang et al. (2011a))	***I. lobata* (pl. 3, Fig. 1)**	**30b**	***I. huckriedei***
Yangou (Sun et al., 2012)	***H. anterodentatus* (Fig. 5Q)**	**LY-24 + 0**	***H. bicuspidatus***
Yangou (Sun et al., 2012)	***H. latidentatus* (Fig. 5T, U)**	**LY-23 + 0**	***H. praeparvus***
Yangou (Sun et al., 2012)	***H. inflatus* (Fig. 4A-D)**	**LY-19 + 35**	***H.* sp. indet**
Dajiang (Jiang et al. (2014))	***H. postparvus* (pl. 1, Fig. 3)**	**DJ 28-4**	***H.* sp. indet**
Dajiang (Jiang et al. (2014))	***H. eurypyge* (pl. 2, Fig. 1, 2)**	**DJ 13, DJ 27**	***H.? praeparvus***
Dajiang (Jiang et al. (2014))	*H. parvus* (pl. 2, Fig. 10, 14)	DJ 28-1, DJ 31	*H.? praeparvus*
Dajiang (Jiang et al. (2014))	*H. sosioensis* (pl. 3, Fig. 13)	DJ 35	*H. postparvus*
Dajiang (Jiang et al. (2014))	*I. prisca* (pl. 4, Fig. 5)	DJ 13	*H. typicalis*
Dajiagou (Yuan et al. (2015))	***H.* sp. (pl. 6, Fig. 25, 26, 28)**	**DJG 1.05-1.10**	***I. inflata***

one of the selected six sections and are thus of no use for correlations. Such species generally heavily contribute to the number of biostratigraphical contradictions (Boulard, 1993; Guex, 1991; Monnet and Bucher, 1999; Monnet et al., 2011; Guex, 1999). They are temporarily removed from the data set and re-integrated only after the biochronological analysis has been performed. The initial data set then includes 26 species distributed among three genera (*Hindeodus*, *Isarcicella*, and *Neogondolella*).

2.2. Standardization of the taxonomy

Table 1 details the revisions we made to insure the consistency of the taxonomic data. When the illustration-based revisions concern the youngest or oldest occurrence of a given species, we modified its range accordingly, thereby assuming that if a less uncertain specimen had been found in the corresponding bed, it would have been illustrated in order to attest the validity of that range. If all of the illustrated conodont elements of a particular species in a particular study suggested a different species definition than the one we used, we discarded the entire range of that species in that study (e.g. *Hindeodus inflatus* and *Hindeodus latidentatus* in the Yangou section; Sun et al., 2012). Undetermined (indet.), compared (cf.) and transitional (trans.) species have been excluded from the data set.

2.3. Unitary associations method

The UAs method (Guex, 1991) is a quantitative and deterministic method that produces biozonations based on discrete (i.e. discontinuous) maximal association zones. This method is described in detail by Guex (1991), Savary and Guex (1991), Guex (1999), Angiolini and Bucher (1999), Monnet and Bucher (2002); see Fig. 2), Monnet et al. (2011); see Figs. 3 and 5), Monnet et al. (2015), and Guex et al. (2015). A dedicated tool (UAGraph) is integrated within the palaeontological analysis freeware Past (Hammer, 2013).

The main advantage of the UA method is to provide a logical, robust, open and iterative tool for solving the biostratigraphical contradictions that are contained in a data set (see sub-Section 3.1 for examples). It also allows discarding under-constrained data sets, disentangling biostratigraphical contradictions and precisely identifying what occurrence in a given bed of a given section generates these contradictions, all being crucial assets unavailable in other methods in quantitative biochronology.

Species with a discontinuous range (ecological exclusion, preservation bias, insufficient sampling) in a single section are assumed to range through between their FO and their last occurrence (LO). In our data set, actual occurrences are indicated by a black '1', whereas virtual occurrences inferred from the range through assumption are indicated in grey (see Appendix A). One can demonstrate (Guex, 1991) that only samples where the set of (actually and virtually) occurring species is maximal (local maximal horizon, LMH) are relevant for constructing the sequence of biochronozones with the highest possible resolution. In other words, beds whose set of species is included in the set of another bed do not add information for the construction of the biozonation.

Four LMHs are found in Wuzhuan, four in Dawen, four in Dajiang, five in Shangsi, seven in Yangou, and five in Meishan (see Table 2). There are two types of biostratigraphical relation: co-occurrence and superposition. The co-occurrence of two species corresponds to the overlap of the ranges of these two species in at least one sample or is logically inferred from virtual occurrences. For instance, if species A is below species B in Section 1 but above B in Section 2, their ranges must overlap in time but not in space. Virtual co-occurrences initially documented in the data are integrally preserved in the final UA zones. All observed biostratigraphical relations of the 26 species of the data set are shown in the biostratigraphical graph G* (Fig. 3B, C). Each vertex of G* represents a species (see codes in Fig. 3A). The edges in the non-oriented part of G* represent co-occurrences and the arcs in the oriented part of G* represent superpositions. The absence of arc or of edges between two species indicates unknown stratigraphical relations.

The analysis of G* allows extracting the complete list of biostratigraphical contradictions. Solving these contradictions allows G* to become an interval graph, i.e. an intersection graph of a family of intervals on the time line (see Guex et al., 2015). The UA method solves such contradictions by identifying which arcs are the most frequently involved in contradictions and by replacing these arcs by virtual co-occurrences that were not observed but that can logically be inferred. Fig. 4A–C shows a general example of the resolution of a subgraph Z_4" (a four-edged circuit with two arcs). The edges between the four species 1 to 4 indicate that their existence domains in time and space overlap in pairs and form a ring. The two arcs 4 > 2 and 3 > 1 correspond to two alternative, contradictory scenarios about the direction of the time axis:

A. Identification of the species in the initial matrix

1	*H. bicuspidatus*	8	*H. praeparvus*	15	*I. staeschei*	22	*N. taylorae*
2	*H. changxingensis*	9	*H. typicalis*	16	*I. turgida*	23	*N. tulongensis*
3	*H. eurypyge*	10	*I. huckriedei*	17	*N. changxingensis*	24	*N. yini*
4	*H. inflatus*	11	*I. inflata*	18	*N. deflecta*	25	*N. zhangi*
5	*H. latidentatus*	12	*I. isarcica*	19	*N. meishanensis*	26	*N. zhejiangensis*
6	*H. parvus*	13	*I. lobata*	20	*N. planata*		
7	*H. postparvus*	14	*I. prisca*	21	*N. subcarinata*		

B. Non-oriented part of the biostratigraphical graph G*: associations of species

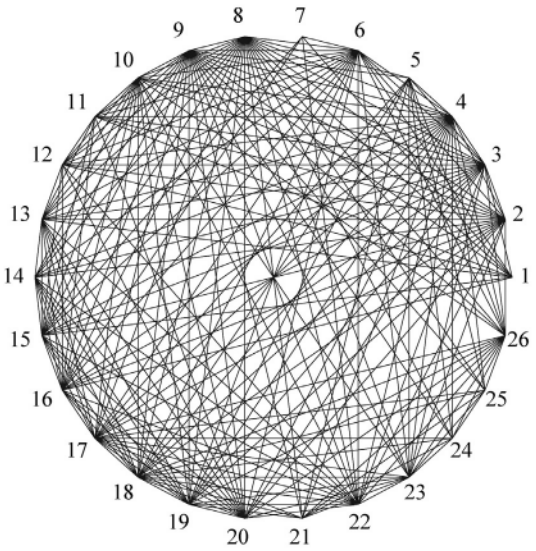

C. Oriented part of the biostratigraphical graph G*: superpositions of species

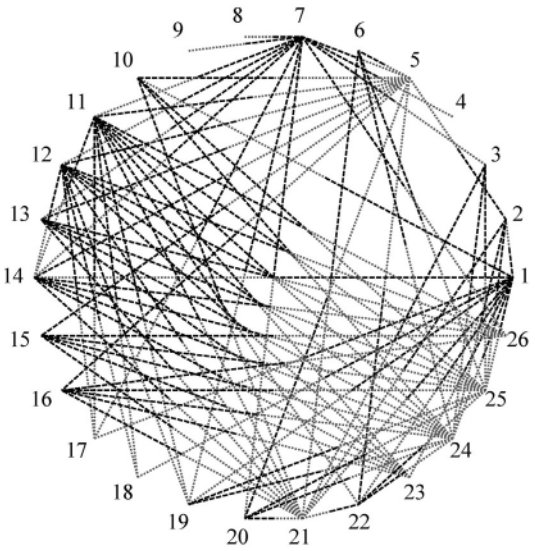

D. Six forbidden subgraphs extracted from G*

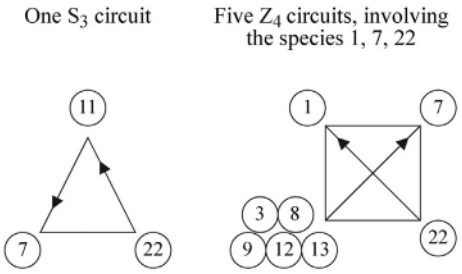

E. Implication of species in the forbidden subgraphs

species involved		Number of Z_4	Number of S_3
1	*H. bicuspidatus*	5	
3	*H. eurypyge*	1	
7	*H. postparvus*	5	1
8	*H. praeparvus*	1	
9	*H. typicalis*	1	
11	*I. inflata*		1
12	*I. isarcica*	1	
13	*I. lobata*	1	
14	*I. prisca*	1	
22	*N. taylorae*	5	1

Fig. 3. Biostratigraphical graph G* and extracted forbidden subgraphs generated during Run 1. In (C), Long dark dashes at the top and short grey dots at the base of an arc. *H*: *Hindeodus*, *I*: *Isarcicella*, *N*: *Neogondolella*.

either the arc 4 > 2 is true (4 older than 2, time T_2) and then the arc 3 > 1 is false and species 1 and 3 must co-occur in time even if not in space (virtual co-occurrence, potential ecological exclusion), or the arc 3 > 1 is true (time T_1) and species 2 and 4 must co-occur in time (Fig. 4D, E).

After addition of these virtual coexistences in the data set, the analysis is run again and we check that the number of contradictions is lower than in the previous run. The same procedure is iterated until the smallest possible number of contradictions is reached. Would the data set be inadequate, i.e. insufficiently constrained in terms of associations and superpositions, the number of contradictions would not decrease but increase. This distinction between adequate and inadequate data sets is an asset unique to the UA method. As opposed to this, all data sets will yield a set of "optimal" solutions when processed with CONOP. CONOP does not assess the quality of the primary data, nor does it extract biostratigraphic contradictions exhaustively and specifically. It only smooths out such contradictions by blindly expanding the ranges of species that do not plot on the line of correlation, thereby generating spurious associations.

3. Conodont zonation

3.1. Run 1

8 UAs; 2 contradictions; 5 Z_4 circuits; 1 S_3 circuit, 0 cycles between cliques.

Run 1 corresponds to the first iteration of the analysis on the initial data set (see Appendix B). The absence of cycles (species A below species B, species B below species C, species C below species A) is an indication of the good quality of the data. The five Z_4 and one S_3 circuits are shown in Fig. 3D. They originate from contradictory relations between

species that generate forbidden subgraphs within G* as shown in Fig. 3B–C. All five Z_4 circuits display the same configuration that involves the same three species: *H. postparvus*, *Hindeodus bicuspidatus*, and *Neogondolella taylorae* (see Fig. 3D). As explained in Fig. 4, one of the two arcs must result from insufficient sampling effort and/or ecological partitioning and should be replaced by a virtual edge. We also note that the two species *H. postparvus* and *N. taylorae* are involved in the S_3 circuit, suggesting that one of these two species or both generate the sum of all these contradictions. *H. postparvus* is documented above species 3, 8, 9, 11, 12, and 13 (Fig. 3D), which are all representatives of *Hindeodus* and *Isarcicella*. On the other hand, *N. taylorae* is a long-ranging species found during the entire Griesbachian in South China (as in the sections included in the present analysis), Kashmir (Matsuda, 1984), Tibet (Orchard et al., 1994), Arctic Canada (Henderson and Baud, 1997), and Spiti (Orchard and Krystyn, 1998). Its record may be strongly influenced by distinct environmental preferences, as this genus is suggested to have dwelled in deeper-water settings during the Early Triassic (Joachimski et al., 2012). In the above contradictions, the arcs involving *N. taylorae* are connected with the shallow-water anchignathodontids (*H. bicuspidatus* and *Isarcicella inflata*), with which it is indeed less likely to co-occur for ecological reasons. Hence, it appears most parsimonious to infer that the discontinuous range of *N. taylorae* is the most likely source of the contradictions. In particular the arc from *N. taylorae* to *H. bicuspidatus* should be replaced by a virtual edge, by extending the range of *N. taylorae* up to that of *H. bicuspidatus*. The upward extension of the range of *N. taylorae* results in five new virtual occurrences in LMH_3 and LMH_4 at Wuzhuan, in LMH_5 and LMH_6 at Yangou, and in LMH_5 at Shangsi (see Appendix B). As a consequence, LMH_1 at Wuzhuan is no longer a maximal horizon.

Table 2
Correspondence between bed numbers, local maximal horizons (LMHs), unitary association zones (UAZs) and interval zones as described in the original papers. The interval of uncertainty of UAZs can sometimes be narrowed thanks to preceding or succeeding beds. In such a case, the new estimation is shown in brackets (e.g. Dajiang DJ-13: the conodont assemblage does not allow to determine whether it belongs to UAZ_4 or UAZ_5, but as the succeeding bed DJ-13B belongs to UAZ_4, DJ-13 cannot extend to UAZ_5).

Sections	Conodont bearing bed number	LMHs	UAZs	Neogondolellid interval zones	Anchignathodontid interval zones
Wuzhuan	O	4	6	?	?
	N		5		
	M		5		
	L	3	5		
	K		5		
	J		4-5		
	I		4-5		
	H		4-5		
	G	2	4-5		
	F		3-5		
	E		3-5		
	D	1	3-5		
	C		1-5		
	B		1-5		
	A		1-5		
Dajiang	DJ-35	4	6	?	*H. sosioensis* Z.
	DJ-34		4-6		
	DJ-33		4-6		
	DJ+20m		4-6		
	DJ-32		4-6		
	DJ-31		4-6		
	DJ-30		4-5		
	DJ-29		4-5		
	DJ-28-4	3	4-5		*I. isarcica* Z.
	DJ-28-3	2	4-5		
	DJ-28-2		4-5		
	DJ-28-1		4-5		*I. lobata* Z.
	DJ-28		4-5		
	D+15m		4-5		*H. parvus* Z.
	DJ-27B		4-5		
	DJ-27		4-5		
	DJ-26		4-5		
	DJ-18		4-5		
	DJ-13B	1	4		
	DJ-13		4		
Shangsi	33		5	?	*I. isarcica* Z.
	32	5	5		
	31B		5		
	31A		4-5		*I. lobata* Z.
	30D		4-6 (4-5)		
	30C		4-7 (4-5)		
	30b		4-8 (4-5)		
	30a		4-8 (4-5)		*H. parvus* Z.
	29D	4	4	*N. taylorae* Z.	
	29C		4		
	29B		4-5 (4)		*H. changxingensis* Z.
	29A		4-5 (4)		
	28D	3	4		
	28C		4-5 (4)		
	28B		4-5 (4)		
	28A		4-5 (4)	*N. meishanensis* Z.	
	27	2	2-4		?
	26	1	1	*N. yini* Z.	?
Dawen	DPT-26	4	6	*N. lehrmanni* Z.	*I. staeschei* Z.
	DPT-25	3	3-6	?	*H. parvus* Z.
	DPT-24		3-6		
	DPT-23		3-6		
	DPT-22		3-6		
	DPT-19		1-5 (2-5)	*N. zhejiangensis* Z.	*H. eurypyge* Z.
	DPT-18		2-5		
	DPT-16	2	2		
	DPT-13	1	2		
	DPT-12		2		
Meishan	29	5	5	?	*I. isarcica* Z.
	28	4	4	*N. taylorae* Z.	*I. staeschei* Z.
	27d	3	3		*H. parvus* Z.
	27c		3		*H. changxingensis* Z.
	27b		3		
	27a		3		
	26		2-3	*N. meishanensis* Z.	*H. praeparvus* Z.
	25	2	2		
	24e	1	1	*N. yini* Z.	
	24d		1		
	24c		1		
	24b		1		
	24a		1		*H. latidentatus* Z.

Table 2 (*continued*)

Yangou	LY-37		5	?	*I. isarcica* Z.
	LY-36	7	5		*I. staeschei* Z.
	LY-35+50	6	5		
	LY-35+37		5		
	LY-35+25		5		
	LY-35+15		5		*H. parvus* Z.
	LY-34+55		5		
	LY-34+45		5		
	LY-34+33		5		
	LY-34+20		5		
	LY-34+10		5		
	LY-33+20		5		
	LY-33+0		5		
	LY-25+0		5		
	LY-24+0		5		
	LY-23+0		3-5 (4-5)		
	LY-22+0		3-5 (4-5)		
	LY-21-5		3-5 (4-5)		
	LY-21-4	5	4-5		
	LY-21-3	4	3-5	*N. taylorae* Z.	?
	LY-21-2		3-5	?	*H. changxingensis* Z.
	LY-21-1	3	3-4		
	LY-20-0		1-4		
	LY-20+30	2	1-2	*N. yini* Z.	?
	LY-20+15		1-4 (1-2)		
	LY-20+0		1-4 (1-2)		
	LY-19+65		1-4 (1-2)		
	LY-19+50		1		
	LY-19+35		1		
	LY-19+10		1		
	LY-18+87		1	*N. changxingensis* Z.	
	LY-18+45	1	1		

3.2. Run 2

8 UAs; 0 contradictions; 0 Z_4 circuits; 0 S_3 circuits; 0 cycles between cliques.

No contradictions are detected in the second run. As in the first run, 8 UAs are recognized, which shows that the modification of the range of *N. taylorae* solved all the contradictions at no cost for the resolution of our biozonation. The sequence of UAs and their composition are detailed in Fig. 5.

3.3. Lateral reproducibility

Only UAs that are laterally reproducible are useful for correlations. The reproducibility matrix (Fig. 6A) indicates in which sections each UA is identified. We observe that the lateral reproducibility is low for the UA_2, UA_3, UA_4 and UA_6, since they are identified in only one section each. By merging some UAs, we obtain UAs with higher lateral reproducibility. Which UAs are merged is guided by the dissimilarity index and the number of arcs between the UAs (Fig. 6B). The dissimilarity index is a measure of dissimilarity between two UAs that ranges

from 0 (equal) to 2 (completely different) (for details, see Hammer (2013)). From the UAs that have the lowest lateral reproducibility, UA_2 and UA_3 are very similar ($D_3 = 0.2000$), which is confirmed by the small number of arcs between them (1). The same is applied to for UA_6 and UA_7 ($D_7 = 0.3766$, 2 arcs). Therefore, we decided to merge UA_2 with UA_3 and UA_6 with UA_7. The sequence of eight preliminary UAs is thus compacted into a sequence of six unitary association zones (UAZs) of higher lateral reproducibility (Fig. 6C). Within a last step, the 13 endemic species that could not be used for the biostratigraphical analysis are re-injected into their respective UAZs (Fig. 7).

4. Results

The optimal result reached after two runs produces a biozonation with six UAZs for the studied interval. The lateral reproducibility of the resulting UAZs (Fig. 8) is generally higher after the merging. For instance, UAZ_1, UAZ_4, UAZ_5 and UAZ_6 have now a higher lateral reproducibility (3 and 4). On the other hand, UAZ_3 still has a very low lateral reproducibility (1), which we could solve by merging it with UAZ_2 or preferentially with UAZ_4 (dissimilarity index D_{Z4} between UAZ_3 and UAZ_4 is slightly lower). UAZ_3 is identified in Meishan only. This is due to the fact that Meishan has been intensively sampled and yields a fauna composed of both *Anchignathodontidae* and *Neogondolellidae*, an ecological association that is rare in other sections (see Section 5, sub-section 5.2). However, as UAZ_3 is identified by pairs of characteristic species traditionally assigned to the Griesbachian and as it partly overlaps with the *H. parvus* interval zone, we decided not to merge it with UAZ_2, nor with UAZ_4. The emended definition of the PTB and the age of *H. parvus* are developed in sub-section 5.5.

UAZs are formally defined by the full range of their characteristic species and the full intersection of the ranges of their characteristic pairs of species. However, note that if the lowermost (or uppermost) sample of a given section falls within a UAZ and not within a separation interval, the base (or the top) of this UAZ remains unknown in this specific section.

- *UAZ_1*
  Content: *Neogondolella yini*, *Neogondolella zhangi*, *N. subcarinata*, *H. latidentatus*, *Neogondolella zhejiangensis*, *Neogondolella tulongensis*, *Neogondolella changxingensis*, *Neogondolella deflecta*, *H. inflatus*, *H. praeparvus*, *Hindeodus typicalis*, *Neogondolella postwangi*, *Neogondolella parasubcarinata*, *Neogondolella carinata*.
  Characteristic species: *N. yini*, *N. zhangi*, *N. postwangi*.
  Age: Changhsingian
  Partial overlap with interval zones: *N. yini* Zone (Yangou, Meishan, Shangsi), *N. changxingensis* Zone (Yangou), and *H. latidentatus* Zone (Meishan).
  Distribution: Meishan, Shangsi, Yangou.
- *UAZ_2*
  Content: *N. subcarinata*, *H. latidentatus*, *N. zhejiangensis*, *N. tulongensis*, *N. changxingensis*, *N. deflecta*, *H. inflatus*, *H. praeparvus*, *H. typicalis*, *Neogondolella meishanensis*, *Hindeodus eurypyge*, *N. carinata*, *Merrillina ultima*.
  Characteristic species: *M. ultima*. Characteristic pairs of species: *N. subcarinata* or *H. latidentatus* with *N. meishanensis* or *H. eurypyge*.
  Age: Changhsingian
  Partial overlap with interval zones: *N. meishanensis* Zone (Meishan), *N. zhejiangensis* Zone (Dawen), *H. praeparvus* Zone (Meishan).
  Distribution: Meishan, Dawen.
- *UAZ_3*

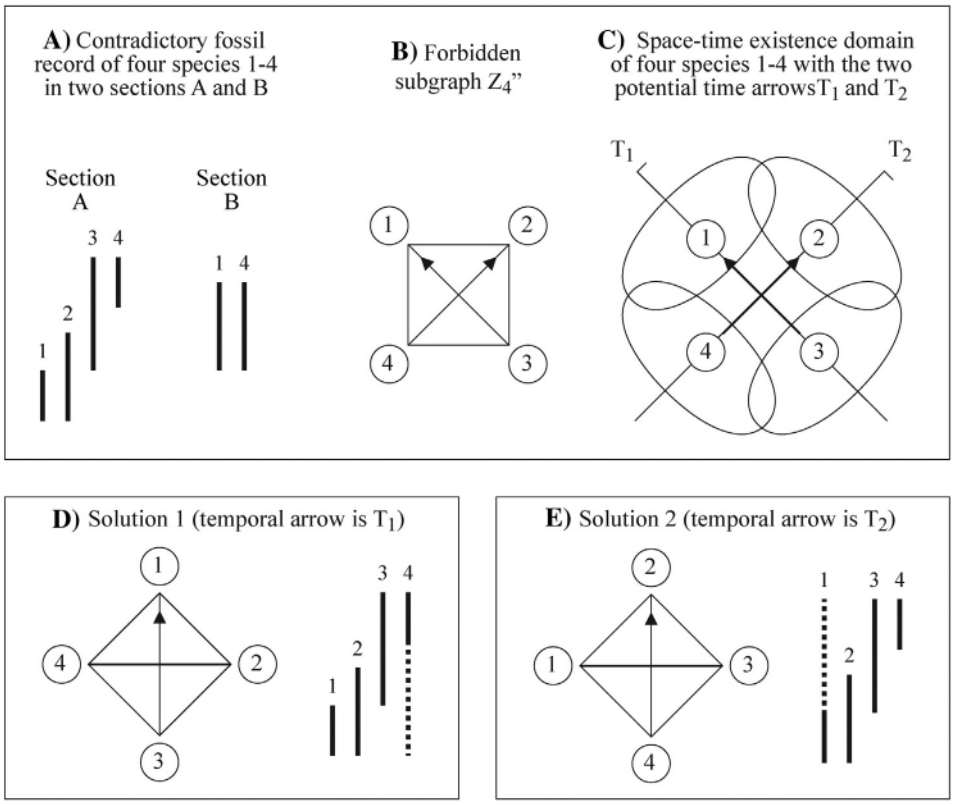

Fig. 4. (A) Example of a contradictory biostratigraphical relation. (B) Generated forbidden subgraph Z_4". (C) Ellipsoids representing the space–time existence domains of the four species 1–4. (D) and (E) The two potential solutions for resolving the contradictions of the Z_4" circuit. (D) Species 2 and 4 are contemporaneous but occupying different areas (ecological exclusion), therefore the arc between 2 and 4 should be transformed into a virtual edge. (E) Species 1 and 3 are contemporaneous. The dotted lines represent the inferred extensions of the range that solve the contradiction.

Content: *N. zhejiangensis*, *N. tulongensis*, *N. changxingensis*, *N. deflecta*, *H. inflatus*, *H. praeparvus*, *H. typicalis*, *N. meishanensis*, *H. eurypyge*, *H. changxingensis*, *Neogondolella planata*, *Isarcicella huckriedei*, *H. parvus*, *N. taylorae*, *N. carinata*, *Hindeodus pisai*.
Characteristic species: *H. pisai*. Characteristic pairs of species: *N. zhejiangensis* or *N. tulongensis* with *I. huckriedei*, *N. planata*, *H. parvus*, *N. taylorae* or *H. changxingensis*.
Age: Griesbachian
Partial overlap with interval zones: *H. parvus* zone (Meishan, Yangou), *N. taylorae* Zone (Meishan).
Distribution: Meishan.

— *UAZ*$_4$
Content: *N. changxingensis*, *N. deflecta*, *H. inflatus*, *H. praeparvus*, *H. typicalis*, *N. meishanensis*, *H. eurypyge*, *N. planata*, *I. huckriedei*, *H. parvus*, *N. taylorae*, *Isarcicella prisca*, *Isarcicella turgida*, *Isarcicella lobata*, *I. staeschei*, *N. carinata*, *Hindeodus anterodentatus*.
Characteristic species: *I. prisca*. Characteristic pairs of species: *N. changxingensis*, *N. deflecta*, *N. meishanensis* or *H. changxingensis* with, *I. turgida*, *I. lobata*, *I. staeschei* or *H. anterodentatus*.
Age: Griesbachian
Partial overlap with interval zones: *I. staeschei* Zone (Meishan and Yangou), *I. lobata* Zone (Dajiang and Shangsi).
Distribution: Meishan, Shangsi, Dajiang.

— *UAZ*$_5$
Content: *H. inflatus*, *H. praeparvus*, *H. typicalis*, *H. eurypyge*, *H. changxingensis*, *N. planata*, *I. huckriedei*, *H. parvus*, *N. taylorae*, *I. turgida*, *I. lobata*, *I. staeschei*, *Isarcicella isarcica*, *Isarcicella inflata*, *H. bicuspidatus*, *N. carinata*, *H. anterodentatus*, *Hindeodus altus*, *Isarcicella peculiaris*, *Hindeodus sosioensis*.
Characteristic species: *I. isarcica*, *I. inflata*, *I. peculiaris*, *H. altus*. Characteristic pairs of species: *H. inflatus*, *H. praeparvus*, *H. typicalis*, *H. eurypyge*, *H. changxingensis*, *N. planata*, *I. huckriedei*, or *I. lobata* with *H. bicuspidatus* or *H. sosioensis*.
Age: Griesbachian

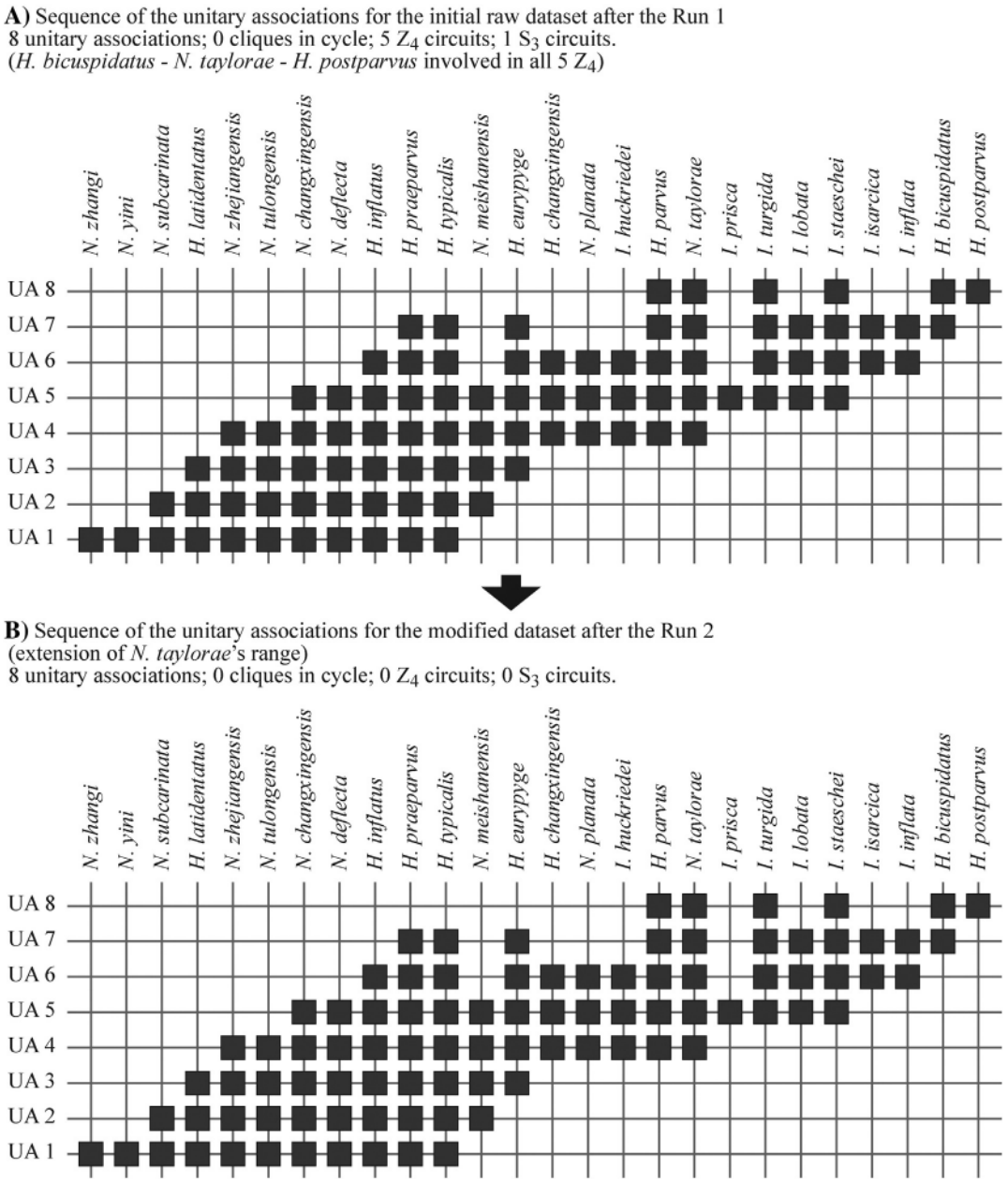

Fig. 5. Sequence of unitary associations (UAs) resulting from the biochronological analyses. Runs 1 and 2 result in the same sequence of UAs. *H*: *Hindeodus*, *I*: *Isarcicella*, *N*: *Neogondolella*.

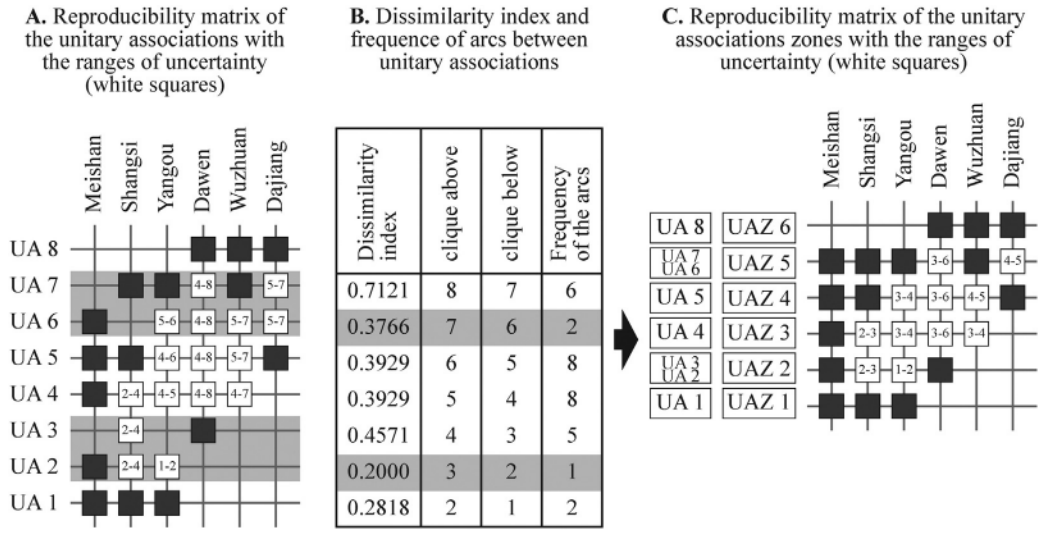

Fig. 6. From unitary associations (UAs) to unitary associations zones (UAZs). Note the poor reproducibility of the UA_2, UA_3, UA_4, and UA_6. The grey shades indicate the UAs that are merged into UAZs. *H*: *Hindeodus*, *I*: *Isarcicella*, *N*: *Neogondolella*.

Partial overlap with interval zones: *I. isarcica* zones (Shangsi, Meishan and Yangou).
Distribution: Meishan, Shangsi, Yangou and Wuzhuan.

— *UAZ_6*
Content: *H. parvus*, *N. taylorae*, *I. turgida*, *I. staeschei*, *H. bicuspidatus*, *H. postparvus*, *H. sosioensis*, *Neogondolella kazi*, *Neogondolella lehrmanni*.

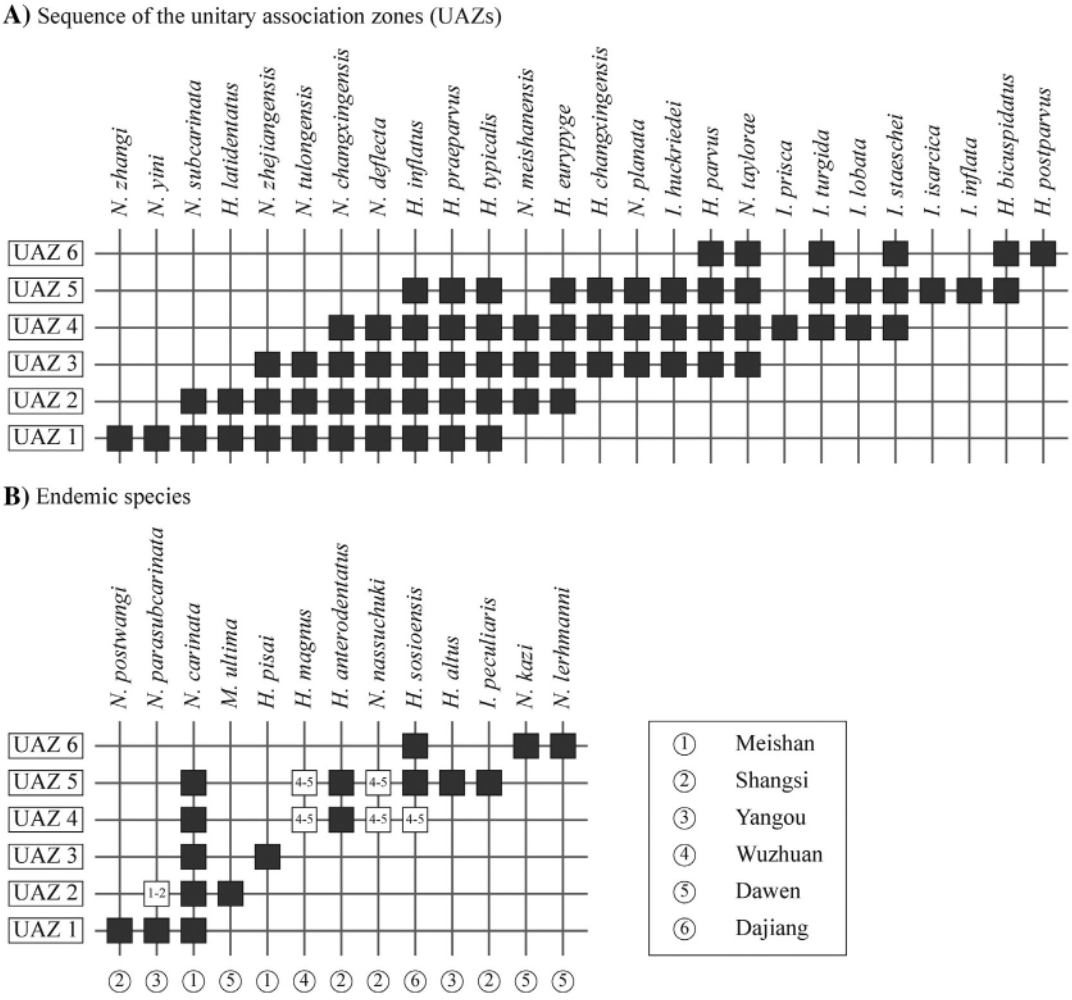

Fig. 7. (A) Sequence of the resulting 6 UAZs. (B) Zonal distribution of the endemic species. The circled numbers refer to the section where the endemic species was found. *H*: *Hindeodus*, *I*: *Isarcicella*, *N*: *Neogondolella*, *M*: *Merrillina*.

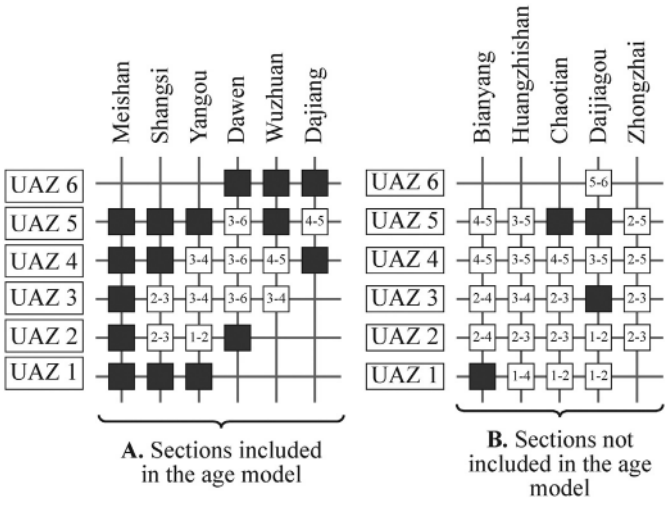

Fig. 8. Reproducibility matrix generated from the final solution given in Fig. 6, including the five sections removed before the analysis. Note that this matrix does not result from another run involving the remaining sections, but from the dating of the remaining sections by means of previous UAZs of Fig. 7. Dark squares represent clear identification of UAZs, white squares represent intervals of uncertainty.

Characteristic species: *H. postparvus*, *N. kazi*, *N. lehrmanni*.
Age: Griesbachian
Partial overlap with interval zones: *H. sosioensis* Zone (Dajiang).
Distribution: Dawen, Wuzhuan, Dajiang.

In the present data set, the FO of *H. parvus* and *N. taylorae* in Meishan fall *within* UAZ_3. Both taxa are traditionally considered as index fossils for the base of the Triassic. Here, we propose that the characteristic species or pairs of species of UAZ_3 are used for the identification of the oldest Triassic conodont biozone. Consequently, the biostratigraphical PTB is within the interval of separation between UAZ_2 and UAZ_3.

5. Discussion

5.1. Contradictory correlations generated by interval zones

Fig. 9 shows the correlations of the six selected sections by means of first occurrences of index species of interval zones. We observe contradictions in the sequence of FOs between the different sections. The most striking example among the long list of contradictions pertains to the FO of *H. parvus*, which has been chosen as the conventional definition for the base of the Triassic (Yin et al., 1988). The FO of *H. parvus* is younger than the FO of *H. praeparvus* in Dawen, Shangsi and Meishan, but older than the FO of *H. praeparvus* at Wuzhuan and Dajiang. We also observe that the FO of *H. parvus* is younger than the FO of *N. taylorae* at Shangsi and Meishan, but older than the FO of *N. taylorae* at Dajiang and Dawen.

One of the most salient cases of diachronous correlations of the PTB by means of the FO of *H. parvus* is found in Xie et al. (2010; see their figure 1). These authors considered the FO of *H. parvus* as a marker of the PTB, and thus located the PTB at the base of the microbial limestone in the Dajiang, Taiping, Zuodeng, and Heping sections, and at the top of the microbial limestone in the Huayinshan, Laolongdong, Cili, Chongyang and Xiushui sections. The Cili section has been re-sampled subsequently (Wang et al., 2016) and *H. parvus* was newly found at the base of the microbial limestone, where the PTB was consequently shifted downwards. This also demonstrates how the location of FOs heavily depends on the sampling effort and does not carry per se robust biochronological significance.

Another interesting case is found in Song et al. (2013a), who reported two pulses of extinction bracketing the PTB. Following the method of Wang and Everson (2007), these authors computed the confidence intervals of taxa from PTB sections in South China before correlating the modified ranges by means of traditional conodont interval zones. Among the seven sections studied by Song et al. (2013a) the Meishan, Shangsi, Yangou and Dajiang sections are also included in our new biozonation, and the lack of superpositional reproducibility of interval zones in these sections is highlighted in Fig. 9. The data set of Song et al. (2013a) also includes the Zhongzhai section, whose conodont assemblages must be taken with the greatest caution in biostratigraphical analyses as discussed in 5.4 (the occurrence of a mixed fauna in the bed LZ28 produces many contradictions).

The correspondences between bed numbers, LMHs, UAZs, and interval zones described in the literature are listed in Table 2. Contrary to interval zones, UAZs have a constant superpositional order allowing reliable correlations. Moreover, all fossil records suffer from uneven sampling effort and geographical or ecological exclusions of species that may lead to artificially stretched or contracted interval zones. For instance, the *I. staeschei* interval zone at Dawen (Chen et al., 2009) appears to be extended because of the absence of *I. isarcica*. UAZs are less affected by such incompleteness of the record because their identification relies on observed occurrences of characteristic taxa or pairs of taxa.

Fig. 10 illustrates the correlation of UAZs across the six studied sections. With the exception of Meishan, which is a highly condensed section, all other sections display thick intervals of separation between samples or beds assigned to UAZs.

5.2. Influence of environment

Joachimski et al. (2012) proposed that *Hindeodus* and *Neogondolella* were thriving in comparable water depths (hence recording similar seawater temperatures) until the latest Changhsingian, and that *Neogondolella* migrated into deeper (and cooler) marine environments during the Griesbachian. The Triassic part of this hypothesis is supported by the predominant occurrence of anchignathodontids in shallower sections such as Dawen, Wuzhuan and Dajiang (see detailed conodont record in Appendix A). The distinct environmental preferences of the two families likely explain the poor lateral reproducibility of UAZ_3, mostly characterized by mixed pairs of neogondolellids and anchignathodontids.

In order to explore the impact of these environmental preferences on the resulting biozonation, we construct two distinct subdatasets: one for neogondolellids (UA.N) and one for anchignathodontids (UA.A). The new UAs sequences with their respective reproducibility matrix are displayed in Fig. 11. $UA.A_3$ is laterally poorly reproducible. Owing to its resemblance with $UA.A_2$ ($D_3 = 0.2576$; see Fig. 11A), we merge $UA.A_2$ with $UA.A_3$ (see procedure described in part 3.3).

The neogondolellid data set leads to three UAs whose lateral reproducibility varies from one ($UA.N_2$) to six ($UA.N_3$). It is however difficult to choose how $UA.N_2$ must be merged, as the dissimilarity index and the frequency of arcs are the same with $UA.N_1$ and $UA.N_3$. The result is a three-UAZ biozonation (Fig. 11C). It is worth of note that the method was applied with and without the virtual extension of the range of *N. taylorae*, and both runs produced the same sequence of UAZ.N.

As mentioned before, we can observe from the respective reproducibility matrices that the anchignathodontids are dominant at Dajiang, Dawen and Wuzhuan, and neogondolellids are dominant at Meishan, Shangsi and Yangou. Fig. 12 shows the correspondence between the sequence of UAZs obtained from the complete data set and the sequences obtained from these two subsets. $UAZ.A_1$ corresponds to UAZ_1–UAZ_2,

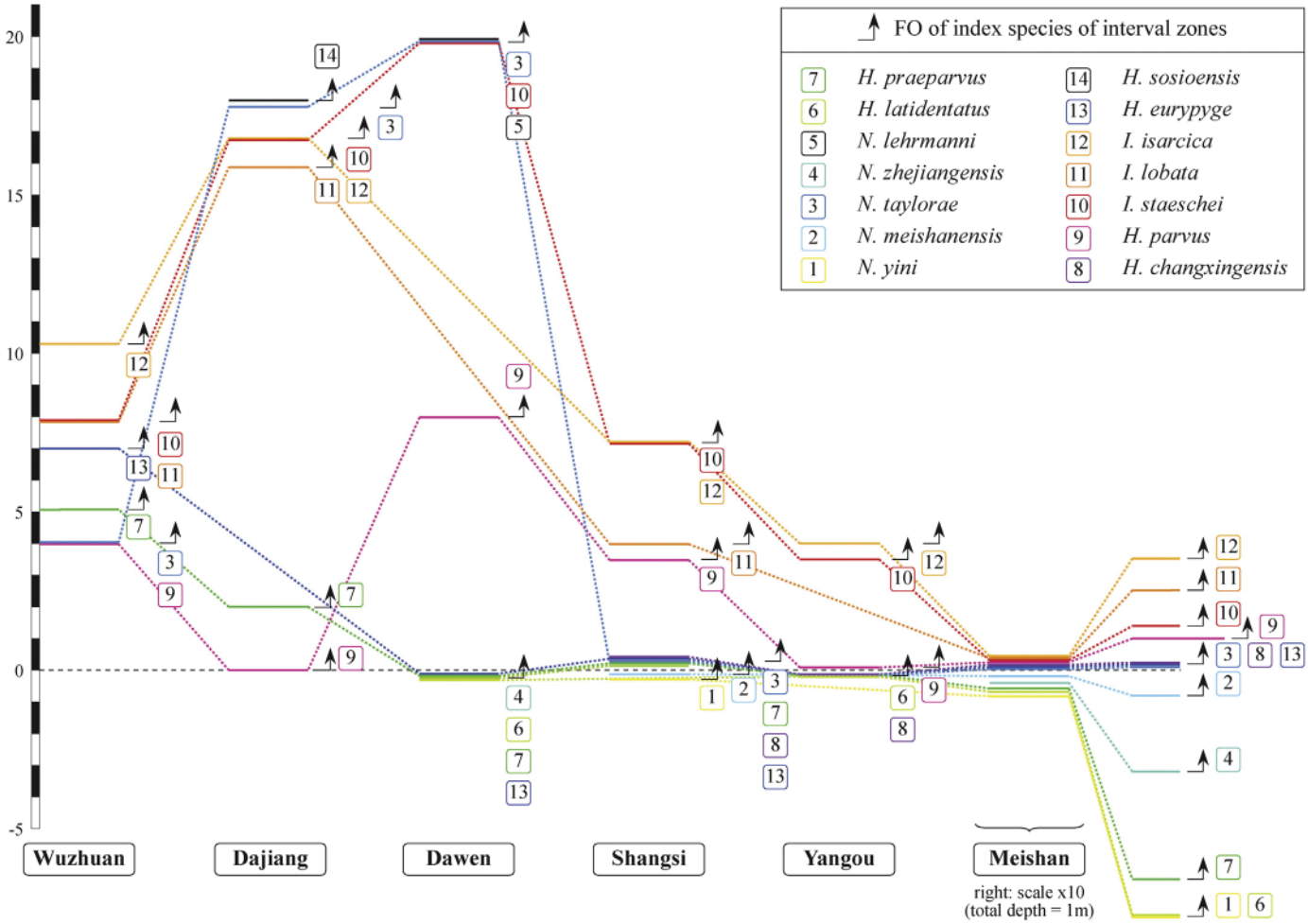

Fig. 9. Biostratigraphical correlations of the Wuzhuan, Dajiang, Dawen, Shangsi, Yangou and Meishan sections by means of first occurrences (FOs). The vertical scale (stratigraphical thickness in metres) is the same for the six sections. *H*: *Hindeodus*, *I*: *Isarcicella*, *N*: *Neogondolella*.

$UA.A_2$ to UAZ_3–UAZ_4 and $UAZ.N_3$ to UAZ_3–UAZ_6. The correspondence is clear between $UAZ.A_3$ and UAZ_5, $UAZ.A_4$ and UAZ_6. Correlations are also clear between $UAZ.N_1$ and UAZ_1, and $UAZ.N_2$ and UAZ_2. Fig. 12 also shows that neogondolellids provide a higher biostratigraphic resolution than anchignathodontids during the Changhsingian, a result which is reversed during the Griesbachian.

The PTB best correlates with a faunal turnover in both families and can be detected in both data sub-sets. The PTB is located between $UAZ.A_1$ and $UAZ.A_2$, and between $UAZ.N_2$ and $UAZ.N_3$. The placement of the PTB in the two subsets is also in full agreement with its position in the complete data set. In addition to the position of the PTB in the complete data set, the occurrence of the anchignathodontids characteristic species *H. changxingensis*, *I. prisca* or *I. huckriedei*, or of the neogondolellids characteristic species *N. planata* or *N. taylorae* can all be considered as equally good proxies for the base of the Triassic.

5.3. Conodonts across the Permian–Triassic transition

Conodonts underwent a gradual decline at family and genus levels throughout the Permian, leading to the extinction of some Tethyan endemic species close to the PTB (Orchard, 2007). Three conodont families (*Neogondolellidae*, *Anchignathodontidae* and *Ellisoniidae*) crossed the Permian–Triassic boundary. About half of the neogondolellid species crossed the PTB and most of post-Griesbachian species stemmed from these (Orchard, 2007). Anchignathodontids evolved rapidly during the latest Permian and both *Hindeodus* and *Isarcicella* experienced a rapid radiation during the early Griesbachian (Nicoll et al., 2002; Perri and Farabegoli, 2003); Ellisoniids seem unaffected by the extinction event (Orchard, 2007).

Fig. 13 shows the temporal evolution (succession of UAZs) of species diversity and faunal turnover for the two main families (anchignathodontids and neogondolellids). As already mentioned in the introduction, the unknown duration of UAZs does not introduce any significant bias when counting taxonomic richness (Escarguel and Bucher, 2004). In the closest agreement with the position of the PTB in Meishan, the PTB is located between UAZ_2 and UAZ_3. The number of species in both families follows a parallel trend from UAZ_1 to UAZ_2, with a rather constant diversity (four to five species of anchignathodontids and seven to six species of neogondolellids). From UAZ_3 onward, anchignathodontids underwent a radiation reaching its climax in UAZ_5 (from four to 13 species), while the number of neogondolellid species decreases drastically from UAZ_4 onward (from seven to one species, see Fig. 13A). In agreement with Orchard (2007), our analysis of taxonomic diversity shows that the radiation of anchignathodontids (from UAZ_3) precedes the extinction of neogondolellids (from UAZ_4). The diversity patterns of the families follow a parallel extinction trend from UAZ_5 onward (decline from 13 to five species of anchignathodontids and from two to one species of neogondolellids). It corresponds to the transition to UAZ_6.

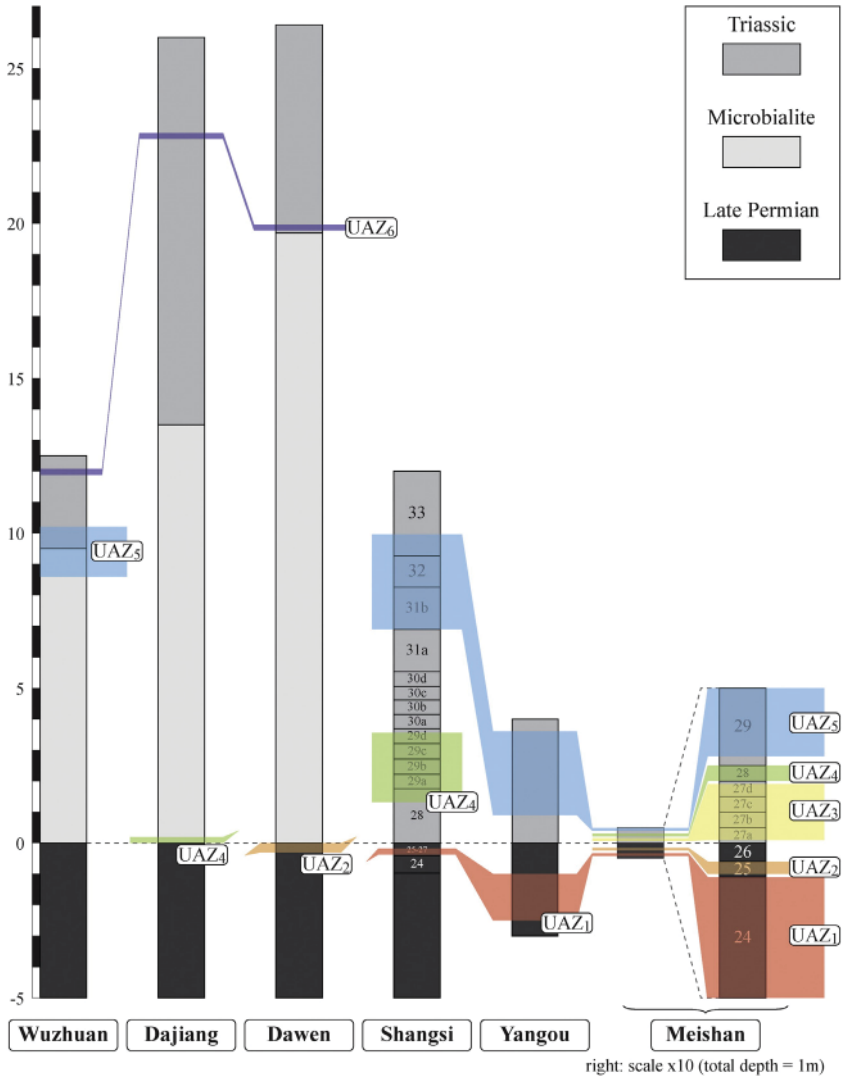

Fig. 10. Position of the 6 UAZ and FOs of index species in the studied sections. The vertical scale (stratigraphical thickness in metres) bar is the same for the six simplified logs.

5.4. Comparison of the age model with other sections

— Age of *Hindeodus parvus*

In Zhongzhai, Zhang et al. (2014) reported the occurrence of the Triassic index fossil *H. parvus* in beds that they interpreted as being Changhsingian in age. The diachronous FO of *H. parvus* is the topic of a long lasting debate (Baud, 1996; Hermann et al., 2010; Li et al., 1996; Zhang et al., 2014). According to Zhang et al. (2014), the last Permian bed at Zhongzhai is bed 28, and the first Griesbachian bed is bed 30, the clay bed 29 being barren. We standardized the taxonomy of Zhongzhai as we did for the other sections (see Table 1). In our opinion, none of the illustrated specimens from bed 28 (Zhang et al., 2014) can be assigned to *H. parvus*. Hence they cannot be used as an evidence for a Permian FO of *H. parvus* in Zhongzhai.

Even if these specimens were considered as true *H. parvus*, then these data would generate no less than 10 contradictions and 6 Z_4 cycles. All Z_4 cycles involve the unusual co-occurrence of *H. bicuspidatus* (found in UAZ_5–UAZ_6) and *H. meishanensis* (found in UAZ_2–UAZ_4). The presence of such an atypical association suggests some contamination, condensation or down-working across an omission surface and, consequently, the conodont record from Zhongzhai must be treated with the greatest caution.

— Age of *Neogondolella taylorae*

N. taylorae was first described as an Early Triassic species by Orchard et al. (1994) from the *Otoceras latilobatum* bed of the Selong section, South Tibet. It has also been found throughout the entire Griesbachian interval in Kashmir (Matsuda, 1984), Arctic Canada (Henderson and Baud, 1997), and in the Guling, Lingti, Muth and Lalung sections of Spiti (Orchard and Krystyn, 1998). *N. taylorae* has also been repeatedly found in China, hitherto only in Early Triassic beds as shown by the selected sections in our data set. On the other hand, Kozur (2004, 2005) reported this species from Permian rocks from Iranian sections at Zal and Jolfa, indicating that its range extends into the Permian in the Tethys. From the 11 initial sections selected for this study, *N. taylorae* is recorded from Permian rocks only at Chaotian (Ji et al., 2007), thus supporting its latest Permian–Griesbachian age range.

5.5. Definition of the PTB and the main extinction interval

The current definition of the PTB at Meishan section is between bed 27b and 27c, as based on the FO of *H. parvus* (found in bed 27c). However, UAZ_3, including *H. parvus* and consequently interpreted as Griesbachian in age, extends down to bed 27a at Meishan, due to the

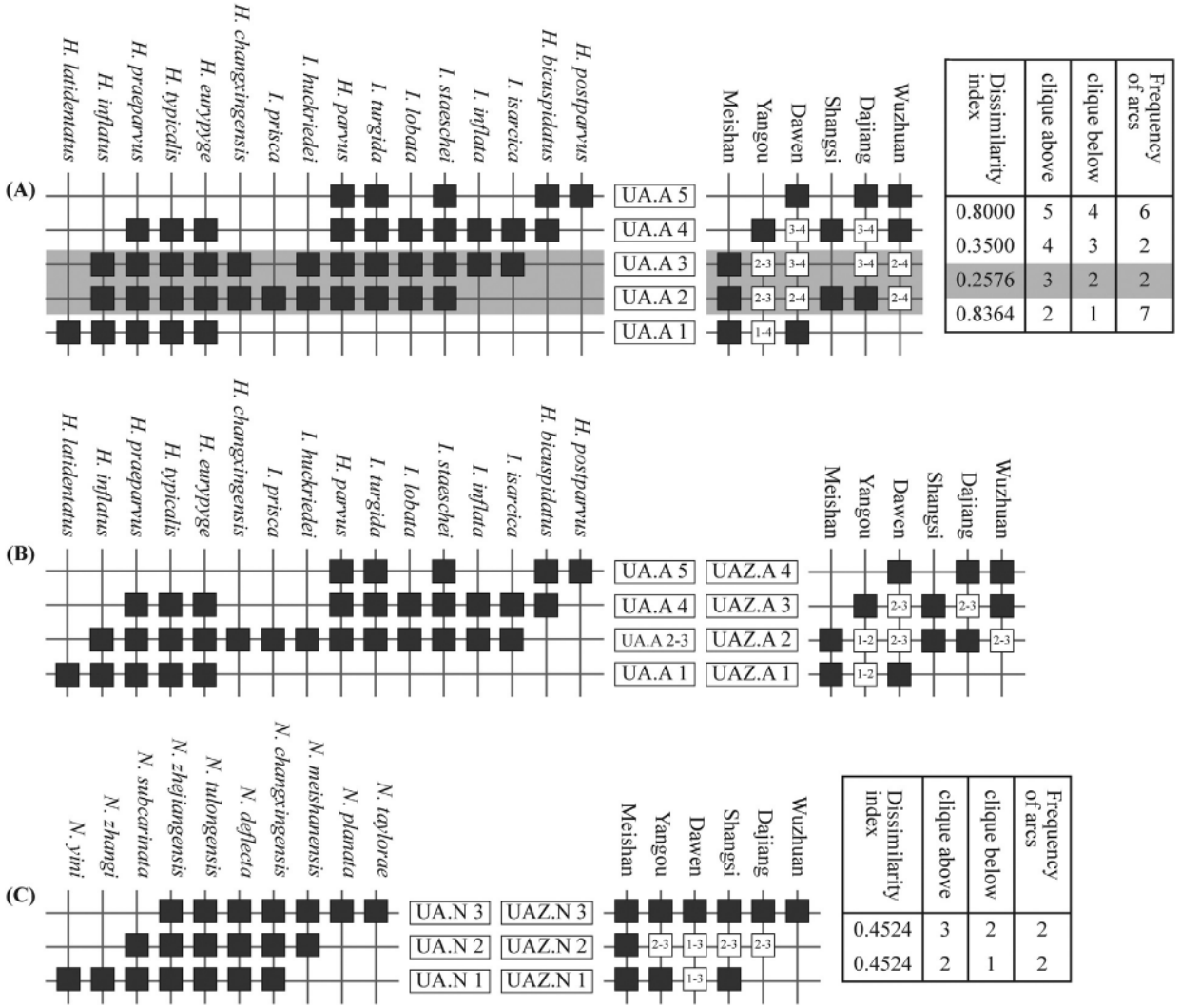

Fig. 11. Sequences of unitary associations (UAs) resulting from anchignathodontids and neogondolellids subsets, respectively. (A) Sequence of UAs, lateral reproducibility, dissimilarity index and arcs between the UAs resulting from the anchignathodontid subset. The grey shades highlight the modification applied to the UA sequence in order to transform them into UA zones (UAZs). B) Sequence of UAZs and lateral reproducibility between the UAZs resulting from the anchignathodontid subset. (C) Sequence of UAs and UAZs, lateral reproducibility, dissimilarity index and arcs between the UAs and UAZs resulting from the neogondolellid subset, no modification was applied on the sequence of UAs. *H*: *Hindeodus*, *I*: *Isarcicella*, *N*: *Neogondolella*.

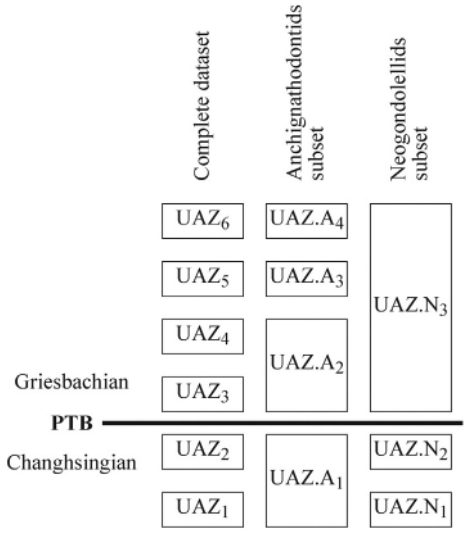

Fig. 12. Correspondence of UAs of the complete data set, with anchignathodontids (A) and neogondolellids (N) subsets.

association of other pairs of characteristic species such as *N. tulongensis* and *N. zhejiangensis* associated with *N. planata*, *N. taylorae*, and *H. changxingensis*. Therefore, as defined by the GSSP (Yin et al., 2001), UAZ_3 is not entirely within the Triassic. Our biochronological analysis supports the placement of the PTB in the separation interval bracketed by UAZ_2 and UAZ_3. In Meishan this interval of separation corresponds to the interval between bed 25 and bed 27a (see Fig. 10).

The five oldest UAZs generated by the method are identified in the Meishan section. UAZ_1, UAZ_2, UAZ_3, UAZ_4, UAZ_5 correspond to beds 24, 25, 27, 28 and 29, respectively, at Meishan (see Table 2). The 5 cm-thick volcanoclastic bed 25 (UAZ_2) and the 4 cm-thick volcanoclastic bed 28 (UAZ_4) were calibrated with U–Pb radio-isotopic zircon ages at 251.941 ± 0.037 and 251.88 ± 0.031 Ma, respectively (Burgess et al., 2014). According to Burgess et al. (2014), the main extinction interval initially characterized by Shen et al. (2011) stretches from beds 25 to 28 in Meishan and its duration is estimated to 61 ± 48 ka. Hence, this duration can also be transposed to sections with different bathymetry (e.g. microbialite-bearing sections). The correspondences between UAZs, bed numbers and numerical ages at Meishan section are shown in Fig. 14A.

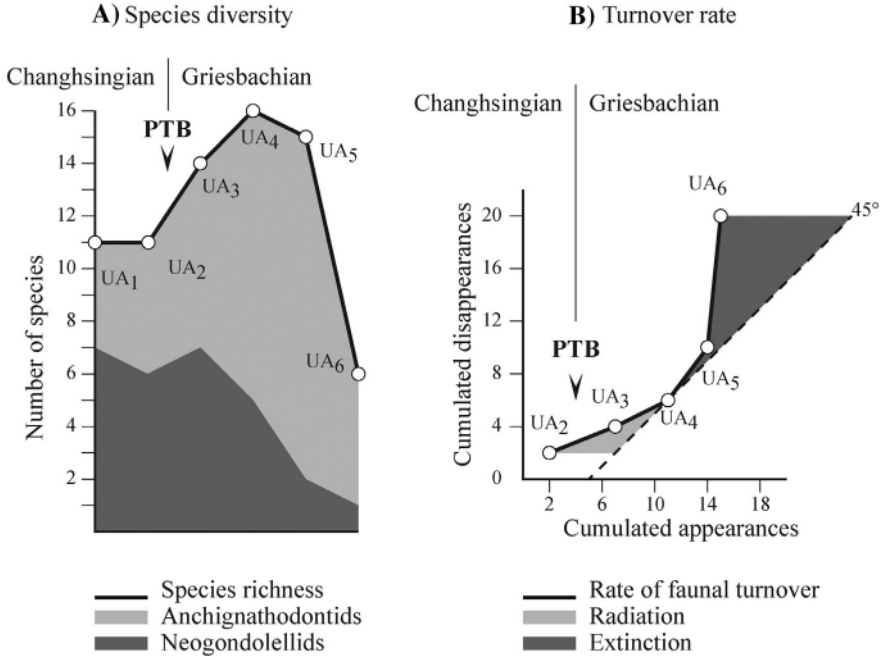

Fig. 13. Species diversity and rates of faunal turnover calculated from the optimal solution given in Fig. 7A. Note the differing behaviour of the two main families anchignathodontids and neogondolellids in (A).

5.6. The microbialite event

The base of the microbial limestone in the Nanpanjiang Basin and in the South China Block has been assigned either to the latest Permian (e.g. Xie et al., 2010) or to the Griesbachian (e.g. Galfetti et al., 2008). Yet, the base of the microbial limestone is generally devoid of any age-diagnostic fossils and rests uncomformably on top of the Permian skeletal limestones. Hence the duration of the gap at the base of the microbial limestone remains unknown. In Dawen, the occurrence of the youngest Permian UAZ_2 indicates that no gap in terms of UAZs can be detected in the uppermost part of the Permian skeletal limestones of this section (Fig. 14B). In Dajiang, the very base of the microbial limestone can be assigned to UAZ_4. Assuming that the base of the microbialite is synchronous between the geographically ca. 1 km distant (Song et al., 2009) Dawen and Dajiang, the gap would thus include the time interval bounded by UAZ_2 and UAZ_4 (see Fig. 14) whose maximal duration is of 61 ± 48 ka (Burgess et al., 2014).

5.7. Comparison with other dating methods

Fig. 15 displays the succession of UAZs along with other stratigraphical data and numerical ages. Note that the radiometric dating at Shangsi (Shen et al., 2011) cannot be directly compared with that at Meishan (Burgess et al., 2014) because these studies used different tracer solutions, different standards, and different error propagation algorithms. Astronomical time scales have been published and interpreted for Shangsi (ARM time series) and Meishan (MS time series) by Wu et al. (2013). However, these astronomical time scales were calibrated with the U–Pb ages of Shen et al. (2011). According to the magnetostratigraphy of Glen et al. (2009), the intervals of normal polarity at Meishan (around beds 24–29) and Shangsi (around beds 25–32) are equivalent. Oxygen isotope records for the Shangsi and Meishan sections were produced by Chen et al. (2015). Carbon isotope records for the Wuzhuan, Dajiang, Dawen, Shangsi, Yangou and Meishan sections were respectively established by Hautmann et al. (2015), Song et al. (2013b), Payne et al. (2004), Shen et al. (2013), Tian et al. (2014) and Cao et al. (2009).

— *UAZ_1 (red in* Fig. 15)
Magnetostratigraphy: UAZ_1 is included within the normal polarity interval at Meishan and Shangsi.
Oxygen isotope record: UAZ_1 is identified within the Permian 20–21‰ plateau at Meishan and Shangsi (sea-water temperatures around 18 °C), before the onset of the "dramatic warming event" that is documented in both sections.
Carbon isotope record: UAZ_1 is identified at Shangsi within the "first order" negative shift from 3 to −1‰ that straddles the PTB (Schobben et al., 2016). In Meishan, beds 24 to 29 and UAZ_1 to UAZ_5 are all within the "first order" negative shift. However, only UAZ_1 included the "second order" excursion of Schobben et al. (2016) in bed 24e, whose age is of 251.950 ± 0.042 Ma (Burgess et al., 2014).
Astronomical time scale: UAZ_1 corresponds to the youngest part of the "~100-kyr-short eccentricity cycle e_1" identified around bed 24 at Meishan, which is in turn within the 405-kyr eccentricity cycle E_0.

— *UAZ_2 (orange in* Fig. 15)
Magnetostratigraphy: UAZ_2 is included within the normal polarity interval at Meishan.
Oxygen isotope record: At Meishan, UAZ_2 immediately precedes the warming event (a 21 to 19‰ negative excursion of the $\delta^{18}O_{apatite}$ record).
Carbon isotope record: UAZ_2 occurs above the abrupt "second-order" excursion in Meishan and within the "first-order" $\delta^{13}C$ trend of Schobben et al. (2016) in Meishan and Dawen.
Astronomical time scale: UAZ_2 corresponds to the base of the Late Permian "~100-kyr-short eccentricity cycle e_2" identified around beds 26–28 at Meishan, which is in turn within the 405-kyr eccentricity cycle E_0.

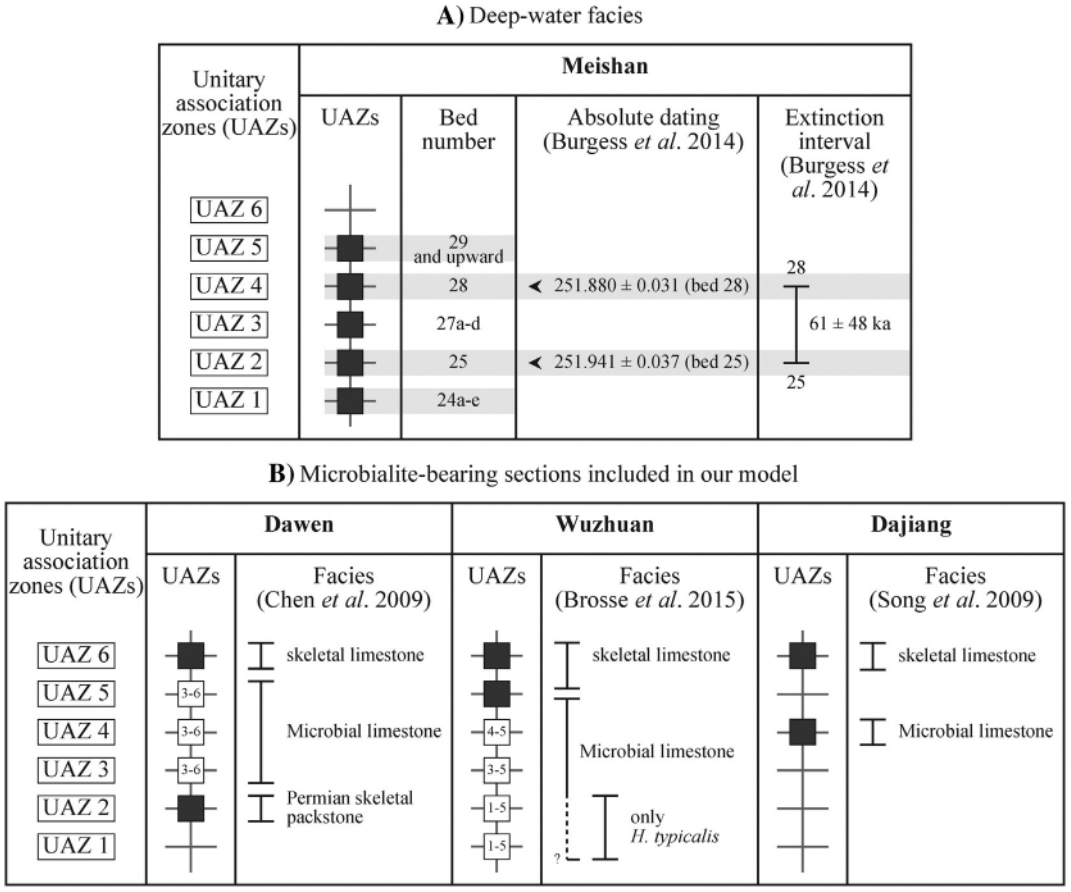

Fig. 14. (A) UAZs and radio-isotopic ages in Meishan. As shown in Table 2, UAZ_1 corresponds to bed 24a-e, UAZ_2 corresponds to bed 25, UAZ_3 corresponds to bed 27a-d and UAZ_4 corresponds to bed 28, allowing us to precisely date some of the UAZs. (B) UAZ ages of facies in microbialite bearing sections.

— *UAZ_3 (yellow in* Fig. 15*)*
Magnetostratigraphy: UAZ_3 is included within the normal polarity interval at Meishan.
Oxygen isotope record: UAZ_3 corresponds to a high temperature interval (~30 °C) at Meishan.
Carbon isotope record: UAZ_3 is identified within a smooth positive excursion at Meishan.
Astronomical time scale: UAZ_3 occurs during the "~100-kyr-short eccentricity cycle e_2" identified around beds 26–28 at Meishan, which is in turn within the 405-kyr eccentricity cycle E_0.
UAZ_3 includes the FO of *H. parvus* at Meishan.

— *UAZ_4 (green in* Fig. 15*)*
Magnetostratigraphy: UAZ_4 is included within the normal polarity interval at Meishan, and at the base of the normal polarity interval that includes possible chrons at Shangsi (around beds 28–31a).
Oxygen isotope record: As for UAZ_3, UAZ_4 corresponds to the interval of high temperatures (~30 °C) at Shangsi and Meishan.
Carbon isotope record: UAZ_4 is coeval with a local positive maximum at Meishan and near a local negative minimum at Shangsi.
Astronomical time scale: UAZ_4 corresponds to the top of the Early Triassic "~100-kyr-short eccentricity cycle e_2" identified around beds 26–28 at Meishan, which is in turn within the 405-kyr eccentricity cycle E_0.
UAZ_4 includes the FO of *H. parvus* at Shangsi and Dajiang.

— *UAZ_5 (blue in* Fig. 15*)*
Magnetostratigraphy: UAZ_5 is included within the reverse polarity interval at Meishan, and overlaps with the transition from normal to reverse polarity at Shangsi.
Oxygen isotope record: As for UAZ_3 and UAZ_4, UAZ_5 is within the same high temperature interval (~30 °C) at Shangsi and Meishan.
Carbon isotope record: UAZ_5 corresponds to a positive 'plateau' of $\delta^{13}C$ at Meishan and to a smooth positive excursion at Shangsi.
Astronomical time scale: UAZ_5 corresponds to the "~100-kyr-short eccentricity cycle e_3" identified around bed 29 at Meishan, which is in turn within the 405-kyr eccentricity cycle E_0.

— *UAZ_6 (purple in* Fig. 15*)*
Carbon isotope record: UAZ_6 occurs within a positive plateau with values around 1–2‰ at Dajiang and within a positive trend at Dawen.

6. Conclusions

1. We propose a new and accurate conodont zonation spanning the PTB in South China. A stringent selection of six sections comprising shallow- and deeper-water successions and 26 conodont species is analysed by means of unitary associations. The UA method produces a discrete sequence of eight UAs subsequently grouped into six UAZs of higher lateral reproducibility.
2. In the closest possible agreement with the Meishan GSSP, we propose to draw the PTB within the interval of separation bracketed by UAZ_2 and UAZ_3. The oldest Triassic UAZ_3 contains the characteristic species *H. pisai* and characteristic pairs of species *N. zhejiangensis* or *N. tulongensis* with *N. planata*, *N. taylorae*, *H. parvus*, *H. changxingensis* or *I. huckriedei*. These characteristic species and pairs of species provide robust alternatives to the first occurrence of *H. parvus* for the base of Triassic. Consequently, beds 27a and

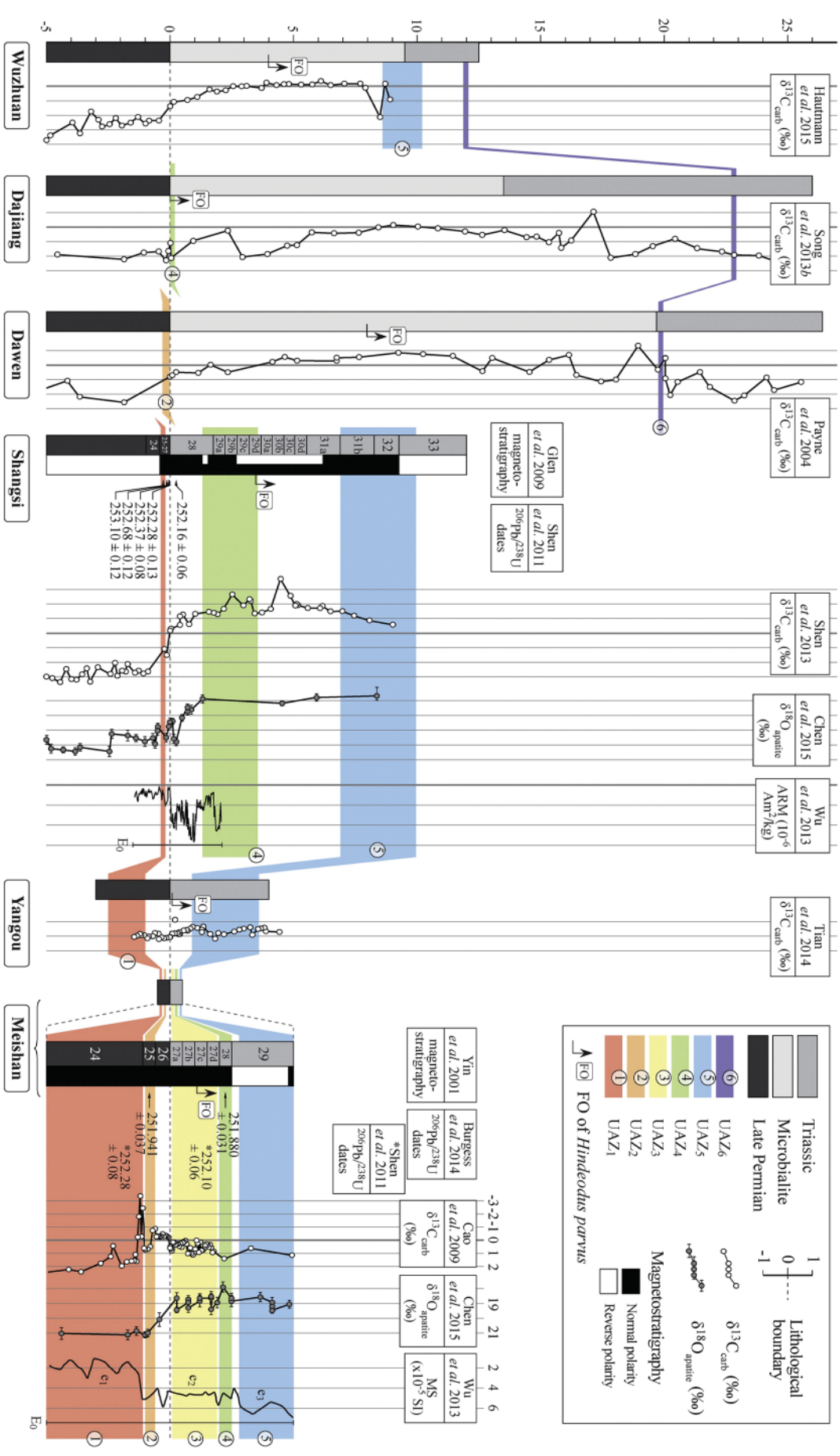

Fig. 15. Comparison of the UAZs with other dating methods for each section included in the model. The 0 on the picture refers to the lithological boundary, for it can be easily identified for every section in most of the studies, and does not reflect the position of the PTB. The other methods include chemostratigraphy (carbon and oxygen isotope records), magnetostratigraphy, astronomical time scale and U–Pb absolute ages. The horizontal scales of carbon and oxygen isotope records respectively are the same between the sections. Former U–Pb ages in Meishan obtained by Shen et al. (2011) are indicated with a star. Vertical scale in metres.

27b at Meishan belong to the Griesbachian and the insufficient faunal content of bed 26 can be assigned either to UAZ_2 or to UAZ_3. The formational boundary between the Changhsing and the Yinkeng formations placed between beds 26 and 27 also falls within the same interval of separation.

3. Separated analyses conducted on anchignathodontids on one hand and neogondolellids on the other reveal that the UAZ-defined PTB also corresponds to a faunal turnover at the species level for both data sets. The occurrences of anchignathodontids characteristic species such as *H. changxingensis*, *I. prisca* or *I. huckriedei* are good proxies for the base of the Triassic in shallow-water depositional environments. The occurrences of neogondolellids characteristic species such as *N. planata* or *N. taylorae* are good proxies for the base of the Triassic in deeper-water depositional environments.
4. Detailed diversity analyses show that the radiation of anchignathodontids starts from UAZ_3 and reaches its climax in UAZ_5. It is followed by a sharp drop between UAZ_5 and UAZ_6. From UAZ_1 to UAZ_3, the diversity of neogondolellids fluctuates between six and seven species. From UAZ_4 to UAZ_6, it displays a sharp and sustained decrease. In agreement with Orchard (2007), we confirm that the radiation of anchignathodontids started earlier than the extinction of neogondolellids and that the extinction of anchignathodontids was thus delayed with respect to that of neogondolellids.
5. The UAs method yields robust intra-basinal correlations, in this case between microbialite-bearing and deeper-water Early Triassic sections. The conodont record within the microbialite-bearing sections shows thick intervals of separation between horizons unequivocally assigned to UAZs. Correlations with Meishan lead to an estimated duration of 61 ± 48 ka for the interval between UAZ_2 and UAZ_4, which corresponds to the main extinction interval and to the maximal duration of the gap at the base of the Triassic microbial limestone in the Dajiang section.

Supplementary data to this article can be found online at http://dx.doi.org/10.1016/j.earscirev.2016.02.003.

Acknowledgments

Kuang Guodun (Nanning), Aymon Baud (Lausanne), Borhan Bagherpour (Zurich) and Åsa Frisk (Uppsala) are thanked for their support in the field and for the insightful discussions. Jonathan Payne (Stanford), Shen Shuzhong (Nanjing) and Thomas J. Algeo (Cincinnati) kindly provided carbon isotope data. Constructive reviews by Ian Metcalfe, an anonymous reviewer and ESR Editor André Strasser greatly improved the manuscript. This work is supported by the Swiss NSF project 200021_135446 (to H.B.) and a French ANR @RAction grant (project EvoDevOdonto to N.G.).

References

Angiolini, L., Bucher, H., 1999. Taxonomy and quantitativebiochronology of Guadalupian brachiopods from the Khuff Formation, Southeastern Oman. Geobios 32 (5), 665–699. http://dx.doi.org/10.1016/S0016-6995(99)80057-6.

Baud, A., 1996. The Permian–Triassic boundary: recent developments, discussion and proposals. Albertiana 18, 6–9.

Boulard, C., 1993. Biochronologie Quantitative: Concepts, méthodes et validité (PhD thesis).

Brosse, M., Bucher, H., Bagherpour, B., Baud, A., Frisk, Å.M., Guodun, K., Goudemand, N., 2015. Conodonts from the Early Triassic microbialite of Guangxi (South China): implications for the definition of the base of the Triassic System. Palaeontology 58 (3), 563–584. http://dx.doi.org/10.1111/pala.12162.

Burgess, S.D., Bowring, S., Shen, S.Z., 2014. High-precision timeline for Earth's most severe extinction. Proc. Natl. Acad. Sci. 111 (9), 3316–3321. http://dx.doi.org/10.1073/pnas.1317692111.

Cao, C., Love, G.D., Hays, L.E., Wang, W., Shen, S., Summons, R.E., 2009. Biogeochemical evidence for euxinic oceans and ecological disturbance presaging the end-Permian mass extinction event. Earth Planet. Sci. Lett. 281 (3), 188–201. http://dx.doi.org/10.1016/j.epsl.2009.02.012.

Chen, J., Henderson, C.M., Shen, S.Z., 2008. Conodont succession around the Permian–Triassic boundary at the Huangzhishan Section, Zhejiang and its stratigraphic correlation. Acta Palaeontol. Sin. 47 (1), 91–114.

Chen, J., Beatty, T.W., Henderson, C.M., Rowe, H., 2009. Conodont biostratigraphy across the Permian–Triassic boundary at the Dawen section, Great Bank of Guizhou, Guizhou Province, South China: implications for the Late Permian extinction and correlation with Meishan. J. Asian Earth Sci. 36 (6), 442–458. http://dx.doi.org/10.1016/j.jseaes.2008.08.002.

Chen, J., Shen, S.Z., Li, X.H., Xu, Y.G., Joachimski, M.M., Bowring, S.A., Erwin, D.H., Yuan, D., Chen, B., Zhang, H., Wang, Y., Cao, C., Zheng, Q., Mu, L., 2015. High-resolution SIMS oxygen isotope analysis on conodont apatite from South China and implications for the end-Permian mass extinction. Palaeogeogr. Palaeoclimatol. Palaeoecol. http://dx.doi.org/10.1016/j.palaeo.2015.11.025.

Clark, D.L., 1959. Conodonts from the Triassic of Nevada and Utah. J. Paleontol. 33 (2), 305–312.

Dai, J., Zhang, J., 1989. Study on the Permian–Triassic Biostratigraphy and Event Stratigraphy of Northern Sichuan and Southern Shaanxi. Ministry Of Geology and Mineral Resources, Geol. Mem., Series 2 p. 435.

Escarguel, G., Bucher, H., 2004. Counting taxonomic richness from discrete biochronozones of unknown duration: a simulation. Palaeogeogr. Palaeoclimatol. Palaeoecol. 202 (3), 181–208. http://dx.doi.org/10.1016/S0031-0182(03)00630-8.

Galfetti, T., Bucher, H., Martini, R., Hochuli, P.A., Weissert, H., Crasquin-Soleau, S., Brayard, A., Goudemand, N., Brühwiler, T., Guodun, K., 2008. Evolution of Early Triassic outer platform paleoenvironments in the Nanpanjiang Basin (South China) and their significance for the biotic recovery. Sediment. Geol. 204 (1), 36–60. http://dx.doi.org/10.1016/j.sedgeo.2007.12.008.

Galster, F., Guex, J., Hammer, O., 2010. Neogene biochronology of Antarctic diatoms: a comparison between two quantitative approaches, CONOP and UAgraph. Palaeogeogr. Palaeoclimatol. Palaeoecol. 285 (3), 237–247. http://dx.doi.org/10.1016/j.palaeo.2009.11.015.

Glen, J.M.G., Nomade, S., Lyons, J.J., Metcalfe, I., Mundil, R., Renne, P.R., 2009. Magnetostratigraphic correlations of Permian–Triassic marine-to-terrestrial sections from China. J. Asian Earth Sci. 36 (6), 521–540. http://dx.doi.org/10.1016/j.jseaes.2009.03.003.

Guex, J., 1991. Biochronological Correlations. Springer Verlag.

Guex, J., Galster, F., Hammer, Ø., 2015. Discrete Biochronological Time Scales.

Hammer, Ø., 2013. PAST: PAleontological STatistics Version 3.01.

Hautmann, M., Bagherpour, B., Brosse, M., Frisk, Å., Hofmann, R., Baud, A., Bucher, H., 2015. Competition in slow motion: the unusual case of benthic marine communities in the wake of the end-Permian mass extinction. Palaeontology 58 (5), 871–901. http://dx.doi.org/10.1111/pala.12186.

Henderson, C.M., Baud, A., 1997. Correlation of the Permian–Triassic boundary in Arctic Canada and comparison with Meishan, China. Proc. 30th Int. Geol. Con. 11, pp. 143–152.

Hermann, E., Hochuli, P.A., Bucher, H., Vigran, J.O., Weissert, H., Bernasconi, S.M., 2010. A close-up view of the Permian–Triassic boundary based on expanded organic carbon isotope records from Norway (Trøndelag and Finnmark Platform). Glob. Planet. Chang. 74 (3), 156–167. http://dx.doi.org/10.1016/j.gloplacha.2010.10.007.

Hochuli, P.A., Vigran, J.O., Hermann, E., Bucher, H., 2010. Multiple climatic changes around the Permian–Triassic boundary event revealed by an expanded palynological record from mid-Norway. Geol. Soc. Am. Bull. 122 (5–6), 884–896. http://dx.doi.org/10.1130/B26551.1.

Ji, Z., Yao, J., Isozaki, Y., Matsuda, T., Wu, G., 2007. Conodont biostratigraphy across the Permian–Triassic boundary at Chaotian, in northern Sichuan, China. Palaeogeogr. Palaeoclimatol. Palaeoecol. 252 (1), 39–55. http://dx.doi.org/10.1016/j.palaeo.2006.11.033.

Jiang, H., Lai, X., Luo, G., Aldridge, R., Zhang, K., Wignall, P., 2007. Restudy of conodont zonation and evolution across the P/T boundary at Meishan section, Changxing, Zhejiang, China. Glob. Planet. Chang. 55 (1), 39–55. http://dx.doi.org/10.1016/j.gloplacha.2006.06.007.

Jiang, H., Lai, X., Yan, C., Aldridge, R.J., Wignall, P., Sun, Y., 2011a. Revised conodont zonation and conodont evolution across the Permian–Triassic boundary at the Shangsi section, Guangyuan, Sichuan, South China. Glob. Planet. Chang. 77 (3), 103–115. http://dx.doi.org/10.1016/j.gloplacha.2011.04.003.

Jiang, H., Aldridge, R.J., Lai, X., Yan, C., Sun, Y., 2011b. Phylogeny of the conodont genera *Hindeodus* and *Isarcicella* across the Permian–Triassic boundary. Lethaia 44 (4), 374–382. http://dx.doi.org/10.1111/j.1502-3931.2010.00248.x.

Jiang, H., Lai, X., Sun, Y., Wignall, P.B., Liu, J., Yan, C., 2014. Permian–Triassic conodonts from Dajiang (Guizhou, South China) and their implication for the age of microbialite deposition in the aftermath of the End-Permian mass extinction. J. Earth Sci. 25 (3), 413–430. http://dx.doi.org/10.1007/s12583-014-0444-4.

Joachimski, M.M., Lai, X., Shen, S., Jiang, H., Luo, G., Chen, B., Chen, J., Sun, Y., 2012. Climate warming in the latest Permian and the Permian–Triassic mass extinction. Geology 40 (3), 195–198. http://dx.doi.org/10.1130/G32707.1.

Kozur, H., 1989. Significance of events in conodont evolution for the Permian and Triassic stratigraphy. Cour. For. Sekenbg. 117, 385–408.

Kozur, H., 1996. The conodonts *Hindeodus*, *Isarcicella* and *Sweetohindeodus* in the uppermost Permian and lowermost Triassic. Geol. Croat. 49 (1), 81–115.

Kozur, H., 2004. Pelagic uppermost Permian and the Permian–Triassic boundary conodonts of Iran: part I: taxonomy. Hall. Jb. Geowiss. 18, 39–68.

Kozur, H., 2005. Pelagic uppermost Permian and the Permian–Triassic boundary conodonts of Iran: part II: Investigated sections and evaluation of the conodont faunas. Hall. Jb. Geowiss. 19, 49–86.

Kozur, H., Pjatakova, M., 1976. Die Conodontenart Anchignathodus Parvus N. Sp., Eine Wichtige Leitform Der Basalen Trias. Knaw. Verhan., Amsterdam. Proceedings, Series B 79 pp. 123–128.

Kozur, H., Mostler, H., Rahimi-Yazd, A., 1975. Beiträge zur mikrofauna permotriadischer schichtfolgen. teil 2: neue conodonten aus dem oberperm und der basalen trias von Nord-und zentraliran. Geol. Paläont. Mitt. Innsbruck 5 (3), 1–23.
Li, Z., Zhan, L., Zhang, S., 1996. Deftnition of the Permian–Triassic Boundary. 30th Int. Geol. Con., Beijing. Abstract Book.
Matsuda, T., 1984. Early Triassic conodonts from Kashmir, India part 4: *Gondolella* and *Platyvillosus*. J. Geosci. Osaka City Univ. 27, 119–141.
Mei, S., Zhang, K., Wardlaw, B.R., 1998. A refined succession of Changhsingian and Griesbachian neogondolellid conodonts from the Meishan section, candidate of the global stratotype section and point of the Permian–Triassic boundary. Palaeogeogr. Palaeoclimatol. Palaeoecol. 143 (4), 213–226. http://dx.doi.org/10.1016/S0031-0182(98)00112-6.
Metcalfe, I., 2013. Gondwana dispersion and Asian accretion: tectonic and palaeogeographic evolution of eastern Tethys. J. Asian Earth Sci. 66, 1–33. http://dx.doi.org/10.1016/j.jseaes.2012.12.020.
Metcalfe, I., Nicoll, R.S., 2007. Conodont biostratigraphic control on transitional marine to non-marine Permian–Triassic boundary sequences in Yunnan–Guizhou, China. Palaeogeogr. Palaeoclimatol. Palaeoecol. 252 (1), 56–65. http://dx.doi.org/10.1016/j.palaeo.2006.11.034.
Metcalfe, I., Nicoll, R.S., Wardlaw, B.R., 2007. Conodont index fossil *Hindeodus changxingensis* Wang fingers greatest mass extinction event. Palaeoworld 16 (1), 202–207. http://dx.doi.org/10.1016/j.palwor.2007.01.001.
Monnet, C., Bucher, H., 1999. Biochronologie quantitative (associations unitaires) des faunes d'ammonites du Cénomanien du sud-est de la France. Bull. Soc. Geol. Fr. 170 (5), 599–610.
Monnet, C., Bucher, H., 2002. Cenomanian (early Late Cretaceous) ammonoid faunas of Western Europe. Part I: biochronology (unitary associations) and diachronism of datums. Eclogae Geol. Helv. 95 (1), 57–74.
Monnet, C., Klug, C., Goudemand, N., De Baets, K., Bucher, H., 2011. Quantitative biochronology of Devonian ammonoids from Morocco and proposals for a refined unitary association method. Lethaia 44 (4), 469–489. http://dx.doi.org/10.1111/j.1502-3931.2010.00256.x.
Monnet, C., Brayard, A., Bucher, H., 2015. Ammonoids and Quantitative Biochronology—A Unitary Association Perspective. Ammonoid Paleobiology: From Macroevolution to Paleogeography. Springer, Netherlands, pp. 277–298 http://dx.doi.org/10.1007/978-94-017-9633-0_11.
Nicoll, R.S., Metcalfe, I., Cheng-Yuan, W., 2002. New species of the conodont Genus *Hindeodus* and the conodont biostratigraphy of the Permian–Triassic boundary interval. J. Asian Earth Sci. 20 (6), 609–631. http://dx.doi.org/10.1016/S1367-9120(02)00021-4.
Orchard, M.J., 2007. Conodont diversity and evolution through the latest Permian and Early Triassic upheavals. Palaeogeogr. Palaeoclimatol. Palaeoecol. 252 (1), 93–117. http://dx.doi.org/10.1016/j.palaeo.2006.11.037.
Orchard, M.J., Krystyn, L., 1998. Conodonts of the lowermost Triassic of Spiti, and new zonation based on *Neogondolella* successions. Riv. Ital. Paleontol. Stratigr. 104 (3), 341–367. http://dx.doi.org/10.13130/2039-4942/5339.
Orchard, M.J., Nassichuk, W.W., Rui, L., 1994. Conodonts from the Lower Griesbachian Otoceras Latilobatum Bed of Selong, Tibet and the position of the Permian–Triassic boundary. Can. Soc. Petrol. Geol. Mem. 17, 823–843.
Payne, J.L., Lehrmann, D.J., Wei, J., Orchard, M.J., Schrag, D.P., Knoll, A.H., 2004. Large perturbations of the carbon cycle during recovery from the end-Permian extinction. Science 305 (5683), 506–509. http://dx.doi.org/10.1126/science.1097023.
Perri, M.C., 1991. Conodont biostratigraphy of the Werfen Formation (Lower Triassic), Southern Alps, Italy. Boll. Soc. Paleontol. Ital. 30 (1), 23–46.
Perri, M.C., Farabegoli, E., 2003. Conodonts across the Permian–Triassic boundary in the Southern Alps. Cour. For. Sekenbg. 245, 281–313.
Raup, D.M., 1979. Size of the Permo-Triassic bottleneck and its evolutionary implications. Science 206 (4415), 217–218.
Retallack, G.J., 1995. Permian–Triassic life crisis on land. Science 267 (5194), 77–80. http://dx.doi.org/10.1126/science.267.5194.77.
Savary, J., Guex, J., 1991. BioGraph: un nouveau programme de construction des corrélations biochronologiques basées sur les associations unitaires. Bull. Soc. Vaud. Sci. Nat. 80 (3), 317–340.
Savary, J., Guex, J., 1999. Discrete Biochronological Scales and Unitary Associations: Description of the BioGraph Computer Program (No. 34). Section des sciences de la terre, Institut de géologie et paléontologie, Université de Lausanne.
Schobben, M., Ullmann, C.V., Leda, L., Korn, D., Struck, U., Reimold, W.U., Ghaderi, A., Algeo, T., Korte, C., 2016. Discerning primary versus diagenetic signals in carbonate carbon and oxygen isotope records: an example from the Permian–Triassic boundary of Iran. Chem. Geol. 422, 94–107. http://dx.doi.org/10.1016/j.chemgeo.2015.12.013.
Shen, S., Crowley, J., Wang, Y., Bowring, S., Erwin, D., Sadler, P., Cao, C., Rothman, D., Henderson, C., Ramezani, J., Zhang, H., Shen, Y., Wang, X., Wang, W., Mu, L., Li, W., Tang, Y., Liu, X., Liu, L., Zeng, Y., Jiang, Y., Jin, Y.G., 2011. Calibrating the end-Permian mass extinction. Science 334 (6061), 1367–1372. http://dx.doi.org/10.1126/science.1213454.
Shen, S.Z., Cao, C.Q., Zhang, H., Bowring, S.A., Henderson, C.M., Payne, J.L., Davydov, V.I., Chen, B., Yuan, D., Zhang, Y., Wang, W., Zheng, Q., 2013. High-resolution δ 13 C carb chemostratigraphy from latest Guadalupian through earliest Triassic in South China and Iran. Earth Planet. Sci. Lett. 375, 156–165. http://dx.doi.org/10.1016/j.epsl.2013.05.020.
Song, H., Tong, J., Chen, Z.Q., Yang, H.A.O., Wang, Y., 2009. End-Permian mass extinction of foraminifers in the Nanpanjiang Basin, South China. J. Paleontol. 83 (05), 718–738. http://dx.doi.org/10.1666/08-175.1.
Song, H., Wignall, P.B., Tong, J., Yin, H., 2013a. Two pulses of extinction during the Permian–Triassic crisis. Nat. Geosci. 6 (1), 52–56. http://dx.doi.org/10.1038/ngeo1649.
Song, H., Tong, J., Algeo, T.J., Horacek, M., Qiu, H., Song, H., Tian, L., Chen, Z.Q., 2013b. Large vertical $\delta^{13}C_{DIC}$ gradients in Early Triassic seas of the South China craton: implications for oceanographic changes related to Siberian Traps volcanism. Glob. Planet. Chang. 105, 7–20. http://dx.doi.org/10.1016/j.gloplacha.2012.10.023.
Sun, D., Tong, J., Xiong, Y., Tian, L., Yin, H., 2012. Conodont biostratigraphy and evolution across Permian–Triassic boundary at Yangou Section, Leping, Jiangxi Province, South China. J. Earth Sci. 23, 311–325. http://dx.doi.org/10.1007/s12583-012-0255-4.
Sweet, W.C., 1970a. Permian and Triassic conodonts from a section at Guryul Ravine, Vihi district, Kashmir. Univ. Kansas Paleontol. Contrib. 49, 2–49.
Sweet, W.C., 1970b. Uppermost Permian and Lower Triassic conodonts of the Salt Range and Trans-Indus Ranges, West Pakistan. Stratigraphic Boundary Problems: Permian and Triassic of West Pakistan, pp. 207–275.
Tian, L., Tong, J., Sun, D., Xiong, Y., Wang, C., Song, H.J., Song, H.Y., Huang, Y.F., 2014. The microfacies and sedimentary responses to the mass extinction during the Permian–Triassic transition at Yangou Section, Jiangxi Province, South China. Sci. China Earth Sci. 57 (9), 2195–2207. http://dx.doi.org/10.1007/s11430-014-4869-5.
Wang, C., 1994. Conodonts of Permian–Triassic boundary beds and biostratigraphic boundary. Acta Palaeontol. Sin. 34 (2), 129–151.
Wang, S.C., Everson, P.J., 2007. Confidence intervals for pulsed mass extinction events. Paleobiology 33 (2). http://dx.doi.org/10.1666/06056.1.
Wang, C., Wang, Z., 1981. Permian conodont biostratigraphy of China. Geol. Soc. Am. Sci. 187, 227–236.
Wang, L., Wignall, P.B., Wang, Y., Jiang, H., Sun, Y., Li, G., Yuan, J., Lai, X., 2016. Depositional conditions and revised age of the Permo-Triassic microbialites at Gaohua section, Cili County (Hunan Province, South China). Palaeogeogr. Palaeoclimatol. Palaeoecol. 443, 156–166. http://dx.doi.org/10.1016/j.palaeo.2015.11.032.
Wu, H., Zhang, S., Hinnov, L.A., Jiang, G., Feng, Q., Li, H., Yang, T., 2013. Time-calibrated Milankovitch cycles for the late Permian. Nat. Commun. 4.
Xie, S., Pancost, R.D., Wang, Y., Yang, H., Wignall, P.B., Luo, G., Jia, C., Chen, L., 2010. Cyanobacterial blooms tied to volcanism during the 5 my Permo-Triassic biotic crisis. Geology 38 (5), 447–450. http://dx.doi.org/10.1130/G30769.1.
Yan, C., Wang, L., Jiang, H., Wignall, P.B., Sun, Y., Chen, Y., Lai, X., 2013. Uppermost Permian to Lower Triassic conodonts at Bianyang section, Guihzou province, South China. PALAIOS 28 (8), 509–522. http://dx.doi.org/10.2110/palo.2012.p12-077r.
Yin, H., Zhang, K., Yang, F., 1988. A new scheme of biostratigraphic delimination between marine Permian and Triassic. Earth Sci. 13 (5), 511–519.
Yin, H., Zhang, K., Tong, J., Yang, Z., Wu, S., 2001. The global stratotype section and point (GSSP) of the Permian–Triassic boundary. Episodes 24 (2), 102–114.
Yuan, D.X., Chen, J., Zhang, Y.C., Zheng, Q.F., Shen, S.Z., 2015. Changhsingian conodont succession and the end-Permian mass extinction event at the Daijiagou section in Chongqing, Southwest China. J. Asian Earth Sci. 105, 234–251. http://dx.doi.org/10.1016/j.jseaes.2015.04.002.
Zhang, K., Lai, X., Ding, M., Liu, J., 1995. Conodont sequence and its global correlation of Permian–Triassic boundary in Meishan section, Changxing, Zhejiang Province. Earth Sci. J. China Univ. Geosci. 20 (6), 669–676.
Zhang, Y., Zhang, K.X., Shi, G.R., He, W.H., Yuan, D.X., Yue, M.L., Yang, T.L., 2014. Restudy of conodont biostratigraphy of the Permian–Triassic boundary section in Zhongzhai, southwestern Guizhou Province, South China. J. Asian Earth Sci. 80, 75–83. http://dx.doi.org/10.1016/j.jseaes.2013.10.032.
Zhao, L., Chen, Y., Chen, Z.Q., Cao, L., 2013. Uppermost Permian to Lower Triassic conodont zonation from Three Gorges area, South China. PALAIOS 28 (8), 523–540. http://dx.doi.org/10.2110/palo.2012.p12-107r.

Appendix A: Conodont occurrences in the sections included in this study. Black font represents observed occurrences, grey font represents virtual deduced occurrences. Black squares indicate taxonomical homogenization. The local maximal horizons (LMHs) are outlined and numbered for each section. The species names in grey appear in more than one section. N, *Neogondolella*; H, *Hindeodus*; I, *Isarcicella*; E, *Ellisonia*.

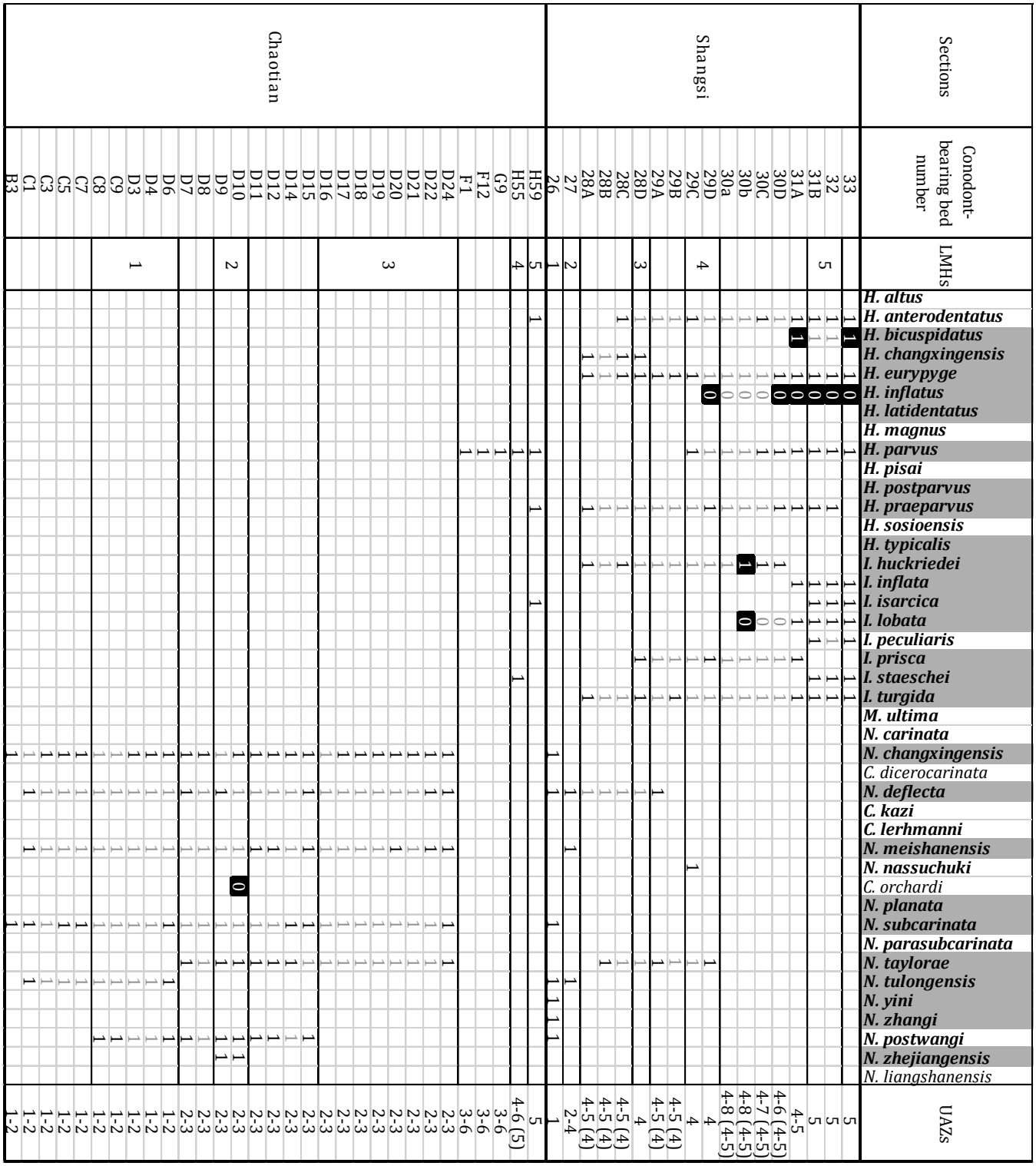

Sections	Conodont-bearing bed number	LMHs	UAZs
Wuzhuan	O	4	6
	N		5
	M		5
	L	3	5
	K		5
	J		4-5
	I		4-5
	H		4-5
	G	2	4-5
	F		3-5
	E		3-5
	D	1	3-5
	C		1-5
	B		1-5
	A		1-5
Dawen	DPT-26	4	6
	DPT-25		3-6
	DPT-24	3	3-6
	DPT-23		3-6
	DPT-22		3-6
	DPT-19		1-5 (2-5)
	DPT-18		2-5
	DPT-16	2	2-5
	DPT-13		2
	DPT-12	1	2
Dajiang	DJ-35	4	6
	DJ-34		4-6
	DJ-33		4-6
	DJ+20m		4-6
	DJ-32		4-6
	DJ-31		4-6
	DJ-30		4-5
	DJ-29		4-5
	DJ-28-4	3	4-5
	DJ-28-3		4-5
	DJ-28-2	2	4-5
	DJ-28-1		4-5
	DJ-28		4-5
	D+15m		4-5
	DJ-27B		4-5
	DJ-27		4-5
	DJ-26		4-5
	DJ-18		4-5
	DJ-13B	1	4
	DJ-13		4

	O	N	M	L	K	J	I	H	G	F	E	D	C	B	A	DPT-26	DPT-25	DPT-24	DPT-23	DPT-22	DPT-19	DPT-18	DPT-16	DPT-13	DPT-12	DJ-35	DJ-34	DJ-33	DJ+20m	DJ-32	DJ-31	DJ-30	DJ-29	DJ-28-4	DJ-28-3	DJ-28-2	DJ-28-1	DJ-28	D+15m	DJ-27B	DJ-27	DJ-26	DJ-18	DJ-13B	DJ-13
H. altus																																													
H. anterodentatus																																													
H. bicuspidatus	1	1	1	1	1	1	1	1	1	1	1	1	1	1	1	1	1	1	1	1	1	1	1	1	1	1	1	1	1	1	1	1	1	1	1	1	1	1	1	1	1	1	1	1
H. changxingensis		1	1																																										
H. eurypyge																																													
H. inflatus																																													
H. latidentatus																																													
H. magnus																																													
H. parvus																																													
H. pisai																																													
H. postparvus																																													
H. praeparvus																																													
H. sosioensis																																													
H. typicalis																																													
I. huckriedei																																													
I. inflata																																													
I. isarcica																																													
I. lobata																																													
I. peculiaris																																													
I. prisca																																													
I. staeschei																																													
I. turgida																																													
M. ultima																																													
N. carinata																																													
N. changxingensis																																													
C. dicerocarinata																																													
N. deflecta																																													
C. kazi																																													
C. lerhmanni																																													
N. meishanensis																																													
N. nassuchuki																																													
C. orchardi																																													
N. planata																																													
N. subcarinata																																													
N. parasubcarinata																																													
N. taylorae																																													
N. tulongensis																																													
N. yini																																													
N. zhangi																																													
N. postwangi																																													
N. zhejiangensis																																													
N. liangshanensis																																													

Sections	Conodont-bearing bed number	LMHs	*H. altus*	*H. anterodentatus*	*H. bicuspidatus*	*H. changxingensis*	*H. eurypyge*	*H. inflatus*	*H. latidentatus*	*H. magnus*	*H. parvus*	*H. pisai*	*H. postparvus*	*H. praeparvus*	*H. sosioensis*	*H. typicalis*	*I. huckriedei*	*I. inflata*	*I. isarcica*	*I. lobata*	*I. peculiaris*	*I. prisca*	*I. staeschei*	*I. turgida*	*M. ultima*	*N. carinata*	*N. changxingensis*	*C. dicerocarinata*	*N. deflecta*	*C. kazi*	*C. lerhmanni*	*N. meishanensis*	*N. nassuchuki*	*C. orchardi*	*N. planata*	*N. subcarinata*	*N. parasubcarinata*	*N. taylorae*	*N. tulongensis*	*N. yini*	*N. zhangi*	*N. postwangi*	*N. zhejiangensis*	*N. liangshanensis*	UAZs
Yangou	LY-37			0	1																																								5
	LY-36	7		0	1		1																1																						5
	LY-35+50	6	1	0	1		1		0		1											1																						5
	LY-35+37			0	1		1		0		1											1																						5
	LY-35+25			0	1		1		0		1											1																						5
	LY-35+15			0	1		1		0		1											1																						5
	LY-34+55			0	1		1		0		1											1																						5
	LY-34+45			0	1		1		0		1											1																						5
	LY-34+33			0	1		1		0		1											1																						5
	LY-34+20			0	1		1		0		1											1																						5
	LY-34+10			0	1		1		0		1											1																						5
	LY-33+20			0	1		1		0		1											1																						5
	LY-33+0			0	1		1		0		1											1																						5
	LY-25+0			0	1		1		0		1											1																						5
	LY-24+0			0	1		1		0		1											1																						5
	LY-23+0						1		0		1											1																						5
	LY-22+0						0		0		1											1																						5
	LY-21-5						0		0		1											1																						5
	LY-21-4	5			1		0		0		1											1																						5
	LY-21-3	4			1		0		0																																		4-5
	LY-21-2				1		0		0																																		4-5
	LY-21-1	3			1		0		0																																		3-5
	LY-20-0																																									3-4
	LY-20+30	2																																								1-4
	LY-20+15																																									1-2
	LY-20+0																																									1-4 (1-2)
	LY-19+65																																									1-4 (1-2)
	LY-19+50																																									1-4 (1-2)
	LY-19+35																																									1
	LY-19+10																																									1
	LY-18+87																																									1
	LY-18+45	1																																								1
Bianyang	BYC-6	4			1	1				1													1																				4-5
	BYC-5	3			1	1				1																																2-4
	BYC-4	2			1																																					2-4
	BYC-3	1																																								1
Meishan	29 (=D/C-12	5			1	1																																				5
	28 (=D/C-11	4			1	1				1																																4
	27d	3			1	1				1	0																															3
	27c				1	1				1																																	3
	27b				1	1				1																																	3
	27a				1	1				1																																	3
	26				1	1				1																																	2-3
	25																																									2
	24e	2																																								1
	24d (=D/C-9)	1										0																														1
	24c (=D/C-10 and AW/C-1)																																									
	24b																																									
	24a																																									

Sections	Conodont-bearing bed number	LMHs	*H. altus*	*H. anterodentatus*	*H. bicuspidatus*	*H. changxingensis*	*H. eurypyge*	*H. inflatus*	*H. latidentatus*	*H. magnus*	*H. parvus*	*H. pisai*	*H. postparvus*	*H. praeparvus*	*H. sosioensis*	*H. typicalis*	*I. huckriedei*	*I. inflata*	*I. isarcica*	*I. lobata*	*I. peculiaris*	*I. prisca*	*I. staeschei*	*I. turgida*	*M. ultima*	*N. carinata*	*N. changxingensis*	*C. dicerocarinata*	*N. deflecta*	*C. kazi*	*C. lerhmanni*	*N. meishanensis*	*N. nassuchuki*	*C. orchardi*	*N. planata*	*N. subcarinata*	*N. parasubcarinata*	*N. taylorae*	*N. tulongensis*	*N. yini*	*N. zhangi*	*N. postwangi*	*N. zhejiangensis*	*N. liangshanensis*	UAZs
Daijiagou	DJG 1.30-1.34									1																																		3-6 (5-6)
	DJG 1.20-1.30									1																																			3-6 (5-6)
	DJG 1.05-1.10	5									1						1																											5
	DJG 0.86-1.0										1																																	3-6 (3-5)
	DJG 0.73-0.75									1			1		1																													3
	DJG 0.58-0.73	4								1			1		1																													1	3
	DJG 0.45-0.5														1																													2-4 (2-3)
	DJG 005	3			1																												1									1		1-2
	DJG 0.15-0.2				1											1																											1		1-2
	DJG 007				1											1																											1		1-2
	DJG 008				1											1																											1		1-2
	DJG 009				1											1																											1		1-2
	DJG 011				1											1																											1		1-2
	DJG 012				1											1																											1		1-2
	DJG 013	2			1											1																1										1		1-2
	DJG 014					1										1																1												2-4 (1-2)
	DJG -15.5					1										1																1												1-4 (1-2)
	DJG -19															1																1												1-4 (1-2)
	DJG -21															1																1												1-4 (1-2)
	DJG -32															1																1												1-4 (1-2)
	DJG -35.1															1																1												1-4 (1-2)
	DJG -39.3															1																1												1-4 (1-2)
	DJG -43.8															1																1												1-4 (1-2)
	DJG -49.5															1																1												1-4 (1-2)
	DJG -53.6															1																1												1-4 (1-2)
	DJG -60.9															1																1												1-4 (1-2)
	DJG -66.6															1																1												1-4 (1-2)
	DJG -70.8															1																					1							1-2
	DJG -75.8	1														1																					1							1-2
	DJG -80															1																					1							1-2
	DJG -82															1																					1							1-2
	DJG -85															1																					1							1-2
	DJG -88.2															1																												1-5 (1-2)
	DJG -91															1																												1-5 (1-2)
	DJG -98															1																												1-5 (1-2)
	DJG +24.3															1																												1-5 (1-2)
	DJG +19.3															1																												1-5 (1-2)
	DJG +9.6															1																												1-5 (1-2)
	DJG 018																																											1	
Zhongzhai	LZ30	2			1					1																															0				2-3
	LZ28	1	1	1							1																																		2-5 (4-5)

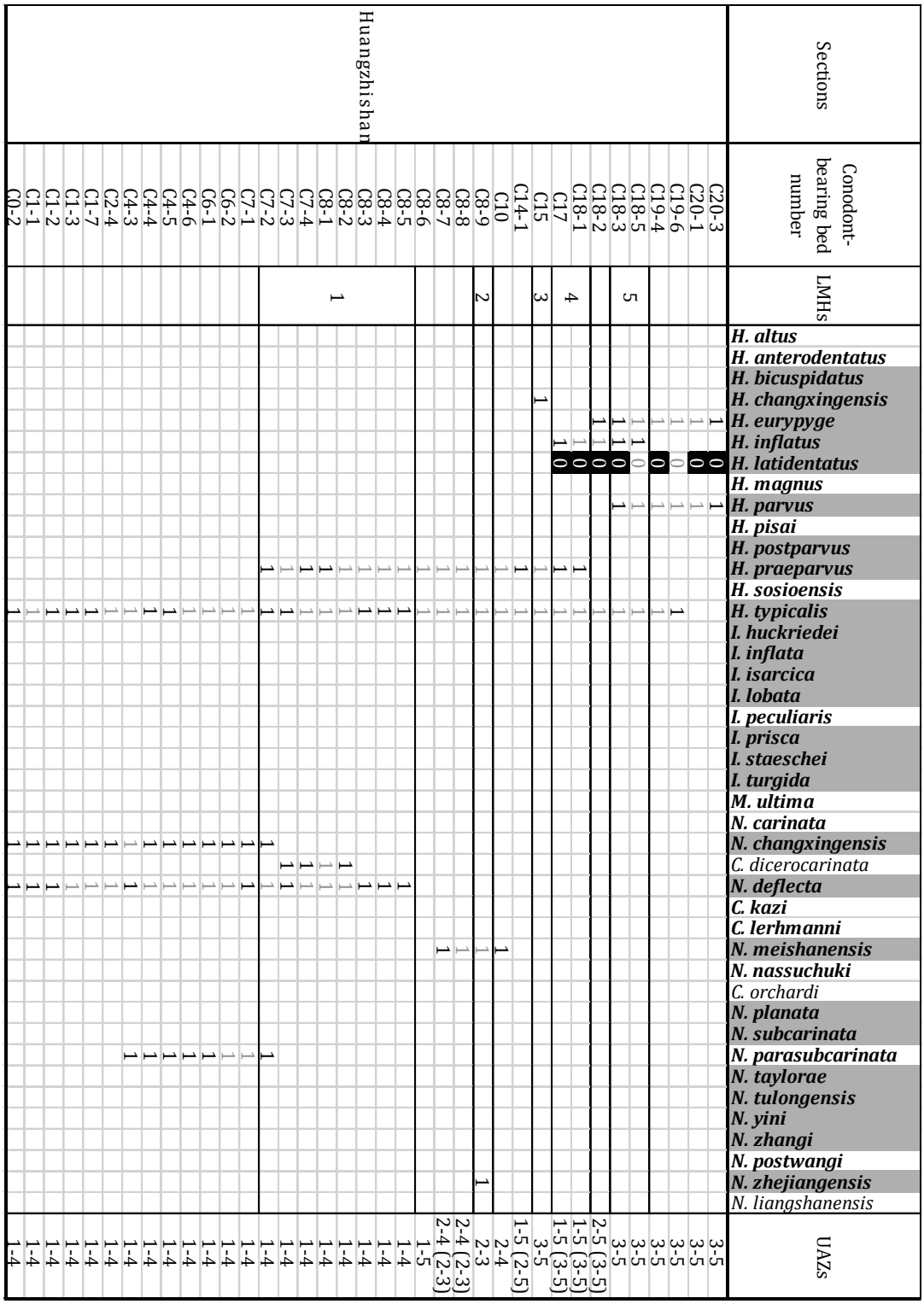
Sections
Conodont-bearing bed number
LMHs
UAZs
Huangzhishan
C20-3
C20-1
C19-6
C19-4
C18-5
C18-3
C18-2
C18-1
C17
C15
C14-1
C10
C8-9
C8-8
C8-7
C8-6
C8-5
C8-4
C8-3
C8-2
C8-1
C7-4
C7-3
C7-2
C7-1
C6-2
C6-1
C4-6
C4-5
C4-4
C4-3
C2-4
C1-7
C1-3
C1-2
C1-1
C0-2
1
2
3
4
5
H. altus
H. anterodentatus
H. bicuspidatus
H. changxingensis
H. eurypyge
H. inflatus
H. latidentatus
H. magnus
H. parvus
H. pisai
H. postparvus
H. praeparvus
H. sosioensis
H. typicalis
I. huckriedei
I. inflata
I. isarcica
I. lobata
I. peculiaris
I. prisca
I. staeschei
I. turgida
M. ultima
N. carinata
N. changxingensis
C. dicerocarinata
N. deflecta
C. kazi
C. lerhmanni
N. meishanensis
N. nassuchuki
C. orchardi
N. planata
N. subcarinata
N. parasubcarinata
N. taylorae
N. tulongensis
N. yini
N. zhangi
N. postwangi
N. zhejiangensis
N. liangshanensis
3-5
3-5
3-5
3-5
3-5
3-5
2-5 (3-5)
1-5 (3-5)
1-5 (3-5)
3-5
1-5 (2-5)
2-4
2-3
2-4 (2-3)
2-4 (2-3)
1-5
1-4
1-4
1-4
1-4
1-4
1-4
1-4
1-4
1-4
1-4
1-4
1-4
1-4
1-4
1-4
1-4
1-4
1-4
1-4
1-4
1-4
1-4
1-4
1-4
1-4
1-4
1-4
1-4

Appendix B: Matrix of occurrence built after the optimization. The first column represents the local maximal horizons (LMHs) of each section. '0' is absence, '1' is presence. The grey squares represent virtual occurrences deduced from the optimization. N, *Neogondolella*; H, *Hindeodus*; I, *Isarcicella*; E, *Ellisonia*.

Sections	Zhongzhai		Bianyang					Daijiagou					Huangzhishan					Chaotian				
LMHs	2	1	5	4	3	2	1	5	4	3	2	1	5	4	3	2	1	5	4	3	2	1
H. bicuspidatus	0	1	0	0	0	0	0	0	0	0	0	0	0	0	0	0	0	0	0	0	0	0
H. changxingensis	0	0	0	0	0	0	0	0	0	0	0	0	0	0	1	0	0	0	0	0	0	0
H. eurypyge	0	0	0	1	1	0	0	0	0	1	0	0	0	0	0	0	0	0	0	0	0	0
H. inflatus	0	0	0	1	0	0	0	0	0	0	0	0	0	1	0	0	0	0	0	0	0	0
H. latidentatus	1	0	0	0	0	0	0	0	0	0	0	0	0	0	0	0	0	0	0	0	0	0
H. parvus	1	1	0	1	0	0	0	1	0	0	0	0	1	0	0	0	0	0	0	0	0	0
H. postparvus	0	0	0	0	0	0	0	0	0	0	0	0	0	0	0	0	0	0	0	0	0	0
H. praeparvus	0	1	0	1	1	0	0	0	0	0	0	0	1	0	1	1	1	0	0	0	0	0
H. typicalis	1	0	0	0	1	0	0	0	1	1	0	0	1	0	1	1	1	0	0	0	0	0
I. huckriede	0	0	0	0	0	0	0	0	0	0	0	0	0	0	0	0	0	0	0	0	0	0
I. inflata	0	0	0	0	0	0	0	1	0	0	0	0	0	0	0	0	0	0	0	0	0	0
I. isarcica	0	0	0	0	0	0	0	0	0	0	0	0	0	0	0	0	0	0	0	0	0	0
I. lobata	0	0	0	0	0	0	0	0	0	0	0	0	0	0	0	0	0	0	0	0	0	0
I. prisca	0	0	0	0	0	0	0	0	0	0	0	0	0	0	0	0	0	0	0	0	0	0
I. staeschei	0	0	0	0	0	0	0	0	0	0	0	0	0	0	0	0	0	0	0	0	0	0
I. turgida	0	0	0	1	0	0	0	0	0	0	0	0	0	0	0	0	0	0	0	0	0	0
N. changxingensis	0	0	0	0	0	0	1	0	0	0	1	0	0	0	0	0	1	0	0	0	1	1
N. deflecta	0	0	0	0	0	1	1	0	0	0	0	0	0	0	0	0	1	0	0	0	1	1
N. meishanensis	0	1	0	0	0	0	0	0	0	1	0	0	0	0	0	1	0	0	0	0	1	1
N. planata	0	0	0	0	0	0	0	0	0	0	0	0	0	0	0	0	0	0	0	0	0	0
N. subcarinata	0	0	0	0	0	0	0	0	0	0	1	0	0	0	0	0	0	0	0	1	1	1
N. taylorae	0	0	0	0	0	0	0	0	0	0	0	0	0	0	0	0	0	0	0	1	1	1
N. tulongensis	0	0	0	0	0	0	0	0	0	0	0	0	0	0	0	0	0	0	0	0	0	1
N. yini	0	0	0	0	0	0	1	0	0	0	1	0	0	0	0	0	0	0	0	0	0	0
N. zhangi	0	0	0	0	0	0	0	0	0	0	0	0	0	0	0	0	0	0	0	0	0	0
N. zhejiangensis	0	0	0	0	0	0	0	0	0	0	0	0	0	0	0	0	1	0	0	0	1	0

Sections	LMHs	*H. bicuspidatus*	*H. changxingensis*	*H. eurypyge*	*H. inflatus*	*H. latidentatus*	*H. parvus*	*H. postparvus*	*H. praeparvus*	*H. typicalis*	*I. huckriede*	*I. inflata*	*I. isarcica*	*I. lobata*	*I. prisca*	*I. staeschei*	*I. turgida*	*N. changxingensis*	*N. deflecta*	*N. meishanensis*	*N. planata*	*N. subcarinata*	*N. taylorae*	*N. tulongensis*	*N. yini*	*N. zhangi*	*N. zhejiangensis*
Wuzhuan	4	1	0	0	0	0	1	1	0	0	0	0	0	0	0	0	0	0	0	0	0	0	0	0	0	0	0
	3	1	0	0	0	0	1	0	1	1	0	1	1	1	0	1	1	0	0	0	0	0	1	0	0	0	0
	2	0	0	1	0	0	1	0	1	1	0	0	0	0	0	0	1	0	0	0	0	0	1	0	0	0	0
	1	0	0	0	0	0	1	0	0	1	0	0	0	0	0	0	0	0	0	0	0	0	1	0	0	0	0
Dawen	4	0	0	0	0	0	0	1	0	0	0	0	0	0	0	1	0	0	0	0	0	0	1	0	0	0	0
	3	0	0	0	0	0	1	0	0	0	0	0	0	0	0	0	0	0	0	0	0	0	0	0	0	0	0
	2	0	0	1	1	1	0	0	1	0	0	0	0	0	0	0	0	0	0	0	0	0	0	0	0	0	0
	1	0	0	1	0	1	0	0	1	1	0	0	0	0	0	0	0	0	0	0	0	0	0	0	0	0	1
Dajiang	4	0	0	0	0	0	1	1	0	0	0	0	0	0	0	0	1	0	0	0	0	0	0	0	0	0	0
	3	0	0	0	0	0	1	0	1	0	0	0	0	1	0	1	1	0	0	0	1	0	1	0	0	0	0
	2	0	0	0	0	0	1	0	1	1	0	0	1	1	0	1	1	0	0	0	0	0	0	0	0	0	0
	1	0	0	0	0	0	1	0	1	1	0	0	0	0	1	0	1	1	0	1	0	0	0	0	0	0	0
Shangsi	5	1	0	1	0	0	1	0	1	0	0	1	1	1	0	1	1	0	0	0	0	0	1	0	0	0	0
	4	0	0	1	0	0	1	0	1	0	1	0	0	0	1	0	1	0	0	0	0	0	1	0	0	0	0
	3	0	1	1	0	0	0	0	1	0	1	0	0	0	1	0	1	0	1	0	0	0	1	0	0	0	0
	2	0	0	0	0	0	0	0	0	0	0	0	0	0	0	0	0	0	1	1	0	0	0	1	0	0	0
	1	0	0	0	0	0	0	0	0	0	0	0	0	0	0	0	0	1	1	0	0	1	0	1	1	1	0
Meishan	5	0	1	0	1	0	0	0	1	0	1	1	1	1	0	1	1	0	0	0	1	0	0	0	0	0	0
	4	0	1	0	1	0	1	0	1	0	1	0	0	1	1	1	0	1	1	1	1	0	1	0	0	0	0
	3	0	1	1	1	0	1	0	1	1	1	0	0	0	0	0	0	1	1	1	1	0	1	1	0	0	1
	2	0	0	0	1	1	0	0	1	1	0	0	0	0	0	0	0	1	1	1	0	1	0	1	0	0	1
	1	0	0	0	1	1	0	0	1	1	0	0	0	0	0	0	0	1	1	0	0	1	0	1	1	1	1
Yangou	7	1	0	1	0	0	1	0	1	0	0	0	1	0	0	1	0	0	0	0	0	0	0	0	0	0	0
	6	1	0	1	0	0	1	0	1	1	0	0	0	0	0	1	0	0	0	0	0	0	1	0	0	0	0
	5	0	1	0	0	0	1	0	1	1	0	0	0	0	0	0	1	0	0	0	0	0	1	0	0	0	0
	4	0	1	0	0	0	0	0	1	1	0	0	0	0	0	0	0	0	0	0	0	0	1	0	0	0	0
	3	0	1	0	0	0	0	0	1	1	0	0	0	0	0	0	0	1	0	0	0	0	0	0	0	0	0
	2	0	0	0	0	0	0	0	1	0	0	0	0	0	0	0	0	1	1	0	0	1	0	0	0	0	0
	1	0	0	0	0	0	0	0	0	0	0	0	0	0	0	0	0	1	0	0	0	0	0	0	0	1	0

CHAPTER II.B

REPLY TO THE COMMENT ON QUANTITATIVE BIOCHRONOLOGY OF THE PERMIAN-TRIASSIC BOUNDARY IN SOUTH CHINA BASED ON CONODONT UNITARY ASSOCIATIONS

Morgane Brosse, Hugo Bucher and Nicolas Goudemand

Accepted in Earth-Science Reviews

“Do not meddle in the affairs of wizards, for they are subtle and quick to anger.”

J.R.R. Tolkien, The Fellowship of the Ring

ARTICLE IN PRESS

EARTH-02345; No of Pages 3

Earth-Science Reviews xxx (2016) xxx–xxx

Contents lists available at ScienceDirect

Earth-Science Reviews

journal homepage: www.elsevier.com/locate/earscirev

Discussion

Reply to the Comment on "Quantitative biochronology of the Permian–Triassic boundary in South China based on conodont unitary associations"

Morgane Brosse [a,*], Hugo Bucher [a], Nicolas Goudemand [a,b]

[a] Paläontologisches Institut und Museum der Universität Zürich, Karl Schmid-Strasse 4, CH 8006 Zürich, Switzerland
[b] Institut de Génomique Fonctionnelle de Lyon, CNRS UMR 5242, Université de Lyon, Université Claude Bernard Lyon 1, Ecole Normale Supérieure de Lyon, 46 Allée d'Italie, Lyon 69364, France

ARTICLE INFO

Article history:
Received 5 July 2016
Received in revised form 20 July 2016
Accepted 21 July 2016
Available online xxxx

1. Introduction

In their Comment, Jiang et al. (2016) claim that the discordance between our zonation (Brosse et al., 2016) and the interval zones does not rest on the use of the Unitary Association method (Guex, 1991; Guex et al., 2015) per se but on our "failure to use the most recent published conodont ranges from some key Chinese sections". They add that our analysis is based on "unreliable taxonomic data sets with unjustified taxonomic re-assessments", and hence, that we did not demonstrate that the Unitary Association method performs better than traditional interval zones.

Additionally, the Comment by Jiang et al. (2016) contains misunderstandings pertaining to the method used in our study (Brosse et al., 2016). Our goal was to apply the Unitary Association Method on a dataset of conodont distributions from South China around the Permian–Triassic boundary (PTB) in order to reassess the quality of the corresponding data and to provide a discrete and robust alternative zonation to the continuous, First-Occurrence-based interval zones. Such interval zones are routinely utilized in Permian and Triassic conodont biostratigraphy, regardless of their abundant internal contradictions.

Three categories of points of contention can be extracted from the Comment of Jiang et al. (2016): method, selection of data and taxonomy, and illustrations. Each of these is addressed separately below.

2. Method

Fig. 1 complies with the recommendation of Jiang et al. (2016) and takes into account all the recent literature, summarizing the most recent published conodont ranges from the relevant sections. The reader will immediately observe that the sequences of First Occurrences (FOs) used in the most recently published interval zones occupy contradictory positions between the different sections. This is precisely the main criticism expressed in our work. This problem cannot be solved by simply standardizing the taxonomy of the considered taxa. Many contradictions do persist after taxonomic homogenization. As conceded by Jiang et al. (2016), FOs are prone to diachronism. But contrary to what Jiang et al. (2016) suggest, sampling effort is not the only nor the main reason for such diachronism and PTB sections from South China are no exceptions in this respect. Fig. 9 of Brosse et al. (2016) demonstrates the contrary. Ironically enough, Jiang et al. (2016) acknowledge that Last Occurrences (LOs) can be diachronous because of local, ecological differences, but they exclude that FOs can be affected. In reality, these authors unduly equate every local FO with an alleged instantaneous spreading of a species across all sections. Incidentally, such an unwarranted assumption also deliberately ignores that speciation is an intrinsically space-restricted evolutionary process.

Contradictions in the superpositional relationships of FOs prevent *reliable* correlations between sections. The main points in using the Unitary Association method are that (1) one can quantitatively assess the quality of the data, in particular one can detect contradictions, even subtle ones implying three or four taxa in circular or sub-circular relationships; (2) one can iteratively use the information drawn from the detected contradictions to critically reassess the quality of the data, occasionally pointing out previously unseen sampling or taxonomic determination biases; (3) one can drastically reduce the impact of diachronism of single taxa on the resulting zonation by considering only maximal associations of taxa; and (4) all constructed biozones are defined in an exclusive way, i.e. by the occurrence of a characteristic taxon or the co-occurrence of characteristic pairs of taxa. For all these reasons, we consider the Unitary Association method as the single major conceptual and practical advance in the field of biochronology during the last three decades. In particular, we consider that the accuracy (understood as trueness of the results) of the resulting zonation is greatly improved.

The improvement in terms of accuracy and robustness may come with a reduction of the "resolution", but it must be noted that the "resolution" obtained with interval zones is misleading in that it only represents a very local measure on which no constraint on lateral reproducibility is applied. As opposed to this, poorly laterally reproducible preliminary Unitary Associations can be merged optimally to ensure that the resulting Unitary Association Zones are laterally reproducible, i.e., that the resulting zones can be effectively employed to build robust correlations between sections.

* Corresponding author.
E-mail address: morgane.brosse@pim.uzh.ch (M. Brosse).

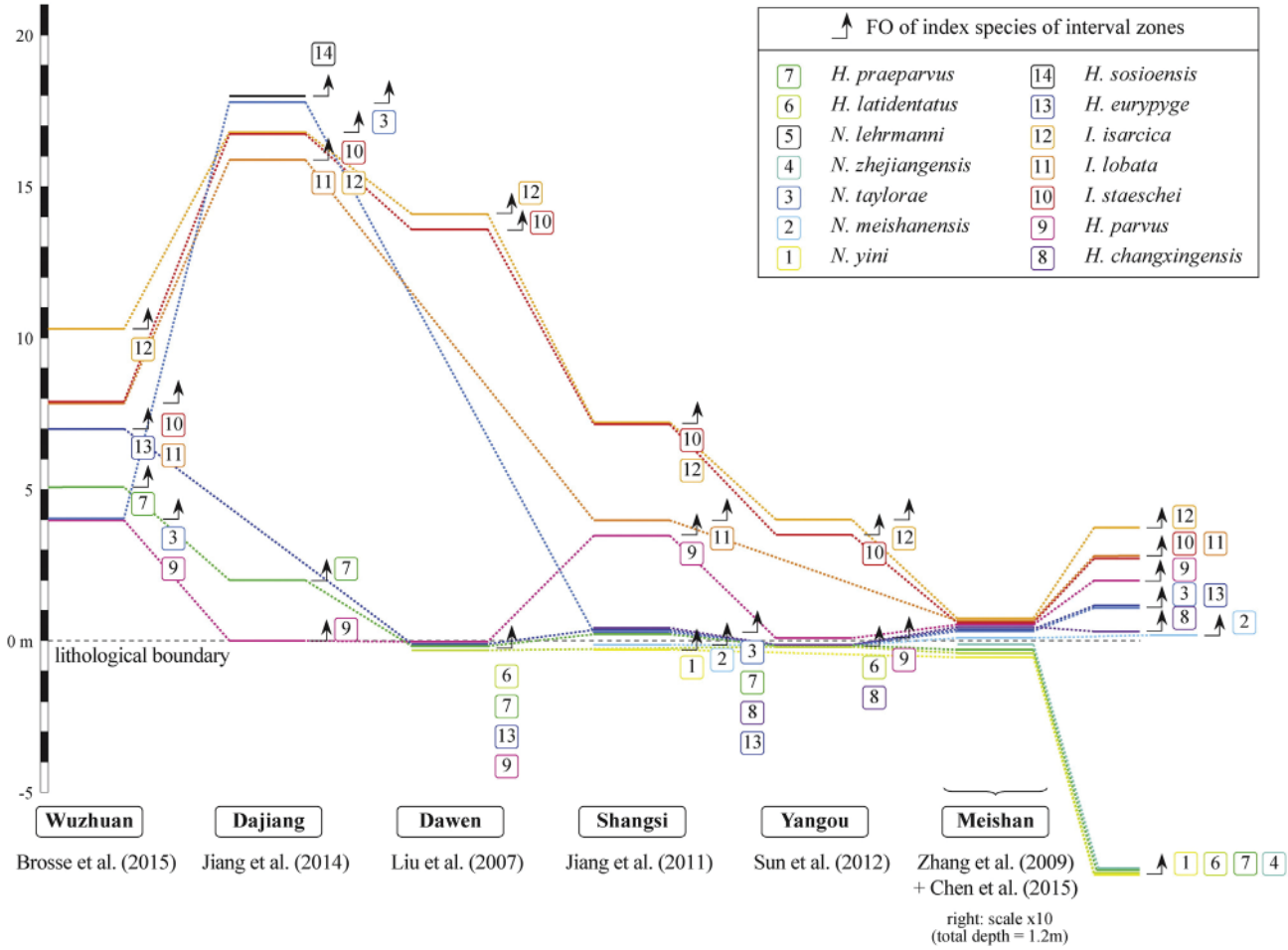

Fig. 1. Biostratigraphical correlations of the Wuzhuan, Dajiang, Dawen, Shangsi, Yangou and Meishan sections by means of first occurrences (FOs). The vertical scale (stratigraphical thickness in metres) is the same for the six sections. The 0 on the picture refers to the lithological boundary. *H: Hindeodus*, *I: Isarcicella*, *N: Neogondolella*.

This advance also comes with the recognition that some beds do not contain enough information to be unequivocally dated. Those beds lie within so-called intervals of separation and reflect the amount of undefined and contradictory stratigraphic relations present in each dataset. Contrary to the Comment of Jiang et al. (2016), the fact that a boundary such as the PTB lies within an interval of separation does not at all imply that it is not precisely located or defined. Thicknesses of intervals of separation tend to correlate negatively with the density of biostratigraphic relations contained in the data set. Only with Unitary Associations will the biostratigrapher be directly confronted to the quality of the data to be processed and its potential consequences. The user will be forced to acknowledge that some data sets can be partly or completely under-constrained and thus inappropriate for constructing zones having constant superposition order and broad lateral reproducibility. Unitary Associations advance the field of biochronology to an unprecedented point where data can be carefully and quantitatively evaluated, where data sets are amenable to optimization and where a measurable degree of uncertainty can be assigned to a biozonation. In contrast and per definition, interval zones have no uncertainty and form a frozen succession of continuous zones.

3. Selection criteria and taxonomy

Jiang et al. (2016) misunderstood the selection criteria used for the construction of our data set. Only publications with raw range charts and adequate illustrations of documented taxa were taken into account. The "missing" papers mentioned in the Comment were not included in our data set because they did not meet with the above-mentioned criteria. Chen et al. (2015) do not provide any illustrations of conodonts, nor a detailed range chart. The range chart of Zhang et al. (2009) cannot be used because illustrations of taxonomic assignments are lacking: their 16 conodont photographs are in fact copied from Zhang et al. (1995), Yin et al. (2001), and Zhang et al. (2007), and are reproduced without any citation of original sources. Liu et al. (2007) provide too few illustrations for assessing their taxonomic assignments and the study of Chen et al. (2009) must therefore be preferred for the Dawen section. The range chart of Jiang et al. (2015; see their Fig. 2) is based on that of Yan et al. (2013), which is included in our data set. Contrary to a statement made in the Comment, the data of Jiang et al. (2011a,b) were included in our analysis. Contrary to the claim of Jiang et al. (2016), our data also includes the updated stratigraphical ranges of the considered sections. These include the taxonomic adjustment made by Jiang et al. (2011b) who re-assigned *I. staeschei* sensu Jiang et al. (2007) from the bed 27d at Meishan to *I. huckriedei*, and moved up the *I. staeschei* IZ to bed 28 (see our Table 1 and Appendix A; Brosse et al., 2016). The same applies to *H. changxingensis*, which we correctly placed in bed 26 (after Nicoll et al., 2002) in our model, as shown in Appendix A (Brosse et al., 2016).

4. Illustrations

We thank Jiang et al. (2016) for spotting a typo in the illustration of the holotype of *Isarcicella lobata* in Fig. 1.10 of Brosse et al. (2016). Our Fig. 1.10 reproduces the illustration of "*I. lobata* morphotype 1" of Perri and Farabegoli (2003; pl. 3, Figs. 27–29). The holotype of *I. lobata*

is illustrated by Perri and Farabegoli (2003) in their plate 3, Figs. 21–23, to which the reader is now correctly referred.

A graphic typo is also correctly found in Figs. 9, 10 and 15. In Meishan, the dashed line separating the Changxing and Yinkeng formations is correctly placed between beds 24 and 25. Graphic misplacement of this boundary has absolutely no influence on the validity of our biochronological results.

Acknowledgments

Editor André Strasser helped improving the Reply. This work is supported by the Swiss NSF project 200021_135446 (to H.B.) and a French ANR @RAction grant (project EvoDevOdonto to N.G.).

References

Brosse, M., Bucher, H., Goudemand, N., 2016. Quantitative biochronology of the Permian–Triassic boundary in South China based on conodont unitary associations. Earth Sci. Rev. 155, 153–171.

Chen, J., Beatty, T.W., Henderson, C.M., Rowe, H., 2009. Conodont biostratigraphy across the Permian–Triassic boundary at the Dawen section, Great Bank of Guizhou, Guizhou Province, South China: implications for the Late Permian extinction and correlation with Meishan. J. Asian Earth Sci. 36 (6):442–458. http://dx.doi.org/10.1016/j.jseaes.2008.08.002.

Chen, Z.Q., Yang, H., Luo, M., Benton, M.J., Kaiho, H., Zhao, L.S., Huang, Y.G., Zhang, K.X., Fang, Y.H., Jiang, H.S., Qiu, H., Li, Y., Tu, C.Y., Shi, L., Zhang, L., Feng, X.Q., Chen, L., 2015. Complete biotic and sedimentary records of the Permian–Triassic transition from Meishan section, South China: ecologically assessing mass extinction and its aftermath. Earth-Sci. Rev. 149, 63–103.

Guex, J., 1991. Biochronological Correlations. Springer Verlag.

Guex, J., Galster, F., Hammer, Ø., 2015. Discrete Biochronological Time Scales.

Jiang, H., Lai, X., Luo, G., Aldridge, R., Zhang, K., Wignall, P., 2007. Restudy of conodont zonation and evolution across the P/T boundary at Meishan section, Changxing, Zhejiang, China. Glob. Planet. Chang. 55 (1):39–55. http://dx.doi.org/10.1016/j.gloplacha.2006.06.007.

Jiang, H., Lai, X., Yan, C., Aldridge, R.J., Wignall, P., Sun, Y., 2011a. Revised conodont zonation and conodont evolution across the Permian–Triassic boundary at the Shangsi section, Guangyuan, Sichuan, South China. Glob. Planet. Chang. 77 (3):103–115. http://dx.doi.org/10.1016/j.gloplacha.2011.04.003.

Jiang, H., Aldridge, R.J., Lai, X., Yan, C., Sun, Y., 2011b. Phylogeny of the conodont genera Hindeodus and Isarcicella across the Permian–Triassic boundary. Lethaia 44 (4): 374–382. http://dx.doi.org/10.1111/j.1502-3931.2010.00248.x.

Jiang, H., Joachimski, M.M., Wignall, P.B., Zhang, M., Lai, X., 2015. A delayed end-Permian extinction in deep-water locations and its relationship to temperature trends (Bianyang, Guizhou Province, South China). Palaeogeogr. Palaeoclimatol. Palaeoecol. 440, 690–695.

Jiang, H.S., Wignall, P.B., Chen, Z.Q., Xie, S.H., Lai, X.L., Song, H.J., Wang, L., 2016. Comment on "Quantitative biochronology of the Permian–Triassic boundary in South China based on conodont unitary associations". Earth Sci. Rev.

Liu, J.B., Ezaki, Y., Yang, S.R., Wang, H.F., Adachi, N., 2007. Age and sedimentology of microbialites after the end-Permian mass extinction in Luodian, Guizhou Province. J. Palaeogeogr. 9, 473–486 (in Chinese with English abstract).

Nicoll, R.S., Metcalfe, I., Cheng-Yuan, W., 2002. New species of the conodont genus *Hindeodus* and the conodont biostratigraphy of the Permian–Triassic boundary interval. J. Asian Earth Sci. 20 (6):609–631. http://dx.doi.org/10.1016/S1367-9120(02)00021-4.

Perri, M.C., Farabegoli, E., 2003. Conodonts across the Permo-Triassic boundary in the Southern Alps. Cour. Forschungsinst. Senck. 281–314.

Yan, C., Wang, L., Jiang, H., Wignall, P.B., Sun, Y., Chen, Y., Lai, X., 2013. Uppermost Permian to Lower Triassic conodonts at Bianyang section, Guihzou province, South China. Palaios 28 (8):509–522. http://dx.doi.org/10.2110/palo.2012.p12-077r.

Yin, H., Zhang, K., Tong, J., Yang, Z., Wu, S., 2001. The global stratotype section and point (GSSP) of the Permian–Triassic boundary. Episodes 24 (2), 102–114.

Zhang, K., Lai, X., Ding, M., Liu, J., 1995. Conodont sequence and its global correlation of Permian–Triassic boundary in Meishan section, Changxing, Zhejiang Province. Earth Sci. J. China Univ. Geosci. 20 (6), 669–676.

Zhang, K., Tong, J., Shi, G.R., Lai, X., Yu, J., He, W., Peng, Y., Jin, Y., 2007. Early Triassic conodont–palynological biostratigraphy of the Meishan D Section in Changxing, Zhejiang Province, South China. Palaeogeogr. Palaeoclimatol. Palaeoecol. 252 (1): 4–23. http://dx.doi.org/10.1016/j.palaeo.2006.11.031.

Zhang, K., Tong, J., Lai, X., Jiang, H., 2009. Progress on study of conodont sequence for the GSSP section at Meishan, Changxing, Zhejiang Province, South China. Acta Palaeontol. Sin. 48, 474–486 (in Chinese with English abstract).

Chapter III

Conodont-based Griesbachian biochronology of the Guryul Ravine section (Induan, Early Triassic, Kashmir, India)

Morgane Brosse, Marc Leu, Aymon Baud, Ghulam Mohmmad Bhat, Hugo Bucher, Torsten Vennemann and Nicolas Goudemand

Formatted for Geobios

Conodont-based Griesbachian biochronology of the Guryul Ravine section (Induan, Early Triassic, Kashmir, India)

Morgane Brosse[a*], Aymon Baud[b], Ghulam Mohmmad Bhat[c], Hugo Bucher[a], Marc Leu[a], Torsten Vennemann[d], Nicolas Goudemand[e, a]

[a]Paläontologisches Institut und Museum der Universität Zürich, Karl Schmid-Strasse 4, CH-8006 Zürich, Switzerland. morgane.brosse@pim.uzh.ch

[b]Geological Museum, Lausanne University, Quartier UNIL-Dorigny, Bâtiment Anthropole, CH-1015 Lausanne, Switzerland.

[c]Department of Geology, University of Jammu, Jammu and Kashmir State, India.

[d]Institute of Earth Surface Dynamics, University of Lausanne, Géopolis, 1015 Lausanne, Switzerland.

[e]Univ. Lyon, ENS de Lyon, CNRS, Univ. Claude Bernard Lyon 1, Institut de Génomique Fonctionnelle de Lyon, UMR 5242, 46 Allée d'Italie, F-69364 Lyon Cedex 07, France.

Abstract

The Guryul Ravine section (Kashmir, India) exposes one the world's most continuous and carbonated rock successions throughout the Permian-Triassic boundary and beyond. Due to political instability in this region, the biostratigraphy of this section has not been updated for nearly three decades. Following our new high resolution sampling, we reassess here the conodont biochronology and isotopic records of the fifteen lowermost stratigraphical metres (Member E) of the Khunamuh Formation at Guryul Ravine section. This interval includes both the Permian-Triassic and the Griesbachian-Dienerian (Induan) boundaries. The FO of *Hindeodus parvus*, the index for the base of the Triassic, is confirmed in the middle of sub-member E_2 (Unit 56 in Matsuda, 1981; our bed GUR09). We calculated 10 Unitary Association zones based on the conodont record from China and from Guryul Ravine. UAZ_{1-2} are Late Permian and identified only in South China, UAZ_{3-10} are identified both in China and Guryul Ravine. The Griesbachian-Dienerian boundary is included within the interval of separation between UAZ_7 and UAZ_8. At Guryul Ravine, the boundary is precisely constrained between beds GUR310 and GUR311 and corresponds to the replacement of segminiplanate (here *Neogondolella*) to segminate (*Sweetospathodus* and *Neospathodus*) conodonts. Above this 40 cm uncertainty interval, we also observe a conspicuous positive excursion of the $d^{13}C$ signal, which records a significant event at least at the scale of the Tethyan realm, and could be used as a secondary proxy for the Griesbachian-Dienerian boundary. This global perturbation of the carbon isotope signal is linked to a climate change at the Griesbachian-Dienerian transition, from a cool and dry to a hot and humid climate. This transition could be the trigger of the migration of neogondolellids towards the high latitude, and of the radiation of neospathodids during the Dienerian.

Keywords

Conodonts, carbon cycle, Permian-Triassic boundary, Griesbachian-Dienerian boundary, Guryul Ravine, Kashmir.

1. Introduction

The Permian-Triassic boundary mass extinction, between 251.941±0.037 and 251.880±0.031 Ma (Burgess et al., 2016) and calculated at 251.956 ± 0.033 Ma (Baresel et al., 2016) is marked by the disappearance of more than 90% of all marine species (Raup, 1979) and by major changes in plant communities (Retallack, 1995; Hochuli et al., 2010). Understanding the mechanisms of this event and of the subsequent biotic recovery requires high-resolution biochronology. The relative abundance, the wide spatial distribution, and the high evolutionary rates of conodont microfossils have made them one of the main biochronological tools for this critical interval.

Contrary to most organisms, conodonts were not much affected by the main extinction event and thrived in the direct aftermath of the extinction (Orchard 2007). Yet, at the Griesbachian-Dienerian (Iower-upper Induan) boundary, presumably much less than 1 Myr after the Permian-Triassic boundary event, conodonts underwent a major faunal turnover, whose cause remains unknown. This boundary is marked also by a positive shift of the carbon isotope record (Horacek et al., 2007; Payne et al., 2004; Corsetti et al., 2005) and a climate change indicated by a major turnover in plant assemblages (swapping from gymnosperm-dominated to a lycopsid spore-dominated assemblages; Hochuli et al., 2016) and by an increase of the riverine $^{87}Sr/^{86}Sr$ lasting until the Smithian (Song et al., 2015). The Griesbachian and Dienerian substages have been defined by Tozer (1965, 1967) in the Canadian Arctic on the basis of ammonoids. Yet, the scarcity of fossils and the discrepancy between the respective records from low and high latitudes, and hence the lack of a consensual global definition of the boundary, have hitherto precluded to correlate the phenomena at the Griesbachian-Dienerian transition with high precision, in particular in equatorial and tropical regions.

Conodont studies on Early Triassic biochronology started in the fifties (e.g. Bender and Kockel, 1963; Bender, 1968; Clark, 1959; 1979; Clark et al., 1979; Huckriede, 1958; Igo, 1994; Koike, 1982, 1996; Kozur and Mostler, 1973; Mosher, 1968, 1970, 1973; Müller, 1956, 1962; Nogami, 1968). After the pioneering works of Hayden (1907) and especially Middlemiss (1909) at Guryul Ravine section, the interest in Guryul Ravine was renewed when Teichert et al. (1970) discovered a putative mixed Permo-Triassic fauna. Ever since Guryul Ravine was considered as one of the world's best locality for the study of the Permian-Triassic boundary (PTB) event: it records indeed a sub-continuous, relatively uniform, fossiliferous (Nakazawa and Kapoor, 1981; Bando, 1981; Sweet, 1970a; Nakazawa et al., 1970, 1975; Sweet 1979; Matsuda, 1981, 1982, 1983, 1984; Agarwal et al., 1980, Agarwal and Singh, 1981) and expanded rock succession straddling the PTB and most of the Early Triassic. For many years, Guryul Ravine was even considered the best candidate for the global stratotype section and point (GSSP) for the base of the Triassic (Kapoor, 1996). Yet, since the eighties and until a few years ago (and sadly, again very recently), the unstable political conditions in Kashmir have precluded access to and sampling of the section. As a consequence most of the recent publications on Guryul Ravine (Baud et al., 1996; Algeo et al., 2007; Brookfield et al., 2003; Wignall et al., 2005) were actually based on material collected more than three decades ago. More recently, a few people, including our group, have resumed fieldwork in Kashmir (Brookfield et al., 2013; Jasper et al., 2016; Singh et al., 2015; Tewari et al., 2015), but hitherto no one has reassessed the conodont record at Guryul Ravine.

However, many advances in conodont biochronology have been realized since the eighties in other parts of the world, in particular in China, where the GSSP for the base of the Triassic has been finally set (Yin et al. 2001) and it has become urgent to reassess the conodont record of this important section in the light of those advances.

In 2012 and 2013, we re-sampled the Guryul Ravine section at high resolution. Here we discuss the results concerning the conodonts from the latest Permian to earliest Dienerian interval (Member E, see Geological settings) and their implications for worldwide correlations.

2. Geological and palaeontological settings

2.1. Geological setting

An IGC Program 630 field workshop has been organized in Kashmir on Nov. 17- 22, 2014. A detailed geological setting can be found in the Guidebook (Baud and Bhat, ed. 2014).

At the end of the Paleozoic, Kashmir was located on the northern margin of Gondwana,

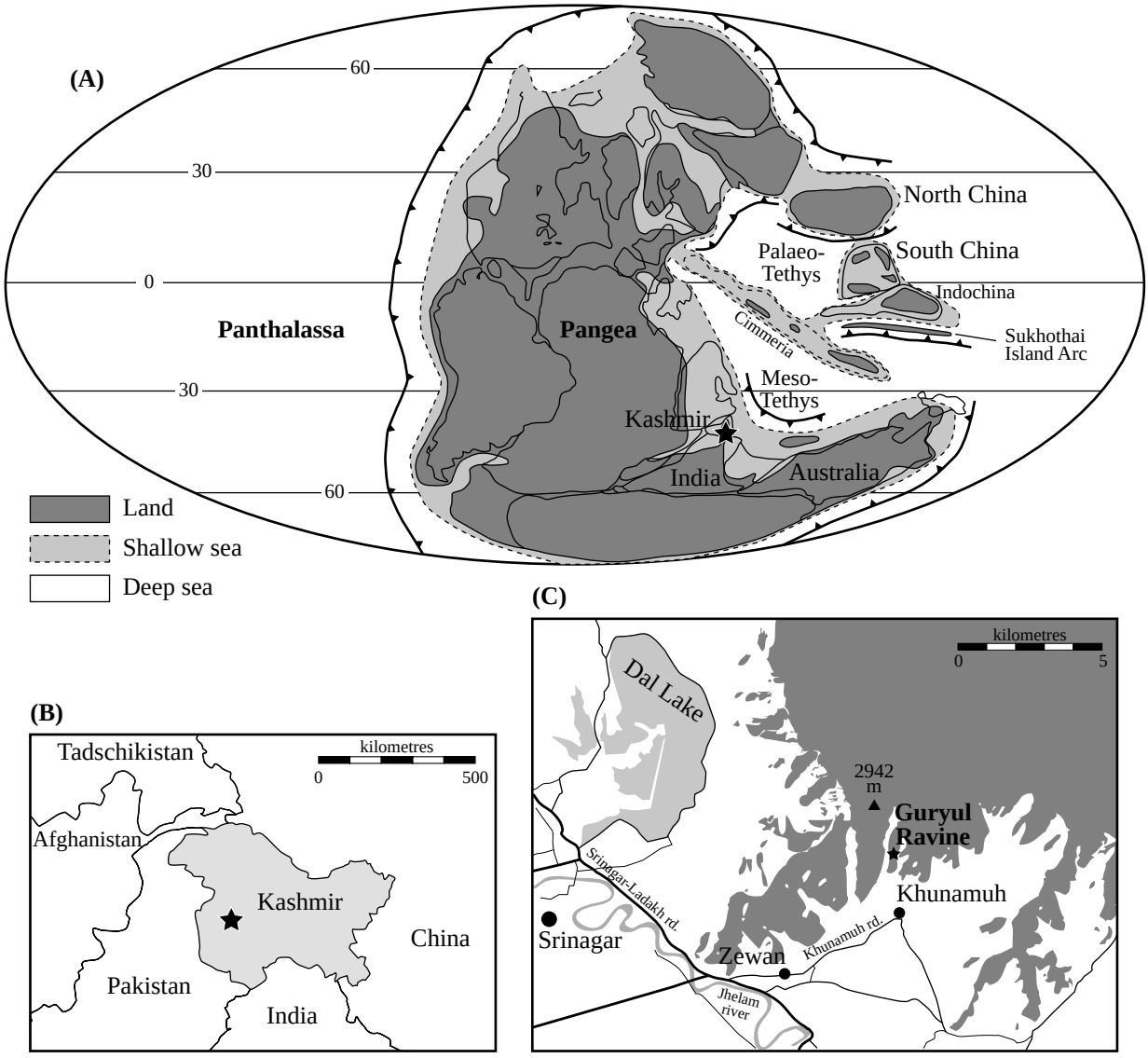

Figure 1: Palaeogeographical and geographical settings of the studied section. (A) Palaeogeographical map of the Earliest Triassic. The black star indicates the region of interest (modified after Metcalfe, 2013). (B-C) Locality map showing the position of Guryul Ravine within Kashmir nowadays.

about 37 degrees South, on the southern side of the Neotethys inner sea (Fig. 1; Scotese, 2014).

The opening of the Neotethys and rifting of the Kashmir margin of Gondwana during the late Permian and Early Triassic led to a rapid thermal subsidence that resulted in the marine submersion of Kashmir and allowed sub-continuous marine sedimentation across the PTB (Bhat, 1982, 1984; Gaetani et al., 1990; Stampfli et al., 1991; Garzanti et al., 1996; Baud et al., 1996; Brookfield, 1993; Brookfield et al., 2003, 2013).

The Permian Zewan Fm. is characterized by calcareous sandstone, deposited in an offshore mixed clastic carbonate deltaic complex, while overlying and mainly Triassic the Khunamuh Fm. records an alternation of marine shales with limestone associated to a deepening (Nakazawa et al., 1975; Baud et al., 1996; Kapoor, 1996).

Guryul Ravine (GPS 34°04.23'N 074°56.49'E) can be reached through the Khunamuh village, located about 15km South-East of Srinagar. Hayden first discovered this section and wrote a short report based on two days of observations (Hayden, 1907). This preliminary work was later completed by the study of Middlemiss (1909).

The Japanese-Indian team realized the most significant re-examination of the Guryul Ravine section (Nakazawa et al., 1975; Nakazawa and Kapoor, 1981). Nakazawa and his collaborators established the sedimentological sub-division of the Zewan and Khunamuh formations that is still in use today: the Zewan Fm. is divided into four members A-D; The Khunamuh Fm. is divided into six members E-J; Member E which includes the PTB, is divided into three sub-members E_1-E_3 (Fig. 2, 4). The reader is referred to Nakazawa et al. (1975) for detailed descriptions.

2.2. Biostratigraphy of the Guryul Ravine section

Sweet (1970a) published the first conodont study of Guryul Ravine, based on 35 bulk samples that were collected by Teichert, Kummel and Kapoor. Sweet (1970a) distinguished four conodont zones across the upper Zewan Fm. and the lower Khunamuh Fm.: the *Hindeodus typicalis*, *Neogondolella carinata*,

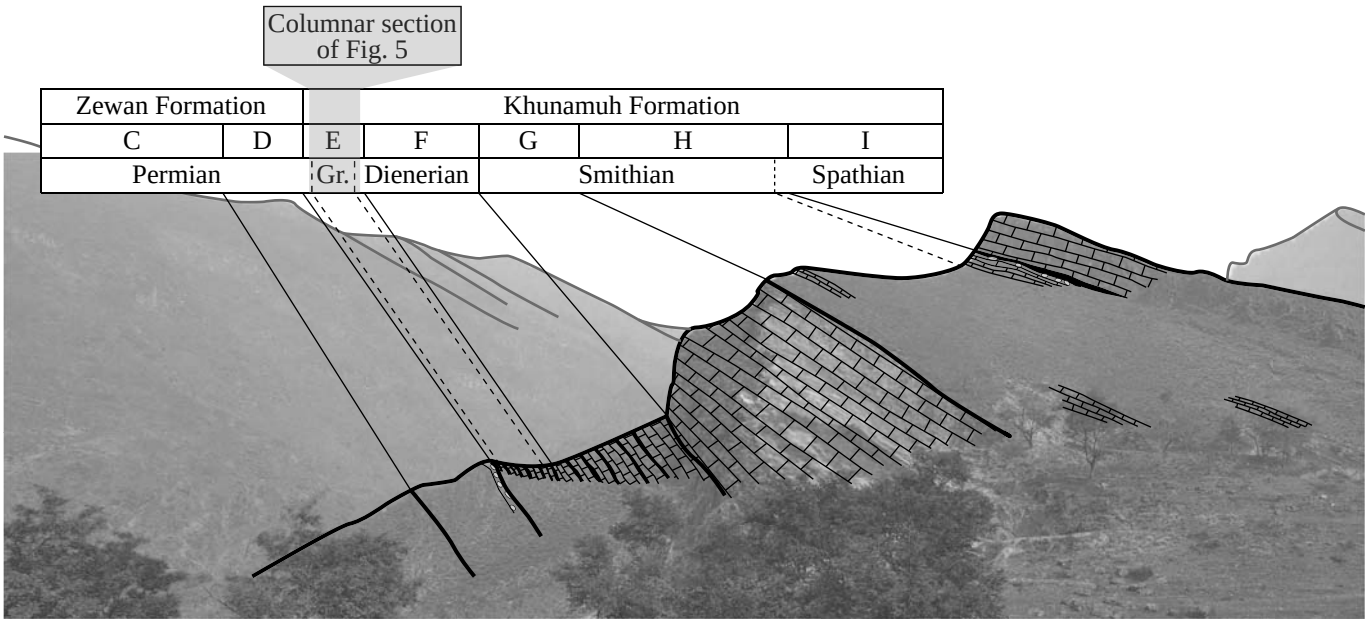

Figure 2: The Guryul Ravine outcrop with the Members defined in Nakazawa et al. (1975).

Neospathodus dieneri and *Neospathodus cristagalli* zones in ascending order. *H. typicalis* being a conodont described from uppermost Permian and lowermost Triassic, the PTB was located within the *H. typicalis* Zone (beds K28-K41; Sweet 1970a), which includes the "mixed fauna" interval of Teichert et al. (1970).

Nakazawa et al. (1975, 1980) reported the occurrence of the ammonoid *Otoceras woodwardi* in Unit 52 and thus proposed to locate the PTB between units 51 and 52 (sub-member E_2; specimen illustrated in Bando 1981). Nogami and Murata (in Nakazawa et al., 1975) studied the conodonts samples and recognized four conodont zones in the Khunamuh Fm.: The *H. typicalis*, *Ng. carinata*, *Ns. cristagalli* and *Neospathodus waageni* zones in ascending order (a few of these conodonts are illustrated in Nakazawa and Kapoor, eds. 1981). Although the occurrence charts of Sweet (1970a) and Nakazawa et al. (1975) show the same sequence of conodonts, the sequence of Nakazawa et al. (1975, see their table 11) is offset towards the base: in particular Nakazawa et al. (1975) reported the FO of *Neospathodus* in Unit 64 (sub-member E_3) (instead of F) whereas Sweet (1970) reported it in the equivalence of Member F. Note that Matsuda (1981, 1982, 1983, and 1984), after having re-sampled the section in 1977, reported also an upper FO of *Ns. cristagalli* in Unit 71 Member F, about 9.5m above Unit 64). Murata (in Nakazawa and Kapoor, 1981, Pl. 21, Fig. 10) illustrated a single specimen of *Ns. cristagalli* from Unit 64 (this specimen is more likely a broken *Ns. dieneri*). Although exact bed by bed correlation is rendered difficult by lateral variations in exposure and thickness (see Methods), it is extremely unlikely that *Ns. cristagalli* or *Ns. dieneri* would occur that low in the section (several meters below the FO of *Sweetospathodus kummeli* in Unit 70) together with hindeodids. Such association is unknown anywhere else and neither Sweet (1970, 1979) nor Matsuda (1981) nor our group were able to reproduce this observation.

When Sweet (1979) re-examined the conodont samples collected by Teichert and his collaborators, he found in Member E specimens of *Isarcicella isarcica*, a species that had not been documented previously. Sweet (1979) discounted the FO) of *Ng. carinata* in member C as reported by Nakazawa et al. (1975) and confirmed it in member D.

Matsuda (1981, 1982, 1983 and 1984) re-sampled the section and proposed a refined conodont biozonation across the members E and F. He notably reported the FO of *Hindeodus parvus*, the index species for the base of the Triassic (Yin et al., 1996), in Unit 56 (sub-member E_2; Matsuda, 1981). It is worth noting that prior to the definition of *H. parvus* by Kozur and Pjatakova (1976), *H. parvus* likely would have been determined as belonging to the long-ranging *Hindeodus typicalis*. In a later study, Nakazawa and Kapoor (1981) reported *H. parvus* from Unit 52 (sub-member E_2), but we interpret the illustrated specimen (Nakazawa and Kapoor, 1981, pl. 21, fig. 2) as belonging to the PTB straddling conodont *Hindeodus typicalis* instead.

Similarly, the specimens illustrated by Matsuda as belonging to *I. isarcica* all correspond to *Isarcicella staeschei* (a species defined by Dai and Zhang in 1989 only). It is likely that the specimens of *I. isarcica* reported by Sweet (1979) also belong to *I. staeschei*.

Finally, several more recent publications have discussed the conodonts at Guryul Ravine (the most recent being Budurov and Gupta (1988) but they involved Gupta, who is famous for having falsified data (Webster, 1993) and hence are not considered here.

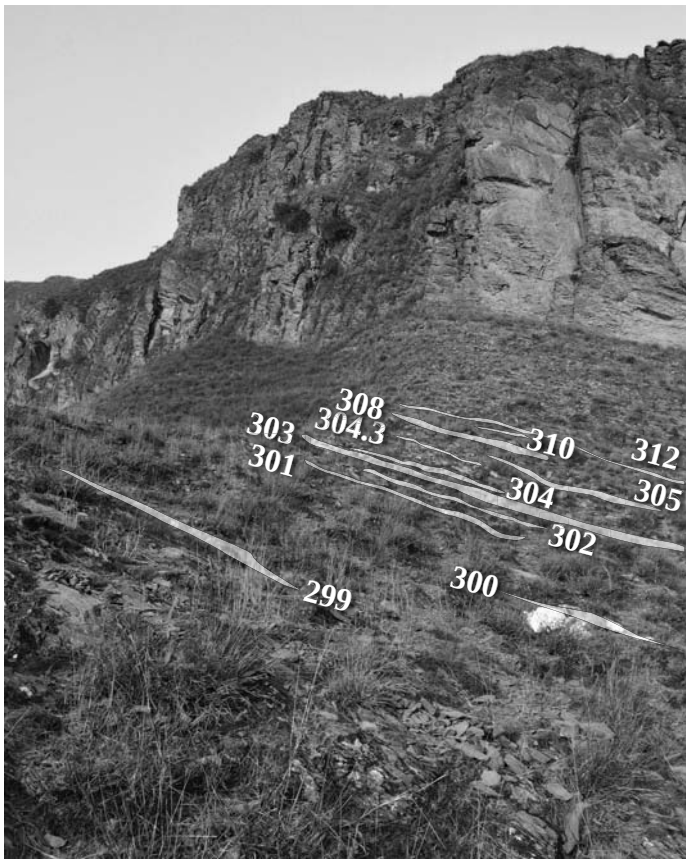

Figure 3: Location of the sampled horizons on the outcrop.

3. Material and methods

3.1. Correlation with the subdivision of Nakazawa et al. (1970, 1975)

The location of some of the sampled horizons on the outcrop is shown in Figure 3. The Member E of the Guryul Ravine outcrop is characterized by intercalating flaggy shales and limestone beds of variable thickness. The limestone beds can be discontinuous or lenticular (e.g. in E_2 and E_3; Nakazawa et al., 1970, 1975) inducing high lateral variability of the sequence. Moreover, as noted by Nakazawa et al. (1975, p. 72), the boundaries between subdivisions of the member E (E_1-E_2, E_2-E_3) were drawn somewhat artificially since changes in lithology are gradual. Comparatively the boundaries between members (D-E, E-F) are much more conspicuous, since they translate in slope changes that are quite obvious in the landscape. As a consequence bed by bed correlation within member E is at places tricky and the correspondence between our bed numbers and those of Nakazawa et al. (1975) is tentative. Yet, there are beds whose correlation can be done with confidence:

- GUR09: this bed is one of a few carbonated beds found approximately in the middle of the E_2 sub-member. This is stratigraphically the lowest bed where we found abundant conodonts, including FO of *Hindeodus parvus*, the index for the base of the Triassic. Although the absence of evidence is not the evidence of absence, it is likely that this bed corresponds to the prominent limestone beds of the units numbered 55 and 56 by Nakazawa et al. (1975).

-GUR13: This bed is the first limestone bed of the more carbonated E_3 sub-member, and hence quite easily recognizable. It is characterized by the exclusive occurrence of *Hindeodus pisai* and the first occurrence of *Hindeodus eurypyge*. We interpret it as corresponding to the lowest part of the prominent limestone bed at the base of Unit 60 of Nakazawa et al. (ibid).

-GUR15: This bed lies at the third of the E_3 sub-member and shows abundant ammonoid cross-sections. This is remarkable because most of E_3 is barren of ammonoids. For this reason and although we have not determined the corresponding ammonoids, we are confident in correlating this bed with Unit 64 of Nakazawa et al. (ibid), where most of Nakazawa et al.'s ammonoids from E_3 were found.

-GUR311: This bed lies in the upper half of sub-member E_3 and our bed by bed sampling showed that it is the only one containing specimens of *Sweetospathodus kummeli*, although the surrounding beds were also rich in conodonts. Hence it is likely to correspond to the base of Unit 70, where Matsuda (1981) found also *S. kummeli*.

-GUR17: This bed is one of the last carbonated beds of Member E and contrary to the nearby beds it contains abundant ammonoids. For these reasons we interpret it as correlating with the prominent limestone bed near the top of Unit 70 of Nakazawa et al. (1975, 1981).

3.2. Conodont sampling and preparation

The sampling was performed on the eastern slope of the Guryul Ravine outcrop, about 20 metres below the crest, where the beds were better preserved. The samples were collected from the limestone beds of sub-members E_1-E_3, i.e. the lowermost 15 stratigraphical metres of the Khunamuh Fm. (Fig. 3). Samples were collected from the limestone beds at about 10-50 cm spacing. In total, 39 samples, each weighing between 1 and 3 kg, were processed.

The samples were dissolved with a ~10% buffered acetic acid solution following the procedure of Jeppsson et al. (1999). The insoluble residues were concentrated by heavy liquid separation using sodium polytungstate (Jeppsson and Anehus 1999), and sieved with a 0.075-mm mesh, and handpicked under a binocular microscope.

3.3. Carbon isotopes

The samples from the studied interval correspond to the beds sampled for conodonts analyses. Limestone samples were critically investigated for stylolites, cracks, veins, weathering and strong recrystallisation. These parts were removed before the samples were cut and drilled with a diamond-tipped drill to produce a fine powder. The isotopic composition of the carbonates were measured with a GasBench II connected to a Finnigan MAT DeltaPlus XL mass spectrometer, using a He-carrier gas system according to a method adapted after Spötl and Vennemann (2003). All samples were processed at the Institute of Mineralogy and Geochemistry of Lausanne University. External reproducibility for the analyses estimated from replicate analyses of the in-house standard (n = 3 per run) was better than 0.1‰ for standards and 0.15‰ for sediment samples.

All reported carbonate carbon isotope results are in the standard δ notation (‰ deviation versus Vienna Pee Dee Belemnite (VPDB)). The samples GUR05, GUR07 and GUR308 had carbonate content too low (<10%) and are considered dubious (Fig. 4).

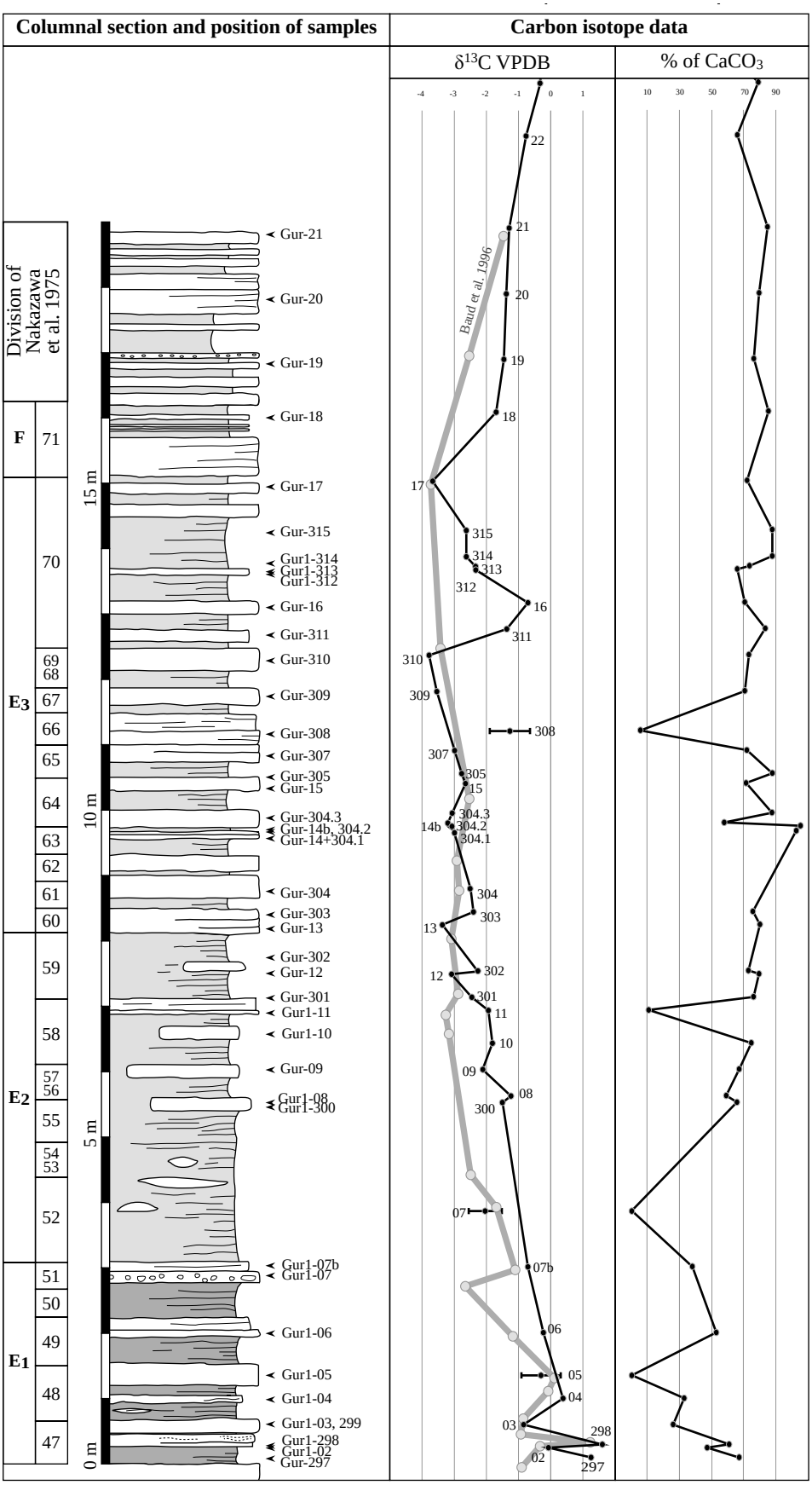

Figure 4: Detailed stratigraphical log of the studied interval of the Guryul Ravine section showing the $\delta^{13}C$ record with the associated % of $CaCO_3$. The samples GUR0, GUR07 and GUR308 that contain less than 10% of CaCO3 and which $\delta^{13}C$ are doubtful and shown with a 99% confidence interval.

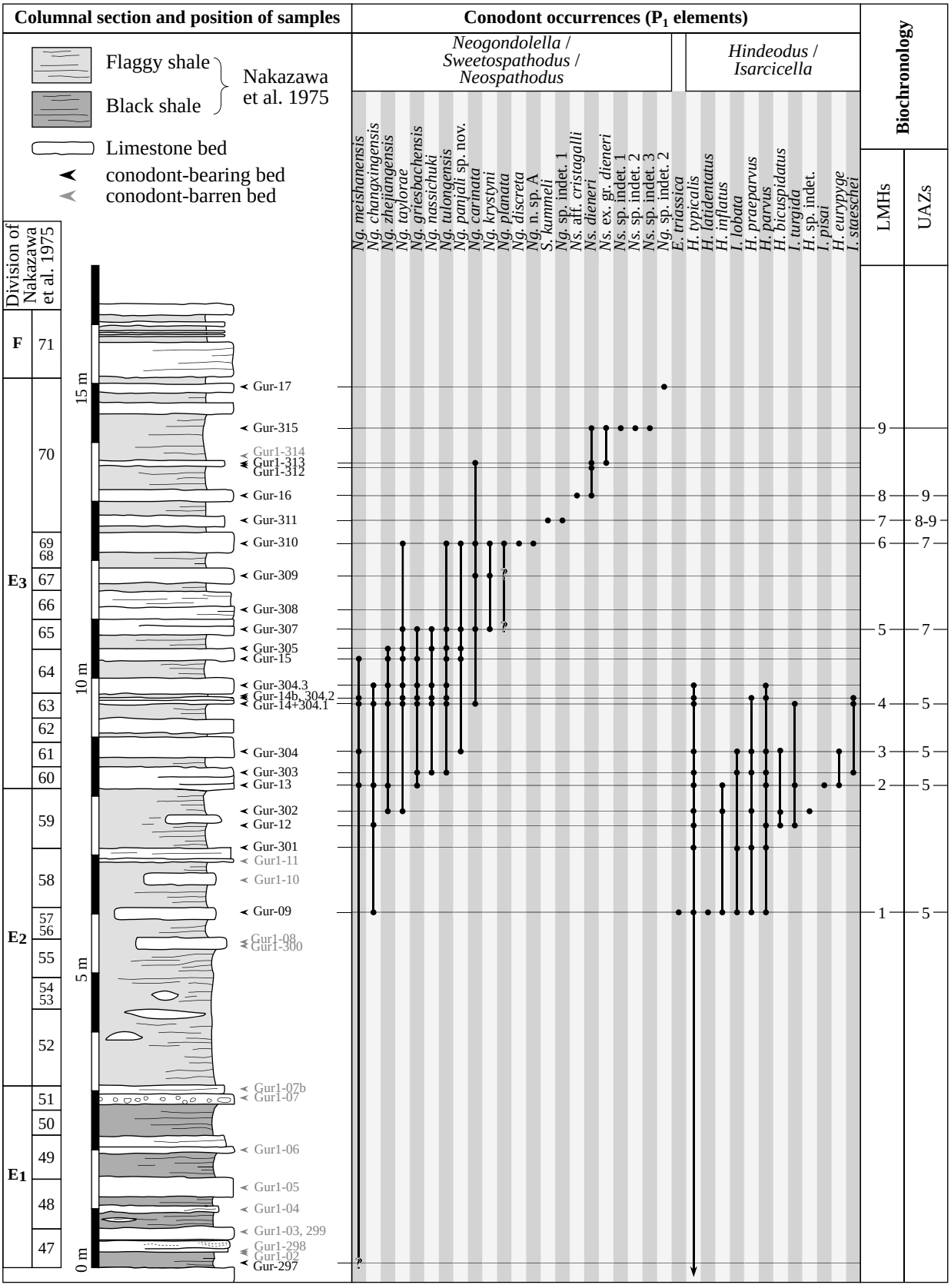

Figure 5: Detailed stratigraphical log of the studied interval of the Guryul Ravine section showing the conodonts occurrence chart. The zero on the vertical scale corresponds to the boundary between the Zewan and the Khunamuh formations. Each limestone bed sampled is indicated. Beds which names are in grey font are conodont-barren. Beds which name are in black font yielded P_1 elements. Ng, *Neogondolella*; H, *Hindeodus*; I, *Isarcicella*; E, *Ellisiona*; S, *Sweetospathodus*; Ns. *Neospathodus.*

4. Results

4.1. Biostratigraphy

Of the 39 samples from the member E of the Khunamuh Fm. that we processed, 22 yielded pectiniform conodont elements. Pectiniform elements are more abundant than ramiform elements in Member E, and 34 species assigned to six genera were identified. *Neogondolella* specimens dominate in abundance most of the samples throughout the studied interval (Table 1), but some samples also yielded *Hindeodus*, *Isarcicella*, *Neospathodus* or *Sweetospathodus* species. The general preservation is good although the colour of the elements is black (CAI = 5).

Figure 5 shows a summary of conodont occurrences. Representative conodont specimens are illustrated in Figures 6-17. The sub-member E_1 is very poor in conodonts: Only sample GUR297 contains a few conodonts. The next bed yielding conodonts, GUR09, is located about 6 metres above the base of the Khunamuh Fm. and belongs to sub-member E_2 (see also Methods). It contains specimens of *Hindeodus parvus* (index species for the base of the Triassic) and is therefore the lowermost bed to which we can confidently assign a Griesbachian age. GUR09 yielded also the Griesbachian *Isarcicella lobata*. The relative abundance of neogondolellids increases from beds GUR09 to GUR307 (across E_2 and E_3), the latter containing exclusively elements of *Neogondolella*.

Towards the top of the E Member, we observe a radical turnover: though from GUR15 to GUR310 all samples yielded only neogondolellids, the next carbonated bed, GUR311, contains mostly specimens of *S. kummeli*. One bed higher, in GUR16, only neospathodids are found. This conodont faunal transition from neogondolellids to neospathodids is known to occur in many places (Orchard 2007) and is a marker of the Griesbachian-Dienerian boundary. It is thought that neospathodids evolved from neogondolellids by platform loss in the P_1 element, the intermediary form being putatively *S. kummeli*, whose populations display a huge variation in platform extent (Sweet, 1970b). Neospathodids seem to have replaced neogondolellids very quickly in equatorial and tropical environments, restricting neogondolellids to the Boreal realm during most of the Dienerian.

The *Neogondolella* sequence at Guryul Ravine is remarkably similar to the sequence described from Spiti (Krystyn and Orchard, 1996; Orchard and Krystyn, 1998), which conodont record is also dominated by neogondolellids. In both localities, the oldest faunas contain the end-Permian survivors *Neogondolella carinata*, *Neogondolella meishanensis*, *Neogondolella zhejiangensis* and *Neogondolella taylorae*, associated with Griesbachian anchignathodontids. The younger species of exclusively Griesbachian age appear in sequence *Neogondolella nassichuki*, *Neogondolella planata*, *Neogondolella krystyni* and *Neogondolella discreta*. The faunal similarities of assemblages between the Griesbachian of Kashmir and Spiti extend to the occurrence of *Neogondolella panjali* nov. sp. that was until now exclusively known from Spiti as *Neogondolella* n. sp. A (Krystyn and Orchard 1996; Orchard and Krystyn, 1998). Contrary to the sequence from Spiti, *Neogondolella kazi*, *Neogondolella orchardi* and *Neogondolella nevadensis* have not been observed in Guryul Ravine.

Hindeodids at Guryul Ravine also show the typical sequence occurring throughout the Griesbachian. Worth noting, *Isarcicella isarcica*, a species common in the Equatorial Realm (Jiang et al., 2011b), is absent from

both Kashmir and Spiti. A striking difference between the faunas from Spiti and Kashmir is that the whole sequence of hindeodids is older than *Ng. krystyni* at Guryul Ravine, while hindeodids range *Ng. krystyni* in Spiti.

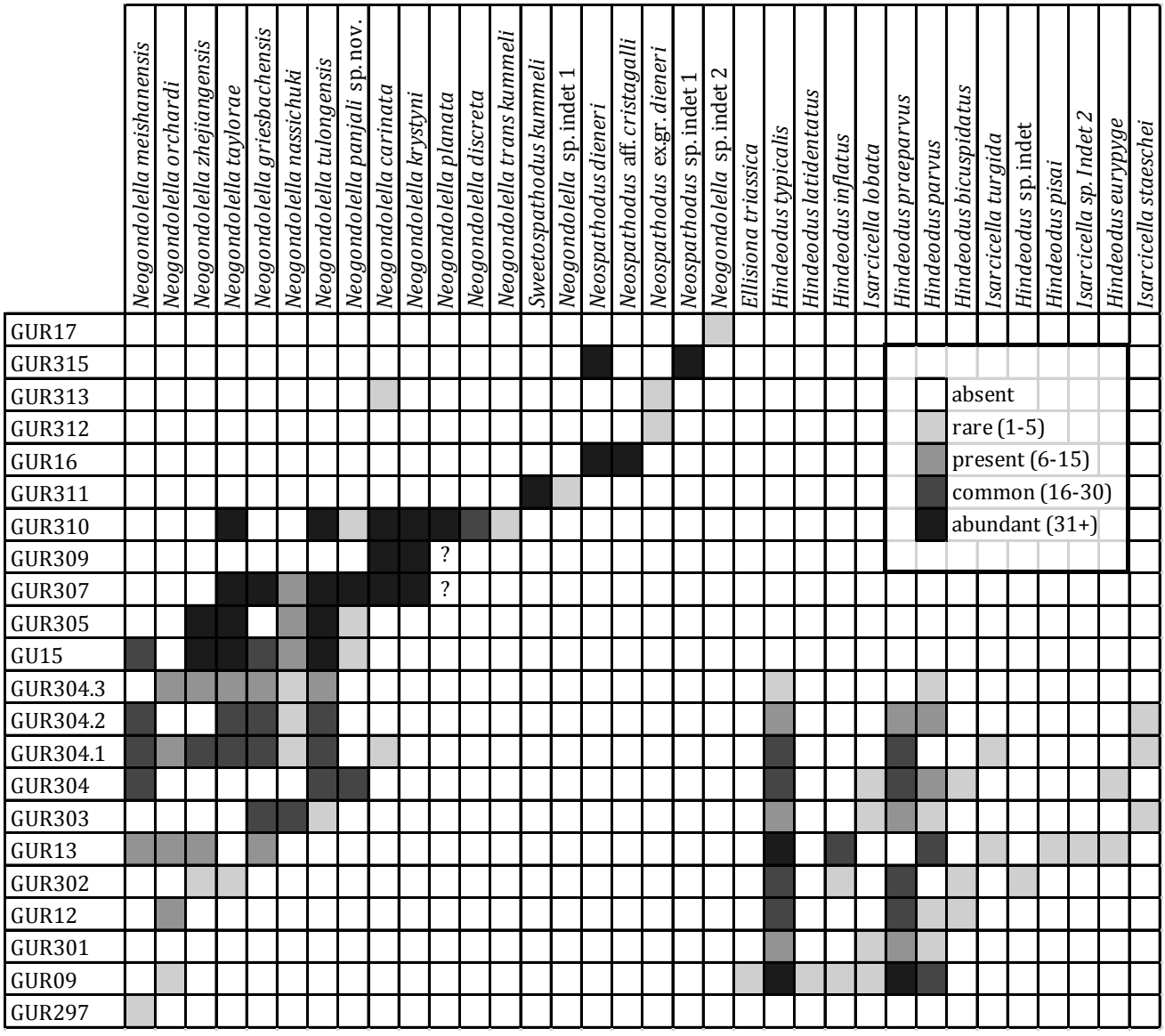

Table 1: Abundance of conodont taxa retrieved from the conodont-bearing beds at the Guryul Ravine section. The intensity of the colour represents the abundance of P_1 elements, from white (zero) to black (more than 30). N, *Neogondolella*; H, *Hindeodus*; I, *Isarcicella*; E, *Ellisiona*; S, *Sweetospathodus*; Ns. *Neospathodus*.

4.2. Systematic palaeontology (Brosse and Goudemand)

Synonymies are limited to key citations and are not intended to be exhaustive lists. All illustrated specimens are shown at the same scale. Figured elements are stored in PIMUZ, Paleontological Institute and Museum of the University of Zurich, Karl Schmid-Strasse 4, 8006 Zurich, Switzerland. Pectiniform elements are far more abundant than ramiform elements in Member E at Guryul Ravine and the traditional biostratigraphy is mostly established from P elements. Consequently, the descriptions of species are exclusively based on P1 elements.

The terminology for the orientation of the element is the traditional one based on the orientation and curvature of the cusp; it refers to the element only, not to its natural orientation within the animal (Purnell et al., 2000). 'Lower' refers to the side of the element from which the basal cavity opens. 'Upper' refers to the opposite side. The term 'cusp' refers only to the cusp sensu stricto. It represents the structure above the apex of the basal cavity (Klapper et al., 1973) and is homologous in distinct conodont elements. The cusp is often larger than the other denticles, but not necessarily. The big denticle that is found on the 'anterior' of carminiscaphate elements of anchignathodontids is appropriately termed 'distal denticle' (as in Agematsu et al., 2014).

As the lower view of the P_1 element is very rarely illustrated even in taxonomical papers, the descriptions focus mostly on the axial part (blade-carina-cusp) and the shape of the platform, especially in the case of neogondolellids.

Class *CONODONTA* Eichenberg, 1930

Order *OZARKODINIDA* Dzik, 1976

Family *ANCHIGNATHODONTIDAE* Clark, 1972

Genus ***Hindeodus*** Rexroad and Furnish, 1964

Type species. *Hindeodus cristulus* Youngquist and Miller, 1949.

Hindeodus bicuspidatus (Kozur, 2004)

Figure 6D, E

1991. *Hindeodus* n. sp. Schönlaub, p. 88, pl. 1, fig. 6 (only).

2004. *Hindeodus bicuspidatus* - Kozur, p. 50, pl. 2, fig. 4.

2011a. *Hindeodus anterodentatus* Dai et al. - Jiang *et al.*, pl. 1, figs 3, 5.

2014. *Hindeodus bicuspidatus* Kozur - Zhang *et al.*, fig. 4(22-24).

2015. *Hindeodus bicuspidatus* Kozur - Brosse *et al*. fig. 3(B-E, ?F).

Occurrence. Iran: Kuh-e-Hambast, section V, bed Aba V-3, lower *Clarkina meishanensis* – *Hindeodus praeparvus* Zone (Kozur, 2004). China: Shangsi section, Sichuan Province, Feixianguan Fm., beds 31A-33 (Jiang et al., 2011a); Zhongzhai section, Guizhou, bed 28 (Zhang et al., 2014); Guangxi, Wuzhuan section, Luolou Fm., beds WUZ.L and WUZ.O (Brosse et al., 2015). Kashmir: Guryul Ravine section, Khunamuh Fm., E_2.

Diagnosis. see Kozur (2004).

Description. The P_1 elements are characterized by two erect distal denticles having a much bigger size than the adjacent denticles of the carina. In the material from Guryul Ravine, these two denticles can reach a very big size and extend as much as the distal denticle of *H. parvus* (Fig. 6D). The two big distal denticles are followed by nine to eleven smaller, triangular and laterally compressed denticles. A tiny denticle is often found on the anterior margin of the blade. The carina is arched posteriorly as a consequence of the progressive decrease in the height of the denticles toward the posterior end. Although

the basal margins are broken in the specimens found at Guryul Ravine, the basal cavity seems narrow.

Hindeodus eurypyge (Nicoll et al., 2002)
Figure 6I

1981. *Hindeodus minutus* Ellison - Matsuda, pl. 1, fig. 1.

1989. *Anchignathodus parvus* Kozur and Pjatakova - Li et al., pl. 39, figs 16, 17 ; pl. 45, figs 22-24.

2002. *Hindeodus eurypyge* - Nicoll et al., p. 616-620, figs 4, 5, 7-9.

2007. *Hindeodus eurypyge* Nicoll et al. - Metcalfe and Nicoll, pl. 1, figs 2-6.

Occurrence. Meishan section, discontinuous from bed 27a to bed D/C-2 in the Yinkeng Fm. (Nicoll et al., 2002); Shangsi section, bed 6405548, *Merrillina ultima-Stepanovites*? *mostleri* Zone (Metcalfe and Nicoll, 2007); Wuzhuan section, Luolou Fm., bed WUZ. G (Brosse et al. 2015). Kashmir: Guryul Ravine section, Khunamuh Fm. E_3.

Diagnosis. see Nicoll et al. (2002).

Description. The P_1 element has a tall, erect and triangular distal denticle. In lateral view the carina is straight and not posteriorly arched, giving the whole element a rectangular outline. The first denticles after the distal one are small and closely appressed while in the posterior half of the carina the denticles are progressively getting broader. In upper view the denticles are laterally compressed and the carina has a straight to stretched S-shape. The carina rises quickly from the flaring cup as a thick and laterally compressed blade (see posterior view, Fig. 6I). The basal cavity is wide with semi-circular margin rounded posteriorly.

Hindeodus inflatus (Nicoll et al., 2002)
Figure 6H

2002. *Hindeodus inflatus* - Nicoll et al., figs 10-12.

2009. *Hindeodus inflatus* Nicoll et al. - Chen et al., fig. 8(9-11).

Occurrence. China: found in the upper Permian and Griesbachian at Meishan section (Nicoll et al., 2002) and in the upper Permian at Dawen section (Chen et al., 2009). Kashmir: Guryul Ravine, Khunamuh Fm., E_2. Only one specimen of *H. inflatus* was found at Guryul Ravine in sub-members E_2-E_3 of Griesbachian age.

Diagnosis. see Nicoll et al. (2002).

Description. In lateral view, the anterior part of the carina after the distal denticle is composed of a few closely appressed and low denticles, while the posterior part shows broader denticles that are less closely spaced. A tiny denticle can be found on the anterior and posterior margins of the carina. The space between the denticles is V-shaped to blunt-V-shaped. The lateral outline is arched posteriorly due to the progressive size decrease of the denticles. The carina rises directly from the inflated cup (see the posterior view). The basal cavity opens directly after the distal denticle. It is somewhat asymmetrical, as the carina is slightly arched laterally. The basal cavity is large, semi-circular, inflated and deeply excavated. The groove that can be observed on the lower view extends throughout the entire length of the element.

Remarks. *H. inflatus* is a rare form that was so far only known from the Nanpanjiang Basin, it is here reported for the first time in the Southern Tethyan realm.

Hindeodus latidentatus (Kozur, Mostler and Rahimi, 1975)

Figure 6F

1975. *Anchignathodus latidentatus* - Kozur, Mostler and Rahimi, p. 4, 5, pl. 2, fig. 6.

1994. *Hindeodus latidentatus* Kozur, Mostler and Rahimi - Orchard et al., pl. 1, fig. 20.

1996. *Hindeodus latidentatus* Kozur, Mostler and Rahimi - Mei, pl. 18.2, fig. 5.

1996. *Hindeodus latidentatus praeparvus* Kozur, pl. I, fig. 10 (only).

1998. *Hindeodus latidentatus* Kozur, Mostler and Rahimi - Orchard and Krystyn, pl. 6, figs 27, 28.

2002. *Hindeodus latidentatus* Kozur, Mostler and Rahimi - Nicoll et al., figs 13, 14.

?2003. *Hindeodus pisai* Perri and Farabegoli, pl. 1, Fig. 15.

2007. *Hindeodus praeparvus* Kozur - Jiang et al., pl. IV, fig. 12.

2007. *Hindeodus latidentatus* Kozur, Mostler and Rahimi - Jiang et al., pl. IV, figs 1-4.

2009. *Hindeodus latidentatus* Kozur, Mostler and Rahimi - Chen et al., pl. 9, figs 1-3.

2014. *Hindeodus praeparvus* Kozur - Yuan et al., pl. VIII, fig. 12 (only).

Occurrence. China: Nanpanjiang basin, uppermost Permian at Shangsi section (Jiang et al., 2011a, Dawen section (Chen et al., 2009), uppermost Permian and lower Griesbachian at Meishan section (Nicoll et al., 2002). Southern Alps: possibly in Bulla section, bed BU12A, last bed in the Werfen Fm. (see synonymy list). Kashmir: Guryul Ravine section, Khunamuh Fm, E_2.

Diagnosis. See the amended diagnosis of Orchard and Krystyn (1998).

Description. The single P_1 element found at Guryul Ravine is small, with a length of about 350 μm and five denticles including the distal one. The distal denticle is twice larger and higher than the adjacent denticles. The denticles are large, triangular in shape and laterally compressed. The first denticle adjacent to the distal denticle is smaller and closely appressed to the adjacent denticles, but the posterior denticles are widely spaced. Anteriorly the space between the denticles is V-shaped, while it has posteriorly the typical U-shape. The cup is broken and precludes further observation.

Remarks. Elements previously included in *H. latidentatus* with V-shaped spaces between posterior denticles have been differentiated by Kozur (1996) as a subspecies, later elevated as *H. praeparvus* at the species level by Orchard and Krystyn (1998).

H. latidentatus sensu Orchard (1998) is a rarer species than *H. praeparvus*, and is mostly found in Late Permian deposits in China. Nicoll et al. (2002), in a re-evaluation of the conodont record at Meishan section, found *H. latidentatus* in abundance at the top of the Permian Changxing Fm., but also documented a few elements (eight in total) in the Triassic Yinkeng Fm. The single element of *H. latidentatus* found at Guryul Ravine is associated with conodonts of a Griesbachian age (*H. parvus* and *H. bicuspidatus*), confirming that the range of *H. latidentatus* extends indeed into Triassic.

Hindeodus parvus (Kozur and Pjatakova, 1976)

Figure 6A-C

1976. *Anchignathodus parvus* - Kozur and Pjatakova, p. 123-125, fig. 1(a, b, e, h).

1981. *Hindeodus parvus* Kozur and Pjatakova - Matsuda, pl. 5, figs 1–3.

1981. *Hindeodus minutus* Ellison - Matsuda, pl. 1, figs 8–12 (only).

1996. *Hindeodus parvus* Kozur and Pjatakova - Koike, fig. 3(3-15).

1996. *Hindeodus parvus* Kozur and Pjatakova - Mei, pl. 18.2, figs 2-4, 14.

1998. *Hindeodus parvus* Kozur and Pjatakova - Orchard and Krystyn, pl. 6, figs 9, 16, 17, 20.

2002. *Hindeodus parvus* Kozur and Pjatakova - Nicoll et al., fig. 15: 1-4, fig. 16(1-3).

2007. *Hindeodus parvus* Kozur and Pjatakova - Jiang et al., pl. 5, figs 1-7.

2008. *Hindeodus parvus* Kozur and Pjatakova - Chen et al., pl. V, figs 1-5.

2009. *Hindeodus parvus* Kozur and Pjatakova - Chen et al., fig. 10(1-13).

2009. *Hindeodus parvus* parvus Kozur and Pjatakova - Chen et al., fig. 10(14–19), fig. 11(1-5).

2013 *Hindeodus parvus* Kozur and Pjatakova - Yan et al., fig. 5(G–L, P, S, U) (only).

2015 *Hindeodus parvus* Kozur and Pjatakova - Brosse et al., fig. 4.

Occurrence. Tibet: Selong section, *Otoceras latilobatum* Zone. Spiti: Guling, Lingti, Lalung sections, *Otoceras woodwardi* Zone. Arctic Canada: Ellesmere Island, *Otoceras boreale* Zone (Henderson and Baud, 1997). China: UAZ_3-UAZ_6 in the Nanpanjiang basin (Brosse et al. 2016). Kashmir: Guryul Ravine section, Khunamuh Fm., E_2-E_3. Salt Range: Kathwai Dolomite (Sweet 1970b). Worldwide during the Griesbachian.

Diagnosis. See Kozur and Pjatakova (1976).

Description. The P_1 element is short with 5-7 denticles following the big distal denticle. The denticle next to the distal denticle is often smaller and more closely appressed with the adjacent ones. All denticles are subequal in size, with the exception of the distal denticle, which is wide and very high. The anterior margin of the distal denticle is straight to arched posteriorly. The carina is laterally compressed and arises from the cup as a high blade (see posterior view). The cup flares quickly from the base of the blade with oval, symmetrical to subsymmetrical margins. In lower view, the basal groove extends throughout the entire length of the element. Its posterior end is slightly arched downward and often bears a tiny denticle.

Remarks. *H. parvus* is the index species for the base of the Triassic (Yin et al., 1986) and was the focus of numerous studies. Kozur (1996) recognized two morphotypes and created the subspecies *H. parvus erectus* (holotype of *H. parvus* and morphotype 1) and *H. parvus parvus* (morphotype 2). *H. parvus erectus* is distinct by its subvertical posterior edge (see Kozur, 1996; pl. II, figs 6, 8; pl. III, figs 1-11; pl. IV, figs 6), *H. parvus parvus* is characterized by a steeply inclined posterior blade bearing a few denticles (see Kozur, 1996, pl. II, fig. 7). Kozur (1996) noted that the two morphotypes are linked with transitional forms in the lower part of their respective ranges. A third morphotype with a less inclined, denticulate posterior edge, referred to as morphotype 3, was described in Meishan (Mei, 1996).

Nicoll et al. (2002), in their re-assessment of the conodont faunas from Meishan, proposed that the subspecies had no clearly distinct stratigraphic ranges and recommended the use of the sole *H. parvus*. We follow here that recommendation.

Hindeodus pisai (Perri and Farabegoli, 2003)
Figure 6G

1998. *Hindeodus* n. sp. A Farabegoli and Perri, pl. 4.3.12, fig. 9.

2003. *Hindeodus pisai* - Perri and Farabegoli, pl. 1, figs 1-12.

?2007. *Hindeodus pisai* Perri and Farabegoli - Jiang et al., pl. IV, fig. 26 (only).

Occurrence. Southern Alps: Bulla section, base of Werfen Fm., upper Permian and lower Griesbachian (Perri and Farabegoli, 2003). China: Meishan section, Yinkeng Fm. (Jiang

et al., 2007). Kashmir: Guryul Ravine section, Khunamuh Fm., E_3.

Diagnosis. See Perri and Farabegoli (2003).

Description. The P_1 element of the single *H. pisai* found at Guryul Ravine is small (less than 350 µm long) and could be a juvenile form. The large distal denticle is followed by 10 needle-like denticles, closely appressed and fused at their base. The anterior margin bears two tiny denticles. The posterior half of the carina is arched downward. In upper view, the carina is laterally compressed and slightly curved. Although broken, the basal cavity seems to be narrow and to open from the base of the high free blade.

Remarks. Our specimen of *H. pisai* is distinct from the holotype as the number of denticles on the carina is smaller, leading to a much lower length/height ratio than all specimens described by Perri and Farabegoli (2003). Nevertheless, the needle-like shape of the denticles is characteristic of *H. pisai*, and our specimen could represent an early ontogenetic stage.

Hindeodus praeparvus (Kozur, 1996)

Figure 6J-L

1994a. *Hindeodus latidentatus* Kozur - Wang, pl. 1, fig. 9.

1996. *Hindeodus parvus erectus* Kozur - Kozur, pl. 4, fig. 7.

1996. *Hindeodus latidentatus praeparvus* - Kozur, p. 93- 94, pl. 2, figs 1-4 (only).

1996. *Hindeodus latidentatus* Kozur - Yin et al., pl. 2, fig. 3 (only).

1998. *Hindeodus praeparvus* Kozur - Orchard and Krystyn, p. 352, pl. 6, figs 22-23.

2002. *Hindeodus praeparvus* Kozur - Nicoll et al., fig. 17.

2007. *Hindeodus latidentatus* Kozur - Jiang et al., pl. IV, fig. 12 (only).

2009. *Hindeodus praeparvus* Kozur - Chen et al., fig. 9(7-14).

2013. *Hindeodus praeparvus* Kozur - Zhao et al., pl. 5, figs V-W.

2015. *Hindeodus praeparvus* Kozur - Brosse et al., fig. 7(A-E).

Occurrence. Spiti: Guling and Lingti sections, *Otoceras woodwardi* Zone. Kashmir: Guryul Ravine section, Khunamuh Fm., E_2-E_3. China: UAZ_1-UAZ_5 in the Nanpanjiang basin (Brosse et al., 2016). Worldwide late Permian and Griesbachian.

Diagnosis. See Kozur (1996).

Description. The specimens of *H. praeparvus* found at Guryul Ravine have 7-9 denticles after the distal denticle. The anterior margin of the distal denticle is straight and gives the distal denticle a triangular shape. The anterior margin also often bears a tiny denticle. In lateral view, the denticles are closely appressed anteriorly and get less appressed, broader and shorter posteriorly, which give the carina a posterior arched outline. In upper view, the carina is laterally compressed. The element in Figure 6L is the only one to show a thickening of the carina. This feature is usually found in *Isarcicella* species, along with a strong development of the distal denticle, which is tall, pointy and inclined posteriorly. The specimen illustrated in Figure 6L lacks the latter and hence is here assigned to *H. praeparvus* only tentatively.

Hindeodus typicalis (Sweet, 1970b)

Figure 6M-P

1970a. *Anchignathodus typicalis* - Sweet, p. 7-8, pl. 1, figs 13, 22.

1970b. *Anchignathodus typicalis* Sweet - Sweet, pl. 1, figs 13, 20.

1976. *Anchignathodus typicalis* Sweet - Sweet

in Teichert and Kummel, pl. 16, figs 6-8.

1981. *Hindeodus minutus* Ellison - Matsuda, p. 78–84, pl. 1, figs 1–7 (only).

1996. *Hindeodus typicalis* Sweet - Mei, p. 146, pl. 18.2, figs 6, 10, 11 (only).

1998. *Hindeodus typicalis* Sweet - Orchard and Krystyn, p. 354, pl. 6, figs 14, 18, 19, 25, 26.

2013. *Hindeodus typicalis* Sweet - Zhao et al., fig. 5(T-U).

2015. *Hindeodus typicalis* Sweet - Yuan et al., pl. 3, figs 16-24, 26, 27.

Occurrence. Greenland: Kap Stosch, straddling the PTB. Tibet: Selong section, *Otoceras latilobatum* Zone. Spiti: Guling, Lingti, Lalung, and Muth sections, *Otoceras woodwardi* and *Ophiceras tibeticum* zones. China: UAZ_1-UAZ_5 in the Nanpanjiang basin (Brosse et al., 2016). Pakistan: Salt Range, Chhidru section, Chhidru Fm. Kashmir: Guryul Ravine, Khunamuh Fm., E_1-E_3. Worldwide late Permian and Griesbachian.

Diagnosis. See Sweet (1970b).

Description. The anterior margin of the P_1 is straight and gives the distal denticle a triangular shape. The denticles are subequal in width and their size decreases progressively posteriorly. Based on the size of the distal denticles, we split our population into two morphotypes: (α) P_1 with broad cusp and, as shown in Figure 6M, N; (β) P_1 with undifferentiated cusp, see Figure 6O, P. Both morphotypes share the same stratigraphical range. Hence their somewhat arbitrary separation is not necessarily useful for biochronological purposes.

α morphotype (Figure 6M, N)

Description. The αmorphotype corresponds to the hypotype (Sweet 1970a; Pl. 1, Fig. 22) from Guryul Ravine. In addition to the typical subequal denticles of the carina, the distal denticle is wide, high and triangular in shape, the number of denticles varies from 7 to 10.

β morphotype (Figure 6O, P)

Description. The β morphotype corresponds to the holotype (Sweet, 1970b; Pl.1, Fig. 20), which was found in Pakistan. The number of denticles varies from 7 to 10. In lateral view, the blade outline is straight to slightly arched. The P_1 of *H. typicalis* β is characterized by a small distal denticle hardly bigger than the adjacent ones at all growth stages.

Remarks. *H. typicalis* has the same stratigraphical and geographical range that *H. praeparvus*, with which it shares the shape of the distal denticle. However, *H. typicalis* is characterized by a more uniform denticle size.

Hindeodus sp. indet.
Figure 7I

Description. This P_1 element is carminiscaphate with a broad triangular distal denticles about twice higher than the adjacent denticles. The carina is composed of 10 denticles that are more closely appressed anteriorly and broader and shorter posteriorly. Consequently, the carina looks arched posteriorly in lateral view. In upper view, the blade appears thickened and S-shaped.

Genus ***Isarcicella*** Kozur, 1975

Type species. *Spathognathodus isarcicus* Huckriede, 1958

Isarcicella lobata (Perri and Farabegoli, 2003)
Figure 7G, H

1964. *Spathognathodus isarcicus* Huckriede -

Staesche, textfig. 61.

1981. *Hindeodus parvus* Kozur and Pjatakova - Matsuda, p. 91-93, pl. 5, figs 1, 3 (only).

1987. *Isarcicella sichuanensis* Ding - Yang et al., pl. 36, figs 7, 8.

1991. *Isarcicella isarcica* Huckriede - Perri, p. 42-43, pl. 3, fig. 7, pl. 4, fig. 8.

1998. *Hindeodus parvus* morphotype 2 Kozur and Pjatakova - Farabegoli and Perri, pl. 4.3.1, fig. 13.

2003. *Isarcicella lobata* - Perri and Farabegoli, p. 298–298, pl. 2, figs 1-3, pl. 3, figs 18-23 (only).

2004. *Isarcicella lobata* Perri and Farabegoli - Perri et al., p. 475, pl. 1, figs 7, 9.

2007. *Isarcicella lobata* Perri and Farabegoli - Jiang et al., pl. 5, figs 17, 18.

2011a. *Isarcicella lobata* Perri and Farabegoli - Jiang et al., pl. 3, figs 2–4 (only).

2014. *Isarcicella lobata* Perri and Farabegoli - Jiang et al., pl. 4, figs 1, 3 (only).

2015. *Isarcicella lobata* Perri and Farabegoli - Brosse et al., fig. 6A-D.

Occurrence. Southern Alps: Bulla, Tesero, San Pellegrino Pass and Agordo-Frassené sections, Werfen Fm., Mazzin Member. Pakistan: Chitral section. China: UAZ_4-UAZ_5 in the Nanpanjiang basin (Brosse et al., 2016). Kashmir: Guryul Ravine section, Khunamuh Fm., E_2-E_3.

Diagnosis. See Perri and Farabegoli (2003).

Description. The distal denticle is bigger and much higher than the succeeding denticles. Its anterior margin is arched posteriorly. It is followed by six to seven smaller denticles whose width increases posteriorly. The carina is developed in a thickened blade in big specimens. The denticles have a rounded section and a rounded tip. The basal cavity is asymmetrical, with a smooth lateral lobe that bears neither a node nor a denticle. The basal cavity is tapered anteriorly below the distal denticle and posteriorly below the last denticle. We can see in lower view that it is not deeply excavated.

Remarks. *Isarcicella lobata* bears resemblances with *H. parvus* (e.g. high cusp), but it differs by the asymmetrical wide basal cavity and a swelling of the carina. It shares with *I. turgida* a swelling of the base of the denticles, but the blade is not as swollen as in the latter and its basal cavity is asymmetrical and more inflated.

Isarcicella staeschei (Dai and Zhang, in Li et al., 1989)

Figure 7D-F

1964. *Spathognathodus isarcicus* Huckriede - Staesche, p. 288, text-figs 62-63.

1981. *Isarcicella isarcica* Huckriede - Matsuda, p. 93-94, pl. 5, figs 4-7.

1981. *Isarcicella*? sp. - Matsuda, p. 94-95, pl. 5, fig. 8.

1989. *Isarcicella staeschei* - Dai and Zhang, pp. 430–431, pl. 45, figs 16–17; pl. 46, figs 4-7, 11–13, 18, 19; pl. 53, figs 13-14.

1996. *Isarcicella isarcica* Huckriede - Kozur, p. 100, pl. 5, figs 6, 9.

1998. *Isarcicella staeschei* Dai and Zhang - Orchard and Krystyn, p. 354, pl. 6, figs 4, 5, 10-12.

2003. *Isarcicella staeschei* Dai and Zhang - Perri and Farabegoli, p. 300, pl. 3, figs 1-14; pl. 4, figs 7–9.

2004. *Isarcicella staeschei* Dai and Zhang - Perri et al., p. 475, pl. 1, figs 1–6; pl. 2, figs 3, 6-14.

2011a. *Isarcicella staeschei* Dai and Zhang - Jiang et al., pl. 3, figs 9-12.

2015. *Isarcicella staeschei* Dai and Zhang - Brosse et al., fig. 6(G-K).

Occurrence. China: UAZ_4-UAZ_6 in the Nanpanjiang basin (Brosse et al., 2016). Southern Alps: Bulla, Tesero, San Pellegrino Pass and Agordo-Frassené sections, Werfen Fm., Mazzin Member. Kashmir: Guryul Ravine section, Khunamuh Fm., E_3.

Diagnosis. See Dai and Zhang (1989).

Description. The P_1 element is characterized by a distal denticle much higher than the following denticles. All denticles have a rounded section, due to the swollen carina. The distal denticle can be slender and conical in small specimens (Fig. 7E) or laterally compressed with a triangular outline in bigger specimen (see Fig. 7D, F). The cup is asymmetrical and has a lateral lobe bearing one or two denticles. The basal cavity is wide and asymmetrical. It tapers anteriorly below the distal denticle and posteriorly below the last denticle. The basal margin of the cup flares around the widest part of the element in big specimens (Fig. 7F).

Remarks. The P_1 elements of the three *Isarcicella* species *I. lobata*, *I. staeschei* and *I. isarcica* have a very high intraspecific variation, with variable number and size of features on their lateral processes, from rudimentary nodes to broad denticles. In lateral view, the three species have a very similar general outline. The three species can be summarized as having: (i) no lateral node or denticle (*I. lobata*), (ii) one lateral process bearing nodes or denticles (*I. staesche*i), (iii) two lateral processes bearing nodes or denticles (*I. isarcica*). These three species are common and the sequence of their respective FOs usually follow the 'development of the lateral lobes' gradient. It is worth noting that *I. isarcica* seems to be absent at Guryul ravine.

I. staeschei is divided into two morphotypes (Perri and Farabegoli, 2003): a 'single lateral denticle' morphotype (Fig. 7D, E) and a 'more than one lateral denticle' morphotype (Fig. 7F), the latter including the holotype. Both morphotypes are found in the same beds at Guryul Ravine.

Isarcicella turgida (Kozur et al., 1975)

Figure 7A-C

1975. *Anchignathodus turgidus* n. sp. - Kozur et al., p. 5, pl. VII, figs 11-12.

1995. *Isarcicella*? *turgida* Kozur et al. - Kozur, p. 72, pl. 2, figs 5, 8.

1996. *Isarcicella*? *turgida* Kozur et al. - Kozur, p. 100, pl. 4, fig. 8.

2003. *Isarcicella turgida* Kozur et al. - Perri and Farabegoli, p. 245, pl. 2, figs 13-15.

2003. *Isarcicella lobata* Perri and Farabegoli - Perri and Farabegoli, pp. 298–298, pl. 3, figs 15-17, 24-29 (only).

2004. *Isarcicella turgida* Kozur et al. - Perri et al., p. 475, pl. 1, fig. 8.

2011a. *Isarcicella turgida* Kozur et al. - Jiang et al., pl. 2, figs 3-6.

2015. *Isarcicella turgida* Kozur et al. - Brosse et al., fig.8(A-J, ?K, ?L).

Occurrence. Iran: Elikah Fm., Unit 64. China: UAZ_4-UAZ_6 in the Nanpanjiang basin (Brosse, et al. 2016). Southern Alps: Bulla, Tesero, San Pellegrino Pass and Agordo-Frassené sections, Werfen Fm., Mazzin Member. Kashmir: Guryul Ravine section, Khunamuh Fm., E_3.

Diagnosis. See Kozur et al. (1975).

Description. The P_1 element has a small length/width ratio, due to the small number of denticles. The distal denticle is much higher than the following denticles, erected and thick, with a rounded section. It precedes five to six denticles which anteriorly are small and closely appressed, and become broader and less closely appressed posteriorly. The denticles are laterally thick with rounded sections and rounded tips. They arise from the very thick and swollen blade. As a consequence of the swollen carina, the basal cavity is wide. The basal cavity is symmetrical and tapers anteriorly below the distal denticle and posteriorly below the last denticle.

Remarks. The outline of *I. lobata* is similar to the one of *I. turgida*, and the former also

shows a swelling of the entire basal cavity. *I. lobata* is distinct in having its asymmetrical basal cavity. In lateral view, *I. turgida* is very similar to *H. parvus*, but is distinct by the swollen carina. Kozur et al. (1996, p. 100) considered *I. turgida* as a transitional form between *H. parvus* and *I. staeschei*. Perri and Farabegoli (2003) revised the phylogeny of anchignathodontids and proposed instead that turgida is a transitional form between *I. prisca* and *I. lobata*. The more rigorous phylogenetical analysis by Jiang et al. (2011b) resulted in the same conclusion than Perri and Farabegoli (2003, Fig. 7, p. 291). This is also supported by the remarkable conodont sequence of Wuzhuan (Brosse et al. 2015, Fig. 2).

H. parvus and *I. turgida* are often associated in Griesbachian deposits, but in agreement with the current hypothesis about their phylogenetical relationships, the FAD of *H. parvus* is considered to be slightly older than the FAD of *I. turgida*. *I. turgida* has been occasionally used as an alternative index species for the base of the Triassic. For instance, at Shangsi section Lai et al. (1996) and Jiang et al. (2011a) placed the base of the Triassic below the FO of *I. turgida* in (bed 28a) rather than below the FO of *H. parvus* (bed 29c).

Family *GONDOLELLIDAE* Lindström, 1970

Genus ***Neogondolella*** Bender and Stoppel, 1965

Type species. *Gondolella mombergensis* Tatge, 1956.

Segminiplanate forms of Carboniferous, Permian and Triassic ages were initially included within the genus *Gondolella* (Stauffer and Plummer, 1932). Bender and Stoppel (1965) later separated Triassic gondolellids as belonging to *Neogondolella*, on the basis that Triassic fonrms would have a more rounded basal cavity and a more extended lanceolate platform.

Similarly, Kozur (1989) introduced *Clarkina* for Late Permian neogondolellid forms and considered *Neogondolella* as restricted to the (Middle) Triassic. The genus *Clarkina* was later extended by various authors to the early Triassic (e.g. Zhang et al., 1996; Korte et al., 2004; Kozur, 2005; Chen et al., 2008, 2009; Zhao et al., 2013; Zhang et al., 2014) on the assumption that this genus went extinct at the end of the Griesbachian and should be kept separated from the Middle Triassic *Neogondolella*. Yet, the long thought gap in neogondolellids during post-Griesbachian Early Triassic was due to ecological exclusion from the Tethyan realm, and migration to the Boreal realm, rather than extinction (Orchard, 2007). Moreover presumed distinctions between *Clarkina* and *Neogondolella* (Kozur, 1989; Henderson and Mei, 2007) rest on little evidence or untested hypotheses (see Orchard and Rieber, 1999; Orchard, 2007). Hence, we follow here Orchard and others (Orchard et al., 1994; Orchard and Krystyn, 1998; Orchard and Rieber, 1999; Jiang et al., 2007, 2011a; Sun et al., 2012) in considering *Clarkina* as a junior synonym of *Neogondolella*.

Neogondolella carinata (Clark, 1959)

Figure 13A-H

1959. *Gondolella carinata* - Clark, pp. 308-309, pl. 44, figs 15-19.

1970b. *Neogondolella carinata* Clark - Sweet, pl. 3, figs 1-17 (only).

1971. *Neogondolella carinata* Clark - Sweet et al., pl. 1, fig. 1-7.

1981. *Gondolella carinata* Clark - Bhatt et al.,

pl. 1, fig. 7.

1982. *Neogondolella carinata* Clark - Tian, pl. 1, fig. 13.

1984. *Gondolella carinata* Clark - Matsuda, pl. 1, figs 7, 11 (only).

1987. *Gondolella carinata* Clark - Yang et al., pl. 34, figs 1, 7 (only).

1994. *Neogondolella carinata* Clark - Orchard et al., pl. 3, figs 1-4, 10-14.

1995. *Clarkina carinata* Clark - Wang and Wang, pl. I, figs 2.

1995. *Gondolella carinata* Clark - Garzanti et al., pl. 1, fig. 5 (only).

1998. *Neogondolella carinata* Clark - Orchard and Krystyn, pl. 4, figs 9, 11, 16, 17, 20.

2007. *Neogondolella carinata* Clark - Zhang et al., fig. 2(8, 9).

2014. *Neogondolella carinata* Clark - Wu et al., pl. 8, figs 4, 13-15.

Occurrence. Nevada: Dinner Spring Canyon. Tibet: Selong section, *Otoceras latilobatum* Zone; Tulong sections *Hindeodus typicalis*-*Hindeodus parvus* Zone, Wenbudangsang section, I. Isarcica Zone. Spiti: Guling, Lingti, Lalung, Muth sections, *Otoceras woodwardi* Zone. Pakistan: Salt Range, Chhidru section, Chhidru Fm. Kashmir: Guryul Ravine section, Khunamuh Fm., E_3. China: Meishan section, beds 24d to 29. Lowermost Triassic worldwide.

Diagnosis. See the amended diagnosis by Orchard and Krystyn (1998).

Description. At Guryul Ravine, the platform of the P_1 shows variable width, from 1/3 to 1/2 of the total length. The platform margins often show mild indentations and flare laterally flat in wide specimens. The carina bears eight to eleven denticles. The denticles are discrete and lowest at mid-length. They consist in low nodes in the oldest forms (Bed GUR304-1, 307 and 309) and high pointy denticles in younger specimens (Bed GUR310). The platform strongly tapers anteriorly around the three first denticles which arise as a free or semi-free blade higher than the adjacent denticle. The cusp is erect to posteriorly inclined and broader and higher than the other denticles. It is surrounded by a small secondary platform, as the platform posteriorly tapers between the cusp and the before last denticles. The secondary platform can also include an additional smaller denticle after the cusp.

Remarks. *Ng. carinata* is known to have a long range across the entire Griesbachian and the base of the Dienerian. We can observe two populations at Guryul Ravine, the youngest, which is restricted to the late Griesbachian GUR310, having distinctively high and pointy denticles.

Ng. carinata was initially the only species of *Neogondolella* described at Guryul Ravine (Matsuda, 1984). Matsuda (1984) wrote that *N. carinata* extended within the Permian at Guryul Ravine. However, Matsuda (1981) reports de FO of *Ng. carinata* in Unit 57, above the FO of *H. parvus* (Unit 56), which would confirms a Griesbachian age for *Ng. carinata* at Guryul Ravine. Note that the only specimen of *Ng. carinata* illustrated by Matsuda (1984; Unit 57, pl. 1, Fig. 1) is revised here as belonging to *Ng. tulongensis*.

The holotype of *Ng. carinata* is re-illustrated in Orchard et al. (1994, figs 1, 2).

Neogondolella changxingensis (Wang and Wang in Zhao et al., 1981)

Figure 8J-L

1981. *Neogondolella subcarinata changxingensis* - Wang and Wang *in* Zhao et al., p. 80, pl. V, figs. 6, 7, 10, 11, pl. VII, figs 7, 8.

1994. *Neogondolella changxingensis* Wang

and Wang - Orchard et al., part, pl. 1,

figs. 7, 8, 10, 13-16., 18, 19.

1998. *Clarkina changxingensis changxingensis* Wang and Wang - Mei et al., pl. I: B-D, F-H, K, pl. II: G.

1998. ?*Neogondolella changxingensis* Wang and Wang - Orchard and Krystyn, pl. 4, fig. 21, 22.

2011a. *Neogondolella changxingensis* Wang and Wang - Jiang et al., pl. 5, figs 1, 2.

2014. *Clarkina changxingensis* Wang and Wang - Yuan et al., pl. IV, figs 1-20, 22-24.

Occurrence. China: Shangsi section (Jiang et al., 2011a), bed 26 (upper Changhsingian); Meishan section (Jiang et al., 2007), beds 24a-28 (upper Changhsingian to Griesbachian). Spiti: Lingti section (Griesbachian). Kashmir: Guryul Ravine, Khunamuh Fm., E_2-E_3, Griesbachian. Upper Changhsingian and Griesbachian worldwide.

Diagnosis. See the amended diagnosis from Mei et al. (1998).

Description. The P_1 element is elongated with subsymmetrical platform margins. The carina is arched and is composed of partially fused low denticles or nodes. It terminates posteriorly by a small erected terminal cusp. As a consequence of the terminal cusp and the laterally arched carina, the posterior margin is slightly truncated. Anteriorly the platform margins tapers sharply and lead to a high fixed blade that can let the first denticle free. The carina can display a small gap between the cusp and the adjacent denticle.

Remarks. Orchard et al. (1994) and later Mei (1996) considered *Ng. changxingensis* as being closest to *Ng. orchardi* (Orchard et al. (1994)'s '*Ng*. aff. c*hangxingensis*') to which it differs in having a bigger cusp, a more elongated curved platform, more fused denticles and a tear-drop outline.

Neogondolella discreta (Orchard and Krystyn, 1998)

Figure 14J-P

1996. *Neogondolella* n. sp. E - Krystyn and Orchard, p. 18, 19.

1997. *Neogondolella* n. sp. E - Orchard and Tozer, p. 677.

1998. *Neogondolella discreta* - Orchard in Orchard and Krystyn, p. 356, pl. 5, figs 4-9.

?2013. *Neogondolella discreta* Orchard - Zhao et al., fig. 6(M-O) (only)

Occurrence. Spiti: Guling section, bed 5. Arctic Canada: Ellesmere Island, Strigatus Zone. Kashmir: Guryul Ravine section, E_3, bed GUR310. China: Hubei Province, Daxiakou section (Zhao et al., 2013). Latest Griesbachian Worldwide.

Diagnosis. See Orchard and Krystyn (1998).

Description. The P_1 element is small with an elliptical to lanceolate outline. In upper view, the narrow platform margins are strongly constricted anteriorly and posteriorly, leaving the anterior- and posterior-most denticles free. The carina is composed of eight to eleven high pointy discrete denticles. The denticles are subequal in size and arise as a blade terminated by a broader cusp inclined posteriorly. The cusp is occasionally followed by an additional smaller denticle. In lateral view, the element is straight to slightly concave upward. In lower view, the attachment surface is broad and flaring posteriorly.

Remarks. *Ng. discreta* differs from *Ng. krystyni* by its reduced platform and by a higher carina with more discrete denticles. It is distinct from *S. kummeli* by more discrete denticles and more developed platform brims. All elements found at Guryul Ravine come from the same bed (GUR310), below the FO of *S. kummeli*.

According to Krystyn and Orchard (1996) Orchard and Krystyn (1998) and Orchard (2007) *Ng. discreta* is included within the *krystyni-discreta-dieneri* lineage. This morphocline is based on the P_1 element and includes the progressive development of the axial part (blade-carina-cusp) together with a reduction of the platform relative size. This conodont faunal transition from neogondolellids to neospathodids is known to occur in many places (Orchard 2007) and is a marker of the Griesbachian-Dienerian boundary.

Neogondolella griesbachensis (Orchard, 2007)

Figure 10A-E

2007. *Neogondolella griesbachensis* - Orchard, p.114, pl. 1, figs 22, 23.

Occurrence. Arctic Canada: Ellesmere Island, Otto Fiord South and Blind fiord, Blind Fiord Formation, *Strigatus* zone. Kashmir: Guryul Ravine section, Khunamuh Fm., E_3.

Diagnosis. See Orchard (2007).

Description. The P_1 elements are elongated and slender (width/length ratio < 1/3). The platform margins are parallel to subparallel and posteriorly constricted around the terminal cusp. The platform narrows slowly in the anterior third of the element around a low fixed blade. The cusp is posteriorly inclined, broad but short. The carina bears numerous (11 to 13) low denticles or nodes. In lower view, the attachment scar is narrow and also has parallel margins.

Remarks. Until now, *Ng. griesbachensis* was exclusively known from the *Strigatus* Zone of the Artic Canada (Orchard, 2007, 2008). It is here reported for the first time in the Tethyan realm.

Neogondolella krystyni (Orchard in Orchard and Krystyn, 1998)

Figure 13I-Q

1996. *Neogondolella* n. sp. D - Krystyn and Orchard, p. 18, 19.

1997. *Neogondolella* n. sp. D - Orchard and Tozer, p. 677.

1998. *Neogondolella krystyni* - Orchard in Orchard and Krystyn, pp. 356-357, pl. 4, figs 25-28, pl. 5, figs 1-3, 10-17, 20, 21.

?2012. *Neogondolella krystyni* Orchard - Yang et al., fig. 5(6).

Occurrence. Spiti: Guling section, bed 3 (*Otoceras woodwardi* Zone), bed 62. Kashmir: Guryul Ravine section, Khunamuh Fm., E_3, bed GUR310. China: Chaohu section (Zhao et al., 2007), Meishan section (Zhang et al., 2007). Late Griesbachian Worldwide.

Diagnosis. See Orchard and Krystyn (1998).

Description. The platform margins strongly taper in the anterior third around a fixed blade. The posterior margin is pointy to narrowly squared around the cusp. The posteriorly inclined cusp is broader and much taller than the other denticles. It can be terminal, subterminal, surrounded by a narrow platform or followed by another denticle that deflects laterally for the biggest specimens. The carina bears 9 to 13 high and discrete denticles. The denticles are subequal in size. The attachment scar is narrow and tear-shaped, or posteriorly squared in the case of an additional denticle posteriorly. The platform shape is very variable and asymmetrical, often slightly constricted posteriorly.

Remarks. The variations of the size and position of the terminal denticle and of the platform shape have been highlighted in Orchard and Krystyn (1998) using the material

from Spiti. We also observe at Guryul Ravine a high intraspecific variability in the shape of the denticles and platform. Compared with the material from Spiti, specimens of *Ng. krystyni* at Guryul Ravine have less fused denticles. This is particularly true in younger hrizons. The common features of the specimens retrieved from Guryul Ravine section are a well-developed carina, a big posteriorly inclined cusp and asymmetrical ondulose platform margins.

Specimens of *Ng. krystyni* have higher denticles than most contemporaneous species. The development of the carina in P_1 elements of *Ng. krystyni* is similar to that of elements of *Ng. kazi*, but their posterior margin is less rounded than in elements of *Ng. kazi*. Elements of *Ng. discreta* are more constricted posteriorly and have an even more developed carina.

Neogondolella meishanensis (Zhang, Lai, Ding and Liu, 1995)

Figure 8A-D

1995. *Clarkina* sp. nov. - Wang, pl. I, fig. 2-4.

1995. *Clarkina meishanensis* - Zhang, Lai, Ding and Liu, p. 674, pl. 2, figs 4, 5, 6.

1995. *Gondolella carinata* Clark - Garzanti et al., pl. 1, fig. 12, pl. 2, fig. 10 (only).

1998. *Neogondolella meishanensis* Zhang et al. - Orchard and Krystyn, pl. 1, figs 10-14, 17, 18, 19, 26-28.

2008. *Clarkina meishanensis meishanensis* Zhang et al. - Chen et al., pl. I, figs 9-14, pl. III, figs 5, 6 (only).

2011a. *Neogondolella* sp. - Jiang et al., pl. 4, fig. 6.

2011a. *Neogondolella meishanensis* Zhang et al. - Jiang et al., pl. 4, figs 7-9.

2015. *Neogondolella meishanensis* Zhang et al. - Yuan et al., pl. 4, figs 1-7 (only).

Occurrence. Tibet: Selong section, *Ophiceras latilobatum* Zones. Spiti: Guling, Lingti, Lalung and Muth sections, *Otoceras woodwardi* and *Ophiceras latilobatum* zones. China: UAZ_2-UAZ_4 in the Nanpanjiang basin (Brosse et al., 2016). Kashmir: Guryul Ravine section, Khunamuh Fm., E_1-E_3.

Diagnosis. See Zhang et al. (1995).

Description. The P_1 has an elongated platform (width-length ratio ≤ 1/3) with biconvex to subparallel margins. The platform margins taper in the anterior third and leave the anteriormost denticles free. It tapers posteriorly toward the prominent terminal cusp. The anterior denticles are fused in a nearly free blade. The cusp is big, inclined posteriorly and slightly arched. It may be less closely spaced with the adjacent denticle than the other denticles of the carina. The carina is otherwise low, with denticles lowest at midlength. The carina bears nine to eleven denticles.

Remarks. As in *Ng. griesbachensis*, the prominent terminal cusp of *Ng. meishanensis* is slightly distant from the adjacent denticle, but *Ng. griesbachensis* has a more slender elongated outline and more parallel platform margins.

Neogondolella nassichuki (Orchard *in* Orchard and Krystyn 1998)

Figure 10F, G

1994. *Neogondolella* aff. *carinata* Clark - Orchard et al., pl. 3, figs 16-19.

1998. *Neogondolella nassichuki* - Orchard in Orchard and Krystyn, p. 358, pl. 5, figs 18-19, 22-30.

2004. *Neogondolella nassichuki* Orchard - Kozur, pl. 2, fig. 26 (only).

2011a. *Neogondolella nassichuki* Orchard - Jiang et al., pl. 4, fig. 10.

Occurrence. Tibet: Selong section, *Ophiceras latilobatum* Zones. Spiti: Guling, Lingti, Lalung and Muth sections, *Otoceras woodwardi* Zone. Iran: Shahreza section, uppermost Hambast Fm., sample Sh62A. China: Shangsi section, bed 29c. Kashmir: Guryul Ravine, E_3.

Diagnosis. See Orchard and Krystyn (1998).

Description. The P_1 element is quite elongated and has an oval outline. The platform margin tapers anteriorly and the anteriormost denticle is free. The platform tapers posteriorly in a narrowly rounded to slightly squared thin posterior margin. As the platform tapers on both sides, the element outline can be rhombic (widest at mid-length, see Figure 10G). The cusp is surrounded by the posterior platform margins and is broader than the adjacent denticles, erect and moderately high. The denticles are low and form a low carina. The carina is composed of 10 to 14 discrete nodes, anteriorly more fused into a low blade.

Remarks. Orchard and Krystyn (1998) suggest that *Ng. nassichuki* is the precursor of *Ng. krystyni* through a development of the posterior carina.

Neogondolella planata (Clark, 1959)

Figure 14A-I

1959. *Neogondolella planata* - Clark, p. 309, pl. 44, figs 8-10.

1977. *Neogondolella planata* Clark - Goel, p. 1099, pl. 3, fig. 5 (only).

1984. *Gondolella carinata* Clark - Matsuda, pp. 119-122, pl. 1, fig. 4, 10 (only).

1994. *Neogondolella planata* Clark - Orchard et al., pl. 3, figs 5, 6.

1995. *Clarkina planata* Clark - Zhang et al., pl. 2, fig. 10.

1998. *Neogondolella planata* Clark - Orchard and Krystyn, pl. 4, figs 1-4, 7, 8, 12-15, 18, 19, 23, 24.

2007. *Neogondolella planata* Clark - Jiang et al., pl. III, figs 8, ?9, ?10.

Occurrence. Nevada: Dinner Springs Canyon, Dinwoody Fm. Tibet: Selong section, *Otoceras latilobatum* Zone. Spiti: Guling, Lingti, Lalung and Muth sections, *Otoceras woodwardi* and *Ophiceras tibeticum* zones. China: UAZ_3-UAZ_5 in the Nanpanjiang basin (Brosse et al., 2016). Kashmir: Guryul Ravine section, Khunamuh Fm., E_3. Lowermost Triassic worldwide.

Diagnosis. See the amended diagnosis of Orchard and Krystyn (1998).

Description. The P_1 element has a well-developed platform. The platform margins are flat in the biggest specimens. Anteriorly, the platform tapers slowly until the first denticles. The platform is rounded posteriorly and the posterior brim is very narrow. The cusp is much broader and higher than the adjacent denticles. The carina is composed of seven to ten discrete nodes or denticles.

Remarks. As for *Ng. carinata*, we can observe two populations of *Ng. planata* at Guryul Ravine, the youngest, which is restricted to the late Griesbachian GUR310, having distinctively high and pointy denticles. The development of the carina of *Ng. planata* has been highlighted in Orchard and Krystyn (1998), who observed higher denticles in younger beds. The holotype, re-illustrated by Orchard et al. (1994, pl. 3, figs 5, 6) and Orchard and Krystyn (1998, pl. 4, fig. 4) corresponds to the "oldest" specimens found at Guryul Ravine.

Ng. planata is distinct from *Ng. taylorae* by the absence of posterior platform brim and a less rounded posterior margin.

Neogondolella taylorae (Orchard in Orchard et al., 1994)

Figure 9A-I

1994. *Neogondolella taylorae* - Orchard in Orchard et al., p. 833, pl. 3, fig. 15 (only).

1995. Gondolella taylorae Orchard - Garzanti et al., pl. 1, fig. 6 (only).

1996. *Clarkina* aff. *planata* Clark - Mei, pl. 18.2, fig. 13.

1998. *Neogondolella taylorae* beta morphotype nov. - Orchard and Krystyn, p. 362, pl. 2, figs 5, 9, 13–16.

2007. *Neogondolella taylorae* Orchard - Jiang et al., pl. II, figs 30-34; pl. III, figs 1-7, 28.

2013. *Clarkina taylorae* Orchard - Zhao et al., pl. 5, figs J-L.

Occurrence. Tibet: Selong section, *Otoceras latilobatum* Zone. Spiti: Guling, Lingti, Lalung and Muth sections, *Otoceras woodwardi* and *Ophiceras tibeticum* zones. Arctic Canada: Otto Fiord South, Blind Fm. (Henderson and Baud, 1997). China: UAZ_3-UAZ_6 in the Nanpanjiang basin (Brosse et al., 2016). Kashmir: Guryul Ravine section, Khunamuh Fm., E_3. Lowermost Triassic worldwide.

Diagnosis. See Orchard et al. (1994).

Description. The P_1 element has an oval platform that can be very large in some specimens and reach a ½ width/length ratio (Fig. 9D). The platform may extend to the anteriormost part of the carina or be strongly constricted anteriorly, leading to a short free blade. The carina is composed of seven to eleven discrete nodes. It terminates posteriorly by a small rounded erect cusp. Anteriorly, the carinal nodes rise and are fused to a low blade. The platform margins are rounded, subsymmetrical (Fig. 9E, F) to indented an asymmetrical (Fig. 9A, D). Posteriorly, the platform is rounded and the platform brim can be well-developed (Fig. 9A). The cusp is more conspicuous in specimens from younger beds (Fig. 9F, I, H).

Remarks. Orchard and Krystyn (1998) recognized three morphotypes of *Ng. taylorae*. *Ng. taylorae* α (including the holotype) has an elongated outline and gradually tapered to strongly constricted anterior platform margins (Fig. 9A-E). *Ng. taylorae* β is a short form with a strongly constricted anterior platform with a bulbous outline posteriorly (Fig. 9F, G). *Ng. taylorae* γ has an elongated and narrow platform (Fig. 9H, I). All three morphotypes can be observed in the material from Guryul Ravine and share the same stratigraphical ranges.

Ng. taylorae α closely resembles *Ng. zhejiangensis* and is distinct from the latter by a laterally wider platform and a wider posterior platform brim. *Ng. taylorae γ* has a similar outline to *Ng. tulongensis*, but a more rounded posterior platform.

We observe in Bed GUR310 that the carina is composed of higher and pointier denticles (Fig. 9F, I, H) than in the older beds. However, *Ng. taylorae* remains distinct from the contemporaneous *Ng. carinata* and *Ng. krystyni* as it does not show as extreme a development of the carina, even in the youngest horizons.

Neogondolella tulongensis (Tian, 1982)

Figure 11A-I

1982. *Neogondolella tulongensis* - Tian, p. 159, pl. 1, figs. 15, 17.

1984. *Gondolella carinata* Clark - Matsuda, pl. 1, fig. 1-3, pl. 2, fig. 1.

1994. *Neogondolella tulongensis* Tian - Orchard et al., pl. 2, fig. 1-4.

1995. *Neogondolella tulongensis* Tian - Wang and Wang, pl. I, figs 17-19.

1995. *Gondolella tulongensis* Tian - Garzanti et al., pl. 1, fig. 3 (only).

1996. *Clarkina tulongensis* Tian - Mei et al., pl. 18.1, figs 1-5.

1998. *Neogondolella tulongensis* Tian - Orchard and Krystyn, pl. 3, figs 1-17.

1998. *Clarkina* aff. *deflecta* Wang and Wang -

Mei et al., pl. V, fig. E.

2000. *Clarkina deflecta* Wang and Wang - Wang and Zhu, pl. II, figs 7-11.

2007. *Neogondolella deflecta* Wang and Wang - Jiang et al., pl. II, figs 13, 14, pl. III, fig. 13.

2007. *Neogondolella tulongensis* Tian - Jiang et al., pl. I, figs 27-33.

2007. *Neogondolella tulongensis* Clark - Zhang et al., fig. 4: 13.

2008. *Clarkina deflecta* Wang and Wang - Chen et al., pl. II, figs 11, 12 (only).

2011a. *Neogondolella deflecta* Wang and Wang - Jiang et al., pl. 4, fig 4, 5 (only).

Occurrence. Tibet, Selong section, *Otoceras latilobaturn* Zone. Spiti: Guling, Lingti, Lalung, and Muth sections, *Otoceras woodwardi* and *Ophiceras tibeticum* zones. China: UAZ_1-UAZ_3 in the Nanpanjiang basin (Brosse et al., 2016). Pakistan: Lingti section, Tamba Kurkur Fm. Kahsmir: Guryul Ravine section, Khunamuh Fm., E_3.

Diagnosis. Amended after Tian (1982) and Orchard and Krystyn (1998). P_1 unit large, arched or strongly arched with a rectangular outline in upper view. Platform long and wide, with a square posterior end, tapering slowly anteriorly. Free blade absent. Carina low, denticles flat and fused. Carina sometimes bifurcated posterior.

Description. The platform is long with subparallel margins, giving the whole element its characteristic rectangular shape. The carina is terminated anteriorly by a fixed blade, posteriorly by an inconspicuous cusp, which is sometimes followed by an additional denticle, or up to two posterior processes. In the former case, the cusp is surrounded by a posterior platform brim.

Remarks. Orchard and Krystyn (1998) differentiated three morphotypes of *Ng. tulongensis* based mainly on the platform shape. *Ng. tulongensis α* has a subsymmetrical platform shape and shows occasional bifurcation (Fig. 11A-E), *Ng. tulongensis β* has indented inner platform margin (Fig. 11F, G), *Ng. tulongensis γ* has a fused carina deflected posteriorly (Fig.11H, I).

Neogondolella zhejiangensis (Mei, 1996)

Figure 8E-I

1994. *Neogondolella* aff. *taylorae* Orchard - Orchard et al., pl. 2, fig. 17-19.

1995. *Clarkina changxingensis* Wang and Wang - Wang, pl. I, fig. 1, 5, 9.

?1995. *Gondolella tulongensis* Tian - Garzanti et al., pl. 1, fig. 10.

1996. *Clarkina zhejiangensis* - Mei, p. 145, pl. 18.2, fig. 16, 17.

1998. *Neogondolella zhejiangensis* Mei - Orchard and Krystyn, pl.1, figs 16, 22-25.

2007. *Neogondolella zhejiangensis* Mei - Jiang et al., pl. II, figs 1, 2.

2008. *Neogondolella zhejiangensis* Mei - *Chen et al.,* pl. III, figs 2, 3.

2011a. *Neogondolella* sp. 3; Jiang et al., pl. V, fig. 4 (only).

2011a. *Neogondolella taylorae* Orchard - Jiang et al., pl. V, fig. 5 (only).

?2014. *Neogondolella taylorae* Orchard - Jiang et al., pl. 6, fig. 6.

Occurrence. Tibet, Selong section, *Otoceras latilobaturn* Zone. Spiti: Guling, Lingti and Lalung sections, *Otoceras woodwardi* Zone. China: UAZ_1-UAZ_3 in the Nanpanjiang basin (Brosse et al., 2016). Kashmir: Guryul Ravine section, Khunamuh Fm., E_3. Worldwide Changhsingian and basal Griesbachian.

Diagnosis. See Mei (1996).

Description. Ng. zhejiangensis has a symmetrical to subsymmetrical platform outline. The platform margin is posteriorly rounded and occasionally subquadrate (Fig. 8H). It tapers anteriorly to a short free blade.

The carina is composed of low denticles or nodes. The cusp is subterminal, low and inconspicuous.

Remarks. Ng. zhejiangensis is distinct from *Ng. taylorae* by the much reduced posterior platform brim.

Neogondolella panjali n. sp.

Figure 12A-G

1995. *Gondolella carinata* Clark - Garzanti et al., pl. 2, fig. 9 (only).

1996. *Neogondolella* n. sp. A - Krystyn and Orchard, p. 17-19.

1998. *Neogondolella* n. sp. A - Orchard and Krystyn, pl. 4, fig. 5-6.

Derivation of name. Named after the Pir Panjal Range, a group of mountains that extends south-eastward for more than 320 km in the western Azad Kashmir area, through southwestern Jammu and Kashmir state to the upper Beas River in northwestern Himachal Pradesh state, India. The Pir Panjal Range geographically includes the PTB sections of Kashmir and Spiti, where this species has been discovered so far.

Holotype. Figure 12A, GUR304, PIMUZ XXXXX.

Type locality and horizon. sub-member E_3, Khunamuh Formation, Guryul Ravine section, Vihi district of Kashmir.

Material. 7 P_1 elements found in beds GUR304 to GUR310, sub-member E_3.

Occurrences. Spiti: "*Otoceras*-bearing strata" at Muth, Guling, Lingti and Lalung sections. Kashmir: Guryul Ravine, sub-member E_3.

Diagnosis. Diagnosis based on P_1 elements. Moderately high carina composed of partially fused denticles with an unremarkable cusp. Carina lowest at midlength, appearing straight in lateral view. Rounded platform margins tapering slowly posteriorly into a narrow posteriorly margin. Very thin posterior platform brim.

Description. The platform is broad and can show asymmetrical indentations. In most cases, it tapers sharply anteriorly so that the first and sometimes second denticles are free. Posteriorly, the platform tapers progressively and the posterior platform margin is narrowly rounded. The posterior platform is reduced to a thin bulge. Moderately high, the carina is composed of even denticles with an unremarkable cusp. The denticles are partly fused (Fig. 12A, C-G), or may be very completely (Fig. 12B)

Remarks. *Ng*. *panjali* n. sp. shares the oblong platform shape and the elevated and partly fused carina with *Ng. kazi*, but the latter has a well differentiated cusp. *Ng*. *panjali* n. sp. is distinct from *Ng. krystyni* in having a less elevated carina with more fused denticles and a more developed platform. Like *Ng. planata*, the carina extends throughout the entire length of the element and the cusp is subterminal to terminal. But *Ng*. *panjali* n. sp. has more closely appressed denticles that may be partially fused, and displays a constriction of the posterior platform margins that is not observed in specimens of *Ng. planata*.

Ng. *panjali* n. sp. was documented only from Spiti (Moth, Guling, Lingti and Lalung).

Neogondolella n. sp. A

Figure 15A-E

Occurrence. Kashmir, Guryul Ravine, sub-member E_3, bed 310.

Description. The carina is composed of numerous (10-15) pointy denticles that,

although often broken, seem to be subequal in size. The cusp is slightly bigger than the adjacent denticles and inclined posteriorly. The platform is slender and extends throughout the entire length of the element and posteriorly around the cusp, which is sometimes followed by an additional denticle. The four P_1 elements we recovered show that the platform develops progressively during the ontogeny and that the adults forms have well-developed platform margins, as illustrated in Figure 15D, E. The attachment scar is narrow and appears nearly straight in lateral view.

Remarks. The platform is not as constricted posteriorly as for co-occurring species like *Ng. krystyni* and *Ng. discreta*. This species could be a precursor of *Sweetospathodus kummeli*, whose elements often bear a platform brim (Sweet 1970b).

Neogondolella sp. indet 1

Figure 15F, G

Occurrence. Kashmir, Guryul Ravine, sub-member E_3, bed 315.

Description. The overall shape of the P_1 element is similar to that of *Ng. taylorae*. The P_1 is characterized by wide, subsymmetrical, flat platform margins. The platform surrounds the cusp posteriorly. Anteriorly, the platform is constricted. Although the preservation of the two elements found is poor, the denticles appear fused and the carina low.

Neogondolella sp. indet 2

Figure 15H, I

Occurrence. Kashmir, Guryul Ravine, sub-member E_3, bed 17.

Description. The overall shape of the P_1 element is similar to that of *Ng. krystyni*. The P_1 element is characterized by a deflection of the carina posteriorly, a terminal cusp and a pointy posterior margin. The cusp is bigger than the adjacent denticles. The denticles can be fused (Fig. 15H) or discrete (Fig. 15I). We retrieved only two elements of *Neogondolella* sp. indet 2 from this bed, a single one being well preserved (Fig. 15I). On this well- preserved element, the platform margins extend until the anterior end.

Genus **Neospathodus** Mosher 1968

Type species. *Spathognathodus cristagalli* Huckriede 1958

Neospathodus aff. *cristagalli* (Huckriede, 1958)

Figure 17A-D

α morphotype

Figure 17A-C

1981. *Neospathodus srivastavai* - Chhabra and Sahni, pl. 1, fig. 30.

Occurrence. Spiti: Mud section (unpublished data). Kashmir, Guryul Ravine, top of sub-member E_3.

Description. This morphotype has widely spaced discrete denticles so that two third of their length is free. The first denticle anterior to the cusp is separated from the cusp by a wider space than between the adjacent denticles and the cusp is conspicuously detached.

β morphotype

Figure 17D

Occurrence. Spiti: Mud section (unpublished data). Kashmir, Guryul Ravine, top of sub-member E_3.

Description. This form has an inverted basal cavity closely resembling that of *Ns. cristagalli* and a fan-shaped denticulation: the posterior denticles are reclined posteriorly and the anterior denticles are slightly inclined anteriorly; the cusp is not differentiated and is as broad as the adjacent denticles.

Neospathodus dieneri (Sweet, 1970a)
Figure 16F-K

1970a. *Neospathodus dieneri* - Sweet, pl. 1, fig. 17.

1970b. *Neospathodus dieneri* Sweet - Sweet, pl. 1, figs 1-4.

1971. *Neospathodus dieneri* Sweet - Sweet et al., pl. 1, fig. 23.

1982. *Neospathodus dieneri* Sweet - Tian et al., pl. 1, fig. 9.

1995. *Neospathodus dieneri* Sweet - Wang and Wang, pl. II, figs 7, 8, 11.

Occurrence. Worldwide early Dienerian.

Diagnosis. See Sweet (1970a).

Description. Zhao et al. (2007) distinguished three morphotypes of *Neospathodus dieneri*, according to the size of the posterior cusp and of the denticulation of the posterior margin of the carina. The material from Guryul Ravine corresponds to the description of the morphotype 3 of Zhao et al. (2007), as the cusp is broader in width and shorter than other denticles. However, we consider the element figured by Zhao et al. as *Ns. dieneri* morphotype 3 (2007, Pl. 1, figs. 11A-C) as belonging to the *cristagalli* group. Sweet's holotype of the species (1970a, Pl. 1, Fig. 17) better corresponds to morphotypes 1 and 2 of Zhao et al. (2007) with a posteriormost denticle smaller than those to the anterior.

Neospathodus ex. gr. *dieneri* (Sweet, 1970a)
Figure 16L-P

Occurrence. Guryul Ravine, sub-member E_3, beds GUR313 and GUR315.

Description. The overall shape of this element is similar to that of *Ns. dieneri* (morphotype 3) but is characterized by a bulge of a platform conspicuous in lateral view.

Neospathodus sp. indet 1
Figure 17F

Occurrence. Guryul Ravine, sub-member E_3, bed GUR315.

Description. The overall shape of this element is similar to that of *Ns. dieneri*, but this element is characterized by a bulge of a platform conspicuous in lateral view and a big anterior denticle that is inclined anteriorly and separated from the carina. This form has an inverted basal cavity closely resembling that of *Ns. cristagalli*. The denticles are subequal in size and width and inclined posteriorly.

Neospathodus sp. indet 2
Figure 17G

Occurrence. Guryul Ravine, sub-member E_3, bed GUR315.

Description. The overall shape of this element is similar to that of *Ns. dieneri*, but this element is characterized by a bulge of a platform conspicuous in lateral view. The denticles are subequal in size and width and inclined posteriorly. The basal cavity is slightly inverted to flat.

Neospathodus sp. indet 3

Figure 17H

Occurrence. Guryul Ravine, sub-member E_3, bed GUR315.

Description. The carina is characterized by 5 thick denticles. The basal cavity is inverted as the one of *Ns. cristagalli*. The denticles are subequal in size and width and inclined posteriorly. The anteriormost denticle is separated from the adjacent denticle by a narrow U-shaped space.

Genus **Sweetospathodus** Kozur, Mostler and Krainer 1998

Type species. *Neospathodus kummeli* Sweet 1970*b*

Sweetospathodus kummeli (Sweet, 1970b)

Figure 1611A-E

1970b*. Neospathodus kummeli* - Sweet, pl. 2, fig. 17, 18, 21 (only).

1971 *Neospathodus kummeli* Sweet - Sweet et al., pl. 1, fig. 9.

1982 *Neospathodus kummeli* Sweet - Tian et al., pl. 1, figs 18, 19.

1995 *Neospathodus kummeli* Sweet - Garzanti, pl. 2, figs 4, 6, 11.

1995 *Neospathodus cristagalli* Huckriede - Wang and Wang, pl. II, figs 12, 14.

?2007 *Neospathodus kummeli* Sweet - Zhang et al. 2007, fig. 3(13).

2013 *Sweetospathodus kummeli* Sweet - Zhao et al. fig. 9(P-Q).

Occurrence. West Pakistan: Salt Range, and Trans-Indus Ranges (Sweet, 1970b). South China, Daxiakou section (Zhao et al. 2013). Tibet: Tulong section (Tian, 1982), Selong section (Wang and Wang 1995). Spiti: Guling section (Garzanti 1995). Kashmir: Guryul Ravine, sub-member E_3, bed GUR311.

Diagnosis. See Sweet (1970b).

Description. Like the material from Pakistan described by Sweet (1970b), *S. kummeli* from Guryul Ravine can show thin platform-like brim. This brim can be widest posteriorly and surrounding the cusp (Fig. 16D) or widest at midlength (Fig. 16E). The posterior end of the element in Figure 16E is slightly laterally deflected. A small node is visible after the posteriormost denticle on the deflected part of the carina. This element bears resemblance with *Sweetospathodus praekummeli*, which diagnosis includes a posteriorly deflected carina and an extra node or denticle (Bhatt et al., 1981).

Remarks. Bhatt *et al*. (1981) described *S. praekummeli* as distinct from *S. kummeli* only by a stronger posterior lateral deflection of P_1 and they estimated that some of the most weakly deflected elements of *S. praekummeli* had likely been assigned to *S. kummeli*. The interpretation of the new species was supported by a large population of posteriorly deflected elements stratigraphically below *S. kummeli* in the Spiti River section. However, the two species co-occur in the Lalung section (Bhatt *et al*. 1981). Sweet has possibly assigned both morphotypes to *S. kummeli* and wrote that the specimen illustrated in lateral view (1970b; pl. 2, Fig. 21) has a 'bifid posterior process', which could induce a deflection of the posterior end. We found only one element with a deflected posterior end within the material of Guryul Ravine, co-occurring with *S. kummeli* (Fig. 16E) in GUR311. We follow here the definition of Sweet (1970b) and assign it to *S. kummeli*.

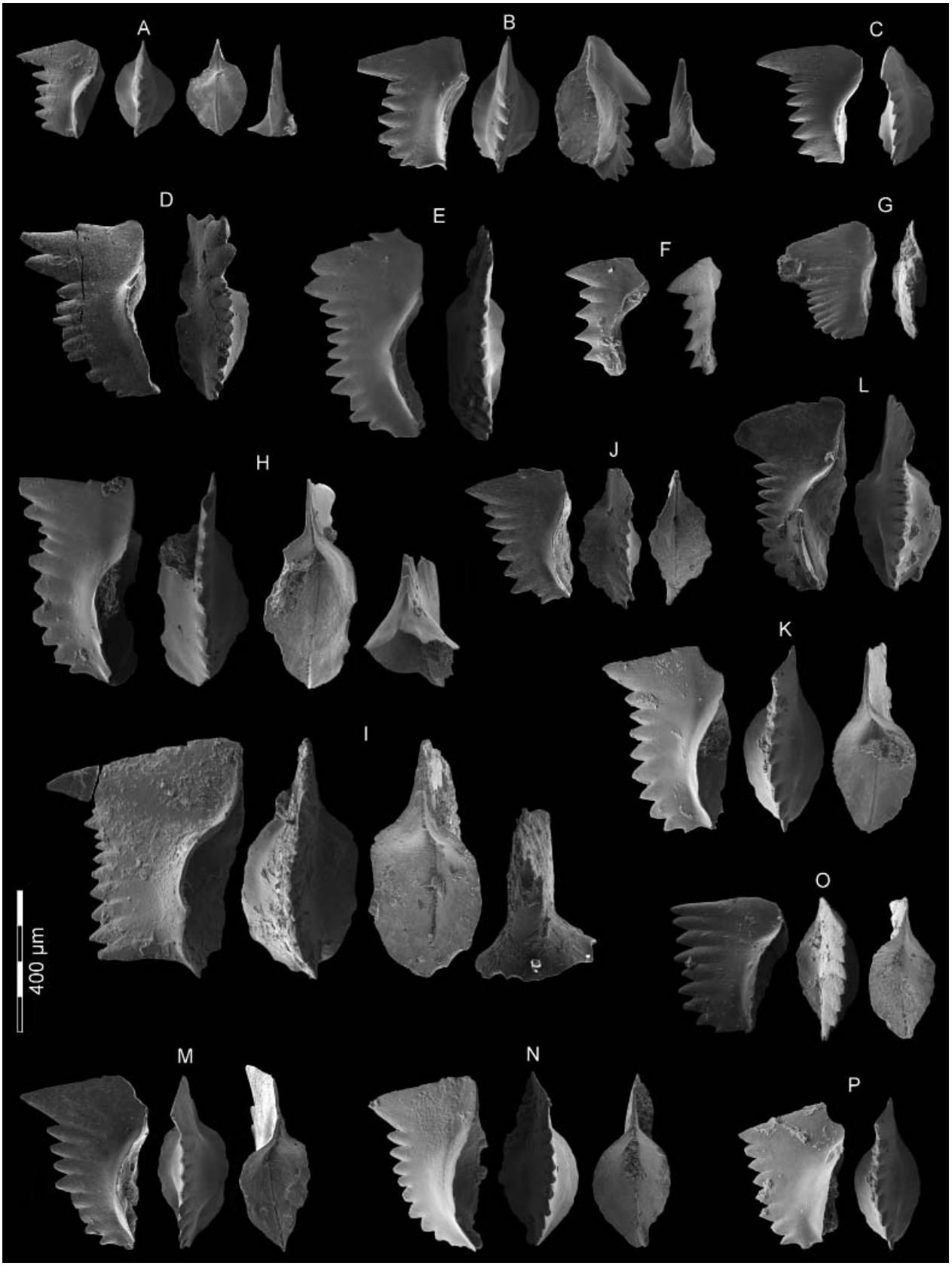

Figure 6: A-C, *Hindeodus parvus* Kozur and Pjatakova 1976; A, GUR13, PIMUZ XXXXX; B, GUR09, PIMUZ XXXXX; C, GUR09, PIMUZ XXXXX. D, E, *Hindeodus bicuspidatus* Kozur 2004; D, GUR302, PIMUZ XXXXX; E, GUR12, PIMUZ XXXXX. F, *Hindeodus latidentatus* Kozur, Mostler and Rahimi 1975, GUR09, PIMUZ XXXXX. G, *Hindeodus pisai* Perri and Farabegoli, GUR13, PIMUZ XXXXX. H, *Hindeodus inflatus* Nicoll et al. 2002, GUR09, PIMUZ XXXXX. I, *Hindeodus eurypyge* Nicoll et al. 2002, GUR13, PIMUZ XXXXX. J-L, *Hindeodus praeparvus* Kozur 1996; J, GUR09, PIMUZ XXXXX; K, GUR303, PIMUZ XXXXX; L. GUR304.2, PIMUZ XXXXX. M-P, *Hindeodus typicalis* Sweet 1970; M, N, new morphotype α; M, GUR304, PIMUZ XXXXX; N, GUR09, PIMUZ XXXXX; O, P, new morphotype β; O, GUR15, PIMUZ XXXXX; P, GUR09, PIMUZ XXXXX.

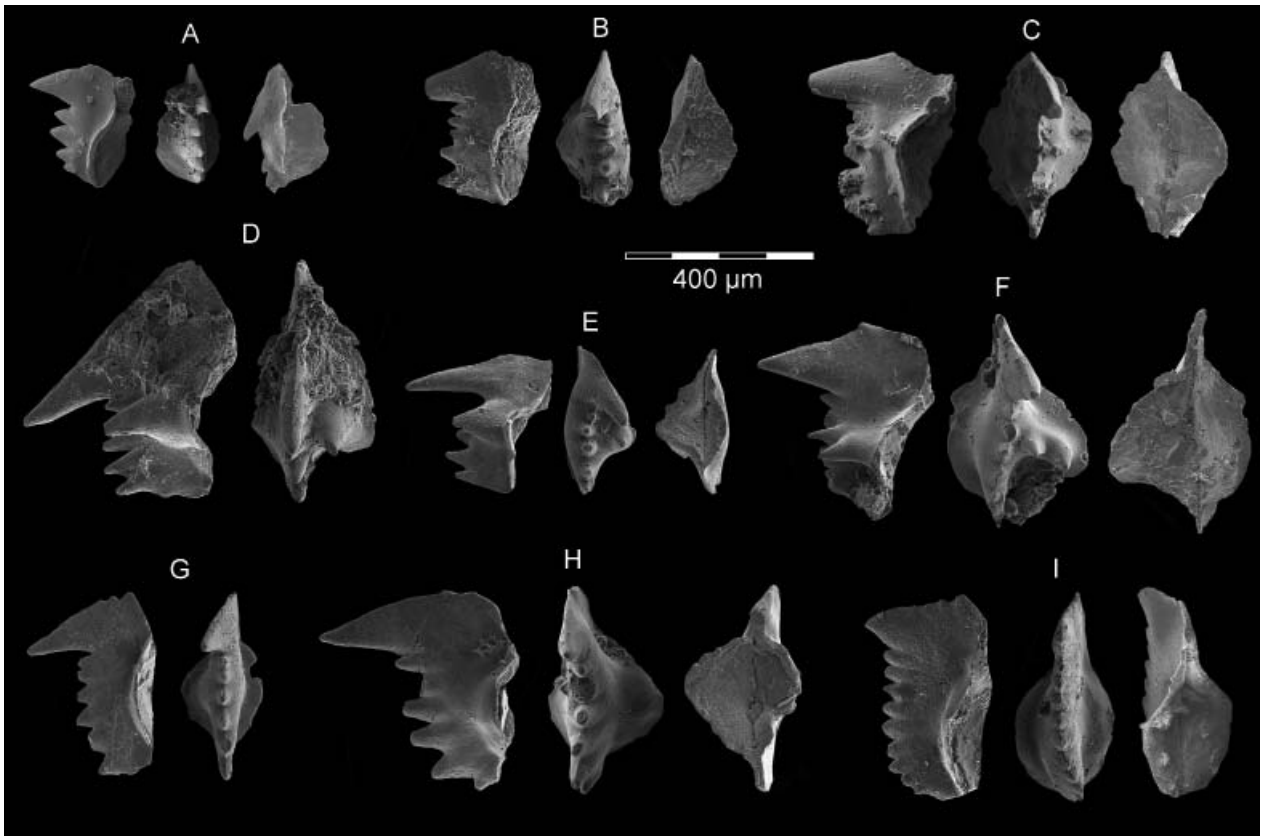

Figure 7: A-C, *Isarcicella turgida* Kozur, Mostler and Rahimi 1975; A, GUR12, PIMUZ XXXXX; B, GUR304.1, PIMUZ XXXXX; C, GUR13, PIMUZ XXXXX. D-F, *Isarcicella staeschei* Dai and Zhang 1989; D, GUR304.2, PIMUZ XXXXX; E, GUR304.1, PIMUZ XXXXX; F, GUR303, PIMUZ XXXXX. G, H, *Isarcicella lobata* Perri and Farabegoli 2003; G, GUR304, PIMUZ XXXXX; H, GUR301, PIMUZ XXXXX. I, *Hindeodus* sp. indet, GUR302, PIMUZ XXXXX.

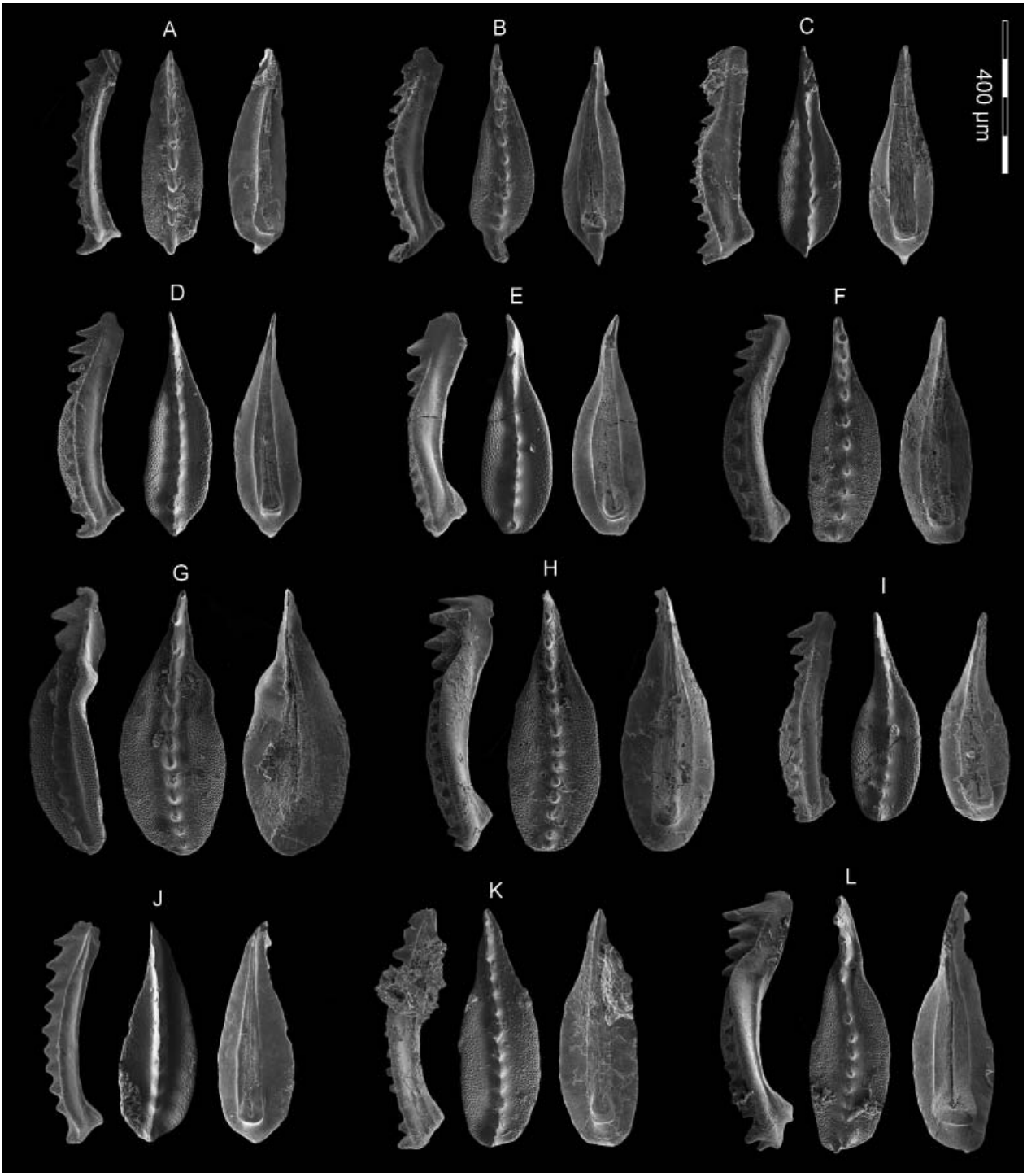

Figure 8: A-D, *Neogondolella meishanensis* Zhang, Lai, Ding and Liu 1995; A, GUR297, PIMUZ XXXXX; B, GUR304, PIMUZ XXXXX; C, GUR13, PIMUZ XXXXX; D, GUR304.2, PIMUZ XXXXX. E-I, *Neogondolella zhejiangensis* Mei 1996; E, GUR304.2, PIMUZ XXXXX; F, GUR304.3, PIMUZ XXXXX; G, GUR304.3, PIMUZ XXXXX; H, GUR305, PIMUZ XXXXX; I, GUR304.2, PIMUZ XXXXX. J-L *Neogondolella changxingensis* Wang and Wang 1981; J, GUR09, PIMUZ XXXXX; K, GUR13, PIMUZ XXXXX; L, GUR304.1, PIMUZ XXXXX.

Figure 9: A-G, *Neogondolella taylorae* Orchard 1994. A-C, α morphotype Orchard and Krystyn 1998: A, GUR307, PIMUZ XXXXX; B, GUR304.1, PIMUZ XXXXX; C, GUR304.2, PIMUZ XXXXX. D-F, β morphotype Orchard and Krystyn 1998; D, GUR305, PIMUZ XXXXX; E, GUR304.2, PIMUZ XXXXX; F, GUR310, PIMUZ XXXXX. I, pathogenic P_1, GUR310, PIMUZ XXXXX. H, G, γ morphotype; H, GUR310, PIMUZ XXXXX; G, GUR304.1, PIMUZ XXXXX.

Figure 10: A-E, *Neogondolella griesbachensis* Orchard 2007; A, GUR303, PIMUZ XXXXX; B, GUR304.1, PIMUZ XXXXX; C, GUR15, PIMUZ XXXXX; D, GUR304.2, PIMUZ XXXXX; E, GUR307, PIMUZ XXXXX. F, G, *Neogondolella nassichuki* Orchard 1998; F, GUR307, PIMUZ XXXXX; G, GUR303, PIMUZ XXXXX.

Figure 11: A-I, *Neogondolella tulongensis* Tian 1982; A-E, α morphotype Orchard and Krystyn 1998; A, GUR305, PIMUZ XXXXX; B, GUR304.2, PIMUZ XXXXX; C, GUR310, PIMUZ XXXXX; D, GUR15, PIMUZ XXXXX; E, GUR310, PIMUZ XXXXX. F, G, β morphotype Orchard and Krystyn 1998; F, GUR304, PIMUZ XXXXX; G, GUR310, PIMUZ XXXXX. H, I, γ morphotype Orchard and Krystyn 1998; H, GUR307, PIMUZ XXXXX; I, GUR303, PIMUZ XXXXX.

Figure 12: A-G, *Neogondolella panjali* nov. sp.; A, GUR304, PIMUZ XXXXX; B, GUR15, PIMUZ XXXXX ; C, GUR15 ; D, GUR305, PIMUZ XXXXX; E, GUR307, PIMUZ XXXXX; F, GUR307, PIMUZ XXXXX; G, GUR310, PIMUZ XXXXX.

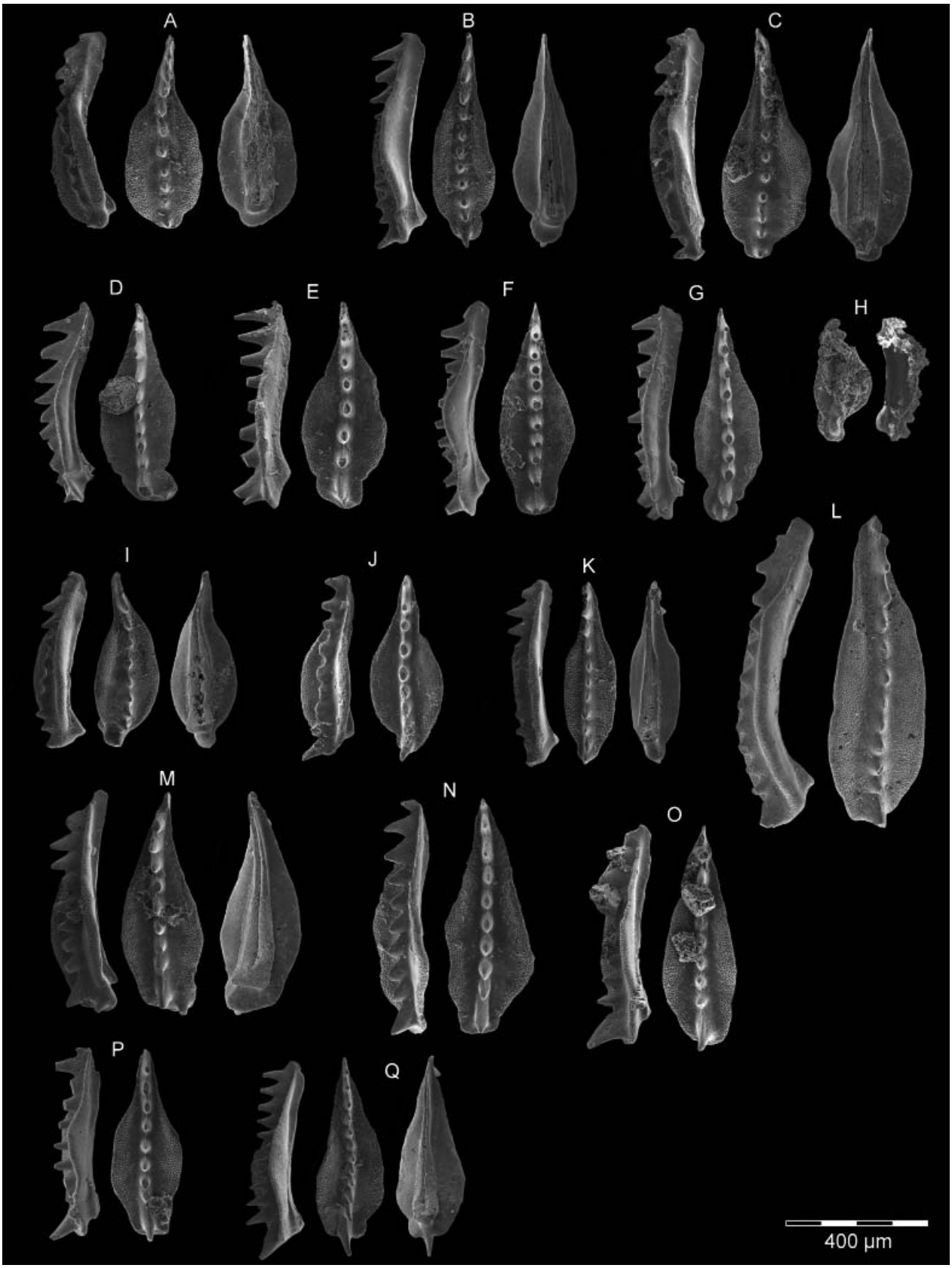

Figure 13: A-H, *Neogondolella carinata* Clark 1959 ; A, GUR304.1, PIMUZ XXXXX ; B, GUR307, PIMUZ XXXXX; C, GUR307, PIMUZ XXXXX; D, GUR310, PIMUZ XXXXX; E, GUR310, PIMUZ XXXXX; F, GUR310, PIMUZ XXXXX; G, GUR310, PIMUZ XXXXX; H, GUR310, PIMUZ XXXXX. I-Q, *Neogondolella krystyni* Orchard 1998; I, GUR307, PIMUZ XXXXX; J, GUR310, PIMUZ XXXXX; K, GUR309, PIMUZ XXXXX; L, GUR307, PIMUZ XXXXX; M, GUR310, PIMUZ XXXXX; N, GUR310, PIMUZ XXXXX; O, GUR310, PIMUZ XXXXX; P, GUR310, PIMUZ XXXXX; Q, GUR310, PIMUZ XXXXX.

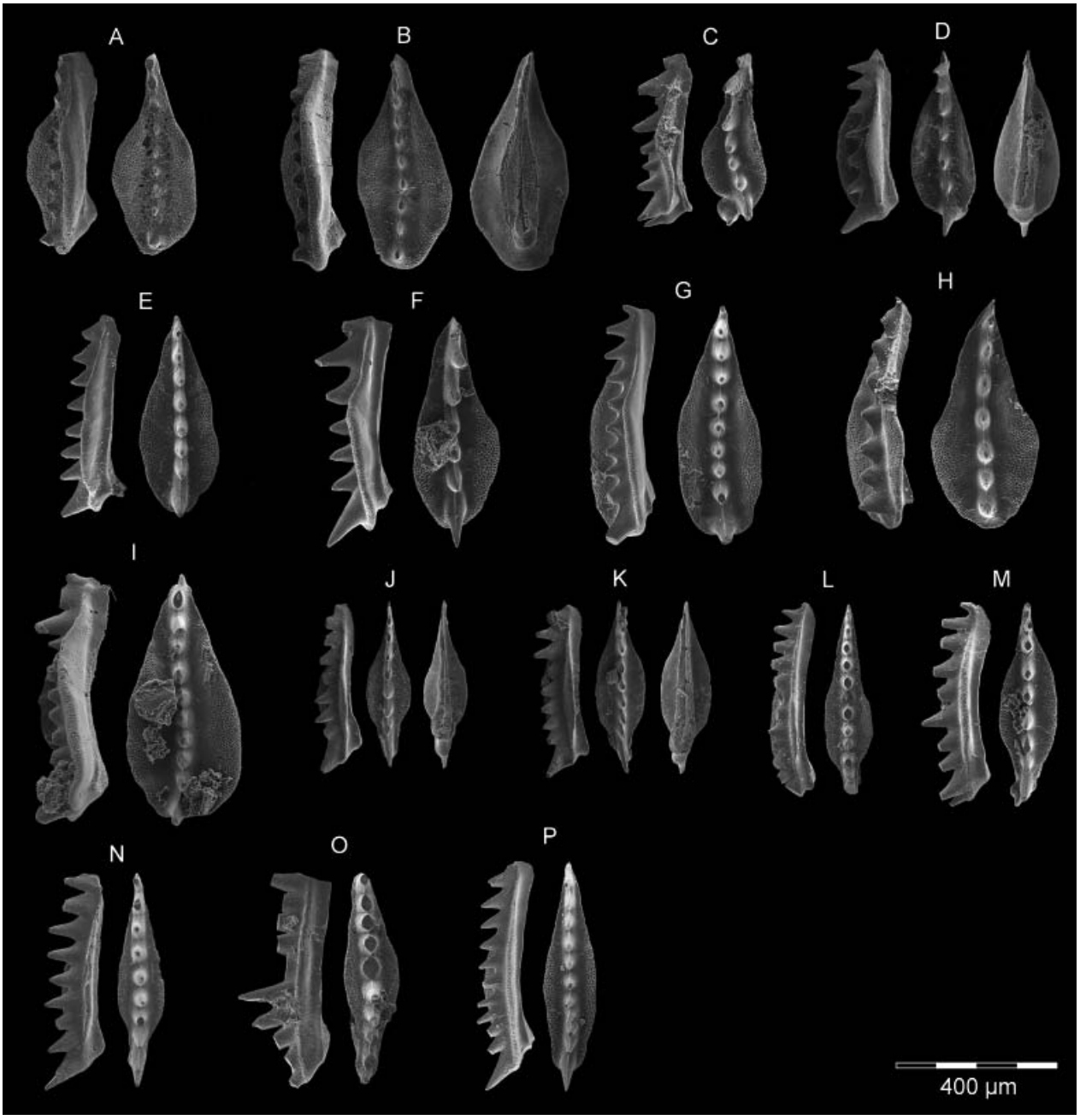

Figure 14: A?, B?, C-I, *Neogondolella planata* Clark 1959; A, GUR307, PIMUZ XXXXX; B, GUR307, PIMUZ XXXXX; C, GUR310, PIMUZ XXXXX; D, GUR310, PIMUZ XXXXX; E, GUR310, PIMUZ XXXXX; F, GUR310, PIMUZ XXXXX; G, GUR310, PIMUZ XXXXX; H, GUR310, PIMUZ XXXXX; I, GUR310, PIMUZ XXXXX. J-P, *Neogondolella discreta* Orchard and Krystyn 1998; J, GUR310, PIMUZ XXXXX; K, GUR310, PIMUZ XXXXX; L, GUR310, PIMUZ XXXXX; M, GUR310, PIMUZ XXXXX; N, GUR310, PIMUZ XXXXX; O, GUR310, PIMUZ XXXXX; P, GUR310, PIMUZ XXXXX.

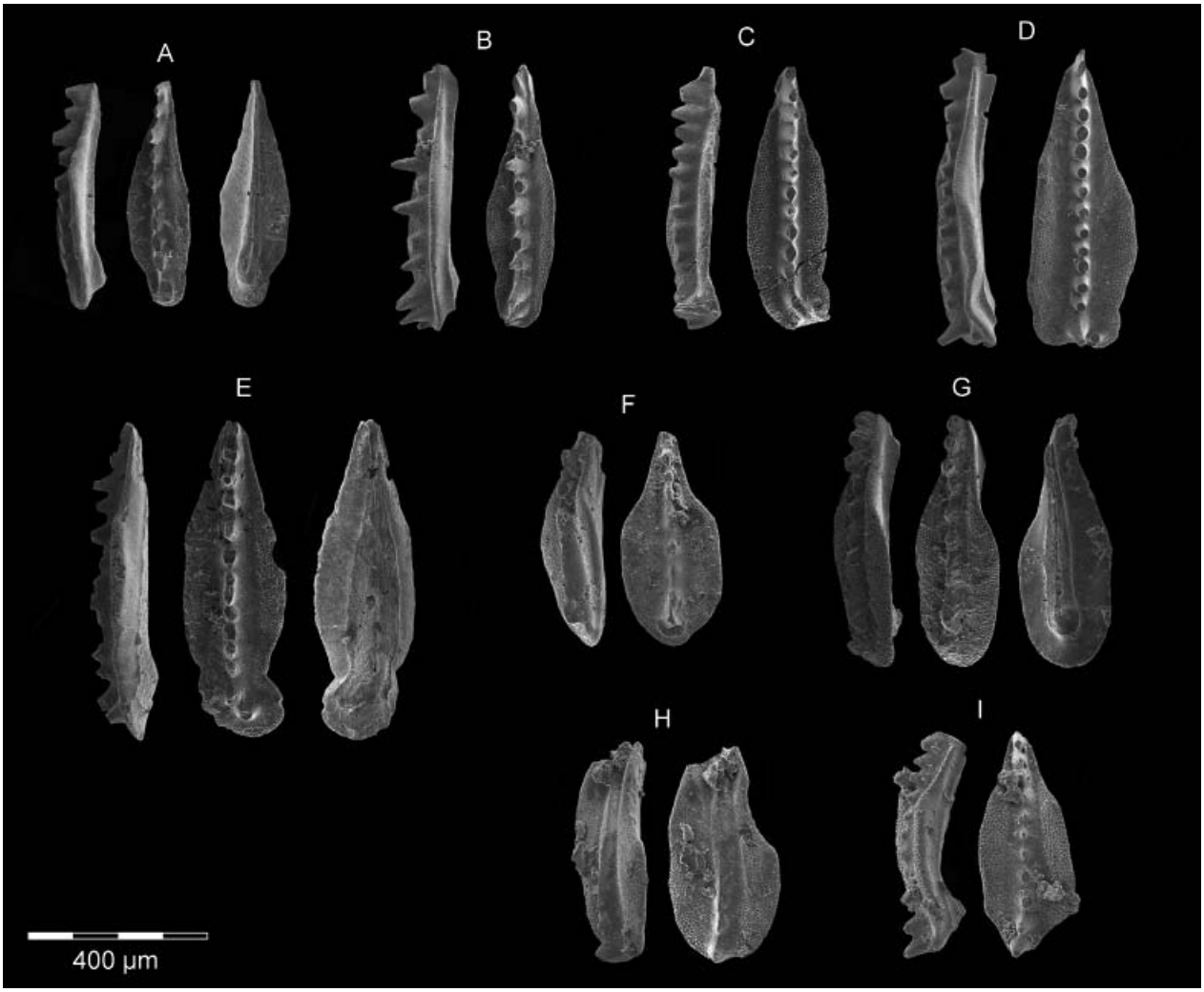

Figure 15: *Neogondolella* sp. A; A, GUR310, PIMUZ XXXXX; B, GUR310, PIMUZ XXXXX; C, GUR310, PIMUZ XXXXX; D, GUR310, PIMUZ XXXXX; E, GUR310, PIMUZ XXXXX. F, G, *Neogondolella* sp. indet. 1; F, GUR311, PIMUZ XXXXX; G, GUR311, PIMUZ XXXXX. H, I, *Neogondolella* sp. indet. 2; H, GUR17, PIMUZ XXXXX; I, GUR17, PIMUZ XXXXX.

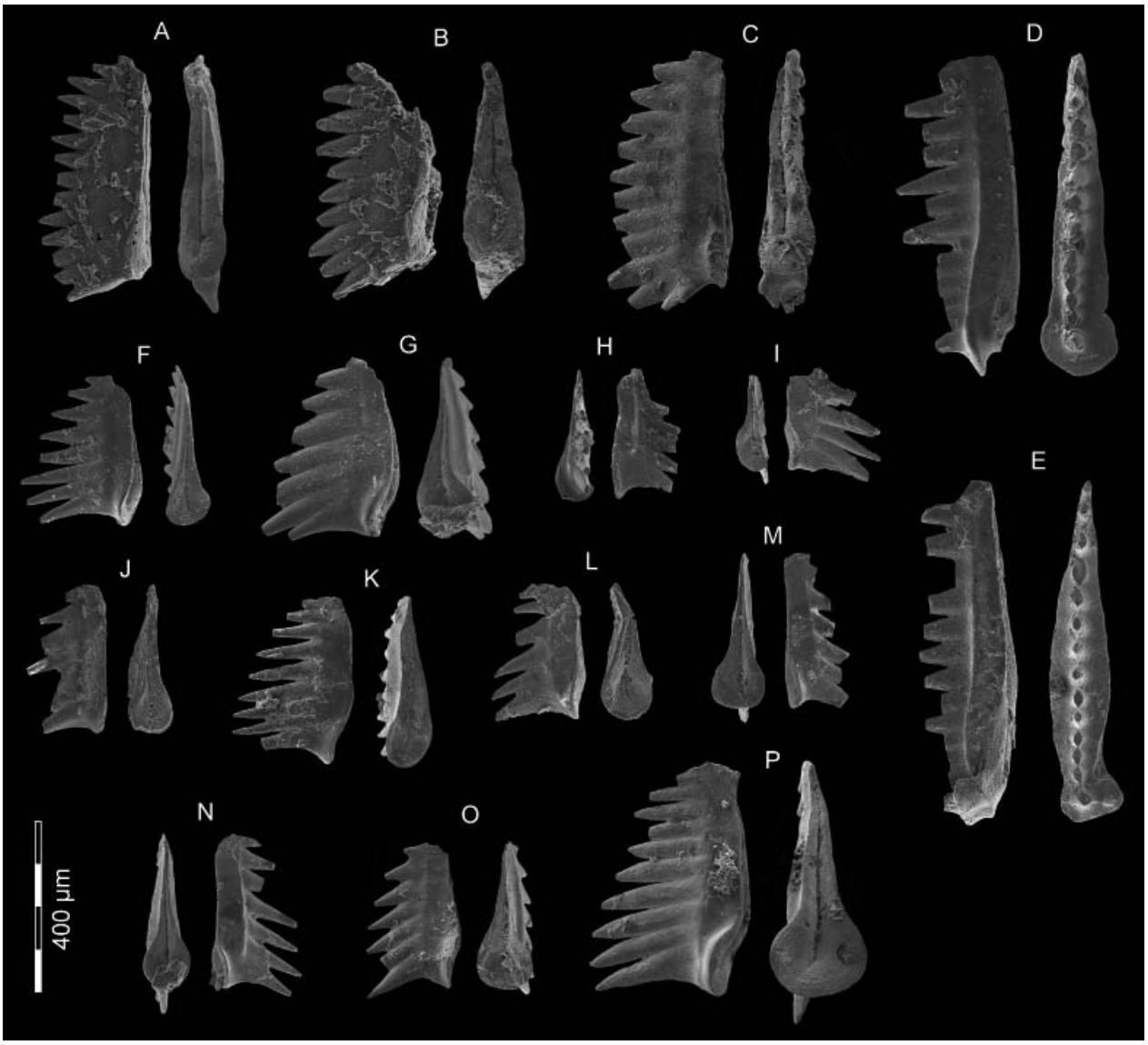

Figure 16: A-E, *Sweetospathodus kummeli* Sweet 1970; A, GUR311, PIMUZ XXXXX; B, GUR311, PIMUZ XXXXX; C, GUR311, PIMUZ XXXXX; D, GUR311, PIMUZ XXXXX; E, GUR311, PIMUZ XXXXX. F-L, *Neospathodus dieneri* Sweet 1970; F, GUR16, PIMUZ XXXXX; G, GUR16, PIMUZ XXXXX; H, GUR312, PIMUZ XXXXX; I, GUR313, PIMUZ XXXXX; J, GUR313, PIMUZ XXXXX; K, GUR315, PIMUZ XXXXX; L-P, *Neospathodus* ex. gr. *dieneri* Sweet 1970; L, GUR313, PIMUZ XXXXX; M, GUR313, PIMUZ XXXXX; N, GUR313, PIMUZ XXXXX; O, GUR315, PIMUZ XXXXX; P, GUR315, PIMUZ XXXXX.

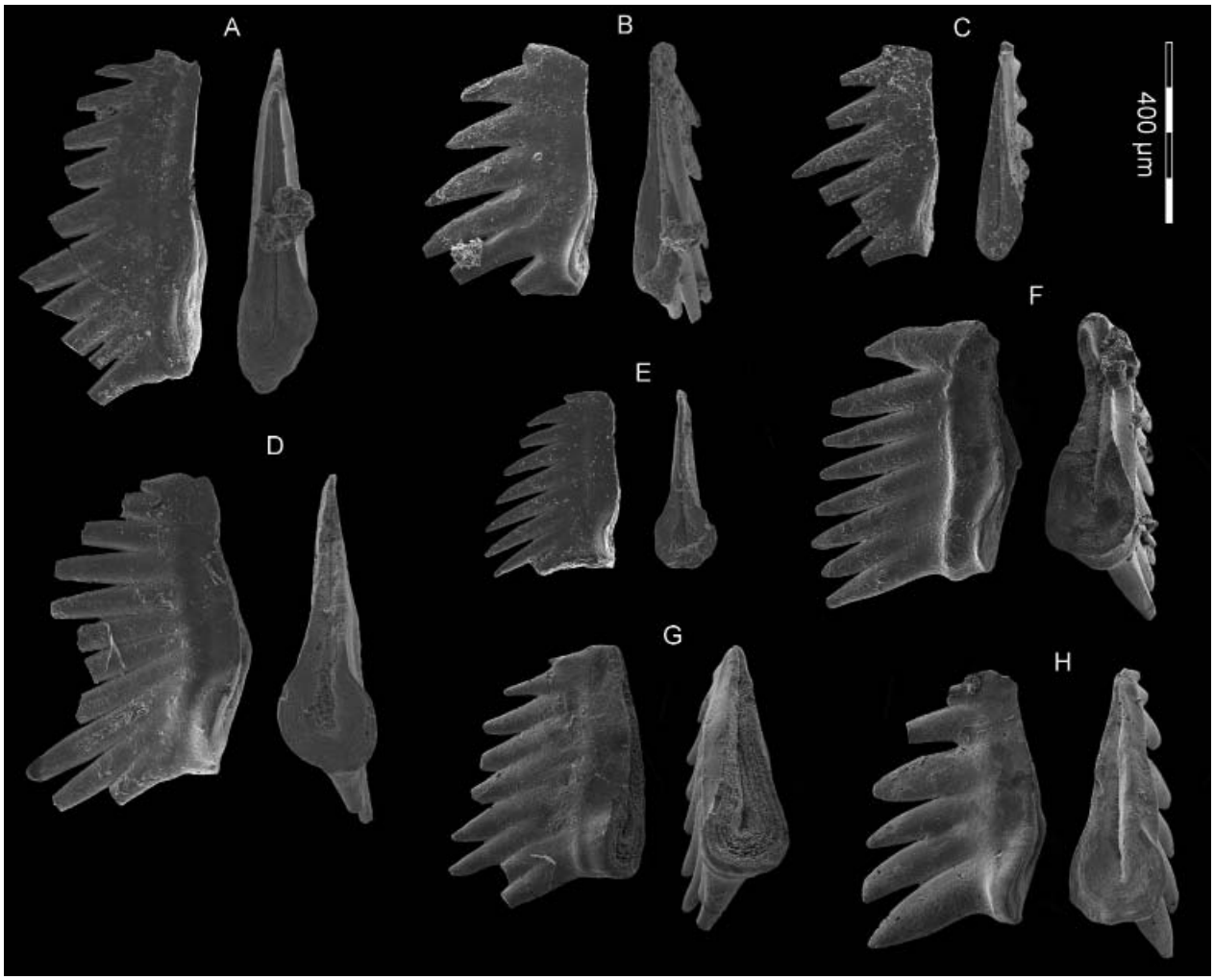

Figure 17: A-E, *Neospathodus* aff. *cristagalli* Huckriede 1958; α morphotype A-C; A GUR16, PIMUZ XXXXX; B, GUR16, PIMUZ XXXXX; C, GUR16, PIMUZ XXXXX; β morphotype, D, GUR16, PIMUZ XXXXX; E, GUR16, PIMUZ XXXXX. F, *Neospathodus* sp. indet. 1, GUR315, PIMUZ XXXXX; G, *Neospathodus* sp. indet. 2, GUR315, PIMUZ XXXXX; H, *Neospathodus* sp. indet. 3, GUR315, PIMUZ XXXXX.

4.3. Quantitative biochronology

We identified nine local maximal horizons (LMHs, beds or cluster of beds that correspond to maximal associations of fossils (see for instance Guex, 1991; Brosse et al., 2016): GUR09, GUR13, GUR304, GUR304.1, GUR307, GUR310, GUR311, GUR16 and GUR315. We conducted Unitary Associations (UAs) analyses using the dataset of Brosse et al. (2016, Appendix A), completed in order to encompass the Griesbachian-Dienerian boundary (GDB) with (1) the conodont record from Guryul Ravine (this work), (2) the data of Zhang et al. (2007) that include the conodont record of Meishan D and (3) the data of Chen et al. (2015a) that described the conodont record from Jiarong section (China). We calculated 10 Unitary Associations Zones (UAZs) which are presented in Figure 18. The intermediate steps of the analyses are detailed in the supplementary material. $UAZ_{1\text{-}6}$ correspond to the $UAZ_{1\text{-}6}$ described in the Nanpanjiang basin (Brosse et al., 2016). $UAZ_{1\text{-}2}$ are Permian, $UAZ_{3\text{-}7}$ are Griesbachian and $UAZ_{8\text{-}10}$ are Dienerian. The PTB is located within the interval of separation between UAZ_2 and UAZ_3 and the GDB is located within the interval of separation between UAZ_7 and UAZ_8. $UAZ_{1\text{-}3}$ are not represented in Guryul Ravine. Hence the location of the PTB in Guryul Ravine is upper bound by the first local maximal horizon in this section which confirm a Griesbachian age for the first local maximal horizon of Griesbachian age but not lower bound by conodonts.

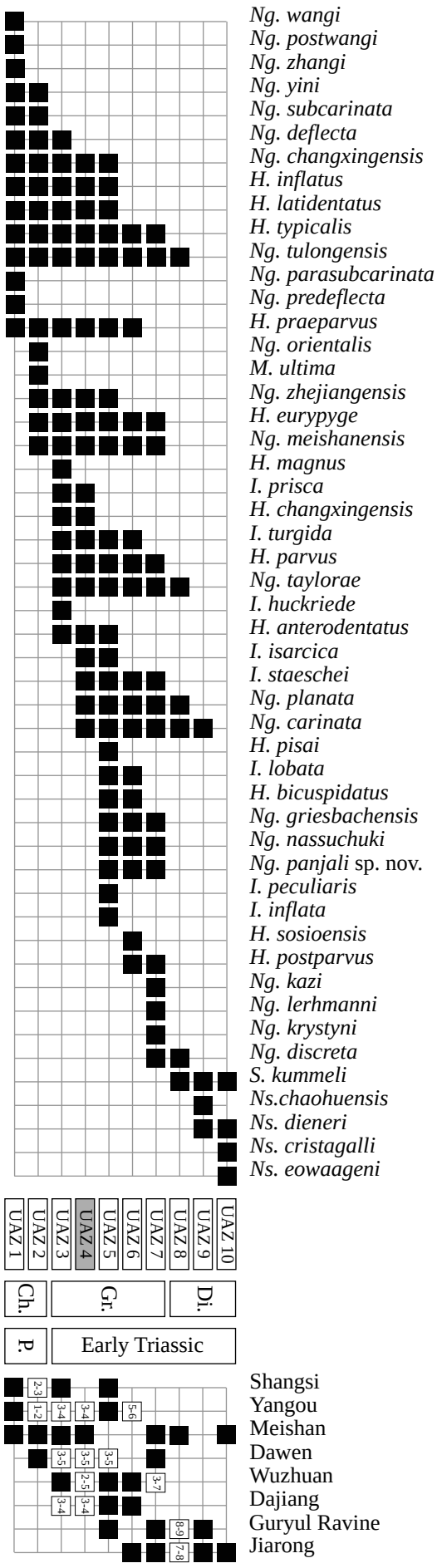

Figure 18: Sequence of the 10 UAZs generated from the eight sections included within the model (Meishan, Yangou, Shangsi, Dawen, Wuzhuan, Dajiang, Dawen, Jiarong and Guryul Ravine) and lateral reproducibility of the UAZ for each section. Ng, *Neogondolella*; H, *Hindeodus*; I, *Isarcicella*; E, *Ellisonia*; S, *Sweetospathodus*; Ns. *Neospathodus*.

5. Discussion

5.1. Location of the Permian-Triassic Boundary

The Permian-Triassic transition is marked worldwide by a prominent negative carbon-isotope excursion (Korte and Kozur, 2010). In Guryul Ravine, the negative excursion is straddling the sub-members E_1 and E_2 (Baud et al., 1996; Atudorei, 1998; Korte et al., 2010), which approximately corresponds to an eight metres thick interval.

The FOs of *H. parvus* (index species of the base of the Triassic) as well as of other typical Griesbachian species are located in the middle of sub-member E_2, in GUR09 (which correlates with Unit 56 of Nakazawa et al. (1970). The scarcity of conodonts in the lower beds unfortunately prevents to constrain the location of the PTB better within Member E. *H. parvus* has been reported at the base of E_2 in Algeo et al. (2007), but this has not been confirmed by illustrations. Pending confirmation, we maintain the FO of *H. parvus* at Guryul Ravine in Unit 56. Contrary to the claims of Korte et al. (2010), the conodonts found in E_1 do not indicate a lower Permian age, as the species in question, *H. typicalis*, and *Ng. carinata* are commonly found within the Griesbachian. The occurrence of *Otoceras woodwardi* in Unit 52 may be used as an additional proxy for locating the base of the Triassic.

5.2. The Griesbachian-Dienerian Boundary (GDB)

5.2.1. Biostratigraphy

The GDB has been defined at Diener Creek, Arctic Canada by Tozer (1965, 1967), as the transition from the ammonoid interval zones *Bukkenites* (=*Pachyproptychites*) *strigatus* Zone to the *Proptychites candidus* Zone. At low latitude, The GDB is identified in South China by the transition from *Ophiceras* beds to *Proptychites candidus* Zone (Brayard and Bucher, 2008; Brühwiler et al., 2008), in Spiti by the transition from *Discophiceras tibeticum* Zone to "*Pleurogyronites*" *planidorsatus* Zone (Krystyn et al., 2004, 2007; Brühwiler et al., 2010) and in Salt Range by the transition from *Ophiceras sakuntala* beds to *Gyronites dubious* beds (Brühwiler et al., 2012; Ware et al., accepted in Fossils and Strata).

The ammonoid index fossils being poorly reproducible, the base of the Dienerian is traditionally identified in lower latitude by the FOs of the conodonts *S. kummeli* (Sweet et al., 1971), *Ns. dieneri* or *Ns. cristagalli* (Krystyn et al., 2004). Although these FOs only roughly correspond to the base of the *candidus* Zone (Orchard. 2008), their occurrences reflect a major faunal turnover in conodonts and are good worldwide proxies of the GDB as defined by Tozer (1965, 1967). This major conodont faunal turnover corresponds to the replacement of segminiplanate forms by segminate forms at low latitudes, for instance in China (Meishan (Zhang et al., 2007), Chaohu (Zhao et al., 2007), Daxiakou (Zhao et al., 2013), Gaimao (Yang et al., 2012), Bianyang (Yan et al., 2013), Jiarong (Chen et al. 2015a) and in Pakistan (Sweet et al., 1970b)). At higher latitudes, *Neogondolella* survived throughout the early Triassic (Orchard, 2007).

At Guryul Ravine, the last occurrences of neogondolellids are observed in GUR310, followed by the FO of *S. kummeli* in GUR311 and the FO of *Ns. dieneri* in the subsequent GUR16. Here we chose to use *S. kummeli* as a proxy for the base of the Dienerian. The GDB is therefore located between beds GUR310 and GUR311 (units 69-70). This transition in the Tethyan realm corresponds to the interval of separation between UAZ_7 and UAZ_8 (Fig. 18).

5.2.2. Carbon isotopes

The carbon isotope record of Guryul Ravine has been first published in Baud et al. (1996) who showed a positive excursion of about 2‰ within the 5m thick interval at the base of Member F. In Abadeh, Zal and Amol sections (Iran), the Dienerian is marked by a positive excursion (Horacek et al., 2007). This pattern is mirrored in Payne et al. (2004), with a positive excursion of nearly 8‰ during the entire Dienerian at Dawen and Dajiang sections (Nanpanjiang basin, China). At Nammal Gorge (Salt Ranges, Pakistan), Corsetti et al. (2005) also reported a "minor positive trend" at the GDB. If these carbon perturbations seem to indicate a Dienerian positive excursion of the carbon cycle of a presumed global scale, it is worth noting that only at the Abadeh section is the base of the Dienerian well constrained by the FO of *Ns. dieneri*. Another positive excursion of the carbon cycle can also be observed at the base of the Dienerian at Kamura B, Japan (Horacek et al., 2009).

We also detected at Guryul Ravine a positive shift of the carbonate carbon isotope profile between beds GUR17 and GUR22 (Fig. 4). This positive excursion is above the first Dienerian bed (GUR311).

These perturbations of the carbon cycle are spanning the entire Early Triassic and have been interpreted as methane release (Horacek et al., 2007), perturbations of the oceanic circulation, oceanic stratification (Corsetti et al., 2005; Horacek et al., 2007, 2009) or a carbon cycle reorganization (Corsetti et al., 2005).

5.2.3. Climate

Sun et al. (2012) indicated a transition from a warm climate during the Griesbachian to a cooler climate during the Dienerian. However, their temperature curve is produced by 'stitching' the oxygen isotope records from the deep water sections Meishan and Shangsi to the oxygen isotope record of the shallower water section Zuodeng, assuming the same environmental settings for the different localities. It is also noteworthy that the equatorial palaeolatitude of the South China block makes it a poor climate-sensitive location.

From a study conducted near Zal, Iran, Sedlacek et al. (2014) detected an increase in the rate of the riverine $^{87}Sr/^{86}Sr$ at the GDB attributed to an increase of weathering. Song et al. (2015) also observed an increase of the riverine $^{87}Sr/^{86}Sr$ at Meishan (China) from the Griesbachian to the Smithian. Song et al. (2015) concluded that the increased continental weathering rates was the consequence of global warming, enhanced hydrological cycle or vegetation die-off.

A recent study published by Hochuli et al. (2016) about the palynology of the Kap Stosch section, Greenland, showed that the Induan was not characterized by a global demise of land plants, but rather by a major turnover in the faunal assemblage. They evidence that the GDB is marked by a swapping from gymnosperm-dominated floral assemblage to a lycopsid spore-dominated floral assemblage. This replacement is also evidenced in Pakistan (Schneebeli-Hermann et al., 2015) and indicates a change of the environmental conditions from a cool and dry to a hot and humid climate at a global scale (Hochuli et al., 2016). The increase of weathering rate discussed above could be due to an enhanced hydrological cycle due to a hot and humid climate rather than to devastated land plants.

6. Conclusion

Our study confirms the FO of *Hindeodus parvus* in Unit 56 (sub-member E_2; Matsuda 1981) but the location of the Permian-Triassic

boundary remains poorly constrained by conodonts.

Our high resolution sampling provides a much better definition of the Griesbachian-Dienerian boundary, both for conodont biochronology and carbon isotope record. We are able to constrain the Griesbachian-Dienerian boundary within 40 cm at Guryul Ravine thanks to our UAZ analysis, between beds GUR310 and GUR311.

The Griesbachian-Dienerian transition at Guryul Ravine is marked by a positive shift of the carbon isotope record that is observed in other Tethyan sections and in Japan (Payne et al., 2004; Corsetti et al., 2005; Horacek et al., 2007; Horacek et al., 2009). The Griesbachian-Dienerian transition is also characterized by a major turnover of the conodont fauna, which we interpret as the disappearance of segminiplanate conodonts from low latitude and their migration to the Boreal Realm during the Dienerian, while segminate conodonts thrived in the Tethyan realm (Orchard, 2007). The conodont turnover at the benefit of the warm-water segminate species, the increase of the weathering during the same time interval (Sedlacek et al., 2014; Song et al., 2015) and the change from gymnosperm-dominated to lycopsid spore-dominated plant assemblages (Hochuli et al., 2016) are consistent with a transition from a Griesbachian dry and cold to a Dienerian hot and humid climate.

Acknowledgments

Maximiliano Meier (Bulles), and the workers from the Geological Survey of Srinagar are thanked for their support in the field. This work is supported by the Swiss NSF project 200021_135446 (to H.B.) and a French ANR @ RAction grant (project EvoDevOdonto to N.G.).

References

Agarwal, P.N., and Singh, S.N., 1981. Regent advances in micropalaeontological investigations of the marine Triassic rocks of India. Journal of the Palaeontological Society of India, 25, pp. 110-129.

Agarwal, P.N., Singh, S.N., and Ashok, S., 1980. Scythian Ostracodes from Kashmir Himalayas. Journal of the Palaeontological Society of India, 23(24), pp. 110-114.

Agematsu, S., Sano, H. and Sashida, K., 2014. Natural assemblages of Hindeodus conodonts from a Permian–Triassic boundary sequence, Japan. Palaeontology, 57 (6), pp. 1277–1289.

Algeo, T.J., Hannigan, R., Rowe, H., Brookfield, M., Baud, A., Krystyn, L., and Ellwood, B.B., 2007. Sequencing events across the Permian–Triassic boundary, Guryul Ravine (Kashmir, India). Palaeogeography, Palaeoclimatology, Palaeoecology, 252 (1), pp. 328-346.

Atudorei, N.V., 1998. Constraints on the Upper Permian to Upper Triassic marine carbon isotope curve: case studies from the Tethys. PhD thesis, University of Lausanne (unpublished).

Bando, Y., 1981. Lower Triassic ammonoids from Guryul ravine and the Spur three kilometres north of Barus. The Upper Permian and Lower Triassic Faunas of Kashmir. Memoirs of the Geological Survey of India Palaeontologia Indica, 46, pp. 135-177.

Baresel, B., Bucher, H., Brosse, M., Cordey, F., Guodun, K., and Schaltegger, U. Precise age for the Permian-Triassic boundary in South China from high precision U-Pb geochronology and Bayesian age-depth modelling, Solid Earth Discuss., doi:10.5194/se-2016-145, in review, 2016.

Baud, A., Bhat, G., and Bachmann, G.H. 2014. Report on the first IGCP 630 field workshop, November 17-22, in Kashmir (India).

Baud, A., Magaritz, M., and Holser, W.T., 1989. Permian-Triassic of the Tethys: Carbon isotope studies. Geologische Rundschau, 78(2), pp. 649-677.

Baud, A., Atudorei, V., and Sharp, Z., 1996. Late Permian and Early Triassic evolution of the Northern Indian margin: carbon isotope and sequence stratigraphy. Geodinamica Acta, 9(2-3), pp. 57-77.

Bender, H., and Kockel, C.W., 1963. Die Conodonten der griechischen Trias. In Annales Géologiques des Pays Helléniques, 14, 436-445.

Bender, H., and Stoppel, D., 1965. Perm-conodonten. Geologisches Jahrbuch, 82(3), pp. 331-364.

Bender, H., 1968. Zur Gliederung der Mediterranen Trias II. Die Conodontenchronologie der Mediterranen Trias. Annales Géologiques des Pays Hélléniques, 19, 465-540.

Bhatt, D. K., Joshi, V. K., and Arora, R. K., 1981. *Neospathodus praekummeli*-a new species of conodont from Lower Triassic of Spiti. Geological Society of India, 22(9), pp. 444-447.

Bhat, M.I., 1982. Thermal and tectonic evolution of the Kashmir basin vis-a-vis petroleum prospects. Tectonophysics, 88(1), pp. 117-132.

Bhat, M.I., 1984. Abor Volcanics: further evidence for the birth of the Tethys Ocean in the Himalayan segment. Journal of the Geological Society, 141(4), pp. 763-775.

Brayard, A. and Bucher, H., 2008. Smithian (Early Triassic) ammonoid faunas from northwestern Guangxi (South China): taxonomy and biochronology. Fossils and Strata 55, pp. 179.

Brookfield, M.E., 1993. The Himalayan passive margin from Precambrian to Cretaceous times. Sedimentary Geology, 84(1), pp. 1-35.

Brookfield, M.E., Twitchett, R.J., and Goodings, C., 2003. Palaeoenvironments of the Permian–Triassic transition sections in Kashmir, India. Palaeogeography, Palaeoclimatology, Palaeoecology, 198 (3), pp. 353-371.

Brookfield, M.E., Algeo, T.J., Hannigan, R., Williams, J., and Bhat, G.M., 2013. Shaken and stirred: Seismites and tsunamites at the Permian-Triassic boundary, Guryul Ravine, Kashmir, India. Palaios, 28(8), pp. 568-582.

Brosse, M., Bucher, H., Bagherpour, B., Baud, A., Frisk, Å.M., Guodun, K., and Goudemand, N., 2015. Conodonts from the Early Triassic microbialite of Guangxi (South China): implications for the definition of the base of the Triassic System. Palaeontology, 58(3), 563-584.

Brosse, M., Bucher, H., and Goudemand, N. 2016. Quantitative biochronology of the Permian–Triassic boundary in South China based on conodont unitary associations. Earth-Science Reviews, 155, pp. 153-171.

Brühwiler, T., Brayard, A., Bucher, H. and Guodun, K., 2008. Griesbachian and Dienerian (Early Triassic) Ammonoid Faunas from Northwestern Guangxi and Southern Guizhou (South China). Palaeontology 51, pp. 1151-1180.

Brühwiler, T., Ware, D., Bucher, H., Krystyn, L. and Goudemand, N., 2010. New Early Triassic ammonoid faunas from the Dienerian/Smithian boundary beds at the Induan/Olenekian GSSP candidate at Mud (Spiti, Northern India). Journal of Asian Earth Sciences 39, pp. 724-739.

Brühwiler, T., Bucher, H., Ware, D., Schneebeli-Hermann, E., Hochuli, P.A., Roohi, G., Rehman, K. and Yaseen, A., 2012. Smithian (Early Triassic) ammonoids from the Salt Range, Pakistan. Special Papers in Palaeontology 88, pp. 1-114.

Budurov, K.J., and Gupta, V.J. 1988. Triassic conodont stratigraphy of some section of Kashmir Himalaya. Bulletin of the Indian Geologists Association, 21(1), pp. 21-39.

Burgess, S.D., Bowring, S., and Shen, S.Z., 2014. High-precision timeline for Earth's most severe extinction. Proceedings of the National Academy of Sciences, 111(9), pp. 3316-3321.

Chauvet, F., Lapierre, H., Bosch, D., Guillot, S., Mascle, G., Vannay, J.C., Cotton, J., Brunet, P., and Keller, F., 2008. Geochemistry of the Panjal Traps basalts (NW Himalaya): records of the Pangea Permian break-up. Bulletin de la Société géologique de France, 179(4), pp. 383-395.

Chen, J., Henderson, C.M., and Shen, S.Z., 2008. Conodont succession around the Permian-Triassic boundary at the Huangzhishan Section, Zhejiang and its stratigraphic correlation. Acta Palaentologica Sinica, 47(1), pp. 91-114.

Chen, J., Beatty, T.W., Henderson, C.M., and Rowe, H., 2009. Conodont biostratigraphy across the Permian–Triassic boundary at the Dawen section, Great Bank of Guizhou, Guizhou Province, South China: implications for the Late Permian extinction and correlation with Meishan. Journal of Asian Earth Sciences, 36(6), pp. 442-458.

Chen, Y., Jiang, H., Lai, X., Yan, C., Richoz, S., Liu, X., and Wang, L., 2015a. Early Triassic conodonts of Jiarong, Nanpanjiang Basin, southern Guizhou Province, South China. Journal of Asian Earth Sciences, 105, pp. 104-121.

Chen, Z. Q., Yang, H., Luo, M., Benton, M. J., Kaiho, K., Zhao, L., Huang, Y., Zhang, K., Fang, Y., Jiang, H., Qiu, H., Li, Y., Tu, C., Shi, L., Zhang, L., Feng, X. and Chen, L., 2015b. Complete biotic and sedimentary records of the Permian–Triassic transition from Meishan section, South China: Ecologically assessing mass extinction and its aftermath. Earth-Science Reviews, 149, pp. 67-107.

Clark, D.L. 1959. Conodonts from the Triassic of Nevada and Utah. Journal of Paleontology, 33(2), pp. 305-312.

Clark, D.L., 1979. Permian-Triassic boundary: Great Basin conodont perspective. Great Basin stratigraphy and paleontology. Brigham Young University Geological Studies, 26(1), 85-90.

Clark, D.L., Paull, R.K., Solien, M.A., and Morgan, W.A., 1979. Triassic conodont biostratigraphy in the Great Basin. Conodont biostratigraphy of the Great Basin and Rocky Mountains: Brigham Young University Geology Studies, 26, 179-186.

Dai, J., and Zhang, J., 1989. Conodonts. Study on the Permian-Triassic biostratigraphy and event

stratigraphy of northern Sichuan and southern Shananxi: Ministry of Geology and Mineral Resources, Geological Memoirs, Series 2, 9, pp. 428-435.

Gaetani, M., Garzanti, E., and Tintori, A., 1990. Permo-Carboniferous stratigraphy in SE Zanskar and NW Lahul (NW Himalaya, India). Eclogae Geologicae Helvetiae, 83(1), pp. 143-161.

Garzanti, E., Jadoul, E., Nicora, A., and Berra, E., 1995. Triassic of Spiti (Tethys Himalaya, N India). Rivista Italiana di Paleontologia e Stratigrafia, 101, pp. 267-300.

Garzanti, E., Critelli, S., and Ingersoll, R.V., 1996. Paleogeographic and paleotectonic evolution of the Himalayan Range as reflected by detrital modes of Tertiary sandstones and modern sands (Indus transect, India and Pakistan). Geological society of america bulletin, 108(6), pp. 631-642.

Guex, J., 1991. Biochronological correlations. Springer Verlag.

Hayden, H.H., 1907. The stratigraphical position of the *Gangamopteris* beds of Kashmir. Records of the Geological Survey of India, 36(1), pp. 23-39.

Henderson, C.M., and Baud, A., 1997. Correlation of the Permian–Triassic boundary in Arctic Canada and comparison with Meishan, China. Proceedings of the 30th International Geological Congress, 11, pp. pp. 143-152.

Henderson, C.M., and Mei, S., 2007. Geographical clines in Permian and lower Triassic gondolellids and its role in taxonomy. Palaeoworld, 16(1), pp. 190-201.

Hochuli, P.A., Vigran, J. O., Hermann, E., and Bucher, H., 2010. Multiple climatic changes around the Permian-Triassic boundary event revealed by an expanded palynological record from mid-Norway. Geological Society of America Bulletin, 122(5-6), pp. 884-896.

Hochuli, P.A., Sanson-Barrera, A., Schneebeli-Hermann, E., and Bucher, H. 2016. Severest crisis overlooked—Worst disruption of terrestrial environments postdates the Permian-Triassic mass extinction. Scientific Reports, 6, pp. 1-7.

Horacek, M., Richoz, S., Brandner, R., Krystyn, L., and Spötl, C., 2007. Evidence for recurrent changes in Lower Triassic oceanic circulation of the Tethys: the δ 13 C record from marine sections in Iran. Palaeogeography, Palaeoclimatology, Palaeoecology, 252(1), pp. 355-369.

Horacek, M., Koike, T., and Richoz, S. 2009. Lower Triassic $\delta^{13}C$ isotope curve from shallow-marine carbonates in Japan, Panthalassa realm: Confirmation of the Tethys $\delta^{13}C$ curve. Journal of Asian Earth Sciences, 36(6), pp. 481-490.

Huckriede, R., 1958. Die Conodonten der mediterranen Trias und ihr stratigraphischer Wert. Paläontologisches Zeitschrift, 32(3/4), 141-175.

Jasper, A., Uhl, D., Agnihotri, D., Tewari, R., Pandita, S.K, Wanderley Benicio, R.R., Pires, E.F., Stock Da Rosa, A.A., Bhat, G.D., and Pillai, S.S., 2016. Evidence of wildfires in the Late Permian (Changsinghian) Zewan Formation of Kashmir, India. Current science, 110(3), pp. 419-423.

Jeppsson, L. and Anehus, R., 1999. A new technique to separate conodont elements from heavier minerals. Alcheringa, 23(1), pp. 57–62.

Jeppsson, L., Anehus, R. and Fredholm D., 1999. The optimal acetate buffered acetic acid technique for extracting phosphatic fossils. Journal of Paleontology, 73(5), pp. 964–972.

Jiang, H., Lai, X., Luo, G., Aldridge, R., Zhang, K., and Wignall, P., 2007. Restudy of conodont zonation and evolution across the P/T boundary at Meishan section, Changxing, Zhejiang, China. Global and Planetary Change, 55(1), pp. 39-55.

Jiang, H., Lai, X., Yan, C., Aldridge, R. J., Wignall, P., and Sun, Y., 2011a. Revised conodont zonation and conodont evolution across the Permian-Triassic boundary at the Shangsi section, Guangyuan, Sichuan, South China. Global and Planetary Change, 77(3), pp. 103-115.

Jiang, H., Aldridge, R.J., Lai, X., Yan, C., and Sun, Y., 2011b. Phylogeny of the conodont genera Hindeodus and Isarcicella across the Permian–Triassic boundary. Lethaia, 44(4), pp. 374-382.

Joachimski, M. M., Lai, X., Shen, S., Jiang, H., Luo, G., Chen, B., Chen, J., and Sun, Y., 2012, Climate warming in the latest Permian and the Permian–Triassic mass extinction: Geology, v. 40, no. 3, p. 195-198.

Kapoor, H.M., 1996. The Guryul ravine section, candidate of the global stratotype and point (GSSP) of the Permian–Triassic boundary (PTB). The Paleozoic–Mesozoic Boundary. Candidates of the Global Stratotype Section and Point of the Permian–Triassic Boundary. Chine University of Geosciences Press, Wuhan, pp. 99-110.

Klapper, G., Lindström, M., Sweet, W.C. aAnd Ziegler, W., 1973. In Ed. Ziegler, W. Catalogue of Conodonts, 1. E. Schweizerbart'sche Verlagsbuchhandlung, Stuttgart.

Koike, T., 1982. Triassic conodont biostratigraphy in Kedah, West Malaysia. Geology and Palaeontology of Southeast Asia, 23, 9-51.

Koike, T., 1996. The first occurrence of Griesbachian conodonts in Japan. Transactions and Proceedings of the Palaeontological Society of Japan, 181, 337–346.

Korte, C., and Kozur, H.W., 2010. Carbon-isotope stratigraphy across the Permian–Triassic boundary: a review. Journal of Asian Earth Sciences, 39(4), pp. 215-235.

Korte, C., Kozur, H.W., Joachimski, M.M., Strauss, H., Veizer, J., and Schwark, L., 2004. Carbon, sulfur, oxygen and strontium isotope records, organic geochemistry and biostratigraphy across the Permian/Triassic boundary in Abadeh, Iran. International Journal of Earth Sciences, 93(4), pp. 565-581.

Korte, C., Pande, P., Kalia, P., Kozur, H.W., Joachimski, M.M., and Oberhänsli, H., 2010. Massive volcanism at the Permian–Triassic boundary and its impact on the isotopic composition of the ocean and atmosphere. Journal of Asian Earth Sciences, 37(4), pp. 293-311.

Kozur, H., and Pjatakova, M., 1976. Die Conodontenart Anchignathodus parvus n. sp., eine wichtige Leitform der basalen Trias. Koninklijke Nederlandse Akademie van Wetenschappen, Amsterdam, Proceedings, Series B, 79, pp. 123-128.

Kozur, H., 1989. The taxonomy of the gondolellid conodonts in the Permian and Triassic. Courier Forschungsinstitut Senckenberg, 117, pp. 409-469.

Kozur, H.W., 2004. Pelagic uppermost Permian and the Permian-Triassic boundary conodonts of Iran: part I: taxonomy. na. Hallesches Jahrbuch für Geowissenschaften, B Geologie, Paläontologie, Mineralogie, 18, pp. 36-68.

Kozur, H.W., 2005. Pelagic uppermost Permian and the Permian-Triassic boundary conodonts of Iran: part II: Investigated sections and evaluation of the conodont faunas. Hallesches Jahrbuch für Geowissenschaften, B Geologie, Paläontologie, Mineralogie, 19, pp. 49-86.

Kozur, H.W. 1996. The conodonts Hindeodus, Isarcicella and Sweetohindeodus in the uppermost Permian and lowermost Triassic. Geologia Croatica, 49(1), pp. 81-115.

Kozur, H.W., and Mostler, H., 1973. Beiträge zur Mikrofauna permotriadischer Schichtfolgen Teil I: Conodonten aus der Tibetzones des Niederen Himalaya (Dolpogebeit, Westnepal). Geol. Paläont. Mitt, Innsbruck, 3(9), pp. 1-23.

Kozur, H.W., Mostler, A., and Rahimi-Yazd, A., 1975. Beiträge zur Mikrofauna permotriadischer Schichtfolgen Teil II: Neue Conodonten aus dem Oberperm und der basalen Trias von Nord- und Zentraliran: Geologisch-Paläontologische Mitteilungen Innsbruck, 5(3), pp. 1-23.

Krystyn, L., and Orchard, M.J., 1996. Lowermost Triassic ammonoid and conodont biostratigraphy of Spiti, India. Albertiana, 17, pp. 10-21.

Krystyn, L., Balini, M., and Nicora, A., 2004. Lower and Middle Triassic stage and substage boundaries in Spiti. Albertiana, 30, pp. 40-53.

Krystyn, L., Bhargava, O.N. and Richoz, S., 2007. A candidate GSSP for the base of the Olenekian Stage: Mud at Pin Valley; district Lahul & Spiti, Himachal Pradesh (Western Himalaya), India. Albertiana 35, pp. 5-29.

Lai, X.L., Yang, F.Q., Hallam, A., and Wignall, P.B. 1996. The Shangsi section, candidate of the global stratotype section and point of the Permian-Triassic boundary. The Paleozoic-Mesozoic Boundary Candidates of Global Stratotype Section and Point of the Permian-Triassic Boundary. China University of Geosciences Press, Wuhan, pp. 113-124.

Matsuda, T., 1981. Early Triassic Conodonts from Kashmir, India part 1: Hindeodus and Isarcicella. Journal of Geosciences Osaka City University, 24, pp. 75-108.

Matsuda, T., 1982. Early Triassic Conodonts from Kashmir, India part 2: Neospathodus 1. Journal of Geosciences Osaka City University, 25, pp. 87-102.

Matsuda, T., 1983. Early Triassic Conodonts from Kashmir, India part 3: Neospathodus 2. Journal of Geosciences Osaka City University, 26, pp. 87-110.

Matsuda, T., 1984. Early Triassic Conodonts from Kashmir, India part 4: Gondolella and Platyvillosus. Journal of Geosciences Osaka City University, 27, pp. 119-141.

Mei, S., 1996. Restudy of conodonts from the Permian–Triassic boundary beds at Selong and Meishan and the natural Permian–Triassic boundary. Eds Wang H., and Wang, X. Centennial memorial volume of Professor Sun Y. China University of Geosciences press, pp. 141-148.

Mei, S., Zhang, K., and Wardlaw, B. R. 1998. A refined succession of Changhsingian and Griesbachian neogondolellid conodonts from the Meishan section, candidate of the global stratotype section and point of the Permian-Triassic boundary. Palaeogeography, Palaeoclimatology, Palaeoecology, 143(4), pp. 213-226.

Metcalfe, I., and Nicoll, R.S., 2007. Conodont biostratigraphic control on transitional marine to non-marine Permian–Triassic boundary sequences in Yunnan–Guizhou, China. Palaeogeography, Palaeoclimatology, Palaeoecology, 252(1), pp. 56-65.

Middlemiss, C.S., 1909. Gondwanas and related marine sedimentary systems of Kashmir. Records of the Geological Survey of India, 37(4), pp. 286-327.

Mosher, L.C., 1968. Triassic Conodonts from Western North America and Europe and Their Correlation. Journal of Paleontology, 42(4), 895-946.

Mosher, L.C., 1970. New Conodonts Species as Triassic Guide Fossils. Journal of Paleontology, 44, 737-742.

Mosher, L.C., 1973. Triassic conodonts from British Columbia and the northern Arctic Islands. Geological Survey of Canada Bulletin 222, 141–193.

Müller, K.J., 1956. Triassic Conodonts from Nevada. Journal of Paleontology, 30(4), 818-830.

Müller, K.J., 1962. Zur systematischen Einteilung der Conodontophoridae. Paläontologisches Zeitschrift, 36, 109-117.

Nakazawa, K., Bando, Y., and Matsuda, T., 1980. The Otoceras woodwardi Zone and the time-gap at the Permian-Triassic boundary in East Asia. Geology and Palaeontology of Southeast Asia, 21, pp. 75-90.

Nakazawa, K., and Kapoor, H.M., 1981. The upper Permian and Lower Triassic faunas of Kashmir. Memoir of the Geological Survey of India, Palaeontologia Indica, 46, pp. 1-204.

Nakazawa, K., Kapoor, H.M., Ishii, K.I., Bando, Y., Maegoya, T., Shimizu, D., Nogami, Y., Tokuoka, T., and Nohda, S., 1970. Preliminary report on the Permo-Trias of Kashmir. Memoirs of the Faculty of Science, Kyoto University. Series of geology and mineralogy, 37(2), pp. 163-172.

Nakazawa, K., Kapoor, H.M., Ishii, K.I., Bando, Y., Okimura, Y., and Tokuoka, T., 1975. The upper Permian and the lower Triassic in Kashmir, India. Memoirs of the Faculty of Science, Kyoto University. Series of geology and mineralogy, 42(1), pp. 1-160.

Nicoll, R.S., Metcalfe, I., and Cheng-Yuan, W., 2002. New species of the conodont Genus Hindeodus and the conodont biostratigraphy of the Permian–Triassic boundary interval. Journal of Asian Earth Sciences, 20(6), pp. 609-631.

Nicora, A., 1991. Conodonts from the Lower Triassic sequence of central Dolpo, Nepal. Rivista italiana di paleontologia e stratigrafia, 97(3-4), pp. 239-268.

Nogami, Y., 1968. Trias-Conodonten von Timor, Malaysien und Japan (Paleontological Study of Portuguese Timor, 5). Memoirs of the Faculty of Science, Kyoto University, Series of Geology and Mineralogy, XXXIV(2), 115-136.

Orchard, M.J., 2007. Conodont diversity and evolution through the latest Permian and Early Triassic upheavals. Palaeogeography, Palaeoclimatology, Palaeoecology, 252(1), pp. 93-117.

Orchard, M.J., 2008. Lower Triassic conodonts from the Canadian Arctic, their intercalibration with ammonoid-based stages and a comparison with other North American Olenekian faunas. Polar Research, 27(3), pp. 393-412.

Orchard, M.J., and Krystyn, L., 1998. Conodonts of the lowermost Triassic of Spiti, and new zonation based on Neogondolella successions. Rivista Italiana di Paleontologia e Stratigrafia, 104(3), pp. 341-368.

Orchard, M.J., abd Rieber, H., 1999. Multielement Neogondolella (Conodonta, upper Permian-middle Triassic). Bollettino-Societa Paleontologica Italiana, 37(2/3), pp. 475-488.

Orchard, M.J., Nassichuk, W.W., and Rui, L., 1994. Conodonts from the Lower Griesbachian Otoceras Latilobatum Bed of Selong, Tibet and the Position of the Permian—Triassic Boundary. Canadian Society or Petroleum Geologists, Memoir 17, pp. 823-843.

Payne, J.L., Lehrmann, D.J., Wei, J., Orchard, M.J., Schrag, D.P., and Knoll, A.H., 2004. Large perturbations of the carbon cycle during recovery from the end-Permian extinction. Science, 305(5683), pp. 506-509.

Perri, M. C., and Farabegoli, E., 2003. Conodonts across the Permian–Triassic boundary in the Southern Alps. Courier Forschungsinstitut Senckenberg, 245, pp. 281-313.

Perri, M.C., Molloy, P.D., and Talent, J.A., 2004. Earliest Triassic conodonts from Chitral, northernmost Pakistan. Rivista Italiana di Paleontologia e Stratigrafia, 110(2), pp. 467-478.

Purnell, M.A., Donoghue, P.C., and Aldridge, R.J., 2000. Orientation and anatomical notation in conodonts. Journal of Paleontology, 74(1), pp. 113-122.

Raup, D.M., 1979. Size of the Permo-Triassic bottleneck and its evolutionary implications. Science, 206(4415), pp. 217-218.

Retallack, G.J., 1995. Permian-Triassic life crisis on land. Science, 267(5194), pp. 77-80.

Schneebeli-Hermann, E., Kürschner, W.M., Kerp, H., Bomfleur, B., Hochuli, P.A., Bucher, H., Ware, D., and Roohi, G., 2015. Vegetation history across the Permian–Triassic boundary in Pakistan (Amb section, Salt Range). Gondwana Research, 27(3), pp. 911-924.

Scotese, C.R., 2014. Atlas of Middle and Late Permian and Triassic Paleogeographic maps, maps 43—48 from volume 3 of the PALEOMAP Atlas for ArcGIS (Jurassic and Triassic) and maps 49–52 from volume 4 of the PALEOMAP PaleoAtlas for ArcGIS (Late Paleozoic). Mollweide Projection, PALEOMAP Project, Evanston.

Sedlacek, A.R., Saltzman, M.R., Algeo, T.J., Horacek, M., Brandner, R., Foland, K., and Denniston, R.F., 2014. $^{87}Sr/^{86}Sr$ stratigraphy from the Early Triassic of Zal, Iran: Linking temperature to weathering rates and the tempo of ecosystem recovery. Geology, 42(9), pp. 779-782.

Singh, V., Pandita, S.K., Tewari, R., van Hengstum, P.J., Pillai, S.S.K., Agnihotri, D., Kumar, K., and Bhat, G.D., 2015. Thecamoebians (Testate Amoebae) Straddling the Permian-Triassic Boundary in the Guryul Ravine Section, India: Evolutionary and Palaeoecological

Implications. PloS one, 10(8), pp. 1-18.

Song, H., Wignall, P. B., Tong, J., Song, H., Chen, J., Chu, D., Tian, L., Luo, M., Zong, K., Chen, Y., Lai, X., Zhang, K., and Wang, H., 2015. Integrated Sr isotope variations and global environmental changes through the Late Permian to early Late Triassic. Earth and Planetary Science Letters, 424, pp. 140-147.

Spötl, C., and Vennemann, T.W., 2003. Continuous-flow isotope ratio mass spectrometric analysis of carbonate minerals. Rapid communications in mass spectrometry, 17(9), pp. 1004-1006.

Stampfli, G., Marcoux, J., and Baud, A., 1991. Tethyan margins in space and time. Palaeogeography, Palaeoclimatology, Palaeoecology, 87(1), pp. 373-409.

Stauffer, C.R., and Plummer, H.J., 1932. Texas Pennsylvanian conodonts and their stratigraphic relations. University of Texas Bulletin, 3201, pp. 13-50.

Sun, D., Tong, J., Xiong, Y., Tian, L., and Yin, H., 2012. Conodont Biostratigraphy and Evolution across Permian-Triassic Boundary at Yangou Section, Leping, Jiangxi Province, South China. Journal of Earth Science, 23, pp. 311-325.

Sun, Y., Joachimski, M. M., Wignall, P. B., Yan, C., Chen, Y., Jiang, H., Wang, L., and Lai, X., 2012. Lethally hot temperatures during the Early Triassic greenhouse. Science, 338(6105), pp. 366-370.

Stauffer, C.R., and Plummer, H.J. 1932. Texas Pennsylvanian conodonts and their stratigraphic relations. University of Texas Bulletin, 3201, pp. 13-50.

Sweet, W.C., 1970a. Permian and Triassic conodonts from a section at Guryul Ravine, Vihi district, Kashmir. University of Kansas, Paleontological contributions, 49, pp. 2-11

Sweet, W.C., 1970b. Uppermost Permian and lower Triassic conodonts of the salt range and Trans-Indus ranges, West Pakistan. Stratigraphic boundary problems: Permian and Triassic of west Pakistan, pp. 207-275.

Sweet, W.C., 1979. Graphic correlation of Permo-Triassic rocks in Kashmir, Pakistan and Iran. Geologica et Palaeontologica, 13, pp. 239-248.

Sweet, W.C., Mosher, L.C., Clark, D.L., Collinson, J.W., and Hasenmueller, W.A., 1971. Conodont biostratigraphy of the Triassic. Geological Society of America Memoirs, pp. 127, 441-466.

Teichert, C., Kummnel, B., and Kapoor, H.M., 1970. Mixed Permian-Triassic fauna, Guryul Ravine, Kashmir. Science, 167(3915), pp. 174-175.

Tewari, R., Pandita, S.K., McLoughlin, S., Agnihotri, D., Pillai, S.S., Singh, V., Kumar, K., and Bhat, G.D., 2015. The Permian–Triassic palynological transition in the Guryul Ravine section, Kashmir, India: implications for Tethyan–Gondwanan correlations. Earth-Science Reviews, 149, pp. 53-66.

Tian, C.R., 1982. Triassic conodonts in the Tulong section from Nyalam County, Xizang (Tibet), China. Contribution to Geology of Qinghai, Xizang (Tibet) Plateau, 7, pp. 153-165.

Tozer, E.T., 1965. Lower Triassic stages and ammonoid zones of Arctic Canada: Geological Survey of Canada, 65-12.

Tozer, E.T., 1967. A standard for Triassic time. Department of Energy, Mines and Resources. Geological Survey of Canada Bulletin, 156(1967), pp. 1-103.

Wang, Z., and Wang, Y., 1995. Permian-Lower Triassic conodonts from Selong Xishan of Nyalam, S. Tibet, China. Acta Micropalaeontologica Sinica, 12(4), pp. 333-348.

Ware, D., Bucher, H., Brühwiler, T., Schneebeli-Hermann, E., Hochuli, P.A., Roohi G., ur-Rehman K., and Yaseen A. Griesbachian and Dienerian (Early Triassic) ammonoids from the Salt Range, Pakistan. Fossils and Strata. Accepted.

Webster, G.D., Rexroad, C.B., and Talent, J.A., 1993. An evaluation of the VJ Gupta conodont papers. Journal of Paleontology, 67(03), pp. 486-493.

Wignall, P.B., Newton, R., and Brookfield, M.E., 2005. Pyrite framboid evidence for oxygen-poor deposition during the Permian–Triassic crisis in Kashmir. Palaeogeography, Palaeoclimatology, Palaeoecology, 216(3), pp. 183-188.

Yan, C., Wang, L., Jiang, H., Wignall, P.B., Sun, Y., Chen, Y., and Lai, X., 2013. Uppermost Permian to Lower Triassic conodonts at Bianyang section, Guihzou province, South China. Palaios, 28(8), pp. 509-522.

Yang, B., Lai, X., Wignall, P.B., Jiang, H., Yan, C., and Sun, Y., 2012. A newly discovered earliest Triassic chert at Gaimao section, Guizhou, southwestern China. Palaeogeography, Palaeoclimatology, Palaeoecology, 344, pp. 69-77.

Yin, H.F., Wu, S.B., Ding, M.H., Zhang, K.X., Tong, J.N., Yang, F.Q., and Lai, X.L., 1996. The Meishan section, candidate of the global stratotype section and point of Permian-Triassic boundary. The Paleozoic-Mesozoic Boundary Candidates of the Global Stratotype Section and Point of the Permian-Triassic Boundary, pp. 31-48.

Yin., H., Zhang, K., Tong, J., Yang, Z., and W., S., 2001. The global stratotype section and point (GSSP) of the Permian-Triassic boundary. Episodes, 24(2), 102-114.

Zhang, K., Lai, X., Ding, M., and Liu, J., 1995. Conodont sequence and its global correlation of Permian–Triassic boundary in Meishan section, Changxing,

Zhejiang Province. Earth Science-Journal of China University of Geosciences, 20(6), pp. 669-676.

Zhang, K.X., Ding, M.H., Lai, X.L., and Liu, J.H., 1996. Conodont sequences of the Permian–Triassic boundary strata at Meishan section, South China. The Palaeozoic–Mesozoic Boundary Candidates of Global Stratotype Section and Point of the Permian–Triassic Boundary. China University of Geosciences Press, Wuhan, pp. 57-64.

Zhang, K., Tong, J., Shi, G.R., Lai, X., Yu, J., He, W., Peng, Y., and Jin, Y., 2007. Early Triassic conodont–palynological biostratigraphy of the Meishan D Section in Changxing, Zhejiang Province, South China. Palaeogeography, Palaeoclimatology, Palaeoecology, 252(1), pp. 4-23.

Zhang, Y., Zhang, K.X., Shi, G.R., He, W.H., Yuan, D.X., Yue, M.L., and Yang, T.L., 2014. Restudy of conodont biostratigraphy of the Permian–Triassic boundary section in Zhongzhai, southwestern Guizhou Province, South China. Journal of Asian Earth Sciences, 80, pp. 75-83.

Zhang, K., Tong, J., Shi, G. R., Lai, X., Yu, J., He, W., Peng, Y., and Jin, Y., 2007. Early Triassic conodont–palynological biostratigraphy of the Meishan D Section in Changxing, Zhejiang Province, South China. Palaeogeography, Palaeoclimatology, Palaeoecology, 252(1), 4-23.

Zhao, L., Orchard, M.J., Tong, J., Sun, Z., Zuo, J., Zhang, S., and Yun, A., 2007. Lower Triassic conodont sequence in Chaohu, Anhui Province, China and its global correlation. Palaeogeography, Palaeoclimatology, Palaeoecology, 252(1), pp. 24-38.

Zhao, L., Chen, Y., Chen, Z.Q., and Cao, L., 2013. Uppermost Permian to Lower Triassic conodont zonation from Three Gorges area, South China. Palaios, 28(8), pp. 523-540.

Appendix A: Fossil range chart of units 47-71 from the Guryul Ravine section. Data gathered from Matsuda (1981-1984) and Nakazawa et al. (1975). The taxonomy of the conodonts (illustrated in Matsuda, 1981-1984) has been revised and updated (grey dots). Note the occurrence of the ammonoid *Otoceras woodwardi* (the best index for the base of the Triassic at Guryul Ravine) in Unit 52.

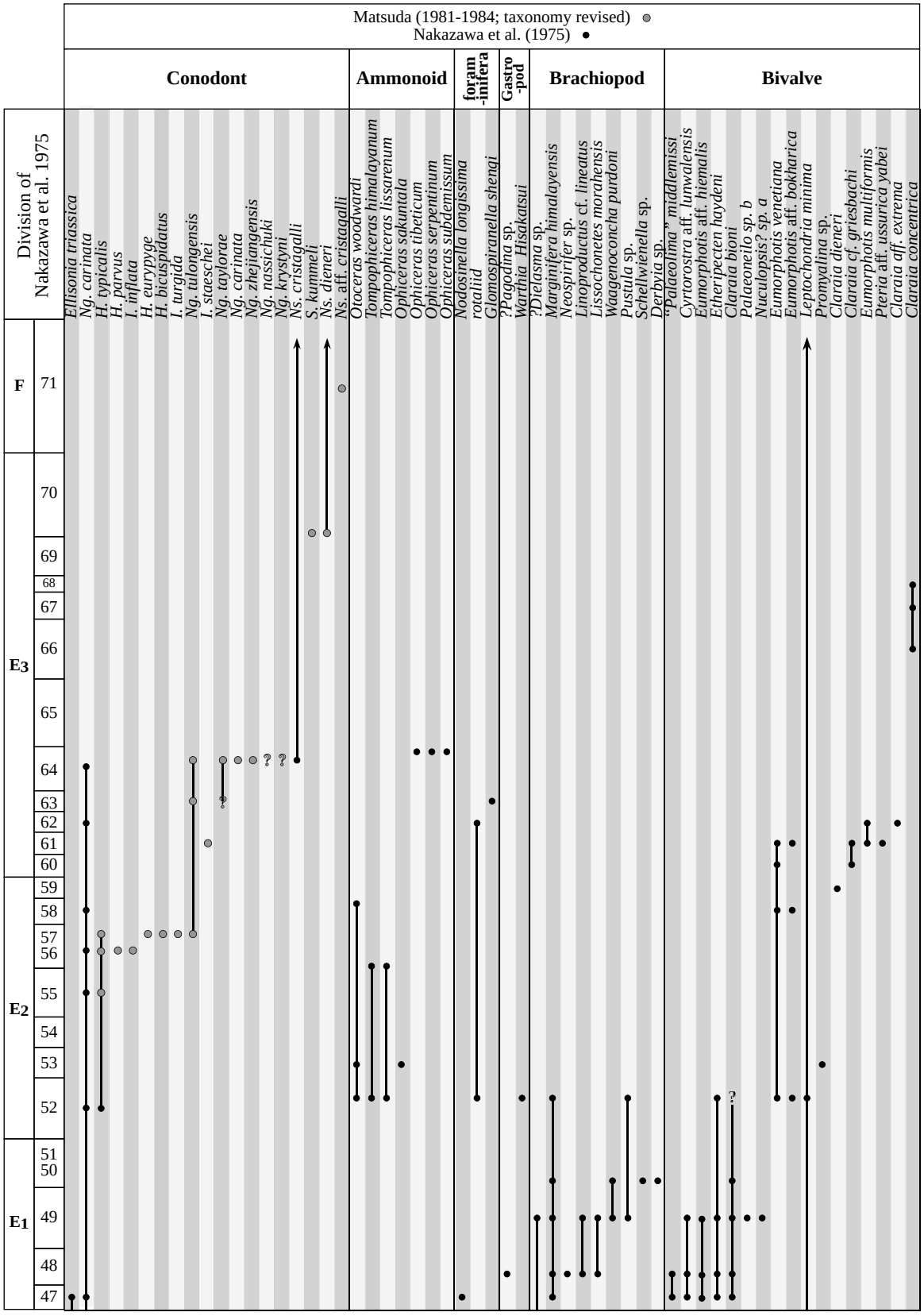

Appendix B: Conodont occurrences in the 8 sections included in this study. Black font represents observed occurrences, grey font represents virtual deduced occurrences. Black squares indicate taxonomical homogenization. The local maximal horizons (LMHs) are outlined and numbered for each section. Ng, *Neogondolella*; H, *Hindeodus*; I, *Isarcicella*; E, *Ellisonia*; S, *Sweetospathodus*; Ns. *Neospathodus*.

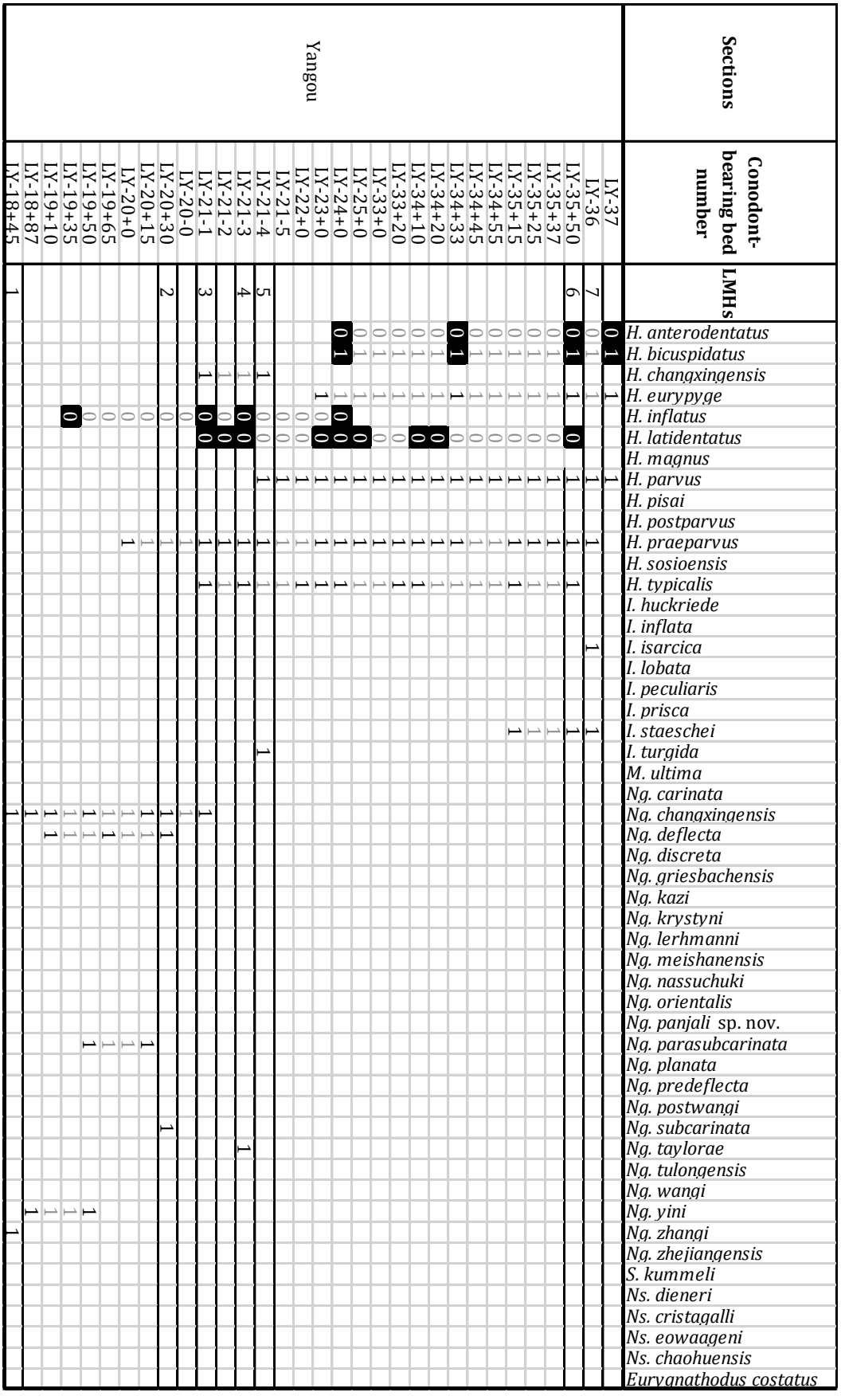

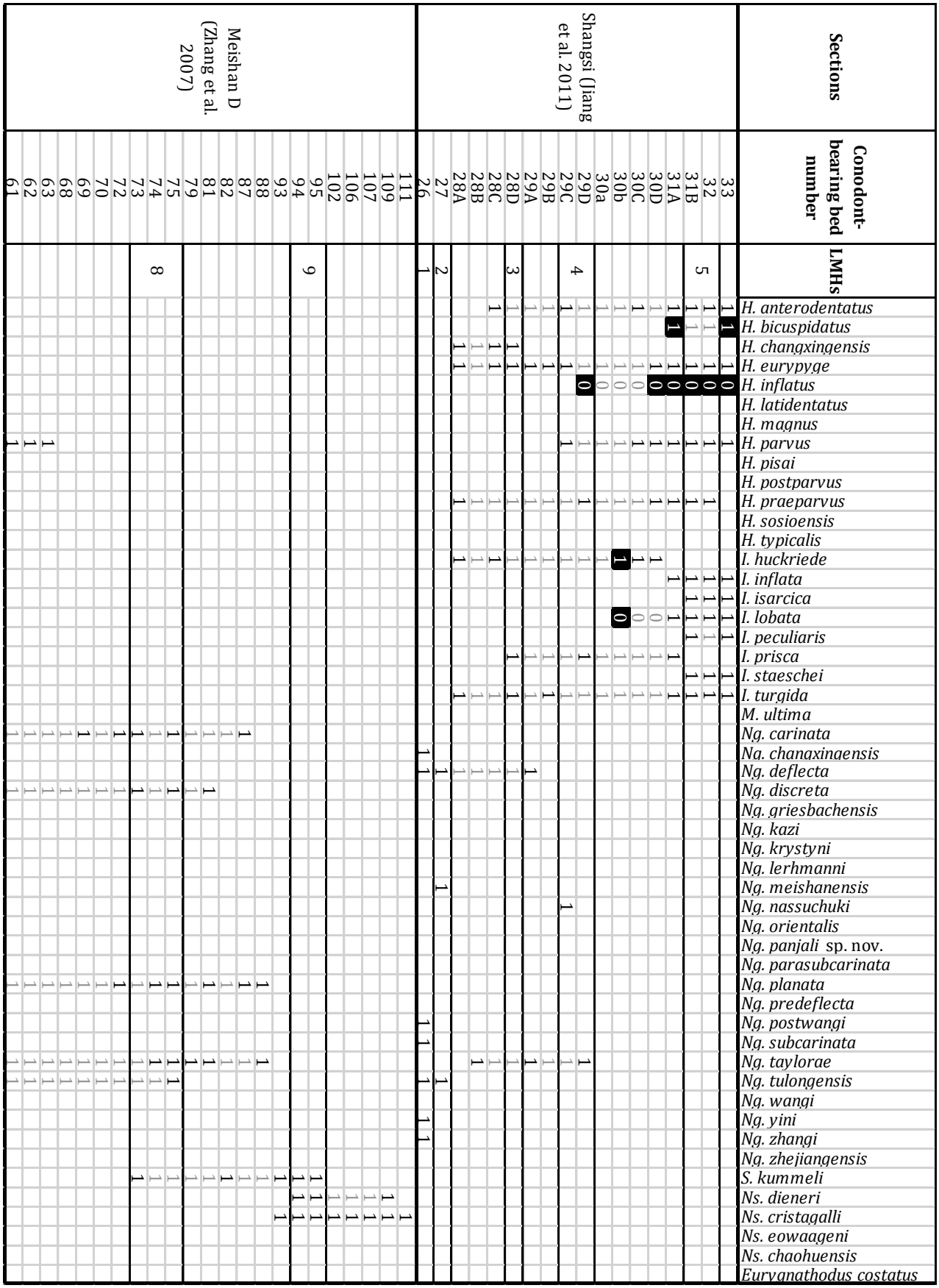
Sections
Conodont-bearing bed number
LMHs
Shangsi (Jiang et al. 2011)
Meishan D (Zhang et al. 2007)
33
32
31B
31A
30D
30C
30b
30a
29D
29C
29B
29A
28D
28C
28B
28A
27
26
111
109
107
106
102
95
94
93
88
87
82
81
79
75
74
73
72
70
69
68
63
62
61
5
4
3
2
9
8
H. anterodentatus
H. bicuspidatus
H. changxingensis
H. eurypyge
H. inflatus
H. latidentatus
H. magnus
H. parvus
H. pisai
H. postparvus
H. praeparvus
H. sosioensis
H. typicalis
I. huckriede
I. inflata
I. isarcica
I. lobata
I. peculiaris
I. prisca
I. staeschei
I. turgida
M. ultima
Ng. carinata
Ng. chanaxingensis
Ng. deflecta
Ng. discreta
Ng. griesbachensis
Ng. kazi
Ng. krystyni
Ng. lerhmanni
Ng. meishanensis
Ng. nassuchuki
Ng. orientalis
Ng. panjali sp. nov.
Ng. parasubcarinata
Ng. planata
Ng. predeflecta
Ng. postwangi
Ng. subcarinata
Ng. taylorae
Ng. tulongensis
Ng. wangi
Ng. yini
Ng. zhangi
Ng. zhejiangensis
S. kummeli
Ns. dieneri
Ns. cristagalli
Ns. eowaageni
Ns. chaohuensis
Eurygnathodus costatus

Sections	Conodont-bearing bed number	LMHs	*H. anterodentatus*	*H. bicuspidatus*	*H. changxingensis*	*H. eurypyge*	*H. inflatus*	*H. latidentatus*	*H. magnus*	*H. parvus*	*H. pisai*	*H. postparvus*	*H. praeparvus*	*H. sosioensis*	*H. typicalis*	*I. huckriede*	*I. inflata*	*I. isarcica*	*I. lobata*	*I. peculiaris*	*I. prisca*	*I. staeschei*	*I. turgida*	*M. ultima*	*Ng. carinata*	*Ng. chanaxingaensis*	*Ng. deflecta*	*Ng. discreta*	*Ng. griesbachensis*	*Ng. kazi*	*Ng. krystyni*	*Ng. lerhmanni*	*Ng. meishanensis*	*Ng. nassuchuki*	*Ng. orientalis*	*Ng. panjali* sp. nov.	*Ng. parasubcarinata*	*Ng. planata*	*Ng. predeflecta*	*Ng. postwangi*	*Ng. subcarinata*	*Ng. taylorae*	*Ng. tulongensis*	*Ng. wangi*	*Ng. yini*	*Ng. zhangi*	*Ng. zhejiangensis*	*S. kummeli*	*Ns. dieneri*	*Ns. cristagalli*	*Ns. eowaageni*	*Ns. chaohuensis*	*Eurygnathodus costatus*
Meishan D (Zhang et al. 2007)	59																																																			
	58					1				1															1							1					1																
	57					1				1															1							1					1																
	56					1				1															1							1					1																
	55					1				1															1							1					1																
	54					1				1															1							1					1																
	53									1															1							1					1																
	52					1				1								1				1			1							1					1																
	51					1				1								1				1			1							1					1																
	50					1				1								1				1			1							1					1																
	47					1				1					1			1				1			1							1					1																
	46					1				1					1			1				1			1							1					1																
	45					1				1					1			1				1			1							1					1																
	44					1				1					1			1				1			1							1					1																
	43					1				1					1			1				1			1							1					1																
	42					1				1					1			1				1			1							1					1																
	41					1				1					1			1				1			1							1					1																
	40					1				1					1			1				1			1							1					1																
	39					1				1					1			1				1			1							1					1																
	38					1				1					1			1				1			1							1					1																
	37					1				1					1			1				1			1							1					1																
	36					1				1					1			1				1			1							1					1																
	35					1				1					1			1				1			1							1					1																
	34					1				1					1			1				1			1							1					1																
	33					1				1					1			1				1			1							1					1																
	31					1				1					1			1				1			1							1					1																
	30					1				1					1			1				1			1							1					1																
	29b					1				1					1			1				1			1							1					1																
	29a					1				1					1			1				1			1							1					1																
	28					1				1					1			1				1			1							1					1																
	27d					1				1					1			1				1			1							1					1																
	27c					1				1					1			1				1			1							1					1																
	27b					1				1					1			1				1			1							1					1																
	27a					1				1					1			1				1			1							1					1																
	26					1				1					1			1				1			1							1					1																
	25					1				1					1			1				1			1							1					1																
	24e					1				1					1			1				1			1							1					1																
	24d					1				1					1			1				1			1							1					1																
	24c					1				1					1			1				1			1							1					1																
	24b					1				1					1			1				1			1							1					1																
	24a					1				1					1			1				1			1							1					1																

Sections	Conodont-bearing bed number	LMHs	*H. anterodentatus*	*H. bicuspidatus*	*H. changxingensis*	*H. eurypyge*	*H. inflatus*	*H. latidentatus*	*H. magnus*	*H. parvus*	*H. pisai*	*H. postparvus*	*H. praeparvus*	*H. sosioensis*	*H. typicalis*	*I. huckriede*	*I. inflata*	*I. isarcica*	*I. lobata*	*I. peculiaris*	*I. prisca*	*I. staeschei*	*I. turgida*	*M. ultima*	*Ng. carinata*	*Ng. changxingensis*	*Ng. deflecta*	*Ng. discreta*	*Ng. griesbachensis*	*Ng. kazi*	*Ng. krystyni*	*Ng. lerhmanni*	*Ng. meishanensis*	*Ng. nassuchuki*	*Ng. orientalis*	*Ng. panjali* sp. nov.	*Ng. parasubcarinata*	*Ng. planata*	*Ng. predeflecta*	*Ng. postwangi*	*Ng. subcarinata*	*Ng. taylorae*	*Ng. tulongensis*	*Ng. wangi*	*Ng. yini*	*Ng. zhangi*	*Ng. zhejiangensis*	*S. kummeli*	*Ns. dieneri*	*Ns. cristagalli*	*Ns. eowaageni*	*Ns. chaohuensis*	*Eurygnathodus costatus*
Wuzhuan (Brosse et al. 2015)	O	4	1							1		1																																								
	N			1						1		1																																								
	M			1						1		1																																								
	L	3			1					1		1																																								
	K									1		1				1	1	1				1	1																												
	I									1		1				1		1	1			1	1																												
	H									1		1				1			1			1	1																												
	G	2			1					1		1											1																												
	F									1		1				1																																			
	E									1		1				1																																			
	D	1								1						1																																		
	C															1																																			
	B															1																																			
	A															1																																			
Dawen (Chen et al. 2009)	DPT-26	4										1																																						
	DPT-25																																																	
	DPT-24											1																																						
	DPT-23	3										1																																						
	DPT-22											1																																						
	DPT-19																																																	
	DPT-18																																																	
	DPT-16	2			1	1	1																	1																										
	DPT-13					1	1																																										
	DPT-12	1				1	1																																										
Dajiang (Jiang et al. 2014)	DI-35	4								1		1																																						
	DI-34									1		1																																						
	DI-33									1		1																																						
	DI+20m									1		1																																						
	DI-32									1		1																																						
	DI-31									1		1																																						
	DI-30									1		1																																						
	DI-29									1		1																																						
	DI-28-4	3								1		1																																						
	DI-28-3									1		1																																						
	DI-28-2	2								1		1																																						
	DI-28-1									1		1																																						
	DI-28									1		1																																						
	D+15m									1		1																																						
	DI-27B									1		1																																						
	DI-27									1		1																																						
	DI-26									1		1																																						
	DI-18									1		1																																						
	DI-13B	1			1					1		1																																						
	DI-13																																																

Sections	Conodont-bearing bed number	LMHs	*H. anterodentatus*	*H. bicuspidatus*	*H. changxingensis*	*H. eurypyge*	*H. inflatus*	*H. latidentatus*	*H. magnus*	*H. parvus*	*H. pisai*	*H. postparvus*	*H. praeparvus*	*H. sosioensis*	*H. typicalis*	*I. huckriede*	*I. inflata*	*I. isarcica*	*I. lobata*	*I. peculiaris*	*I. prisca*	*I. staeschei*	*I. turgida*	*M. ultima*	*Ng. carinata*	*Ng. changxingensis*	*Ng. deflecta*	*Ng. discreta*	*Ng. griesbachensis*	*Ng. kazi*	*Ng. krystyni*	*Ng. lerhmanni*	*Ng. meishanensis*	*Ng. nassuchuki*	*Ng. orientalis*	*Ng. panjali* sp. nov.	*Ng. parasubcarinata*	*Ng. planata*	*Ng. predeflecta*	*Ng. postwangi*	*Ng. subcarinata*	*Ng. taylorae*	*Ng. tulongensis*	*Ng. wangi*	*Ng. yini*	*Ng. zhangi*	*Ng. zhejiangensis*	*S. kummeli*	*Ns. dieneri*	*Ns. cristagalli*	*Ns. eowaageni*	*Ns. chaohuensis*	*Eurygnathodus costatus*
Jiarong Chen et al. 2015	GIR-13																																																					
	IR-04	5																																																				
	GIR-16																																																					
	GIR-17																																																					
	IR-03	5																																																			
	XIR-26	4																																																			
	XIR-20	3																																																			
	XIR-18																																																					
	XIR-17	2																																																			
	XIR-01	1																																																			
	XIR-02																																																					
	XIR-05																																																					
	XIR-10																																																					
	XIR-11																																																					
	XIR-13																																																					
Guryul Ravine	GUR315																																																						
	GUR313																																																					
	GUR312																																																					
	GUR16	8																																																			
	GUR311	7																																																			
	GUR310	6																																																			
	GUR309																																																					
	GUR307	5																																																			
	GUR305																																																					
	GUR15																																																					
	GUR304.3																																																				
	GUR304.2																																																				
	GUR304.1																																																				
	GUR304	4																																																			
	GUR303	3																																																		
	GUR13																																																				
	GUR302	2																																																		
	GUR12																																																				
	GUR301																																																				
	GUR09	1																																																		
	GUR297																																																				

Appendix C: Successive steps of the optimization. The optimization of the matrix has for goal to detect the missing occurrences due to sample bias, ecological exclusions, etc… Here the optimization requires 28 steps in order to reach a minimal stable number of 4 contradictions. We study the contradictions between the most similar sections before to extend the calculation to all sections (e.g. the first steps focus on the microbialite bearing section in shallow-water environmental settings). The stratigraphical ranges of species that are involved in most contradictions are the ranges that are completed with virtual occurrences (see method in Guex et al., 1991). Ng, *Neogondolella*; H, *Hindeodus*; I, *Isarcicella*; E, *Ellisonia*; S, *Sweetospathodus*; Ns. *Neospathodus*.

groups of sections considered	Step	Matrix name	steps involved in the addition of virtual ranges	species involved in most of the contradictions
Microbialite-bearing sections	0	0	**Wuzhuan + Dajiang + Dawen**	Ng. taylorae
	1	1	Ng. taylorae occurs with H. postparvus at Dajiang and Dawen: virtual edge between Ng. taylorae and H. postparvusat Wuzhuan	H. parvus, I. staeschei
	2	2	H. parvus occurs with I. staeschei at Dajiang and Wuzhuan: virtual edge between H. parvus and I. staeschei at Dawen	H. typicalis
	3	3	H. typicalis occurs with I. staeschei at Dajiang and Wuzhuan: virtual edge between H. typicalis and I. staeschei at Dawen	
Deeper water sections	4	3	**Shangsi + Meishan**	Ng. tulongensis, H. typicalis
	5	4	Ng. tulongensis occurs with S. kummeli at Meishan: upward irtual range of Ng. tulongensis at Shangsi	Ng. zhangi, Ng. tulongensis, Ng. orientalis
	6	5	Ng. meishanensis occurs with Isarcicella species at Meishan: virtual edge between Ng. meishanensis and Isarcicella species at Shangsi	Ng. zhangi, Ng. tulongensis, Ng. orientalis
	7	6	Ng. tulongensis occurs with Ng. yini and Ng. zhangi at Shangsi: virtual edge between Ng. tulongensis and Ng, yini + Ng. zhangi at Meishan	Ng. taylorae, Ng. discreta
	8	7	Ng. taylorae occurs with Ng. discreta at Meishan: virtual edge between Ng. tayorae and Ng. discreta at Shangsi	
	9	7	**Shangsi + Meishan + Yangou**	
Microbialite + Jiarong	10	7	**Wuzhuan + Dajiang + Dawen + Jiarong**	Ng. planata
	11	8	Ng. planata occurs with H. parvus at Dajiang: virtual edge between Ng. planata and H. parvus at Jiarong	Ng. planata, H. typicalis
	12	9	H. typicalis occurs with H. postparvus in many sections: virtual edge between typicalis and H. postparvus at Dajiang	
Deeper water China	13	9	**Shangsi + Meishan + Yangou + Jiarong**	Ng. krystyni, H. parvus, Ng. discreta
	14	10	H. parvus occurs with Ng. discreta at Meishan: virtual edge between H. parvus and Ng. discreta at Jiarong	Ng. tulongensis, H. sosioensis
	15	11	Ng. tulongensis occurs with H. parvus at Meishan: virtual edge between Ng. tulongensis and H. parvus at Jiarong	

groups of sections considered	Step	Matrix name	steps involved in the addition of virtual ranges	species involved in most of the contradictions
All chinese sections	16	11	**Wuzhuan + Dajiang + Dawen + Jiarong + Shangsi + Meishan + Yangou**	Ng. discreta, H. sosioensis, Ng. meishanensis
	17	12	H. sosioensis occurs with Ng. planata at Jiarong: virtual edge between H. sosioensis and Ng. planata at Dajiang	Ng. discreta, H. sosioensis, Ng. meishanensis
	18	13	Ng. meishanensis occurs with Ng. planata at Meishan: virtual range upwards of Ng. meishanensis at Dajiang	H. eurypyge
	19	14	H. eurypyge occurs with Ng. discreta at Meishan: Virtual edge between H. eurypyge and Ng. discreta at Dawen	H. inflatus, Ng. zhejiangensis
	20	15	H. inflatus occur with Ng. wangi, Ng. yini and Ng. zhangi at Meishan: virtual range of H. inflatus downward at Dawen	
All sections	21	15	**Wuzhuan + Dajiang + Dawen + Jiarong + Shangsi + Meishan + Yangou + Guryul Ravine**	Ng. carinata, Ng. changxingensis
	22	16	Ng. carinata occurs with Ng. yini and Ng. zhangi at Meishan (Jiang et al. 2007): virtual range of Ng. carinata downward at Guryul	I. staeschei, I. huckriedei, Ng. deflecta
	23	17	Ng. planata occurs with I. staeschei at Meishan: virtual edge between Ng. planata and I. staeschei at Guryul Ravine	I. staeschei, H. pisai, Ng. discreta, Ng. griesbachensis, Ng. nassichuki, Ng. meishanensis, Ng. eurypyge
	24	18	H. latidentatus occurs with I. staeschei at Meishan: Virtual edge between H. latidentatus and I. staeschei at Guryul Ravine	Ng. discreta, Ng. griesbachensis, Ng. nassichuki, Ng. meishanensis, Ng. eurypyge
	25	19	Ng. tulongensis occur with H. pisai at Meishan (Jiang et al. 2007): virtual edges between H. pisai and Ng. tulongensis at Guryul Ravine	H. pisai, Ng. planata, Ng. tulongensis, I. staeschei, Ng. discreta, Ng. griesbachensis, Ng. nassichuki
	26	20	H.inflatus occur with I. staeschei at Meishan: virtual edge between I. staeschei and H. inflatus at Guryul Ravine	I. staeschei, H. pisai, Ng. discreta, Ng. griesbachensis, Ng nassichuki, Ng. meishanensis, Ng. eurypyge, Ng. zhejiangensis
	27	21	Ng. zhejiangensis occurs with H. parvus at Guryul Ravine: virtual edge between Ng. zhejiangensis and H. parvus at Dawen	H. huckriedei, Ng. changxingensis, Ng. discreta, Ng. griesbachensis, Ng. nassichuki
	28	22	Ng changxingensis occur with H. parvus at Guryul Ravine and Meishan: virtual edge between Ng. changxingensis and H. parvus at Shangsi and Yangou	Ng. discreta, Ng. griesbachensis, Ng. nassichuki

Appendix D: Some details of the 28 steps of the optimization. We only show the 3 first contradictions for each step, which were used to detect the species involved the most in contradictions. The lines indicate superpositional relationship: grey points toward the old species and black towards the young species. The numbers above and below each lines represent species (list below). Ng, *Neogondolella*; H, *Hindeodus*; I, *Isarcicella*; E, *Ellisonia*; S, *Sweetospathodus*; Ns. *Neospathodus*.

Step 0	
Residual horizons	10
maximal cliques	10
unitary associations	7
contradictions	10
clique in cycles	0

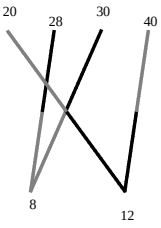

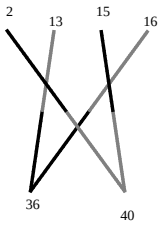

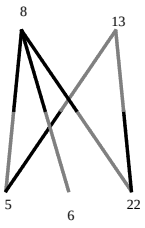

Step 1	
Residual horizons	9
maximal cliques	9
unitary associations	7
contradictions	4
clique in cycles	0

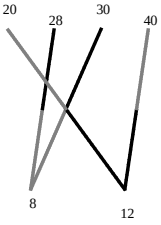

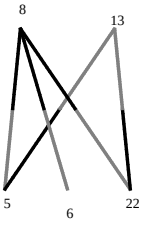

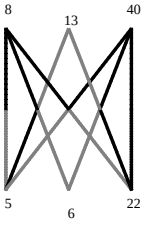

Step 2	
Residual horizons	9
maximal cliques	9
unitary associations	8
contradictions	3
clique in cycles	0

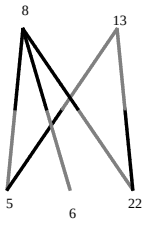

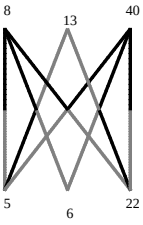

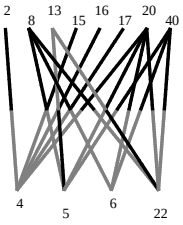

Step 3	
Residual horizons	9
maximal cliques	9
unitary associations	9
contradictions	1
clique in cycles	0

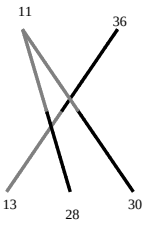

Step 4	
Residual horizons	14
maximal cliques	13
unitary associations	11
contradictions	11
clique in cycles	0

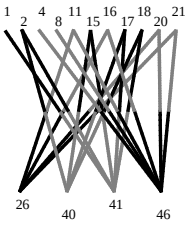

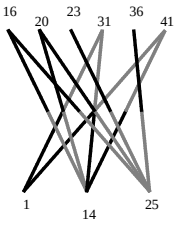

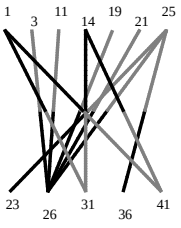

Step 5	
Residual horizons	14
maximal cliques	13
unitary associations	11
contradictions	10
clique in cycles	0

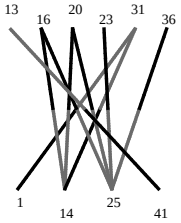

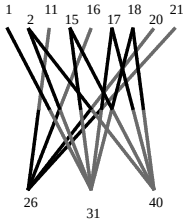

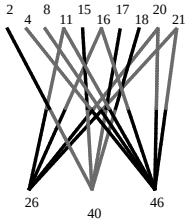

Step 6	
Residual horizons	13
maximal cliques	12
unitary associations	10
contradictions	7
clique in cycles	0

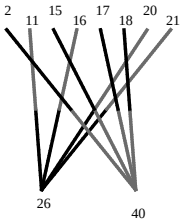

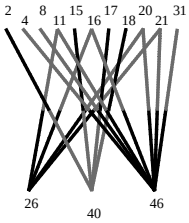

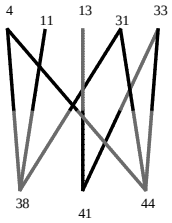

Step 7	
Residual horizons	12
maximal cliques	11
unitary associations	9
contradictions	2
clique in cycles	0

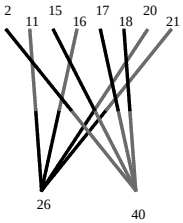

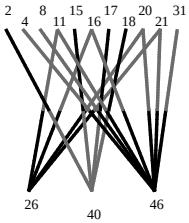

Step 8	
Residual horizons	12
maximal cliques	1
unitary associations	10
contradictions	0
clique in cycles	0

Step 9	
Residual horizons	13
maximal cliques	12
unitary associations	10
contradictions	0
clique in cycles	0

Step 10	
Residual horizons	13
maximal cliques	13
unitary associations	13
contradictions	3
clique in cycles	0

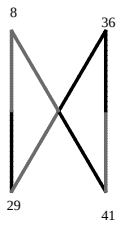

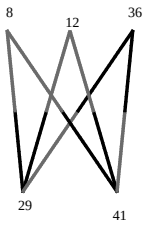

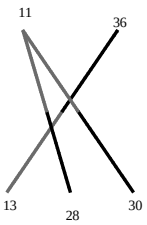

Step 11	
Residual horizons	14
maximal cliques	13
unitary associations	13
contradictions	1
clique in cycles	0

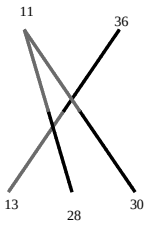

Step 12	
Residual horizons	14
maximal cliques	13
unitary associations	12
contradictions	0
clique in cycles	0

Step 13	
Residual horizons	17
maximal cliques	16
unitary associations	11
contradictions	7
clique in cycles	0

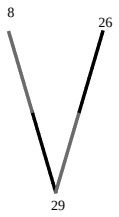

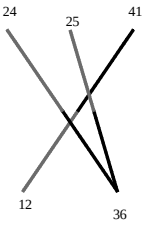

Step 14	
Residual horizons	17
maximal cliques	16
unitary associations	11
contradictions	6
clique in cycles	0

Step 15	
Residual horizons	17
maximal cliques	16
unitary associations	11
contradictions	0
clique in cycles	0

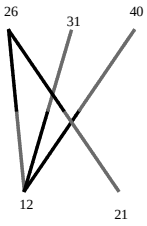

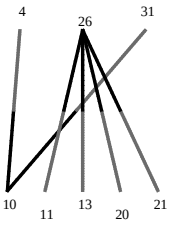

Step 16	
Residual horizons	26
maximal cliques	23
unitary associations	16
contradictions	9
clique in cycles	5

Step 17	
Residual horizons	25
maximal cliques	22
unitary associations	15
contradictions	6
clique in cycles	0

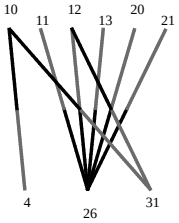

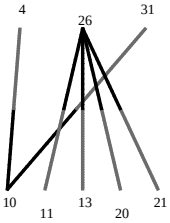

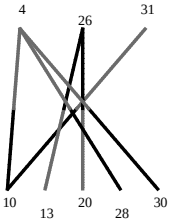

Step 18	
Residual horizons	26
maximal cliques	22
unitary associations	15
contradictions	5
clique in cycles	0

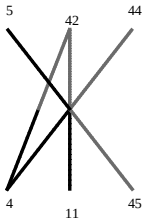

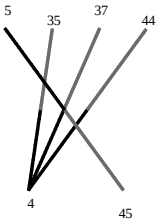

Step 19	
Residual horizons	26
maximal cliques	22
unitary associations	14
contradictions	2
clique in cycles	0

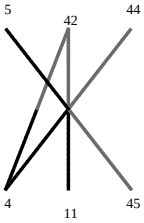

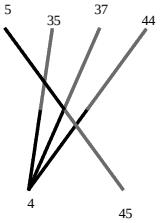

Step 20	
Residual horizons	26
maximal cliques	22
unitary associations	14
contradictions	0
clique in cycles	0

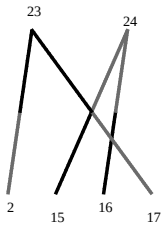

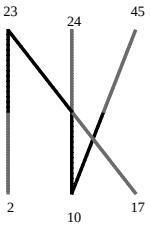

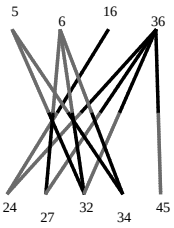

Step 21	
Residual horizons	32
maximal cliques	29
unitary associations	16
contradictions	45
clique in cycles	4

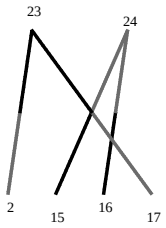

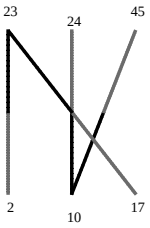

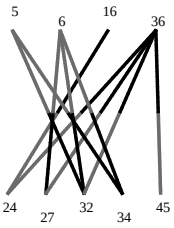

Step 22	
Residual horizons	31
maximal cliques	28
unitary associations	17
contradictions	26
clique in cycles	0

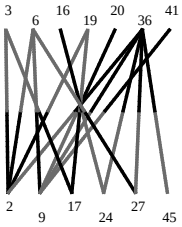

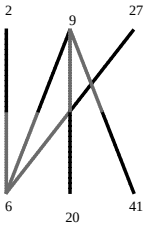

Step 23	
Residual horizons	31
maximal cliques	28
unitary associations	15
contradictions	19
clique in cycles	0

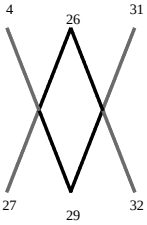

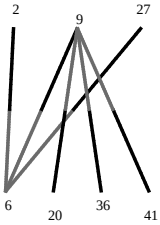

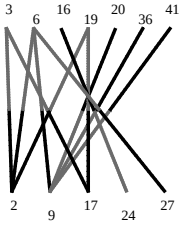

Step 24	
Residual horizons	29
maximal cliques	27
unitary associations	15
contradictions	15
clique in cycles	0

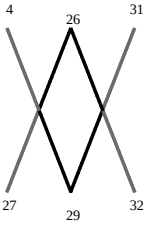

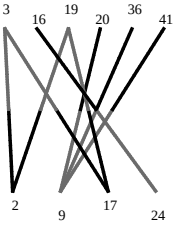

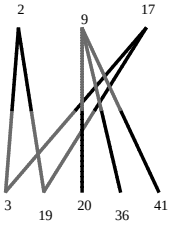

Step 25	
Residual horizons	29
maximal cliques	27
unitary associations	15
contradictions	10
clique in cycles	0

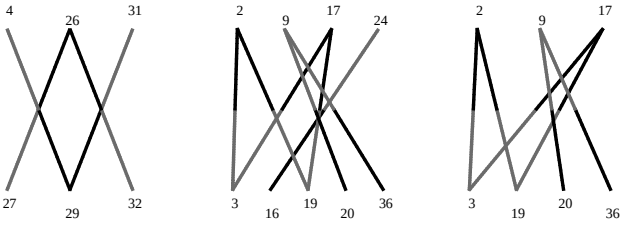

Step 26	
Residual horizons	29
maximal cliques	27
unitary associations	15
contradictions	9
clique in cycles	0

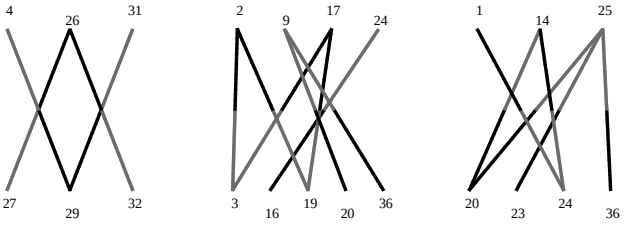

Step 27	
Residual horizons	29
maximal cliques	27
unitary associations	15
contradictions	7
clique in cycles	0

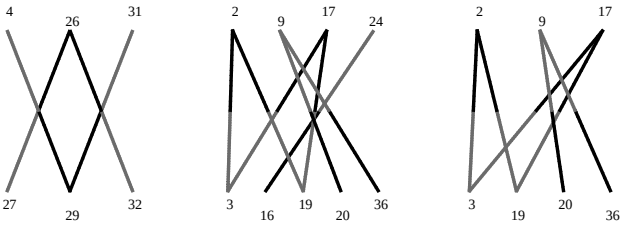

Step 28	
Residual horizons	30
maximal cliques	27
unitary associations	14
contradictions	4
clique in cycles	0

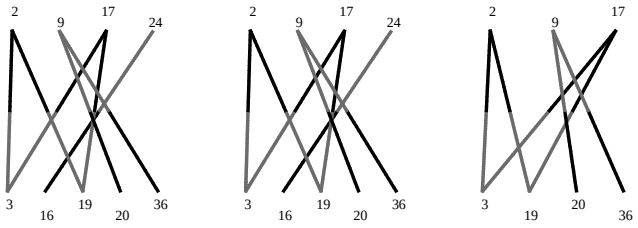

1 *H. anterodentatus*
2 *H. bicuspidatus*
3 *H. changxingensis*
4 *H. eurypyge*
5 *H. inflatus*
6 *H. latidentatus*
7 *H. magnus*
8 *H. parvus*
9 *H. pisai*
10 *H. postparvus*
11 *H. praeparvus*
12 *H. sosioensis*
13 *H. typicalis*
14 *I. huckriede*
15 *I. inflata*
16 *I. isarcica*
17 *I. lobata*
18 *I. peculiaris*
19 *I. prisca*
20 *I. staeschei*
21 *I. turgida*
22 *M. ultima*
23 *Ng. carinata*
24 *Ng. changxingensis*
25 *Ng. deflecta*
26 *Ng. discreta*
27 *Ng. griesbachensis*
28 *Ng. kazi*
29 *Ng. krystyni*
30 *Ng. lerhmanni*
31 *Ng. meishanensis*
32 *Ng. nassuchuki*
33 *Ng. orientalis*
34 *Ng. panjali sp. nov.*
35 *Ng. parasubcarinata*
36 *Ng. planata*
37 *Ng. predeflecta*
38 *Ng. postwangi*
39 *Ng. subcarinata*
40 *Ng. taylorae*
41 *Ng. tulongensis*
42 *Ng. wangi*
43 *Ng. yini*
44 *Ng. zhangi*
45 *Ng. zhejiangensis*
46 *S. kummeli*
47 *Ns. dieneri*
48 *Ns. cristagalli*
49 *Ns. eowaageni*
50 *Ns. chaohuensis*

Appendix E: Matrix of occurrence built after the optimization. The first column represents the local maximal horizons (LMHs) of each section. '0' is absence, '1' is presence. The grey squares represent virtual occurrences deduced from the optimization. Ng, *Neogondolella*; H, *Hindeodus*; I, *Isarcicella*; E, *Ellisonia*; S, *Sweetospathodus*; Ns. *Neospathodus*.

LMHs			*H. anterodentatus*	*H. bicuspidatus*	*H. changxingensis*	*H. eurypyge*	*H. inflatus*	*H. latidentatus*	*H. magnus*	*H. parvus*	*H. pisai*	*H. postparvus*	*H. praeparvus*	*H. sosioensis*	*H. typicalis*	*I. huckriede*	*I. inflata*	*I. isarcica*	*I. lobata*	*I. peculiaris*	*I. prisca*	*I. staeschei*	*I. turgida*	*M. ultima*	*Ng. carinata*	*Ng. changxingensis*	*Ng. deflecta*	*Ng. discreta*	*Ng. griesbachensis*	*Ng. kazi*	*Ng. krystyni*	*Ng. lerhmanni*	*Ng. meishanensis*	*Ng. nassuchuki*	*Ng. orientalis*	*Ng. panjali* sp. nov.	*Ng. parasubcarinata*	*Ng. planata*	*Ng. predeflecta*	*Ng. postwangi*	*Ng. subcarinata*	*Ng. taylorae*	*Ng. tulongensis*	*Ng. wangi*	*Ng. yini*	*Ng. zhangi*	*Ng. zhejiangensis*	*S. kummeli*	*Ns. dieneri*	*Ns. cristagalli*	*Ns. eowaageni*	*Ns. chaohuensis*	*Eurygnathodus costatus*	UAZs	UAs
7	Yangou	Yangou	0	1	0	1	0	0	0	1	0	0	1	0	0	0	0	1	0	0	0	1	0	0	0	0	0	0	0	0	0	0	0	0	0	0	0	0	0	0	0	0	0	0	0	0	0	0	0	0	0	0	0	0	0	0	6-8	5
6	Yangou	Yangou	0	1	0	1	0	0	0	1	0	0	1	0	0	0	1	0	0	0	0	1	0	0	0	0	0	0	0	0	0	0	0	0	0	0	0	0	0	0	0	0	0	0	0	0	0	0	0	0	0	0	0	0	0	0	6-8	5
5	Yangou	Yangou	0	0	1	0	0	0	1	0	0	1	0	0	0	1	0	0	0	0	1	0	0	0	1	0	0	0	0	0	0	0	0	0	0	0	0	0	0	0	0	0	0	0	0	0	0	0	0	0	0	0	0	0	0	0	4-5	3-4
4	Yangou	Yangou	0	0	1	0	0	0	0	0	1	0	1	0	0	0	0	0	1	0	0	0	0	0	0	0	0	0	0	0	0	0	0	0	0	0	0	0	0	0	0	0	0	0	0	0	0	0	0	0	0	0	0	0	0	0	4-5	3-4
3	Yangou	Yangou	0	0	1	0	0	0	0	0	1	0	1	0	0	0	0	0	1	0	0	0	0	0	0	0	0	0	0	0	0	0	0	0	0	0	0	0	0	0	0	0	0	0	0	0	0	0	0	0	0	0	0	0	0	0	4-5	3-4
2	Yangou	Yangou	0	0	0	0	0	0	0	0	0	1	0	0	0	0	0	0	0	0	0	0	0	0	0	0	0	0	0	0	0	0	0	0	0	0	0	0	0	0	0	0	0	0	0	0	0	0	0	0	0	0	0	0	0	0	2-3	1-2
1	Yangou	Yangou	0	0	0	0	0	0	0	0	0	0	0	0	0	0	0	0	0	0	0	0	0	0	0	0	0	0	0	1	0	0	0	0	0	0	0	0	0	0	0	0	0	0	0	0	0	0	0	0	0	0	0	0	0	0	1-2	1
5	Jiarong	Jiarong	0	0	0	0	0	0	0	0	0	0	0	0	0	0	0	0	0	0	0	0	0	0	0	0	0	0	0	0	0	0	0	0	0	0	0	0	0	0	0	0	0	0	0	0	0	0	0	0	0	0	0	0	0	0	11-12	7-8
4	Jiarong	Jiarong	0	0	0	0	0	0	0	0	0	0	0	0	0	0	0	0	0	0	0	0	0	0	0	0	0	0	0	0	0	0	0	0	0	0	0	0	0	0	0	0	0	0	0	0	0	0	0	0	0	0	0	0	0	0	11-12	7-8
3	Jiarong	Jiarong	0	0	0	0	0	0	0	0	0	0	0	0	0	0	0	0	0	0	0	0	0	0	0	0	0	0	0	0	0	0	0	0	0	0	0	0	0	0	0	0	0	0	0	0	0	0	0	0	0	0	0	0	0	0	11-12	7-8
2	Jiarong	Jiarong	0	0	0	0	0	0	0	0	0	0	0	0	0	0	0	0	0	0	0	0	0	0	0	0	0	0	0	0	0	0	0	0	0	0	0	0	0	0	0	0	0	0	0	0	0	0	0	0	0	0	0	0	0	0	11	77
1	Jiarong	Jiarong	0	0	0	0	0	0	0	0	1	0	0	0	0	1	0	0	0	0	0	0	0	0	0	0	0	0	0	0	0	0	0	0	0	0	0	0	0	0	0	0	0	0	0	0	0	0	0	0	0	0	0	0	0	0	9	6
8	Guryul Ravine	Guryul Ravine	0	0	0	0	0	0	0	0	0	0	0	0	0	0	0	0	0	0	0	0	0	0	0	0	0	0	0	0	0	0	0	0	0	0	0	0	0	0	0	0	0	0	0	0	0	0	0	0	0	0	0	0	0	0	13	9
7	Guryul Ravine	Guryul Ravine	0	0	0	0	0	0	0	0	0	0	0	0	0	0	0	0	0	0	0	0	0	0	0	0	0	0	0	0	0	0	0	0	0	0	0	0	0	0	0	0	0	0	0	0	0	0	0	0	0	0	0	0	0	0	12-13	8-9
6	Guryul Ravine	Guryul Ravine	0	0	0	0	0	0	0	0	0	0	0	0	0	0	0	0	0	0	0	0	0	0	0	0	0	0	0	0	0	0	0	0	0	0	0	0	0	0	0	0	0	0	0	0	0	0	0	0	0	0	0	0	0	0	11	7
5	Guryul Ravine	Guryul Ravine	0	0	0	0	0	0	0	0	0	0	0	0	0	0	0	0	0	0	0	0	0	0	0	0	0	0	0	0	0	0	0	0	0	0	0	0	0	0	0	0	0	0	0	0	0	0	0	0	0	0	0	0	0	0	11	7
4	Guryul Ravine	Guryul Ravine	0	0	0	0	0	1	1	0	1	0	0	0	0	1	0	0	1	0	0	0	0	0	0	0	0	0	0	0	0	0	0	0	0	0	0	0	0	0	0	0	0	0	0	0	0	0	0	0	0	0	0	0	0	0	7	5
3	Guryul Ravine	Guryul Ravine	0	1	0	1	1	1	0	1	0	0	1	0	0	0	0	0	0	0	0	0	0	0	0	0	0	1	1	0	0	1	0	0	0	0	0	0	0	0	0	0	0	0	0	0	0	0	0	0	0	0	0	0	0	0	7	5
2	Guryul Ravine	Guryul Ravine	0	1	0	1	1	1	0	1	1	0	0	0	0	0	0	0	0	0	0	0	0	0	0	0	0	0	1	0	0	0	0	0	0	0	0	0	0	0	0	0	0	0	0	0	0	0	0	0	0	0	0	0	0	0	6	5
1	Guryul Ravine	Guryul Ravine	0	0	0	0	1	1	0	1	0	0	1	0	0	0	0	0	0	0	0	0	0	0	0	0	0	1	1	0	0	0	0	0	0	0	0	0	0	0	0	0	0	0	0	0	0	0	0	0	0	0	0	0	0	0	6	5

LMHs	1	2	3	4	5	6	7	8	9	1	2	3	4	5	1	2	3	4	1	2	3	4	1	2	3	4
	Meishan D	Meishan D	Meishan D	Meishan D	Meishan D	Meishan D	Meishan D	Meishan D	Meishan D	Shangsi	Shangsi	Shangsi	Shangsi	Shangsi	Dajiang	Dajiang	Dajiang	Dajiang	Dawen	Dawen	Dawen	Dawen	Wuzhuan	Wuzhuan	Wuzhuan	Wuzhuan
H. anterodentatus	0	0	0	0	0	0	0	0	0	0	0	1	1	1	0	0	0	0	0	0	0	0	0	0	0	0
H. bicuspidatus	0	0	0	0	0	0	0	0	0	0	0	0	0	1	0	0	0	0	0	0	0	0	0	0	1	1
H. changxingensis	0	0	0	1	1	0	0	0	0	0	0	1	0	1	0	0	0	0	0	0	0	0	0	0	0	0
H. eurypyge	0	0	1	1	1	1	1	0	0	0	0	1	1	1	0	0	0	0	1	1	1	1	0	1	0	0
H. inflatus	1	1	1	1	1	1	0	0	0	0	0	0	0	0	0	0	0	0	1	1	0	0	0	0	0	0
H. latidentatus	1	1	1	1	1	1	0	0	0	0	0	0	0	0	0	0	0	0	1	1	0	0	0	0	0	0
H. magnus	0	0	0	0	0	0	0	0	0	0	0	0	0	0	0	0	0	0	0	0	0	0	0	1	0	0
H. parvus	0	0	0	1	1	1	1	0	0	0	0	0	1	1	1	1	1	1	0	0	1	1	1	1	1	1
H. pisai	0	0	0	0	0	0	0	0	0	0	0	0	0	0	0	0	0	0	0	0	0	0	0	0	0	0
H. postparvus	0	0	0	0	0	0	0	0	0	0	0	0	0	0	0	0	1	1	0	0	0	1	0	0	1	1
H. praeparvus	0	1	1	1	1	1	0	0	0	0	0	1	1	1	1	1	1	0	1	1	0	0	0	1	1	0
H. sosioensis	0	0	0	0	0	0	0	0	0	0	0	0	0	0	0	0	1	1	0	0	0	0	0	0	0	0
H. typicalis	1	1	1	1	1	0	0	0	0	0	0	0	0	0	1	1	1	0	1	1	1	1	1	1	1	0
I. huckriede	0	0	0	0	0	0	0	0	0	0	0	1	1	0	0	0	0	0	0	0	0	0	0	0	0	0
I. inflata	0	0	0	0	0	0	0	0	0	0	0	0	0	1	0	0	0	0	0	0	0	0	0	0	1	0
I. isarcica	0	0	0	0	1	1	0	0	0	0	0	0	0	1	0	1	0	0	0	0	0	0	0	0	1	0
I. lobata	0	0	0	0	0	0	0	0	0	0	0	0	0	1	0	1	1	0	0	0	0	0	0	0	1	0
I. peculiaris	0	0	0	0	0	0	0	0	0	0	0	0	0	1	0	0	0	0	0	0	0	0	0	0	0	0
I. prisca	0	0	0	1	1	1	0	0	0	0	0	1	1	0	1	0	0	0	0	0	0	0	0	0	0	0
I. staeschei	0	0	0	0	1	1	0	0	0	0	0	0	0	1	0	1	1	0	0	0	0	1	0	0	1	0
I. turgida	0	0	0	0	1	0	0	0	0	0	0	1	1	1	1	1	1	1	0	0	0	0	0	1	1	0
M. ultima	0	0	0	0	0	0	0	0	0	0	0	0	0	0	0	0	0	0	0	1	0	0	0	0	0	0
Ng. carinata	1	1	1	1	1	1	1	1	0	0	0	0	0	0	0	0	0	0	0	0	0	0	0	0	0	0
Ng. changxingensis	1	1	1	1	0	0	0	0	0	1	1	1	1	0	1	0	0	0	0	0	0	0	0	0	0	0
Ng. deflecta	1	1	1	1	0	0	0	0	0	1	1	1	0	0	0	0	0	0	0	0	0	0	0	0	0	0
Ng. discreta	0	0	0	0	0	0	1	1	0	0	0	0	0	0	0	0	0	0	0	0	0	0	0	0	0	0
Ng. griesbachensis	0	0	0	0	0	0	0	0	0	0	0	0	0	0	0	0	0	0	0	0	0	0	0	0	0	0
Ng. kazi	0	0	0	0	0	0	0	0	0	0	0	0	0	0	0	0	0	0	0	0	0	1	0	0	0	0
Ng. krystyni	0	0	0	0	0	0	0	0	0	0	0	0	0	0	0	0	0	0	0	0	0	0	0	0	0	0
Ng. lerhmanni	0	0	0	0	0	0	0	0	0	0	0	0	0	0	0	0	0	0	0	0	0	1	0	0	0	0
Ng. meishanensis	0	0	1	1	1	1	1	0	0	0	1	1	1	1	1	1	1	0	0	0	0	0	0	0	0	0
Ng. nassuchuki	0	0	0	0	0	0	0	0	0	0	0	0	0	0	0	0	0	0	0	0	0	0	0	0	0	0
Ng. orientalis	0	0	1	0	0	0	0	0	0	0	0	0	0	0	0	0	0	0	0	0	0	0	0	0	0	0
Ng. panjali sp. nov.	0	0	0	0	0	0	0	0	0	0	0	0	0	0	0	0	0	0	0	0	0	0	0	0	0	0
Ng. parasubcarinata	0	1	0	0	0	0	0	0	0	0	0	0	0	0	0	0	0	0	0	0	0	0	0	0	0	0
Ng. planata	0	0	0	0	1	1	1	1	0	0	0	0	0	0	0	0	1	0	0	0	0	0	0	0	0	0
Ng. predeflecta	0	1	0	0	0	0	0	0	0	0	0	0	0	0	0	0	0	0	0	0	0	0	0	0	0	0
Ng. postwangi	0	0	0	0	0	0	0	0	0	1	0	0	0	0	0	0	0	0	0	0	0	0	0	0	0	0
Ng. subcarinata	1	1	1	0	0	0	0	0	0	1	0	0	0	0	0	0	0	0	0	0	0	0	0	0	0	0
Ng. taylorae	0	0	0	1	1	1	1	1	0	0	0	1	1	1	0	0	1	0	0	0	0	1	1	1	1	1
Ng. tulongensis	1	1	1	1	1	1	1	1	0	1	1	1	1	1	0	0	0	0	0	0	0	0	0	0	0	0
Ng. wangi	1	0	0	0	0	0	0	0	0	0	0	0	0	0	0	0	0	0	0	0	0	0	0	0	0	0
Ng. yini	1	1	1	0	0	0	0	0	0	1	0	0	0	0	0	0	0	0	0	0	0	0	0	0	0	0
Ng. zhangi	1	1	0	0	0	0	0	0	0	1	0	0	0	0	0	0	0	0	0	0	0	0	0	0	0	0
Ng. zhejiangensis	0	0	0	0	0	0	0	0	0	0	0	0	0	0	0	0	0	0	1	1	1	0	0	0	0	0
S. kummeli	0	0	0	0	0	0	0	1	1	0	0	0	0	0	0	0	0	0	0	0	0	0	0	0	0	0
Ns. dieneri	0	0	0	0	0	0	0	0	1	0	0	0	0	0	0	0	0	0	0	0	0	0	0	0	0	0
Ns. cristagalli	0	0	0	0	0	0	0	0	1	0	0	0	0	0	0	0	0	0	0	0	0	0	0	0	0	0
Ns. eowaageni	0	0	0	0	0	0	0	0	0	0	0	0	0	0	0	0	0	0	0	0	0	0	0	0	0	0
Ns. chaohuensis	0	0	0	0	0	0	0	0	0	0	0	0	0	0	0	0	0	0	0	0	0	0	0	0	0	0
Eurygnathodus costatus	0	0	0	0	0	0	0	0	0	0	0	0	0	0	0	0	0	0	0	0	0	0	0	0	0	0
UAZs	1	1	3	4	5	5	11	12	14	1	3-4	4	4	8	4-5	6-8	9	9	3-7	3	4-7	10	4-10	4	8	9
UAs	1	1	2	3	4	4	7	8	10	1	2-3	3	3	5	3-4	5	6	6	2-5	2	3-5	7	3-7	3	5	6

Appendix F: Sequences of Unitary Associations (UAs) and Unitary Association Zones (UAZs). The lateral reproducibility, dissimilarity between UAs and real arcs (superpositional relationships) between UAs are taken into account in order to choose which UAs can be merged together into UAZs. The first UAs that should be merged have the lowest reproducibility and the lowest dissimilarities. For instance, UA_6 and UA_7 are detected in only one section each (lateral reproducibility of 1), are very similar (low dissimilarity index of 0.1385) and have only two superpositional arcs: they are the first ones to be merged together. The fusions are highlighted in grey in the table.

Dissimilarity index	UA above	UA below	Frequency of the arcs
0.8000	14	13	3
1.2670	13	12	10
0.7500	12	11	7
0.5000	11	10	4
0.4111	10	9	2
0.3838	9	8	5
0.1818	8	7	2
0.1385	7	6	2
0.2957	6	5	4
0.3772	5	4	8
0.7302	4	3	21
0.6071	3	2	9
0.4318	2	1	4

Dissimilarity index and frequence of arcs between UAZs

Appendix G: carbon isotope data (‰ deviation versus Vienna Pee Dee Belemnite (VPDB)), % of carbonate content and calculated error margins at 95% and 99%.

Sample name	δ13C VPDB	Yield % as CaCO3	Elevation (m)	sd	margin of error (n=3; 99%)	lower bound 99%	upper bound 99%	margin of error (n=3; 95%)	lower bound 95%	upper bound 95%
GUR 29	0.44	59.15	26.80	0.05	0.08	0.36	0.52	0.06	0.38	0.50
GUR 28	-0.12	76.72	25.80	0.04	0.06	-0.18	-0.06	0.05	-0.17	-0.07
GUR 27	0.57	57.93	25.00	0.05	0.07	0.50	0.64	0.05	0.52	0.62
GUR 26	-1.24	88.07	23.80	0.05	0.08	-1.32	-1.17	0.06	-1.30	-1.18
GUR 25	0.01	62.68	22.60	0.05	0.07	-0.07	0.08	0.06	-0.05	0.06
GUR 24	-0.30	46.46	21.80	0.05	0.07	-0.37	-0.23	0.05	-0.35	-0.24
GUR 23	-0.32	79.07	21.00	0.07	0.11	-0.43	-0.22	0.08	-0.40	-0.24
GUR 22	-0.76	66.01	20.20	0.05	0.07	-0.83	-0.69	0.06	-0.82	-0.70
GUR 21	-1.28	84.85	18.80	0.05	0.08	-1.36	-1.21	0.06	-1.34	-1.23
GUR 20	-1.37	79.58	17.80	0.08	0.11	-1.49	-1.26	0.09	-1.46	-1.29
GUR 19	-1.45	76.32	16.80	0.05	0.07	-1.52	-1.38	0.05	-1.50	-1.40
GUR 18	-1.69	85.41	16.00	0.08	0.11	-1.80	-1.57	0.09	-1.77	-1.60
GUR 17	-3.66	72.10	14.95	0.03	0.05	-3.71	-3.61	0.04	-3.70	-3.63
GUR 315	-2.62	87.81	14.20	0.06	0.09	-2.71	-2.52	0.07	-2.69	-2.55
GUR 314	-2.62	87.81	13.80	0.04	0.06	-2.68	-2.55	0.05	-2.67	-2.57
GUR 313	-2.33	73.63	13.65	0.05	0.08	-2.41	-2.25	0.06	-2.39	-2.27
GUR 312	-2.32	65.99	13.60	0.07	0.11	-2.43	-2.22	0.08	-2.41	-2.24
GUR 16	-0.70	70.64	13.10	0.04	0.06	-0.76	-0.64	0.04	-0.75	-0.66
GUR 311	-1.36	83.41	12.70	0.06	0.09	-1.45	-1.27	0.07	-1.43	-1.29
GUR 310	-3.77	73.25	12.30	0.08	0.12	-3.90	-3.65	0.09	-3.87	-3.68
GUR 309	-3.53	70.67	11.75	0.06	0.09	-3.63	-3.44	0.07	-3.60	-3.46
GUR 308	-1.26	5.65	11.15	0.42	0.63	-1.89	-0.64	0.48	-1.74	-0.79
GUR 307	-2.98	71.95	10.85	0.06	0.09	-3.07	-2.89	0.07	-3.05	-2.91
GUR 305	-2.76	87.84	10.50	0.06	0.09	-2.85	-2.66	0.07	-2.83	-2.69
GUR 15	-2.64	71.49	10.35	0.05	0.07	-2.71	-2.57	0.05	-2.69	-2.59
GUR 304.3	-3.05	87.62	9.90	0.04	0.06	-3.11	-3.00	0.04	-3.10	-3.01
GUR 14b	-3.19	57.84	9.75	0.05	0.08	-3.27	-3.11	0.06	-3.25	-3.13
GUR 304.2	-3.06	105.41	9.70	0.04	0.06	-3.13	-3.00	0.05	-3.11	-3.02
GUR 304.1	-2.99	102.17	9.60	0.04	0.06	-3.05	-2.92	0.05	-3.03	-2.94
GUR 304	-2.50		8.75	?						
GUR 303	-2.39	75.74	8.40	0.06	0.10	-2.49	-2.30	0.07	-2.47	-2.32
GUR 13	-3.36	80.12	8.20	0.03	0.04	-3.40	-3.32	0.03	-3.39	-3.33
GUR 302	-2.26	72.94	7.50	0.06	0.08	-2.34	-2.18	0.06	-2.32	-2.20
GUR 12	-3.07	79.52	7.45	0.04	0.06	-3.13	-3.01	0.05	-3.12	-3.03
GUR 301	-2.45	76.13	7.10	0.05	0.07	-2.52	-2.37	0.06	-2.50	-2.39
GUR 11	-1.93	10.77	6.90	0.10	0.16	-2.09	-1.78	0.12	-2.05	-1.81
GUR 10	-1.80	74.74	6.40	0.03	0.05	-1.86	-1.75	0.04	-1.84	-1.76
GUR 9	-2.10	67.18	6.00	0.05	0.08	-2.18	-2.02	0.06	-2.16	-2.04
GUR 8	-1.23	59.11	5.60	0.04	0.06	-1.29	-1.17	0.05	-1.28	-1.18
GUR 300	-1.50	65.78	5.50	0.07	0.10	-1.60	-1.39	0.08	-1.57	-1.42
GUR 7	-2.03	0.24	3.85	0.34	0.51	-2.54	-1.52	0.39	-2.42	-1.64
GUR 07b	-0.70	38.01	3.00	0.06	0.09	-0.79	-0.61	0.07	-0.77	-0.63
GUR 6	-0.22	52.90	2.00	0.04	0.06	-0.28	-0.16	0.04	-0.26	-0.18
GUR 5	-0.29	0.35	1.35	0.41	0.61	-0.90	0.32	0.46	-0.76	0.17
GUR 4	0.39	32.89	1.00	0.05	0.07	0.32	0.47	0.05	0.34	0.45
GUR 3	-0.84	26.03	0.60	0.07	0.11	-0.94	-0.73	0.08	-0.92	-0.76
GUR 299			0.50							
GUR 2	1.61	60.91	0.30	0.02	0.03	1.59	1.64	0.02	1.59	1.63
GUR 298	-0.06	47.21	0.25	0.07	0.10	-0.16	0.04	0.08	-0.14	0.02
GUR 297	1.26	67.16	0.10	0.05	0.07	1.19	1.33	0.05	1.21	1.31

CHAPTER IV

UNTANGLING THE TAXONOMY OF *NEOGONDOLELLA*: CLUSTER ANALYSES VS. TYPOLOGICAL TAXONOMY. THE CASE OF GRIESBACHIAN CONODONTS FROM GURYUL RAVINE, KASHMIR

Morgane Brosse & Louise Souquet

Untangling the taxonomy of *Neogondolella*: Cluster analyses vs. traditional typological taxonomy. The Griesbachian conodonts from Guryul Ravine, Kashmir

Morgane Brosse[a] & Louise Souquet[b]

[a]Paläontologisches Institut und Museum der Universität Zürich, Karl Schmid-Strasse 4, CH-8006 Zürich, Switzerland. morgane.brosse@pim.uzh.ch

[b]Univ. Lyon, ENS de Lyon, CNRS, Univ. Claude Bernard Lyon 1, Institut de Génomique Fonctionnelle de Lyon, UMR 5242, 46 Allée d'Italie, F-69364 Lyon Cedex 07, France.

Abstract

This work is involved in a vast project in collaboration with the IGFL (ENS Lyon, France) that aims at quantifying the morphological variability of conodonts thanks to empirical (as opposed to conceptual) classifications. We focus here on the genus *Neogondolella*, one of the most critical conodont utilized worldwide in building biochronological scales to calibrate the Permian-Triassic boundary, the mother of all mass-extinctions. For this exploratory study, we built a data set of categorical variables from a population of *Neogondolella* from the Guryul Ravine outcrop supplemented with 10 holotypes of *Neogondolella* frequently encountered during the studied time interval. The cluster analysis generates 5 clusters of high statistical power, thus grouping several holotypes together (e.g. *Neogondolella planata* and *Neogondolella discreta*). The size of the cohort (N=183) does not allow a statistical partitioning into more than five groups, but we nevertheless show that non-statistical groups can still distribute the holotypes and produce rather homogeneous clusters.

Keywords:

Conodonts, Griesbachian, morphology, statistic, hierarchical clustering.

1. Introduction

The Permian-Triassic boundary (251.956 ± 0.033 Ma; Baresel et al., 2016) was the most devastating of all mass extinctions in the history of life. The great abundance, global spatial distribution and high evolutionary rates of conodont marine microfossils make them one of the main biochronological tools for the Palaeozoic and the Triassic. Contrary to most organisms, conodonts remained comparatively unscathed across the Permian-Triassic boundary and therefore became prominent fossil indexes for this time interval.

Among all conodont genera that survived the mass extinction, neogondolellids and anchignathodontids are of paramount importance for Late Permian and lowermost Triassic biostratigraphical scales (see Orchard, 2007 and references therein). Neogondolellids were ubiquitous and abundant across the Permian-Triassic boundary, but it has been argued that their high morphological variability precluded establishing reliable fossil indexes (Kozur et al., 1995), which eventually led to elect the anchignathodontid *Hindeodus parvus* as index fossil for the base of the Triassic (Yin et al., 1996). This interpretation has later been contested by Orchard and Krystyn (1998), who proposed a high resolution interval zone series exclusively based on neogondolellids from the Griesbachian (basal Triassic) of Spiti. Neogondolellids were thriving in deeper and colder environments than anchignathodontids during the Griesbachian (Joachimski et al., 2012), and building a neogondolellid-based biochronological scale provides major advantage in deep-water sections. Neogondolellids were more diverse than anchignathodontids during the latest Permian. They underwent an extinction at the Permian-Triassic boundary, followed by the radiation of anchignathodontids at the beginning of the Griesbachian (Brosse et al., 2016). It is therefore of major importance not to neglect these families in building biostratigraphical scales across the Permian Triassic boundary.

Orchard and Krystyn (1998) adopted a typological approach and created four news species of *Neogondolella* that are nowadays commonly used for the biostratigraphy of the Griesbachian, as well as six morphotypes of previously existing species (*Neogondolella tulongensis* α, β, γ and *Neogondolella taylorae* α, β, γ). This method allows the selection of key diagnostic characters to identify species, as shown in Table 1 (reproduced after Orchard and Krystyn, 1998). Although the typological approach permits to achieve high resolution in biostratigraphical studies, it is based on an ideal type that does not necessarily reflect empirical reality.

Brosse et al. (in prep.; Chapter III) recently retrieved very similar conodont assemblages than the ones found in Spiti, from the Member E of the Guryul Ravine section (Vihi district of Kashmir). The populations of conodonts from both sections are dominated by *Neogondolella* and encompass the Griesbachian time interval, which allows making comparisons between the two localities. Following the typological approach, both Orchard and Krystyn (1998) and Brosse et al. (in prep.; Chapter III) were able to build precise biostratigraphical and biochronological scales, but did not document the intra-specific variability.

Our goal is to test the possibility to statistically sort the population of *Neogondolella* thanks to a set of categorical variables that describe the shape of the elements.

We base our study on multiple correspondence and cluster analyses of P_1 elements of *Neogondolella*. The analyses focus on the population of conodonts of Griesbachian age from Member E of the

Ng. carinata	broad platform, maximum width medially, posteriorly indented
Ng. discreta	narrow platform; high discrete carinal denticles
Ng. kazi	broad posteriorly rounded platform; high and fused carinal denticles
Ng. krystyni	platform margins parallel to undulose; elevated posterior carina
Ng. meishanensis	upturned platform margins, straight carina, high terminal cusp
Ng. nassichuki	narrow, evenly tapered platform with maximum width medially
Ng. nevadensis	broad platform, maximum width near posterior end; carina extends to or beyond posterior end
Ng. orchardi	narrow, curved and pointed platform with terminal cusp
Ng. planata	broad, evenly tapered platform with maximum width medially
Ng. taylorae	broad, rounded posterior margin, prominent cusp with posterior brim
Ng. taylorae α	as holotype; length:width ratio = 2:1
Ng. taylorae β	relatively short bulbous platform due to anterior narrowing
Ng. taylorae γ	relatively narrow, long platform; length:width ratio = 3:1
Ng. tulongensis	subquadrate platform +/-sinuous margin
Ng. tulongensis α	symmetrical quadrate platform
Ng. tulongensis β	platform with sinuous inner margin
Ng. tulongensis γ	form with strongly deflected posterior carina
Ng. zhejiangensis	elongate-oval platform, rounded posterior margin, low carinal nodes, indistinct cusp +/-accessory posterior denticles
Ng. sp. A	oblong platform, high carina, sinuous margin

Table 1: Summary of diagnostic morphological characteristics of *Neogondolella* (Ng.) species occurring in the lowermost Triassic. After Orchard and Krystyn, 1998.

Guryul Ravine section, but also includes holotypes of typical latest Permian and Griesbachian species (*Neogondolella carinata*, *Neogondolella changxingensis*, *Neogondolella deflecta*, *Neogondolella discreta, Neogondolella griesbachensis*, *Neogondolella kazi*, *Neogondolella krystyni*, *Neogondolella meishanensis*, *Neogondolella nassichuki*, *Neogondolella nevadensis*, *Neogondolella orchardi*, *Neogondolella planata*, *Neogondolella taylorae*, *Neogondolella tulongensis*, *Neogondolella yini* and *Neogondolella zhejiangensis*).

2. Material and methods

2.1. Selection of variables for analyses

We selected 19 variables based on the upper and lateral views of the P_1 element. These variables are common features used in diagnoses of *Neogondolella* species. When possible, we attempted to express continuous characters as ratios-based discrete characters. For instance, the platform width character is expressed as the length/width ratio and split into two categories: “wide”- L/W>3 and “narrow”- L/W<3 categories. Table 2 shows the list of variables with their categories.

The cohort contains 215 specimens (199 from the Guryul Ravine population and 16 previously published holotypes, see Appendix). Complete data for all these variables, necessary for principal component and cluster analyses are available for 183 specimens. The group of 32 specimens excluded from the analyses consists of poorly preserved elements or insufficient illustrations (only the holotypes of *Neogondolella carinata*, *Neogondolella discreta, Neogondolella griesbachensis*, *Neogondolella kazi*, *Neogondolella krystyni*, *Neogondolella nassichuki*, *Neogondolella orchardi*, *Neogondolella planata*, *Neogondolella taylorae* and *Neogondolella zhejiangensis* are retained). The specimens were retrieved from different horizons but are all of Griesbachian age.

view of the P1 considered	N°	variables	categories
upper view	V1	indentation on lateral margin	(0) no indentation (1) weak indentation (2) strong indentation
upper view	V2	symmetrical indentations of posterior platform	(0) no indentation (1) weak indentation (2) strong indentation = posterior platform
upper view	V3	platform width	(0) narrow: L/maximalW>3 (1) wide: L/maximalW<=3
upper view	V4	location of the platform maximal width	(0) parallel platforms (1) anterior 3/5th (2) posterior 2/5th
upper and lateral view	V5	thickness of the posterior platform brim	(0) no platform brim (cusp terminal) (1) bulge (cusp subterminal) (2) thin brim (< cusp diametre) (3) thick brim (>=)
upper view	V6	occurrence of a free anterior blade	(0) no free blade (1) one denticle free (2) more than one denticle free
upper view	V7	occurrence of a free posterior blade	(0) absence (1) occurrence
upper view	V8	deflection of the carina (main process)	(0) no deflection (1) weak deflection (2) strong deflection
upper view	V9	accessory denticle after the cusp	(0) absence (1) occurrence of excactly one denticle
upper view	V10	accessory process after the cusp	(0) absence (1) at least 2 denticles after the cusp (2) 2 extensions
lateral view	V11	denticle fused (only tip free)	(0) denticles discrete or space between denticle' tip <= 2*height (1) closely appressed to weakly fused (2) strongly fused
lateral view	V12	cusp projects posteriorly further than the posterior margin	(0) absence (1) occurrence
upper and lateral view	V13	space between cusp and carina	(0) equal to space between other denticles (1) larger
lateral view	V14	relative size of denticles (without cusp)	(0) denticles lowest at midlenght or decreasing posteriorly (1) denticles subequal
lateral view	V15	high denticles (midlenght)	(0) low denticle (1) high denticles
upper and lateral view	V16	broad cusp	(0) cusp diametre smaller or equal than adjacent denticles (1) diametre larger
lateral view	V17	cusp higher than adjacent denticle	(0) absence (1) occurrence
upper view	V18	Posterior platform shape	(0) rounded (1) subquadrate to quadrate (2) constricted to pointy
lateral view	V19	lateral shape of the attachment scar	(0) flat: angle between anterior part and posterior part >= 150° (1) angulate: <150°

Table 2: list of the 19 variables and their categories.

2.2. Factorial analyses and hierarchical classification

Factorial analyses were conducted using the R "FactoMineR" package (Lê et al. 2008), dedicated to multivariate data analysis.

The relationships between the 19 categorical variables were studied using multiple correspondence analyses (MCA; see Husson et al., 2016 for detailed description of the function). In a multidimensional dataset of non-linear data, MCA identify associations between multiple categorical variables. Similarly to other multivariate methods, it is dimension reducing: it represents the data as points in a few dimensional spaces that summarizes the variance of the dataset.

Variables are clustered using hierarchical classification (HCPC; see Husson et al., 2016 for detailed description of the function). The cluster analysis produces a hierarchical tree that sorts individuals according to their coordinates within the MCA's principal components morphospace. The hierarchical clusters are presented in a dendrogram.

3. Results

3.1. Principal components

The components generated by the MCA are presented in Table 3, Component 1 representing for the highest variance. The first three components account for 28.32% of the total variance, respectively for 12.53, 8.52, and 7.17% (Table 3). We calculated the pairwise Euclidian distances between all individuals based on their scores on the 16 first dimensions of the MCA (accounting for 80% of the total variance).

3.2. Hierarchical clustering

The dendrogram resulting from the 16 dimensions is indexed by the within-inertia gain. The total inertia (total variance) is the sum of the between- and within-group variance and characterizes the homogeneity of a cluster. It is decomposed thanks to the Ward's criterion detailed in Husson et al. (2010). We based the initial number of clusters on the optimal growth of inertia calculated by the HCPC function. The optimal growth of inertia being four, the population is grouped into five clusters (Fig. 1).

Components	Eigenvalues	% Variance	Cum % Variance
1	0.19	12.53	12.53
2	0.13	8.52	21.06
3	0.11	7.27	28.32
4	0.09	5.84	34.16
5	0.08	5.31	39.47
6	0.08	5.13	44.60
7	0.07	4.55	49.15
8	0.07	4.37	53.53
9	0.06	4.19	57.72
10	0.06	3.61	61.33
11	0.05	3.49	64.82
12	0.05	3.44	68.26
13	0.05	3.18	71.44
14	0.05	2.96	74.40
15	0.04	2.69	77.08
16	0.04	2.65	79.73
17	0.04	2.32	82.05
18	0.03	2.12	84.17
19	0.03	2.04	86.20

Table 3: Eigenvalue, % of variance explained and cumulated % of variance for each component generated by the MCA. The part highlighted by the grey shade indicates the 16 first components that were used to compute the hierarchical classification.

3.3. Description of the clusters

Each cluster is described in Table 4. The clusters are very unequal in number of individuals, from 7 in Cluster 5 to 81 in Cluster 3. The population of each cluster can be described thanks to the categories that are most frequently displayed (Table 4). For instance,

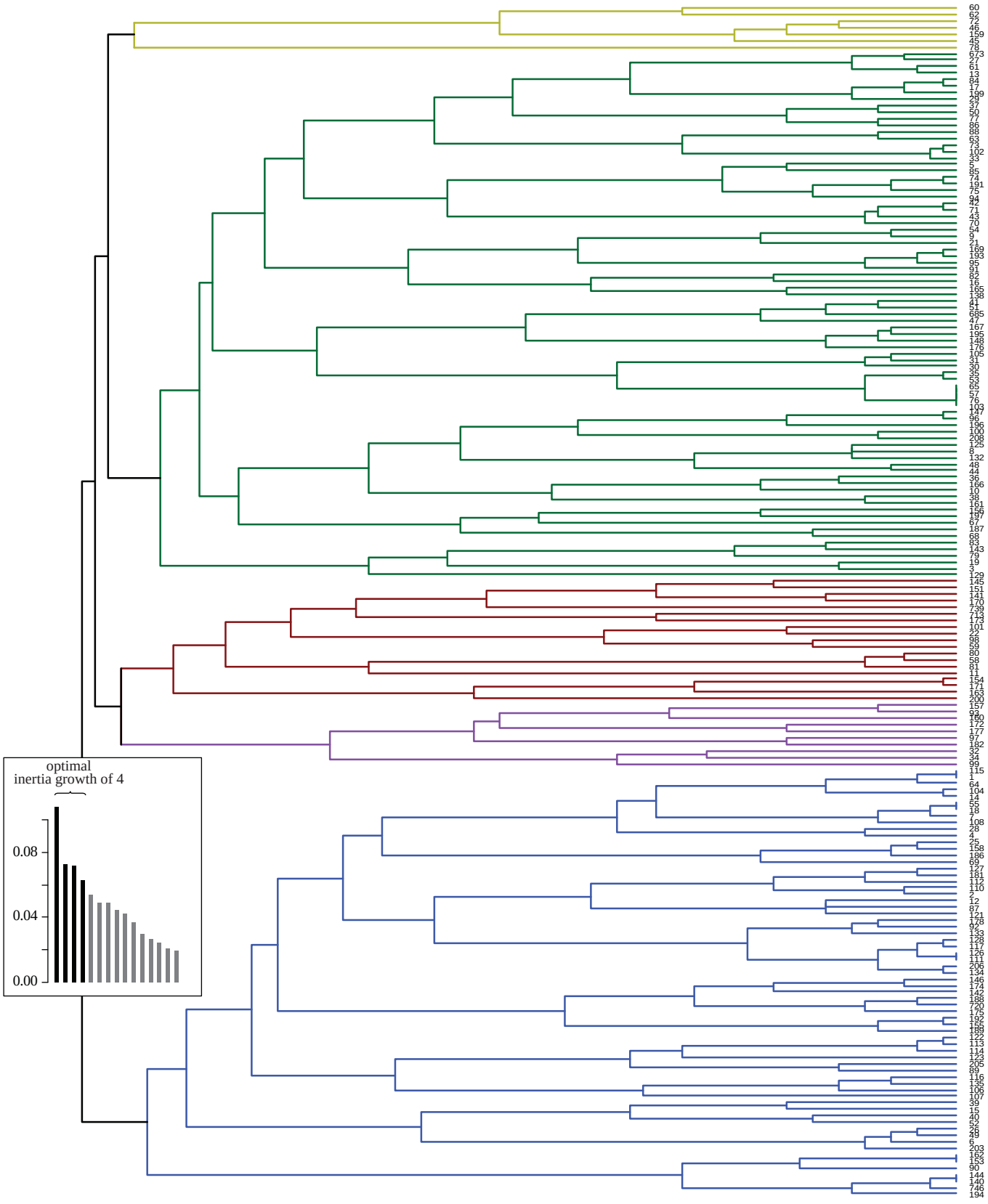

Figure 1: Dendrogram illustrating the results of the cluster analysis of morphological variables. Each horizontal line represents an individual. The original individuals are optimally grouped into five major clusters highlighted by the different colours.

Clusters	Variable_category	Considered variables and categories (for each cluster)	% of individuals included within the cluster (>=50%)	Holotypes included within the cluster
1 (n=66)	V7_1	occurrence of a free posterior blade	100	*Ng. discreta* *Ng. griesbachensis* *Ng. planata* *Ng. nevadensis*
	V18_2	constricted to pointy posterior platform	85	
	V5_0	no platform brim (cusp terminal)	78.87	
	V12_1	cusp projects posteriorly further than the posterior margin	73.77	
	V4_0	parallel platform margins	66.67	
	V8_0	no deflection of the carina (main process	51.81	
2 (n=10)	V2_1	Weak constriction of the posterior platform	100	
3 (n=81)	V1_2	weak indentation on lateral margin	85.71	*Ng. taylorae* *Ng. yini* *Ng. nassichuki*
	V5_2	thin posterior brim (< cusp diametre)	71.05	
	V18_0	posterior platform rounded	68.42	
	VV5_1	posterior bulge (cusp subterminal)	66.67	
	V17_0	cusp not higher than adjacent denticle	64.58	
	V11_1	denticles closely appressed to weakly fused	62.07	
	V12_0	cusp does not projects posteriorly	60.66	
	V13_1	space between cusp and carina larger than space between other denticles	60.00	
	V5_3	thick posterior brim	57.45	
	V8_1	weak deflection of the carina	56.52	
	V16_0	cusp diameter smaller or equal than adjacent denticles	53.75	
	V15_0	low denticles at midlenght	53.62	
	V19_1	attachment scar angulate laterally	52.73	
4 (n=19)	V2_2	secondary posterior platform	80.00	*Ng. carinata* *Ng. krystyni* *Ng. kazi*
	V9_1	occurrence of exactly one extra denticle posteriorly	59.09	
	V11_2	denticles strongly fused	56.25	
5 (n=7)	V10_2	two posterior extension of the carina	100.00	
	V10_1	one posterior extension	85.71	

Table 4: description of the 5 computed clusters. The column to the right corresponds to the percentage of individuals showing the corresponding category. We only show here the categories that are represented by at least 50% of the cluster population.

100% of the individuals in Cluster 2 show a weak constriction of the posterior platform and the other categories are not much represented. 100% of the individuals in Cluster 1 have a free posterior blade (including the holotype of *Ng. discreta*). 100% of the individuals in Cluster 5 have one or two extension of the carina, posteriorly from the cusp. 80% of the individuals in Cluster 4 have a secondary posterior platform (including the holotype of *Ng. carinata*). 85% of the individuals in Cluster 3 feature an asymmetrical weak indentation of the lateral margin and 71% have a thin posterior brim (including the holotype of *Ng. taylorae*, *Ng. nassichuki* and *Ng. yini*).

4. Discussion

Following the standard typological approach, Orchard and Krystyn detected 13 species of *Neogondolella* in Spiti and Brosse et al. (in prep.; Chapter III) identified 13 species in the Griesbachian material from Guryul Ravine. Both localities have 10 species in common. In contrast, the optimal inertia growth generates five clusters, i.e. about 40% of the number of species expected.

The multivariate method also groups morphotypes that are clearly separated by the typological approach, such as the holotypes of *Ng. planata* and *Ng. discreta* in Cluster 1 (Fig. 2).

We thus decided to split further the hierarchical tree to get closer from the expected number of 10-13 species and chose an inertia growth of 10 that splits the hierarchical tree accordingly into 11 subgroups. The Cluster 1 is divided into 3 subgroups 1A-C, Cluster 3 into 3 sub-groups 3A-C, Cluster 4 into 2 subgroups 4A, B, and Cluster 5 into 2 subgroups 5A, B. The five clusters and their subgroups are displayed in Figures 2-6.

Interestingly, the holotypes of *Ng. planata* and *Ng. discreta* are now separated into two different subgroups (1A and 1C) in this new partition. In fact, the subgroup including the holotype of *Ng. discreta* appears to be the most consistent, as all individuals feature the posterior free blade diagnostic of this species. Another relatively consistent subgroup of Cluster 1 includes the holotype of *Ng. griesbachensis* and individuals with parallel platform margins (subgroup 1B). The partitioning of Cluster 3 also presents interesting result, as the new sub-division allows to separate the holotype of *Ng. yini* with terminal cusp (subgroup 3B) and the holotypes of *Ng. taylorae* and *Ng. nassichuki* with a posterior platform brim (subgroup 3C).

Cluster 3A is clearly discriminated mostly on the base of an asymmetrical lateral indentation of the platform margins. It is worth noting that from every diagnosis of *Neogondolella* species that are mentioned here (see the summary in Table 1), the asymmetrical indentation is never used as a diagnostic character, although being plainly featured on the holotype of *Ng. kazi* (Orchard and Krystyn, 1998; Pl. 2, Fig. 10-12). The overall platform shape itself is however often considered as a major diagnostic character: *Ng. tulongensis* (Tian, 1982) is identified thanks to a squared posterior platform and a rectangular platform outline; the holotype of *Ng. carinata* (Clark, 1959; Pl. 44, Fig. 16-17) features a strong constriction of the platform posteriorly nowadays considered diagnostic for some authors (Orchard et al., 1994; Orchard and Krystyn, 1998); *Ng. krystyni* (Orchard and Krystyn, 1998) is characterized by "undulose margins". Mei (1996) introduced the square-, rounded- and narrow-morphotypes when referring to *Neogondolella* species. The square-morphotype has a squared and oblique posterior end and includes *Ng. tulongensis*; the rounded-morphotype has a teardrop platform outline and includes *Ng. changxingensis*, *Ng.*

zhejiangensis and *Ng. taylorae*; the narrow-morphotype has a narrow posterior end and a lenticular platform outline and includes *Ng. meishanensis* and *Ng. orchardi*. Mei et al. (1998) in their re-evaluation of the taxonomy of Permian-Triassic conodonts from China, also used the three morphotypes, but concluded that "the general configuration of the denticles is the most consistent and reliable characteristic". This hypothesis was independently proposed in Krystyn and Orchard (1996) and in Orchard and Krystyn (1998), who argued that Griesbachian *Neogondolella* species are mostly distinct by the axial part (blade-carina-cusp). To summarize, the diagnostic characters are eventually the authors' own choice, and the relative importance of the platform shape or the axial part in taxonomy has never been more than tacitly admitted.

5. Conclusion and perspectives

Although the size of the cohort does not allow a statistical partitioning into more than five groups, we observe that even non-statistical groups can still distribute the holotypes. Increasing the sample size would achieve a higher statistical power, but we also propose here a number of perspectives and solutions in order to improve the method in future analyses.

According to Mei et al. (1998), to Krystyn and Orchard (1996) and to Orchard and Krystyn (1998), Griesbachian *Neogondolella* species are mostly distinguished by the axial part. By this standards, a subgroup mostly defined by the occurrence of a lateral indentation like subgroup 3A is considered a taxonomical dead-end. Although this has never been quantified, it is generally admitted that the platform margins in *Neogondolella* display a high variability (Kozur et al., 1995), and that asymmetrical lateral indentation is occurring independently in different species. Would the axial part bear the most important diagnostic features, the list of variables should focus more on the blade-carina-cusp than on the platform shape.

The difficulty to interpret continuous characters as categorical variables led to approximations that generate "noise" within the final signal, resulting into high within-group inertia. A multivariate method including quantitative measurements would lead to a more objective classification. A Fourier analysis on outlines of the platforms and the carina might produce a better outcome as well as an estimation of the importance of the platform shape as a diagnostic character.

Aknowledgments

This work is supported by the Swiss NSF project 200021_135446 (to H.B.) and a French ANR @RAction grant (project EvoDevOdonto to N.G.). We are very grateful to IE P. Joncour (IGFL, ENS Lyon, France) for her help using the R software and to N. Goudemand for providing a friendly review of the manuscript.

Reference

Clark, D., 1959. Conodonts from the Triassic of Nevada and Utah. Journal of Paleontology, 33(2), 305-312.

Husson, F., Josse, J., and Pages, J., 2010. Principal component methods-hierarchical clustering-partitional clustering: why would we need to choose for visualizing data. Applied Mathematics Department.

Husson, F., Josse, J., Lê, S., Mazet, J., and Husson, F., 2016. Package 'FactoMineR'.

Kozur H., Ramovs A., Wang E. and Zakharov Y., 1995. The importance of Hindeodus parvus (Conodonta) for the definition of the Permian-Triassic boundary and evaluation of the proposed sections for a global stratotype section and point (GSSP) for the base of the Triassic. Geologija, 37(8), 173-213, Ljubljana.

Krystyn, L., and Orchard, M., 199). Lowermost Triassic ammonoid and conodont biostratigraphy of Spiti, India. Albertiana, 17, 10-21.

Lê, S., Josse, J., and Husson, F., 2008. FactoMineR: an R package for multivariate analysis. Journal of statistical software, 25(1), 1-18.

Mei, S., 1996. Restudy of conodonts from the Permian–Triassic boundary beds at Selong and Meishan and the natural Permian–Triassic boundary. Centennial memorial volume of Professor Sun Yunzhu (Sun YC). Stratigraphy and palaeontology, 141-148.

Mei, S., Zhang, K., and Wardlaw, B., 1998. A refined succession of Changhsingian and Griesbachian neogondolellid conodonts from the Meishan section, candidate of the global stratotype section and point of the Permian–Triassic boundary. Palaeogeography, Palaeoclimatology, Palaeoecology, 143(4), 213-226.

Orchard, M., 2007. Conodont diversity and evolution through the latest Permian and Early Triassic upheavals. Palaeogeography, Palaeoclimatology, Palaeoecology, 252(1), 93-117.

Orchard, M.J., and Krystyn, L., 1998. Conodonts of the lowermost Triassic of Spiti, and new zonation based on Neogondolella successions. Rivista Italiana di Paleontologia e Stratigrafia, 104(3), 341-368.

Orchard, M., Nassichuk, W. W., and Rui, L., 1994. Conodonts from the Lower Griesbachian Otoceras Latilobatum Bed of Selong, Tibet and the Position of the Permian-Triassic Boundary. Canadian Society of Petroleum Geologists, memoire 17, 823-843.

Tian, C., 1982. Triassic conodonts in the Tulong section from Nyalam County, Xizang (Tibet), China. Contribution to Geology of Qinghai, Xizang (Tibet) Plateau, vol. 10.

Yin, H., Wu, S., Ding, M., Zhang, K., Tong, J., Yang, F., and Lai, X., 1996. The Meishan section, candidate of the global stratotype section and point of Permian-Triassic boundary. The Paleozoic-Mesozoic Boundary Candidates of the Global Stratotype Section and Point of the Permian-Triassic Boundary, 31-48.

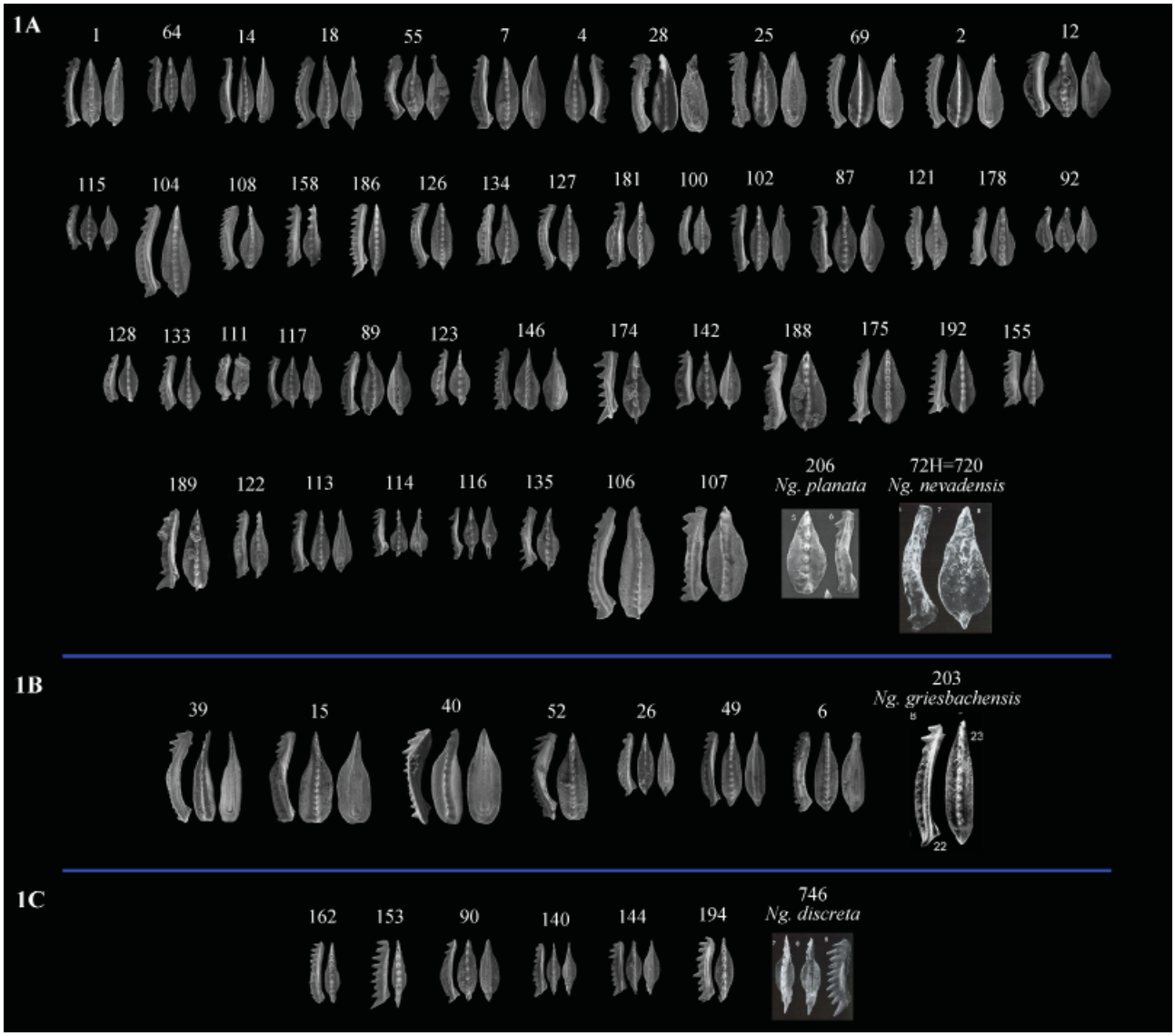

Figure 2: cluster 1 (blue on the dendrogram), including 66 individuals. Numbers above the individuals correspond to the number in figure 2.

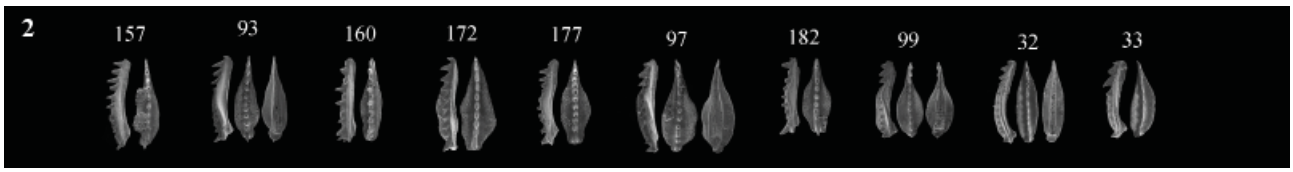

Figure 3: cluster 2 (purple on the dendrogram), including 10 individuals. Numbers above the individuals correspond to the number in figure 2.

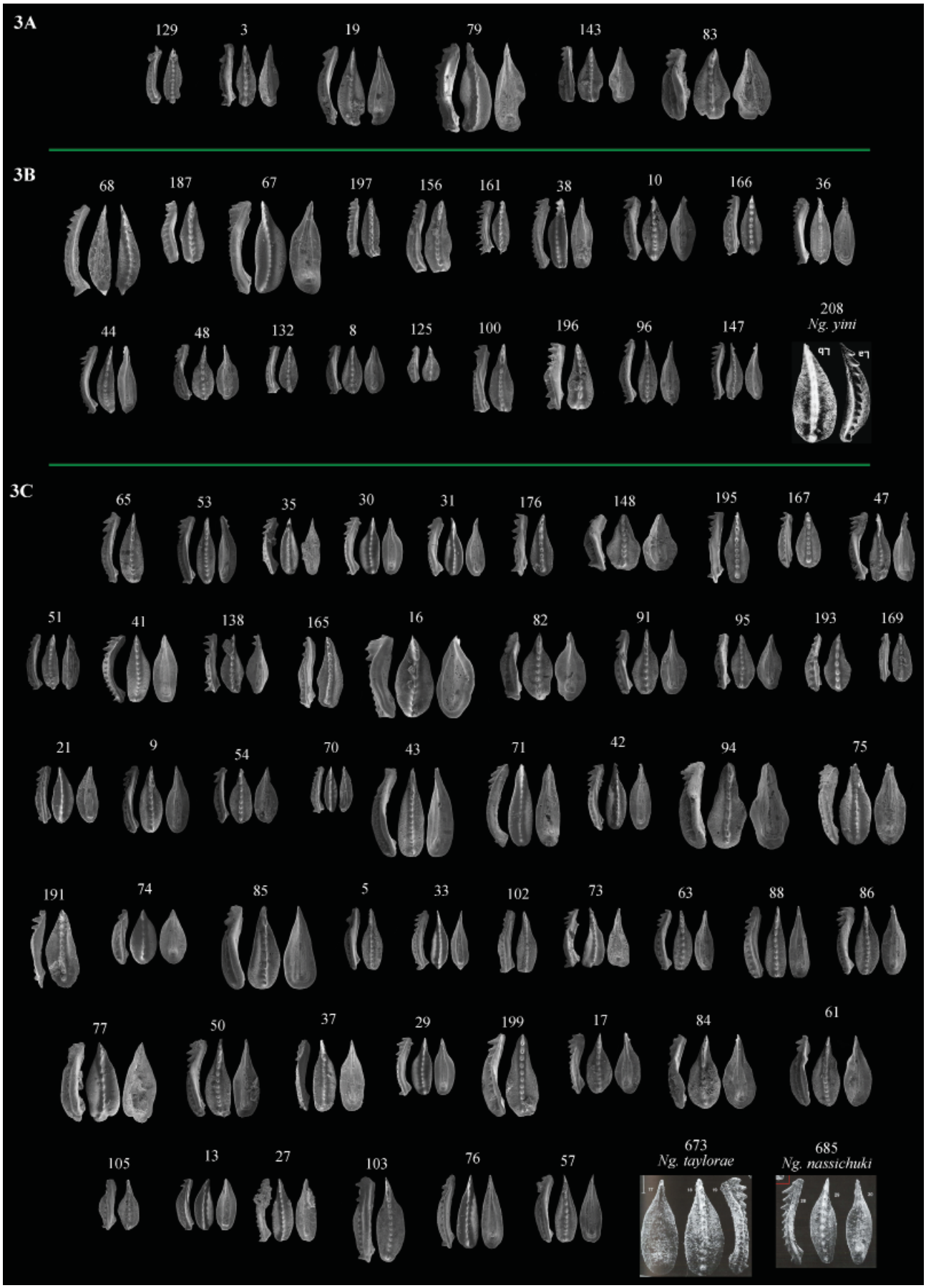

Figure 4: cluster 3 (green on the dendrogram), including 81 individuals. Numbers above the individuals correspond to the number in figure 2.

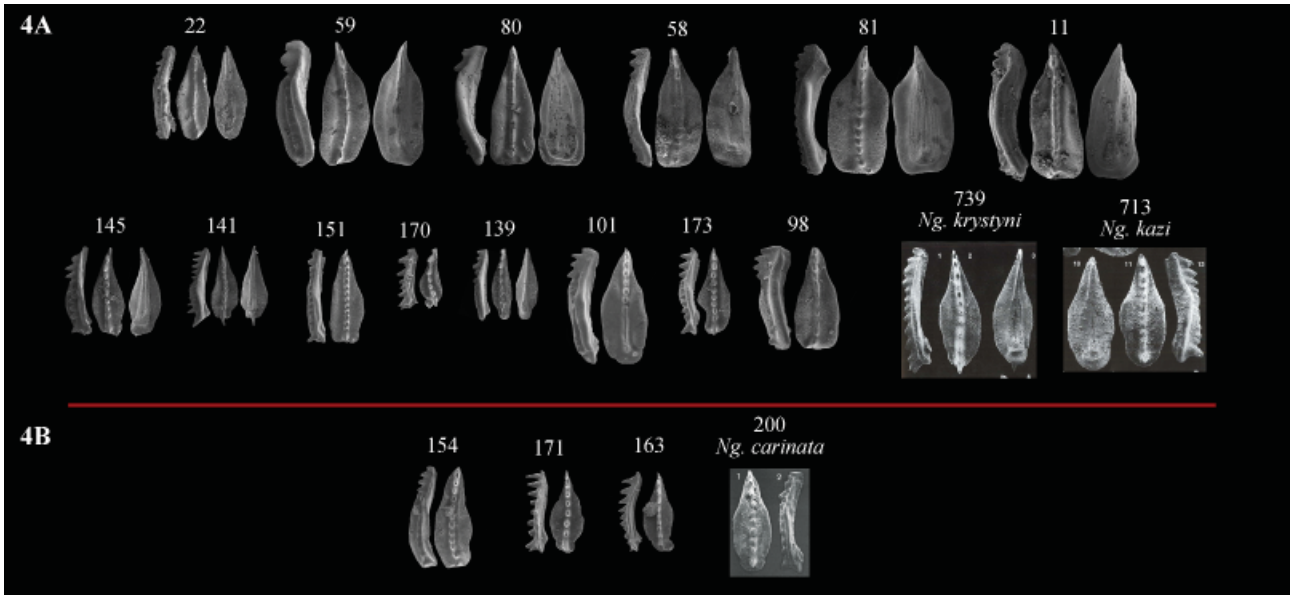

Figure 5: cluster 4 (red on the dendrogram), including 19 individuals. Numbers above the individuals correspond to the number in figure 2.

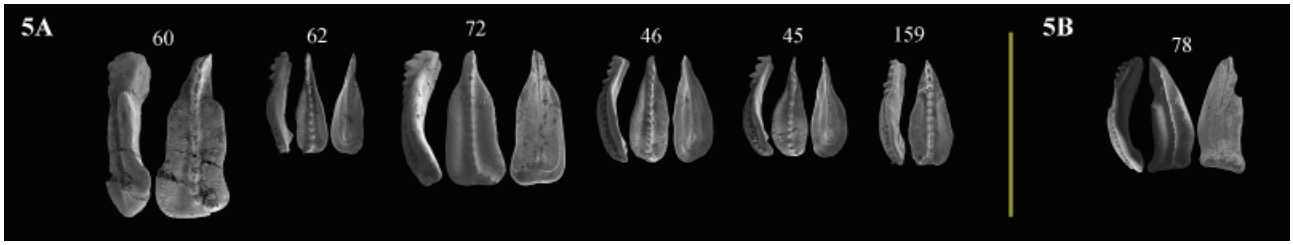

Figure 6: cluster 5 (yellow on the dendrogram), including 7 individuals. Numbers above the individuals correspond to the number in figure 2.

Appendix A: Matrix of the 215 individuals included in the multivariate analyses. The first column represents each variable as described in Table 2. The top row represents each individual as numbered in Figures 2-6. The number ranging from 0 to 2 in the matrix represent the categories (also detailed in Table 2). We coded as non-applicable, "na", when the variable could not be categorized (e.g. poorly preserved elements or insufficient illustrations). These elements were automatically discarded by the MCA.

	1	2	3	4	5	6	7	8	9	10	11	12	13	14	15	16	17	18	19	20	21	22	23	24	25	26	27	28	29	30	31	32	33	34
V1	0	0	2	0	0	0	0	0	0	0	1	0	0	0	0	0	0	0	2	0	0	0	0	0	0	0	0	0	0	0	0	0	0	0
V2	0	0	0	0	0	0	0	0	0	0	0	0	0	0	0	0	0	0	0	0	0	0	0	0	0	0	0	0	0	0	0	1	0	1
V3	0	1	0	0	0	0	0	1	1	1	1	1	0	0	1	1	1	0	1	1	1	1	1	1	0	0	0	0	0	1	0	0	0	0
V4	2	2	2	2	1	0	2	2	2	1	0	1	2	2	0	2	2	2	2	1	1	1	2	2	2	0	2	2	2	1	2	2	2	2
V5	0	0	2	0	3	0	0	1	2	1	3	0	2	0	1	2	3	0	2	2	2	0	2	na	0	0	0	0	0	2	2	2	0	0
V6	0	0	0	1	0	0	0	0	1	1	1	0	0	2	2	0	2	2	0	0	0	0	0	0	2	0	0	1	2	2	2	0	2	1
V7	0	0	0	0	0	0	0	0	0	0	0	0	0	0	0	0	0	0	0	0	0	0	0	0	0	0	0	0	0	0	0	0	0	0
V8	0	1	1	1	0	0	1	0	0	0	0	0	1	1	0	1	1	1	1	0	1	1	0	0	0	0	1	1	1	1	1	0	1	1
V9	0	0	0	0	0	0	0	0	0	0	0	0	0	0	0	0	0	0	0	1	0	0	0	0	1	0	0	1	0	0	0	0	0	0
V10	0	0	0	0	0	0	0	0	0	0	1	0	0	0	0	0	0	0	0	0	0	0	0	0	0	0	0	0	0	0	0	0	0	0
V11	0	1	0	0	1	1	1	0	1	1	2	1	1	0	1	2	0	1	1	na	1	2	0	0	0	0	1	0	0	0	0	1	1	0
V12	1	1	0	1	0	1	1	0	0	0	0	0	0	1	0	0	0	1	0	0	0	0	0	0	1	1	0	1	0	0	0	0	0	0
V13	0	1	1	1	0	1	1	1	0	1	0	0	0	1	0	0	0	1	0	0	0	0	0	0	0	1	0	1	0	1	1	1	0	1
V14	1	1	1	1	1	1	1	1	1	1	0	1	1	1	1	0	1	1	1	na	1	1	1	0	1	1	1	1	1	1	1	1	1	1
V15	0	1	0	0	0	0	0	0	0	0	0	0	0	0	0	1	0	0	0	0	1	0	0	0	1	0	0	0	0	0	0	0	0	0
V16	1	0	1	1	0	1	1	0	1	1	0	1	0	1	1	0	1	1	1	1	1	0	na	na	0	0	0	0	0	1	1	1	0	1
V17	1	0	1	1	0	1	1	1	1	1	1	1	1	1	1	0	0	1	1	1	0	0	0	0	1	1	1	1	0	1	1	1	1	1
V18	2	2	0	0	1	2	2	0	0	2	0	2	0	2	1	0	0	2	0	1	0	0	0	0	2	2	0	2	0	0	0	0	1	2
V19	1	1	0	1	1	1	1	1	1	1	1	1	1	0	1	1	1	1	1	1	0	0	0	0	0	1	1	1	0	1	1	1	1	1

	35	36	37	38	39	40	41	42	43	44	45	46	47	48	49	50	51	52	53	54	55	56	57	58	59	60	61	62	63	64	65	66	67	68
V1	0	0	0	0	0	0	0	0	0	0	0	0	0	0	0	0	0	0	0	0	0	0	0	0	0	1	0	0	0	0	0	0	0	0
V2	0	0	0	0	0	0	0	0	0	0	0	0	0	0	0	0	0	0	0	0	0	0	0	0	0	0	0	0	0	0	0	0	0	0
V3	0	0	0	0	0	0	1	0	0	0	1	1	0	1	0	0	0	1	0	1	0	na	0	1	1	1	1	0	0	0	0	na	0	0
V4	2	2	1	1	0	0	1	2	2	2	2	2	2	2	0	1	1	0	2	2	2	0	2	0	2	2	2	2	2	2	2	2	1	2
V5	2	1	3	1	2	3	3	3	3	1	3	3	3	1	0	3	0	3	2	2	0	2	2	3	0	3	2	3	2	0	2	3	1	0
V6	1	1	2	1	2	0	0	0	1	2	2	0	2	2	2	2	0	0	1	1	2	na	1	1	1	0	2	2	2	0	1	na	2	0
V7	0	0	0	0	0	0	0	0	0	0	0	0	0	0	0	0	0	0	0	0	0	0	0	0	0	0	0	0	0	0	0	0	0	0
V8	0	0	1	0	1	0	1	0	0	1	1	0	1	1	0	1	1	0	0	0	1	1	1	1	1	2	1	2	1	0	1	na	2	2
V9	0	0	0	0	0	0	0	0	0	0	0	0	1	0	0	1	0	0	0	0	0	0	0	1	1	0	0	0	0	0	0	0	1	0
V10	0	0	0	0	0	0	0	0	0	0	1	1	0	0	0	0	0	0	0	0	0	0	0	0	0	1	0	1	0	0	0	0	0	0
V11	0	1	1	0	1	0	0	1	1	0	0	1	0	0	0	0	0	1	0	1	1	2	0	2	2	2	1	0	0	0	0	na	1	1
V12	0	1	0	0	0	0	0	0	0	0	0	0	0	0	1	0	0	0	0	0	1	0	0	0	0	0	0	0	0	1	0	0	0	1
V13	1	1	0	0	0	1	1	0	1	1	0	0	1	1	1	0	1	1	1	1	1	0	1	0	0	0	0	0	0	1	1	0	0	1
V14	1	1	1	1	1	0	1	1	1	1	1	1	1	1	1	1	1	1	1	1	1	1	1	1	1	1	1	1	1	1	1	1	1	1
V15	0	0	0	0	0	0	0	0	0	0	0	0	0	0	0	0	0	0	0	0	0	0	0	0	0	0	0	0	0	0	0	0	0	0
V16	1	1	0	0	0	0	0	1	1	1	0	0	1	0	1	0	1	1	1	0	1	0	1	0	0	0	0	0	0	1	1	0	0	1
V17	0	1	0	0	1	1	1	1	1	1	0	0	1	1	1	0	1	1	1	0	1	0	1	0	1	0	0	0	0	1	1	0	0	1
V18	0	0	0	0	1	1	1	0	0	2	0	1	1	0	2	0	1	0	0	0	2	0	0	1	1	1	0	1	1	2	0	0	0	2
V19	1	1	1	1	1	1	1	1	1	1	1	1	1	1	1	1	1	1	1	0	1	na	1	1	1	0	1	1	1	0	1	1	1	1

	69	70	71	72	73	74	75	76	77	78	79	80	81	82	83	84	85	86	87	88	89	90	91	92	93	94	95	96	97	98	99	100	101	102
V1	0	0	0	1	0	0	0	0	0	1	2	1	1	1	2	0	0	0	0	0	0	0	0	1	1	1	0	0	0	0	0	0	0	0
V2	0	0	0	0	0	0	0	0	0	0	0	0	0	0	0	0	0	0	0	0	0	0	0	0	1	0	0	0	1	0	1	0	0	0
V3	0	0	0	1	0	1	1	0	1	1	0	1	1	1	1	1	0	0	1	0	0	0	1	1	0	1	1	0	1	1	1	1	1	0
V4	2	2	2	2	2	2	1	2	2	2	1	0	0	1	2	2	2	2	1	2	2	2	2	2	2	2	2	2	1	2	2	2	1	2
V5	0	2	3	3	0	3	3	2	3	3	3	3	3	2	3	3	3	3	0	2	0	0	2	0	1	3	2	1	1	2	0	1	3	0
V6	2	0	0	1	2	0	0	1	0	0	2	1	1	1	0	2	1	2	2	1	2	0	2	0	2	0	0	2	2	0	2	1	0	2
V7	0	0	0	0	0	0	0	0	0	0	0	0	0	0	0	0	0	0	0	0	0	1	0	0	0	0	0	0	0	0	0	0	0	0
V8	1	0	0	1	1	0	0	1	1	2	1	0	1	0	1	1	0	1	0	1	1	0	0	1	0	0	1	1	1	1	0	1	0	1
V9	0	0	0	0	0	0	0	0	1	0	0	1	1	0	0	0	0	1	0	0	0	0	0	0	0	0	0	0	0	1	0	0	1	0
V10	0	0	0	1	0	0	0	0	0	2	0	0	0	0	0	0	0	0	0	0	0	0	0	0	0	0	0	0	0	0	0	0	0	0
V11	1	1	1	1	1	1	1	0	1	1	2	2	0	1	2	0	1	1	0	1	0	0	0	0	0	1	0	0	0	2	0	1	2	1
V12	1	0	0	0	0	0	0	0	0	0	0	0	0	0	0	0	0	0	0	0	0	1	0	1	0	0	0	1	0	0	0	0	0	0
V13	0	1	1	0	1	0	0	1	0	0	0	0	0	0	0	0	0	0	1	0	0	0	0	0	0	0	1	0	1	0	0	0	0	1
V14	1	1	1	1	1	1	1	1	1	1	1	1	1	0	1	1	1	1	1	1	0	1	1	1	1	1	1	0	1	1	0	0	1	1
V15	1	0	0	0	0	0	0	0	0	0	1	0	0	0	0	0	0	0	0	0	0	0	0	0	1	0	0	0	0	0	0	0	0	0
V16	0	1	1	0	0	0	0	1	0	0	0	0	0	0	0	0	0	0	1	0	1	1	0	0	0	0	0	1	0	0	1	0	0	0
V17	0	1	1	0	1	0	0	1	0	0	0	0	0	0	0	0	0	0	1	0	1	1	0	1	1	1	1	1	1	1	1	1	0	1
V18	2	0	0	1	1	0	0	0	0	1	0	1	1	0	0	0	0	0	2	1	2	2	0	2	0	0	0	0	0	1	2	0	1	1
V19	1	1	1	1	1	1	1	1	1	1	1	1	1	1	1	1	1	1	0	0	1	1	0	0	0	0	0	1	0	0	1	0	0	0

	103	104	105	106	107	108	109	110	111	112	113	114	115	116	117	118	119	120	121	122	123	124	125	126	127	128	129	130	131	132	133
V1	0	0	1	0	0	0	0	0	0	0	0	0	0	0	0	0	0	0	0	0	0	0	0	0	0	0	2	0	0	0	0
V2	0	0	0	0	0	0	0	0	0	0	0	0	0	0	0	0	0	0	0	0	0	0	0	0	0	0	2	0	0	0	0
V3	0	0	1	0	1	1	na	1	1	0	0	1	0	1	1	1	0	1	1	0	1	na	1	1	0	1	0	na	na	1	1
V4	2	2	2	2	1	2	0	2	2	1	2	2	2	2	2	2	2	2	1	2	2	0	2	2	2	2	1	0	2	2	2
V5	2	0	2	0	0	0	0	0	0	0	0	0	0	0	0	0	0	na	0	0	0	2	1	0	0	0	1	na	2	1	0
V6	1	0	2	1	1	2	0	0	0	2	2	2	0	1	0	0	0	0	0	2	2	na	0	0	0	0	0	na	na	0	2
V7	0	0	0	0	0	0	0	0	0	0	0	0	0	0	0	0	0	0	0	0	1	0	0	0	0	0	0	na	0	0	0
V8	1	1	1	0	0	1	1	0	1	0	0	0	0	0	1	0	na	0	0	0	1	na	1	1	0	1	0	1	1	1	1
V9	0	0	0	0	0	0	0	0	0	0	0	0	0	0	0	0	na	0	0	0	0	0	0	0	0	0	0	0	0	0	0
V10	0	0	0	0	0	0	0	0	0	0	0	0	0	0	0	0	0	0	0	0	0	0	0	0	0	0	0	0	0	0	0
V11	0	0	0	2	2	1	0	1	0	1	0	0	0	0	0	0	0	0	0	0	0	0	0	0	1	0	0	0	2	0	0
V12	0	1	0	0	0	0	0	0	0	1	1	1	1	1	1	1	0	1	1	1	0	0	0	0	1	0	0	0	1	1	0
V13	1	1	1	0	0	1	0	0	0	0	0	0	0	0	0	0	0	0	0	0	0	0	0	0	0	0	0	0	0	0	0
V14	1	1	1	1	0	1	1	1	1	1	0	0	1	1	1	1	1	1	0	0	0	1	1	1	1	1	1	1	1	1	1
V15	0	0	0	0	1	1	0	0	0	0	1	1	0	0	0	0	0	0	0	0	0	0	0	0	0	0	0	0	0	0	1
V16	1	1	1	1	1	1	0	0	0	1	1	1	1	1	1	1	1	0	1	1	1	0	0	0	1	1	1	1	0	0	1
V17	1	1	1	1	1	1	1	1	1	1	1	1	1	1	1	na	1	0	1	1	1	na	0	1	1	1	1	1	0	1	1
V18	0	2	2	2	2	2	2	2	2	2	2	0	2	2	2	2	2	0	2	2	2	0	0	2	2	2	0	na	0	2	2
V19	1	0	1	1	1	1	1	1	1	0	1	1	1	1	1	0	0	1	0	0	0	1	0	1	1	1	1	1	1	1	0

	134	135	136	137	138	139	140	141	142	143	144	145	146	147	148	149	150	151	152	153	154	155	156	157	158	159	160	161	162	163	164
V1	0	0	0	2	1	1	0	1	0	2	0	1	0	0	0	na	0	1	0	0	1	0	1	1	0	0	1	0	0	1	0
V2	0	0	0	2	0	1	0	0	0	0	0	0	0	0	0	0	0	0	0	0	2	0	0	1	0	0	1	0	0	2	0
V3	1	1	na	0	1	0	0	0	0	1	0	1	0	1	1	na	1	1	0	0	0	1	1	0	0	1	0	0	0	1	1
V4	2	2	1	1	2	2	1	2	2	1	1	2	2	2	1	0	2	2	1	2	2	2	2	2	2	2	2	1	2	1	2
V5	0	0	1	3	3	2	0	0	0	0	1	3	2	1	3	0	1	2	0	0	3	1	2	1	0	3	3	1	0	3	na
V6	0	1	0	0	2	1	2	1	1	0	2	1	2	2	0	0	1	0	2	2	2	2	0	2	2	0	2	1	2	1	1
V7	0	0	0	0	0	1	0	0	0	0	1	0	0	0	0	0	0	0	1	0	0	0	0	0	0	0	0	0	1	0	0
V8	1	0	1	0	0	0	1	0	0	1	0	0	1	1	1	1	0	1	1	0	0	0	2	1	0	0	0	0	0	0	0
V9	0	0	0	1	0	0	1	1	0	0	1	0	0	0	0	0	0	0	0	1	0	1	0	0	0	1	0	0	0	0	0
V10	0	0	0	na	0	0	0	0	0	1	0	0	0	0	0	0	0	0	0	0	0	0	1	0	2	0	0	0	0	0	0
V11	0	0	0	na	0	0	0	0	0	0	0	0	0	0	0	0	0	0	0	0	0	0	1	0	0	2	0	0	0	0	0
V12	0	1	0	0	0	0	1	1	0	0	1	0	0	0	0	0	1	0	1	1	0	1	0	1	0	0	0	1	0	0	1
V13	0	0	1	0	0	0	0	0	0	0	0	0	0	0	0	0	0	0	0	0	0	0	0	1	0	0	0	1	0	0	0
V14	1	0	1	na	0	na	1	1	1	1	1	1	1	1	1	1	na	1	1	1	1	1	1	1	1	0	1	0	1	1	0
V15	0	0	0	0	0	0	0	0	0	0	0	0	0	0	0	0	0	0	0	0	0	0	0	0	0	0	0	0	0	0	0
V16	1	1	0	0	1	1	1	1	1	1	1	1	1	1	1	0	1	1	0	0	1	1	0	0	0	0	0	0	0	1	1
V17	1	1	na	na	1	na	1	1	1	0	1	1	1	1	1	0	0	1	na	1	1	1	0	0	1	0	1	0	1	1	1
V18	2	2	2	0	0	0	2	1	0	0	2	0	0	0	0	0	0	1	2	2	0	2	1	0	2	1	0	0	2	0	2
V19	0	1	1	0	0	0	0	0	0	0	0	0	0	1	0	1	0	0	0	0	0	0	1	0	0	0	0	0	0	0	0

	165	166	167	168	169	170	171	172	173	174	175	176	177	178	179	180	181	182	183	184	185	186	187	188	189	190	191	192	193	194	195
V1	1	0	0	na	0	1	1	1	2	0	0	0	1	0	0	na	0	0	na	1	1	0	0	1	1	0	0	0	0	0	0
V2	0	0	0	0	0	0	2	1	0	0	0	0	1	0	0	2	0	1	0	0	0	0	1	0	0	0	0	0	0	0	0
V3	1	0	1	0	0	1	1	0	0	1	1	1	1	1	na	0	1	na	0	0	0	1	1	0	0	1	1	0	0	0	0
V4	2	2	2	1	2	2	2	1	2	2	2	1	2	2	1	2	2	1	0	1	2	1	2	2	2	1	2	2	2	1	1
V5	2	1	3	0	2	0	3	2	2	2	3	2	0	3	2	0	1	1	3	2	0	0	0	1	2	3	1	2	0	3	3
V6	0	1	0	1	1	2	1	1	0	0	1	2	0	na	na	0	2	2	1	2	0	2	0	0	0	0	0	0	2	0	0
V7	0	0	0	0	0	0	0	0	0	0	0	0	0	0	na	0	0	0	1	0	0	0	0	0	0	0	0	0	0	1	0
V8	1	1	0	1	1	1	1	0	0	0	0	0	0	0	na	1	0	0	0	0	0	1	2	0	0	1	0	0	1	0	0
V9	0	0	0	0	0	1	0	0	0	0	0	0	0	0	0	na	0	1	0	0	0	0	0	0	0	0	0	0	0	0	0
V10	0	0	0	0	0	0	0	0	0	0	0	0	0	0	0	na	0	0	0	0	0	0	0	0	0	0	0	0	0	0	0
V11	1	0	0	0	0	0	0	0	0	0	0	0	0	0	0	1	0	0	0	0	0	0	0	1	0	0	0	0	0	0	0
V12	0	0	0	0	0	0	0	0	0	0	0	0	0	0	0	0	0	0	0	0	0	0	0	0	0	0	0	0	0	0	0
V13	0	0	0	0	0	0	0	0	0	0	0	0	0	0	0	0	0	0	0	0	0	0	0	0	0	0	0	0	0	0	0
V14	1	0	1	na	0	na	1	1	1	1	1	1	1	1	1	1	na	1	1	1	1	1	1	1	1	0	1	0	1	1	0
V15	0	0	0	0	0	0	0	0	0	0	0	0	0	0	0	0	0	0	0	0	0	0	0	0	0	0	0	0	0	0	0
V16	1	1	0	0	1	1	1	1	1	1	1	1	1	1	1	0	1	1	0	0	1	1	0	0	0	0	0	0	0	1	1
V17	1	1	na	na	1	na	1	1	1	0	1	1	1	1	1	0	0	1	na	1	1	1	0	0	1	0	1	0	1	1	1
V18	0	0	2	0	2	0	0	0	0	0	0	0	0	0	0	2	0	0	2	0	2	0	0	0	0	0	0	0	0	0	0
V19	0	0	0	1	0	0	0	0	0	0	0	0	0	0	na	0	0	0	0	0	0	1	0	0	0	0	0	0	0	0	0

	196	197	198	199
V1	0	1	1	0
V2	0	0	0	0
V3	0	1	0	1
V4	2	2	2	2
V5	1	1	na	3
V6	2	0	0	0
V7	0	0	0	0
V8	1	2	1	1
V9	0	0	1	0
V10	0	0	0	0
V11	0	1	na	0
V12	1	0	0	0
V13	0	0	0	1
V14	1	1	na	1
V15	1	0	1	0
V16	1	0	0	0
V17	1	1	na	0
V18	2	0	0	0
V19	1	0	0	1

Holotypes	200	201	202	746	203	713	739	204	685	72H	205	206	673	207	208	209	196	197	198	199
Ng. carinata	1	na	na	0	1	0	1	na	1	0	1	0	0	1	0	0	0	1	0	0
Ng. changxingensis	na	0	1	0	0	1	0	0	0	0	0	0	0	0	0	0	0	0	0	0
Ng. deflecta	na	1	0	2	2	1	2	0	0	0	0	0	0	0	0	0	0	0	0	0
Ng. discreta	0	2	0	1	1	0	1	0	0	0	0	0	0	0	0	0	0	0	0	0
Ng. griesbachensis	1	2	0	1	1	0	1	0	0	0	0	0	0	0	0	0	0	0	0	0
Ng. kazi	0	0	0	0	1	1	0	0	0	0	0	0	0	0	0	0	0	0	0	0
Ng. krystyni	0	1	0	0	0	0	1	0	0	0	0	0	0	0	0	0	0	0	0	0
Ng. meishanensis	na	2	0	0	0	0	1	0	0	0	0	0	0	0	0	0	0	0	0	0
Ng. nassichuki	1	0	0	0	0	0	0	0	0	0	0	0	0	0	0	0	0	0	0	0
Ng. nevadensis	1	0	1	0	0	0	0	0	0	0	0	0	0	0	0	0	0	0	0	0
Ng. orchardi	1	2	0	0	0	0	0	0	0	0	0	0	0	0	0	0	0	0	0	0
Ng. planata	0	0	0	0	0	0	0	0	0	0	0	0	0	0	0	0	0	0	0	0
Ng. taylorae	1	0	0	0	0	0	0	0	0	0	0	0	0	0	0	0	0	0	0	0
Ng. tulongensis	na	1	na	na	na	na	na	na	na	na	na	na	na	0	0	0	0	0	0	0
Ng. yini	1	0	0	0	0	0	0	0	0	0	0	0	0	0	0	0	0	0	0	0
Ng. zhejiangensis	na	0	na	na	na	na	na	na	na	na	na	na	na	na	0	0	0	0	0	0
Ng. carinata	1	0	0	0	0	0	0	0	0	0	0	0	0	0	0	0	0	0	0	0
Ng. changxingensis	0	0	1	0	1	1	0	0	0	0	0	0	0	0	0	0	0	0	0	0
Ng. deflecta	0	1	0	1	0	0	1	0	0	0	0	0	0	0	0	0	0	0	0	0
Ng. discreta	1	0	0	0	0	0	0	0	0	0	0	0	0	0	0	0	0	0	0	0

CHAPTER V

THE BIOTIC RECOVERY IN THE AFTERMATH OF THE PERMIAN-TRIASSIC BOUNDARY
NEW DATA FROM THE GRIESBACHIAN OF OMAN

Morgane Brosse, Hugo Bucher, Aymon Baud, Hans Hagdorn, Alexander Nützel, David Ware, Åsa M. Frisk and Nicolas Goudemand

Formatted for Palaeogeography, Palaeoclimatology, Palaeoecology

“The fact that we live at the bottom of a deep gravity well, on the surface of a gas covered planet going around a nuclear fireball 90 million miles away and think this to be normal is obviously some indication of how skewed our perspective tends to be.”

Douglas Adams, The Salmon of Doubt: Hitchhiking the Galaxy One Last Time

The biotic recovery in the aftermath of the Permian-Triassic Boundary: New data from The Griesbachian of Oman

Morgane Brosse[a*], Hugo Bucher[a], Aymon Baud[b], Hans Hagdorn[c], Alexander Nützel[d], David Ware[a], Åsa M. Frisk[e], Nicolas Goudemand[f, a]

[a]Paläontologisches Institut und Museum der Universität Zürich, Karl Schmid-Strasse 4, CH-8006 Zürich, Switzerland. morgane.brosse@pim.uzh.ch

[b]Geological Museum, Lausanne University, Quartier UNIL-Dorigny, Bâtiment Anthropole, CH-1015 Lausanne, Switzerland. aymon.baud@unil.ch

[c]Muschelkalkmuseum, Schlossstraße 11, 74653 Ingelfingen, Germany.

[d]Bayerische Staatssammlung für Paläontologie und Geologie Richard-Wagner-Str. 10 80333 München, Germany. a.nuetzel@lrz.uni-muenchen.de

[e]Palaeobiology, Department of Earth Sciences, Uppsala University, Villavägen 16, 753 36, Uppsala, Sweden. asa.frisk@geo.uu.se

[f]Institut de Génomique Fonctionnelle de Lyon, CNRS UMR 5242, Université de Lyon, Université Claude Bernard Lyon 1, Ecole Normale Supérieure de Lyon, 46 Allée d'Italie, Lyon, 69364, France. nicolas.goudemand@ens-lyon.fr

Abstract

A new marine fauna from the basal Early Triassic of Oman challenges anew the traditional view of devastated ecosystems in the immediate aftermath of the Permian-Triassic boundary mass extinction. The new Griesbachian Asselah boulder yielded diverse pelagic and benthic faunas, including conodonts, ammonoids, gastropods and crinoid ossicles in mass abundance. This association of Permian survivors with Triassic taxa is hardly reconcilable with previous interpretation which saw comparably diverse assemblages as ecological refugium. Moreover, similarities between these tropical faunas and the coeval equatorial shelly benthos from South China and the silicified assemblages from the Boreal realm indicate that marine communities were (1) not affected by a delayed recovery and (2) the recovery was synchronous across the whole range of latitudes. Furthermore, the amount of species inherited from the Permian suggests that the Griesbachian was not a time of devastated ecosystems, but a time of transient diversity preceding the Dienerian minimum. Such unusually diverse Griesbachian assemblages also suggest that the previous view of a devastated Griesbachian marine fauna resulted from a preservation bias.

Keywords

Permian-Triassic boundary, Griesbachian, Oman, biotic recovery, crinoidal limestone, Permian holdovers.

1. Introduction

Following the Permian-Triassic boundary mass extinction (PTBME), a delayed biotic recovery extending throughout the entire Early Triassic (Griesbachian, Dienerian, Smithian and Spathian, in ascending order) through persistence of harsh environmental conditions (e.g. Erwin, 2001) represents the traditional view. Two causes are routinely called upon for this apparently slow recovery. The first cause refers to an oxygen minimum zone (OMZ) that impinged on continental shelves. Early Triassic expanded OMZ are usually interpreted as the result of global transgressions (e.g. Hallam, 1991; Isozaki, 1997). The second cause refers to a generalized greenhouse climate that supposedly peaked during the Griesbachian and the late Smithian (Sun et al., 2012). The best candidates for causing the delayed biotic recovery to extend over the entire Early Triassic are a global transgression (Hallam, 1991; Isozaki, 1997), a greenhouse climate leading to 'lethally hot' temperatures during the Griesbachian (Sun et al., 2012), or a combination of both (Song et al., 2014).

However, a revision of the age calibration of the composite oxygen isotope curve of Sun et al. (2012) by Goudemand et al. (2013) demonstrates that there is no thermal maximum during the Griesbachian and that the late Smithian thermal maximum of Sun et al. (2012) falls within the Spathian. Moreover, a second oxygen isotope record from a single section benefitting from an optimally resolved paleontological age control by Romano et al. (2013) revealed marked differences in the timing and amplitude of temperature changes in comparison to that of Sun et al. (2012). This second record confirmed the absence of any Griesbachian thermal maximum and documented that both Griesbachian and early Smithian times were significantly cooler than the Dienerian.

The diversity of Early Triassic nektonic organisms characterized by high average evolutionary rates (e.g. ammonoids, conodonts) gives strong evidence for successive recovery pulses (Brayard et al., 2006, 2009, Ware et al., 2015, Orchard et al., 2007). The Dienerian witnessed an obvious diversity low, but where the Griesbachian diversity of these nektonic clades exactly stands with respect of that of the Dienerian is still unclear. Although much less well documented than for the nekton, a different diversity pattern seems to emerge from Early Triassic benthic shelly faunas, with a first peak in the Griesbachian (Krystyn et al., 2003; Hautmann et al., 2011, 2015) and a second one in the Spathian (Neri and Posenato, 1985; Wassmer et al., 2012; Hautmann et al., 2013). However, sampling effort and selective preservation cannot be excluded to significantly interfere in these figures. Early Triassic terrestrial plants also display a sequence of extremely contrasted ecological assemblages faithfully mirroring abrupt climatic changes (Hermann et al. 2011, 2012; Hochuli et al 2016). Spore and pollen records from NE Greenland and from the Salt Range reveal a massive spore spike at the Griesbachien-Dienerian boundary, which represents a major and global shift toward a greenhouse climate (Hermann et al., 2011; Hochuli et al., 2016).

Expanded fossiliferous succession of Permian to Griesbachian age are only few and occur preferentially in the high palaeolatitude (Spörli et al., 2007; Hermann et al., 2010; Hochuli et al., 2010; Hori et al., 2011; Sanson-Barrera et al., 2015). Earlier interpretations of the ichnological record suffered from the comparative scarcity of low latitude Griesbachian records, which led to the incorrect inference of an earlier recovery in the high latitudes (Twitchett and Barras,

2004). This biased view was subsequently corrected by careful studies of the low latitude record, as summarized by Hofmann (2016). To summarize, Griesbachian times were apparently more hospitable both in sea and on land than subsequent Dienerian times. Earliest Triassic greenhouse climatic conditions were not reached prior to Dienerian times, i.e. ca. 500 ky after the PTBME.

Griesbachian marine benthic communities are classically interpreted as being devastated, low-diversity assemblages with opportunistic, cosmopolitan taxa (e.g. Erwin, 2001; Schubert and Bottjer, 1992; Rodland and Bottjer, 2001; Fraiser and Bottjer, 2009). Crinoids undergo a dramatic extinction at the PTB bottleneck (Benton & Twitchett, 2003; Paul, 1988) and do not re-appear in the fossil record until the Smithian (Schubert et al., 1992). With their less incomplete record, gastropods are also

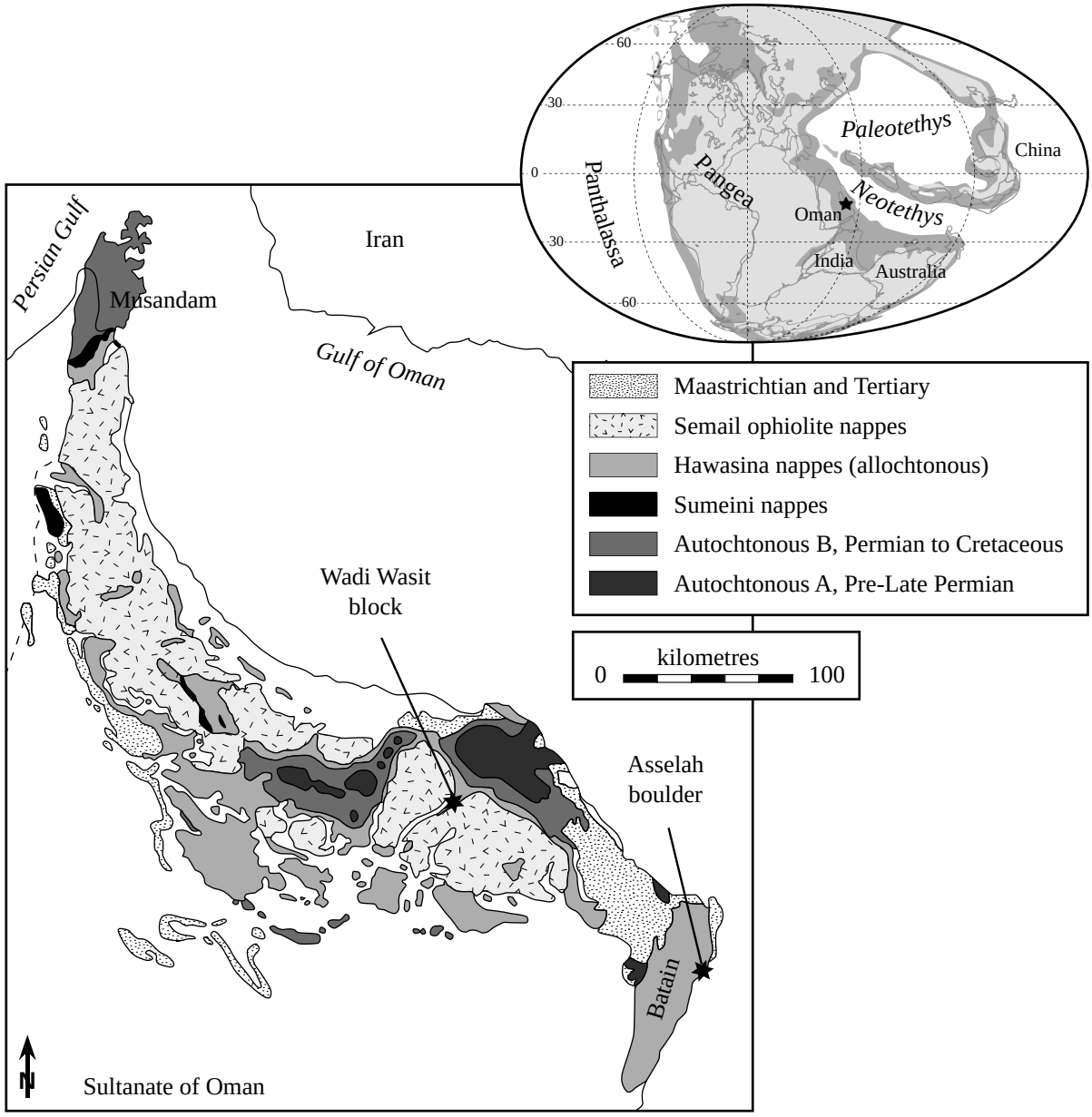

Figure 1. Palaeogeographical worldwide map of the Early Triassic (modified after PALEOMAP project www.scotese.com) and simplified map of the Oman Mountains with the location of the Oman allochthonous blocks (modified from Krystyn et al., 2003 after an original sketch of Glennie, 1973): the Wadi Wasit area in the Hawasina nappes and the Asselah locality in the Batain Plain.

perceived as suffering from a size reduction during the Griesbachian (Fraiser and Bottjer, 2004; Fraiser et al., 2005; Payne, 2005; Twitchett, 2007).

Recent studies on benthic foraminifers (Song et al., 2009a, b, 2011), trace fossils (e.g. Hofmann et al., 2011; Hofmann, 2016), bivalves (Krystyn et al., 2003; Hautmann et al., 2011, 2015) are all at marked variance with the view of a devastated Griesbachian.

Supporting the alternative model of non-devastated Griesbachian times, diverse Griesbachian and Dienerian assemblages were first documented from the Oman record at Wadi Wasit (Krystyn et al., 2003). The Wadi Wasit exotic block (Hawasina nappes) yielded a diversified community of bivalves, gastropods, crinoids, conodonts and ammonoids, indicating a well-oxygenated environment in the immediate aftermath of the PTB. Here, we describe a new exotic block of Griesbachian age from the Batain Plain (eastern Oman), which contains another well-preserved and diversified assemblage that substantially differs in its composition from that of Wadi Wasit. This new assemblage significantly adds to our understanding of the diversity and the ecology of Griesbachian marine faunas and leads to a more prudent application of the refugium concept immediately after the PTBME.

2. Geological setting

At the end of the Palaeozoic, continents were accreted into the supercontinent Pangea. Oman was located on the Gondwana margin and within the Tropical Realm. The Neotethys opened during the Permian with the northward drift of the Cimmerian block (Baud et al., 1993, 2001a, b). During the middle Jurassic, rock of Permian-Triassic age were reworked and redeposited as olistromes within Jurassic sediments (Baud et al., 2012). This allochthonous material indicates an intense tectonic phase in which former offshore seamounts were involved. In Oman, these so-called exotics are found in the Hawasina Basin (Baud et al., 2012) and the Batain Plain (Fig. 1).

Rocks of Griesbachian and Dienerian age were so far unknown from the Batain exotics. According to Hauser et al. (2001), 'records of Late Permian and lowermost Triassic conodonts are completely missing and it may be that sediments of this age were either

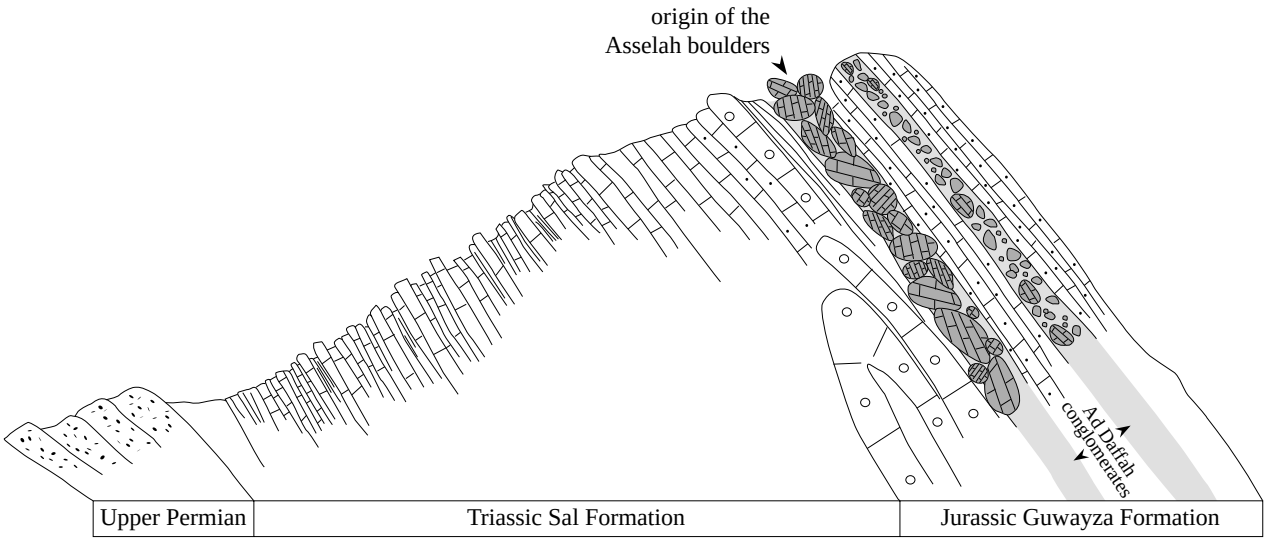

Figure 2. Cross section of the Asselah hill. Modified from Hauser, 2001.

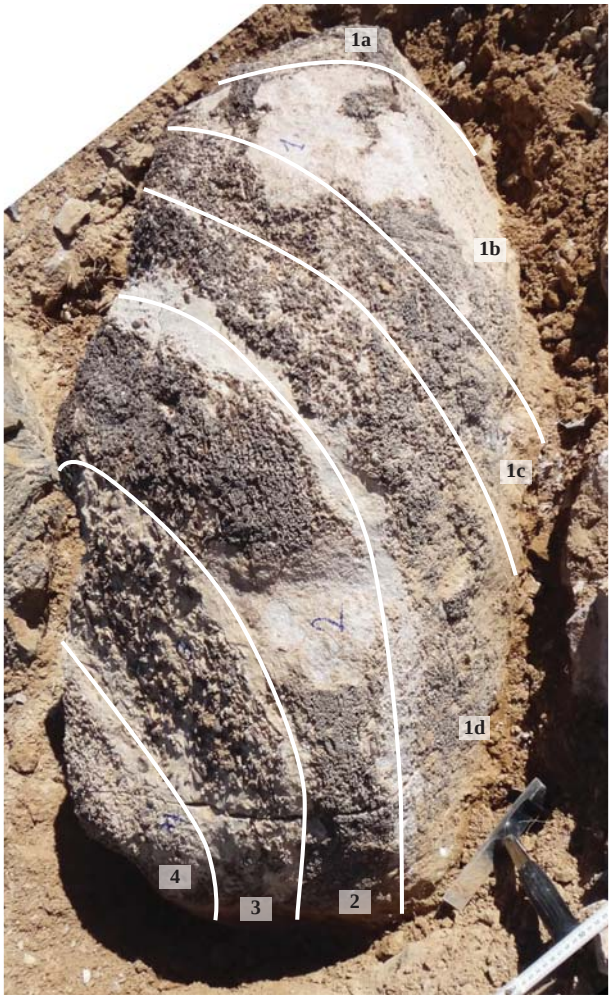

Figure 3. The Asselah outcrop on the field, with the main subdivisions.

not deposited or were removed prior to the deposition of the Sal Formation'. This 'gap' is now completely filled by our recent work.

The studied boulder is located South-West of Asselah village (21°56'36.29"N; 59°36'43.41"E). The hills ESE of Asselah expose a succession comprising Upper Permian quartzite, followed by the Triassic Sal Fm., which is in turn overlain by the Jurassic Guwayza Fm. The Guwayza Fm. is interbedded with the Ad Daffah conglomerates, which are reworked material after the deposition of the Sal Fm. (Hauser, 2001). Several boulders of Griesbachian age were discovered within the Ad Daffah conglomerate in Asselah hills (Fig. 2). These boulders show striking differences in their dominant ecological characteristics, ranging from bivalve-dominated to crinoids-dominated assemblages. This study focuses on the crinoids-dominated assemblage, herein referred to as the 'Asselah boulder'.

The Asselah boulder is ca. 1 m in stratigraphical thickness. The limestone has a light to yellow colour and the coarse crystalline texture common to all crinoidal limestone. The boulder is mainly composed of disarticulated crinoid ossicles in the millimetre size range, but also includes small ammonoids, numerous gastropods and fragmentary bivalves and brachiopods. Four units were recognized by means of abundance and type of macrofossils (Fig. 3). Bioclastic limestone of Unit 1 (65 cm thick) contains strongly cemented gastropods and ammonoids in its upper half. It also yields ostracods and echinoderm spines, microconchids, and sponge spicules. Units 2 to 4 contain more macrofossils, including many small ammonoids and numerous gastropods (Fig. 4).

3. Methods

Fossils were extracted from seven bulk samples corresponding to the 7 subunits of the boulder (Fig. 3, 4), with an average spacing of 15 cm.

Eleven samples were selected throughout the block for microfacies analyses. Petrographic classification of the limestone samples follows the Dunham (1962) classification. Weathered surface of the boulder exposes a few microgastropods that can hardly be extracted because of superficial silicification. However, macrofossils from within the ground mass can be mechanically prepared in the lab.

Crinoid ossicles and conodont elements were extracted chemically. Conodonts were retrieved from seven carbonate samples, each weighting 1 kg, that were dissolved

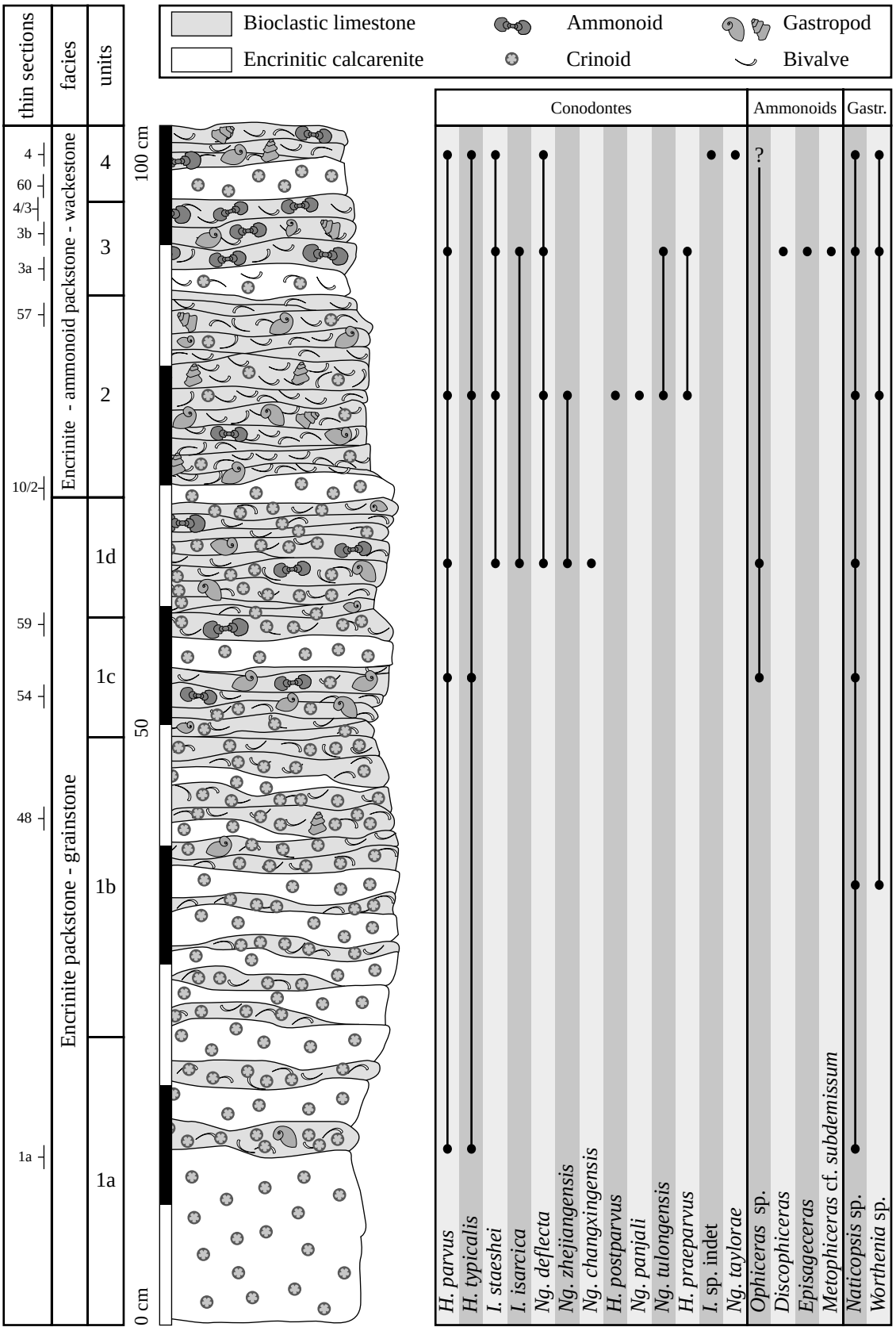

Figure 4. Columnal section of the Asselah block displaying the fossil occurrences and the thin sections.

with a ~10% buffered acetic acid solution following the procedure of Jeppsson *et al.* (1999). Insoluble residues were concentrated by heavy liquid separation (Jeppsson and Anehus 1999). Heavy fraction was sieved with a 0.075-mm mesh, handpicked and studied under a binocular microscope. Crinoid ossicles were extracted from 5 kg sample located over units 2 and 3 dissolved with ~10% buffered acetic acid. The same heavy liquid separation procedure was applied and the light fraction was analysed under a binocular microscope.

4. Results

4.1. Microfacies analyses

Three main microfacies can be recognized on the basis of hydrodynamism and types of dominating bioclasts.

Facies 1 (Fig. 5A-B). Ammonoid floatstone with crinoidal grainstone matrix.

Thin sections from Unit 1 reveal poorly sorted bioclasts dominated by crinoid ossicles and ammonoids, fragments of bivalves, brachiopods, gastropods, echinoid spines, ostracods (thin and thick shelled), microconchids and sponge spicules. The size of the bioclasts ranges up to several centimetres (ammonoids). Anisopachous fibrous calcite cement occurs around some of the bioclasts. Some convex shells are filled up with lime mud and fine bioclastic grains (see geopetal texture in Fig. 5B). The concave (or upper) part of the cavities is surrounded by fibrous calcite cement and by blocky calcite spar in the remaining empty space. Later replacement by dolomite rhombs may occur in the filled-up lime mud (Fig. 5B). This high energy, bioclastic cement-grain supported facies suggests deposition of proximal tempestites in a $CaCO_3$ a saturated water.

Facies 2 (Fig. 5C-F). Encrinitic wackestone-packstone (top of Unit 1 and lower Unit 4)

Moderately well sorted bioclasts are largely dominated by crinoid ossicles (Fig. 5D) with subordinate bivalve fragments, ostracods (thin and thick shelled; Fig. 5F), microconchids, echinoid spines and well-preserved gastropods and ammonoids. Between 20-40% of the micritic calcite is replaced by dolomite rhombs (Fig. 5E, F). Fibrous cements grow on some of the bioclasts and is associated with blocky calcite in the largest cavities. Although this facies includes more micrite than Facies 1, it still has a substantial bioclastic fraction. This moderately high energy, bioclastic facies indicates a more distal tempestite deposition, mixed with lime mud matrix.

Facies 3 (Fig. 5G). Floatstone-rudstone with micritic matrix (Unit 2, Unit 3 and top of Unit 4)

This facies displays poorly sorted bioclasts dominated by ammonoids and large fragments bivalves, with a few crinoid ossicles, microconchids, echinoid spines, gastropods and ostracods. Many bioclasts are centimetric in size. The coiling plane of ammonoids and geopetal structures are parallel, indicating absence of lateral transport of shells. Geopetal structures are composed of fibrous cement and blocky calcite, indicating at least two successive diagenetic phases of cement. Good preservation of the bioclasts and orientation of the geopetal infills both suggest minimal reworking. Between 20-40% of the micritic calcite is replaced by dolomite rhombs. This facies contains more micrite than facies 1-2 and is mud-supported. It suggests a low energy depositional setting in a deeper environment.

Facies 1 and 2 largely predominate in the boulder and suggest deposition above storm wave base. In contrast, facies 3 is represents depositional environments below storm wave base. The entire succession represents a deepening upward trend.

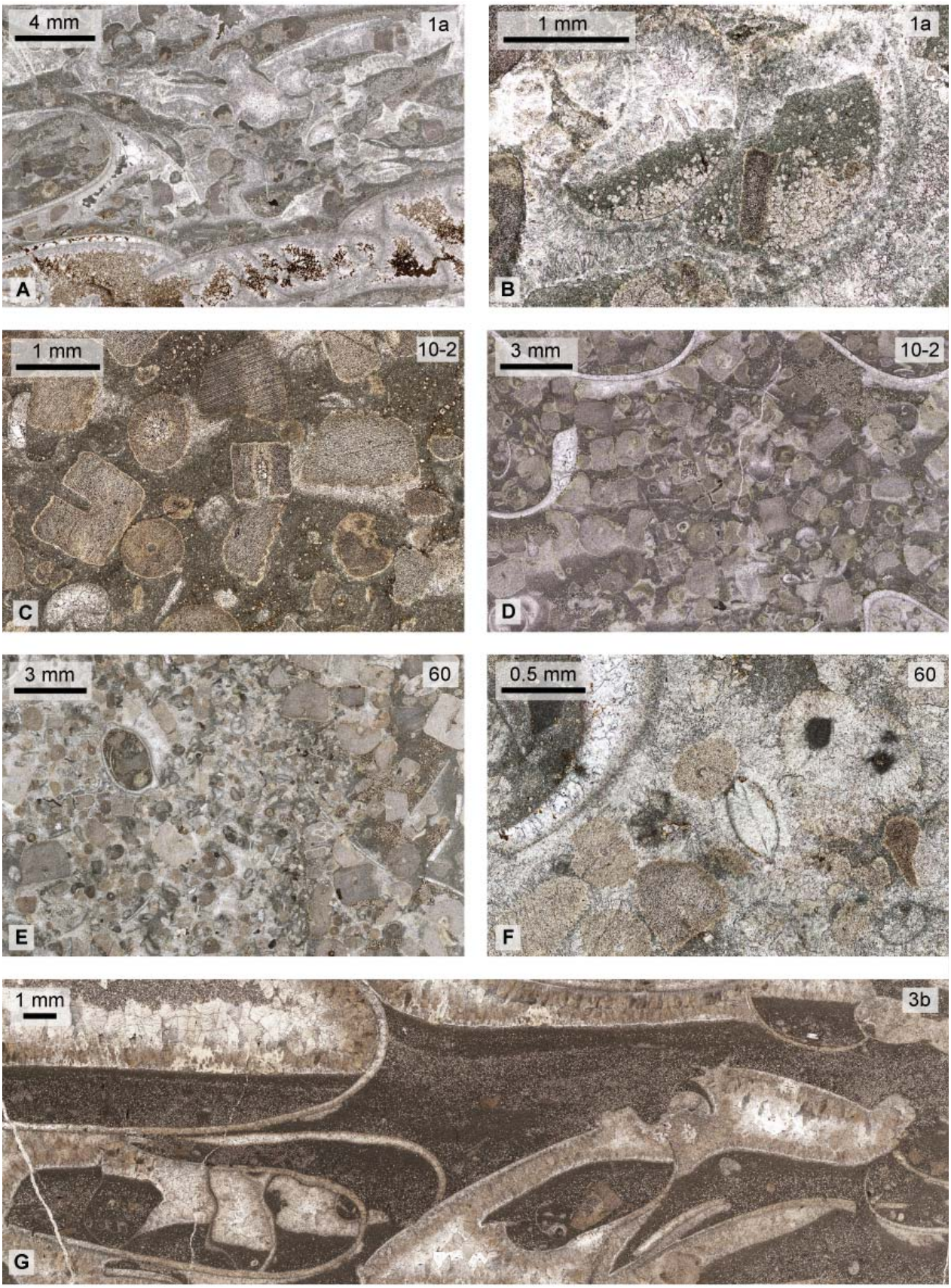

Figures 5. Photomicrographs of the three main facies corresponding to the three main depositional environments observed throughout the Asselah boulder. (A) and (B) Ammonoid floatstone with crinoidal grainstone matrix from sample 60, Unit 1. (C) - (F) Encrinitic wackestone-packstone from sample 10-2, top of Unit 1 and Unit 4. (G) Floatstone-rudstone with micritic matrix from sample 3b, Unit 3. Note the parallel orientation of the ammonoid clasts.

4.2 Conodonts

Six out of seven (sample 1b is barren) samples yielded a grand total of 158 P_1 elements, many of which are fragmentary. The CAI is 1-2. The conodont elements are more frequent in the upper part of the boulder (units 2-4), amounting to more than 80% of the recovered specimens. We identified 11 species belonging to three genera *Hindeodus*, *Isarcicella* and *Neogondolella* (Fig. 6-11). About half of the species are Permian holdovers (e.g. *Hindeodus typicalis*, *Hindeodus praeparvus*, *Neogondolella changxingensis*, *Neogondolella zhejiangensis*). However, occurrence of *Hindeodus parvus* (the index fossil for the base of the Triassic; Yin et al., 1996), *Hindeodus postparvus* and diverse *Isarcicella* species clearly indicates a lower Griesbachian age for the entire Asselah boulder. The higher abundance of conodonts towards the top of the boulder together with the occurrence of more *Neogondolella* (a genus more abundant in deeper water environments during the Griesbachian; Joachimsky et al., 2012) corroborates the trend documented from the facies analyses (Fig. 4).

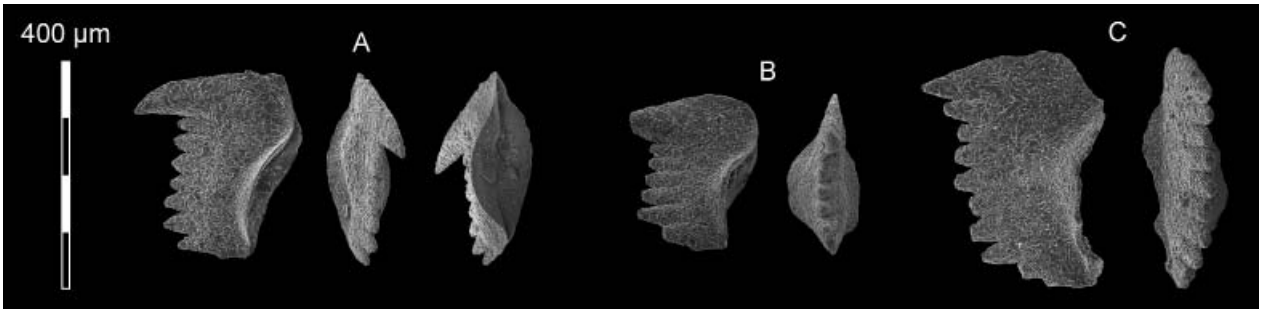

Figure 6: P_1 conodont elements from Unit A1. A, B, *Hindeodus parvus* Kozur and Pjatakova 1976; A, Unit A1-A, PIMUZ XXXXX; B, Unit A1-C PIMUZ XXXXX. C, *Hindeodus typicalis* Sweet 1970, Unit A1-C, PIMUZ XXXXX.

Figure 7: P_1 conodont elements from Unit A1-D. A, *Hindeodus parvus* Kozur and Pjatakova 1976, PIMUZ XXXXX. B, *Isarcicella staeschei* Dai and Zhang 1989, PIMUZ XXXXX. C, *Isarcicella isarcica* Huckriede 1985, PIMUZ XXXXX. D-E, *Neogondolella zhejiangensis* Mei 1996; D, PIMUZ XXXXX; E, PIMUZ XXXXX. G, *Neogondolella changxingensis* Wang and Wang 1981, PIMUZ XXXXX. F, H, *Neogondolella* ?*deflecta* Wang and Wang 1981; F, PIMUZ XXXXX, H, PIMUZ XXXXX.

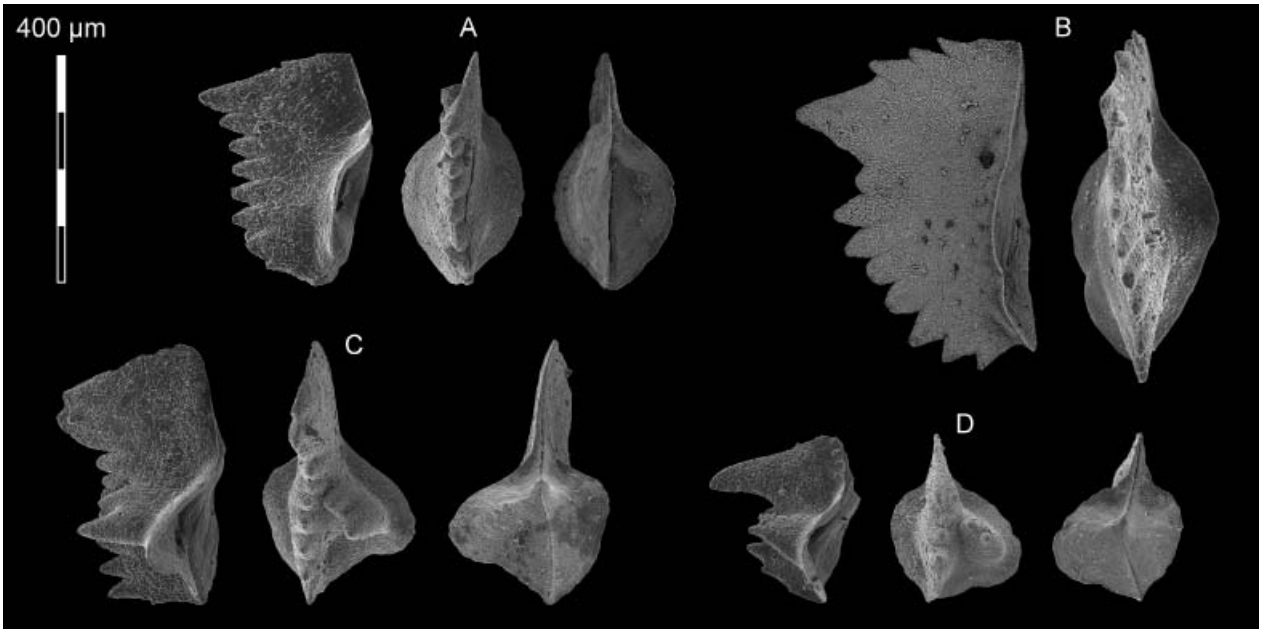

Figure 8: P_1 conodont elements from Unit A2. A, *Hindeodus praeparvus* Kozur 1996, PIMUZ XXXXX. B, *Hindeodus postparvus* Kozur 1989, PIMUZ XXXXX. C, D, *Isarcicella staeschei* Dai and Zhang 1989; C, PIMUZ XXXXX; D, PIMUZ XXXXX.

Figure 9: P_1 conodont elements from Unit A2. A-C, *Neogondolella ?deflecta* Wang and Wang 1981; A, PIMUZ XXXXX; B, PIMUZ XXXXX; C, PIMUZ XXXXX. D, *Neogondolella tulongensis* Tian 1982, PIMUZ XXXXX. E, *Neogondolella panjali* Brosse and Goudemand 2016, PIMUZ XXXXX. F, *Neogondolella zhejiangensis* Mei 1996, PIMUZ XXXXX.

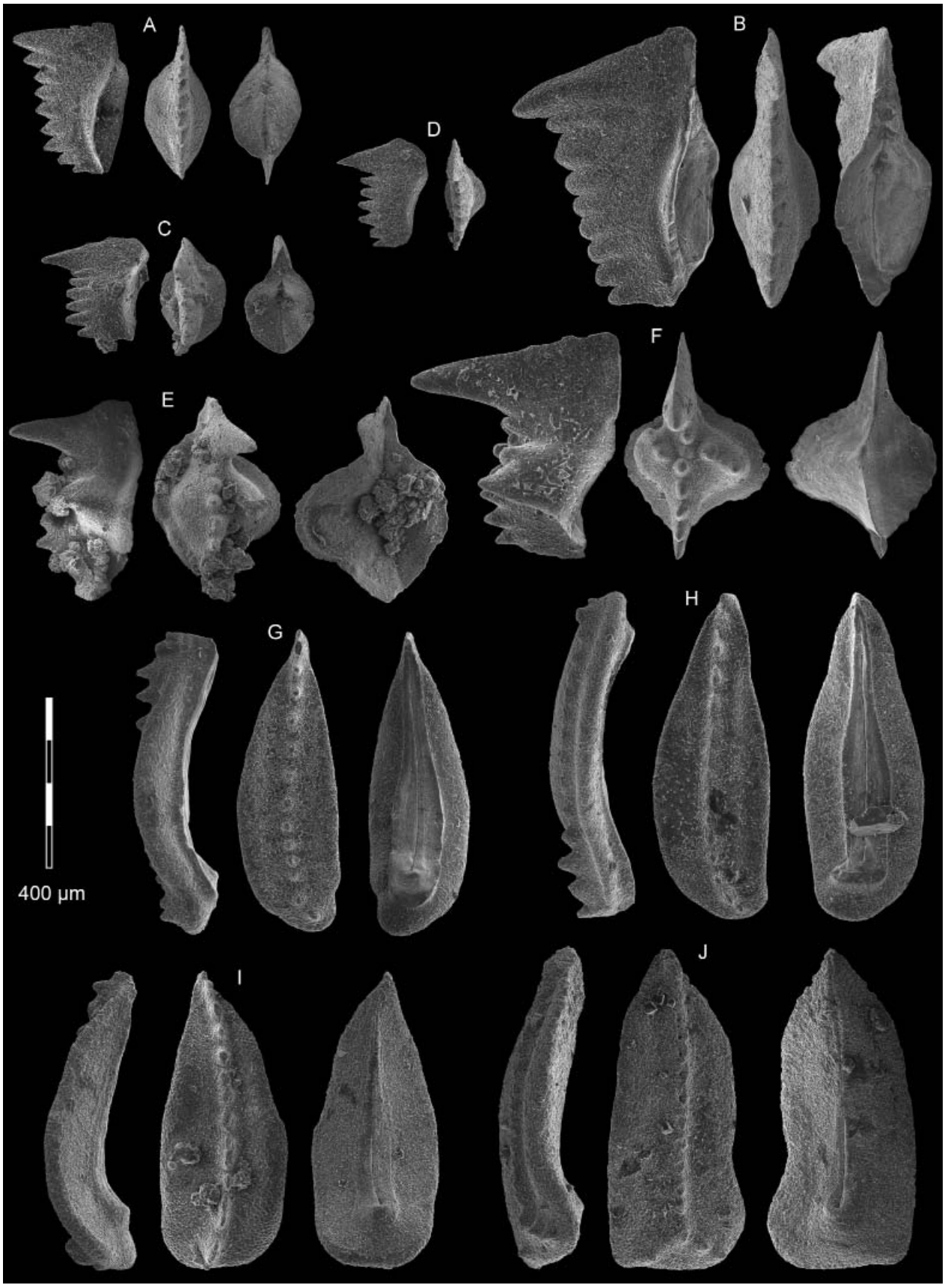

Figure 10: P_1 conodont elements from Unit A3. A, B, *Hindeodus typicalis* Sweet 1970; A, PIMUZ XXXXX; B, PIMUZ XXXXX. C, D, *Hindeodus parvus* Kozur and Pjatakova 1976; C, PIMUZ XXXXX; D, PIMUZ XXXXX. E, *Isarcicella staeschei* Dai and Zhang 1989, PIMUZ XXXXX. F, *Isarcicella isarcica* Huckriede 1985, PIMUZ XXXXX. G-I, *Neogondolella* ?*deflecta* Wang and Wang 1981; G, PIMUZ XXXXX; H, PIMUZ XXXXX; I, PIMUZ XXXXX. J, *Neogondolella tulongensis* Tian 1982, PIMUZ XXXXX.

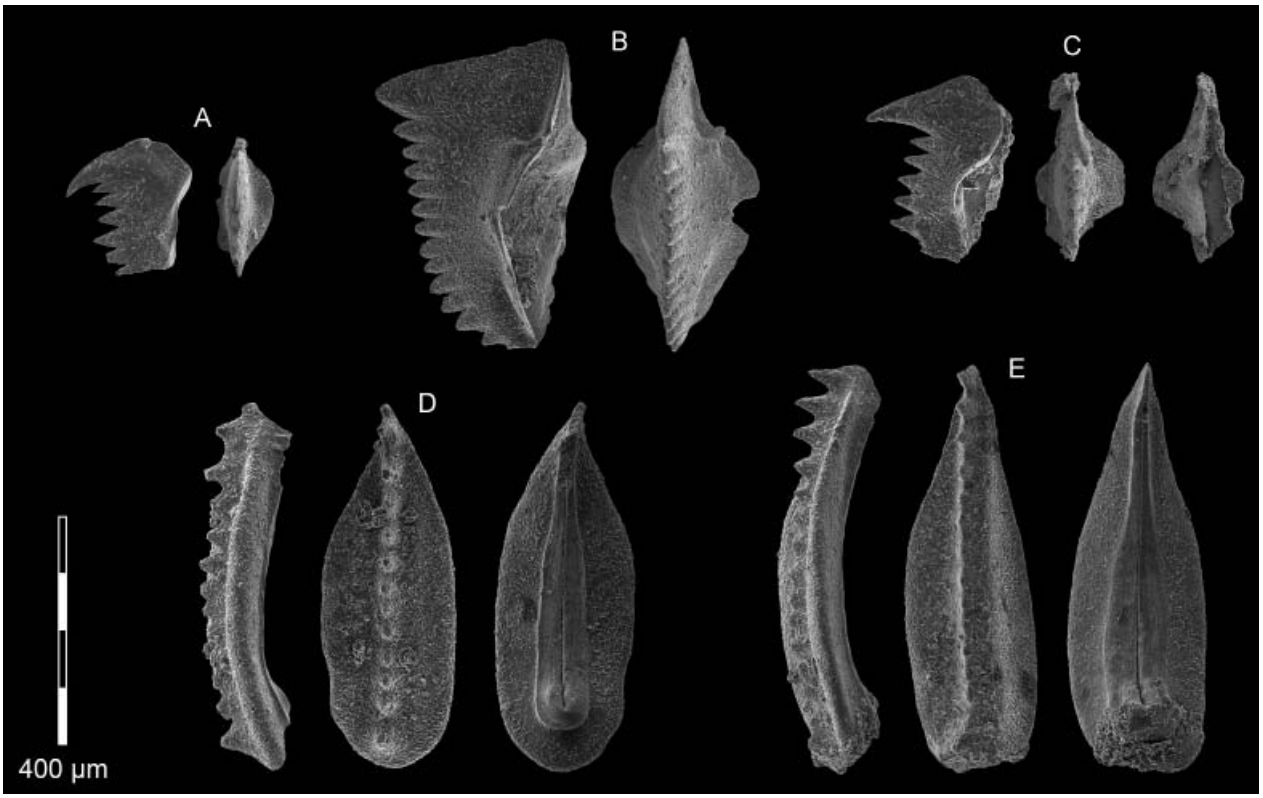

Figure 11: P_1 conodont elements from Unit A4. A, *Hindeodus* ?*parvus* Kozur and Pjatakova 1976 (juvenile), PIMUZ XXXXX. B, *Hindeodus typicalis* Sweet 1970, PIMUZ XXXXX. C, *Isarcicella* sp. indet., PIMUZ XXXXX. D, *Neogondolella taylorae* Orchard 1994, PIMUZ XXXXX. E, *Neogondolella* ?*deflecta* Wang and Wang 1981, PIMUZ XXXXX.

4.3 Gastropods

Nineteen specimens of *Worthenia* sp. and 160 specimens of *Naticopsis* sp. (Fig. 12-13) were recovered. Both genera are well known the Permian (Erwin and Pan Hua-Zhang, 1996). Similar *Naticopsis* species have been reported from the Griesbachian microbial limestone in South China at Shanggan, Wuzhuan and Longyan (Kaim et al., 2010; Hautmann et al., 2015) and from the Smithian-Spathian rocks of the Salt Range, Pakistan (Kaim et al., 2013). This material from Pakistan and China has also been reported in open nomenclature as *Naticopsis* sp. *Naticopsis* specimens from Asselah have a very low spire and in this regard are distinct from the high-spired *Naticopsis* reported from the Wadi Wasit block (Fig. 2N-O in Wheeley and Twitchett, 2005; Twitchett et al., 2004). Width of the *Naticopsis* specimens from Asselah ranges up to 23 mm and is 10.2 mm in average. 50% of the *Naticopsis* specimens have a width larger than 10 mm, a width that is considered the threshold between microgastropods and standard gastropods (Fraiser and Bottjer, 2004). The neritimorph *Naticopsis* is probably closely related to platyceratids (Frýda et al., 2009). The platyceratid group is known for being often associated with crinoids as coprophagous, predator or parasite (see Rollins & Brezinski (1988) and references therein for discussion). Such a mode of life is compatible with the occurrence of *Naticopsis* sp. in the Asselah crinoidal limestone. However, *Naticopsis* can also abound in fine siliclastics such as is the case for the Wordie Creek Fm. in NE Greenland (Fraiser et al., 2005).

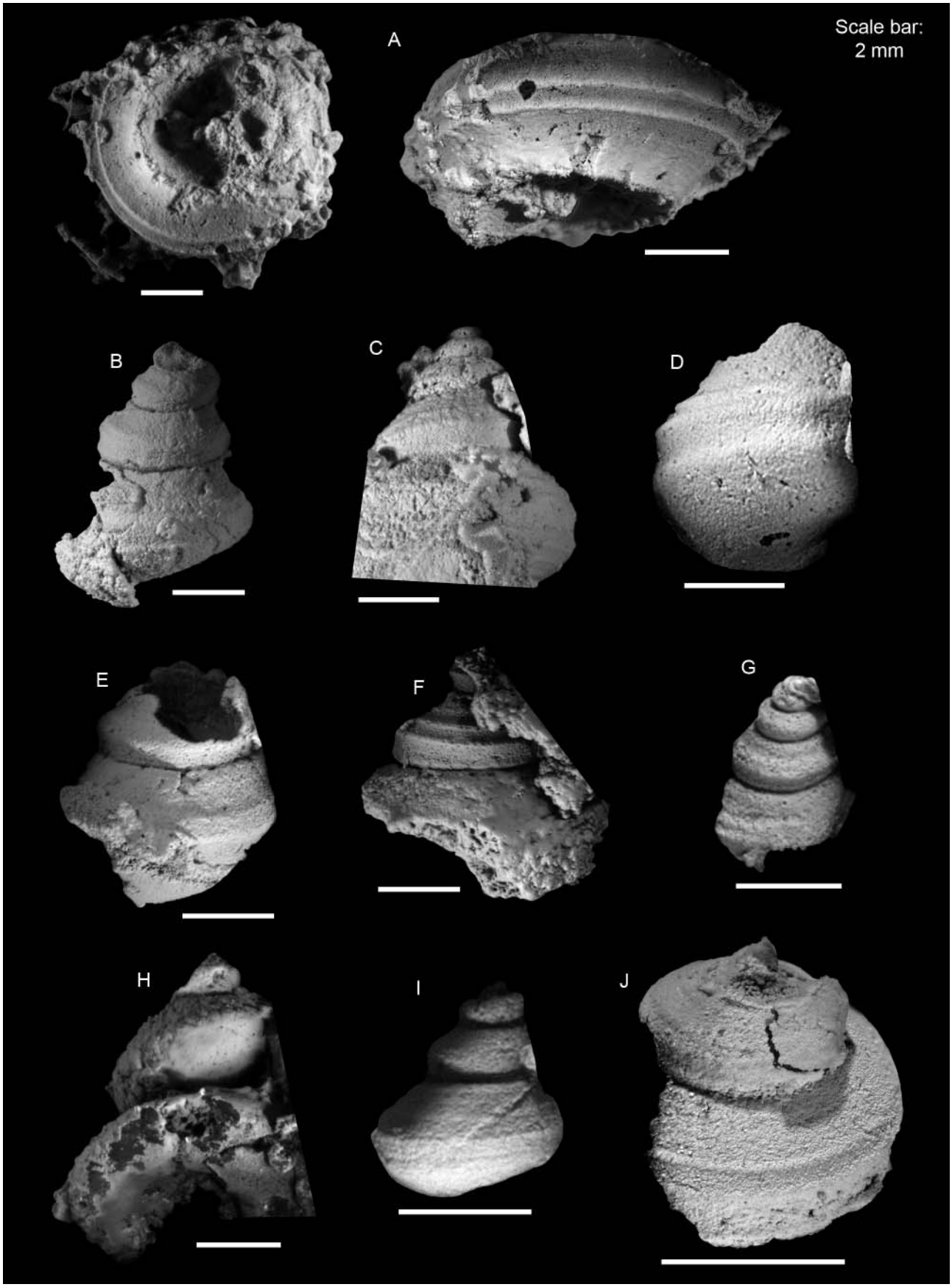

Figure 12: Gastropods from the Asselah boudler. A-J, *Worthenia* sp.; A, PIMUZ XXXXX; B, PIMUZ XXXXX; C, PIMUZ XXXXX; D, PIMUZ XXXXX; E, PIMUZ XXXXX; F, PIMUZ XXXXX; G, PIMUZ XXXXX; H, PIMUZ XXXXX; I, PIMUZ XXXXX; J, PIMUZ XXXXX.

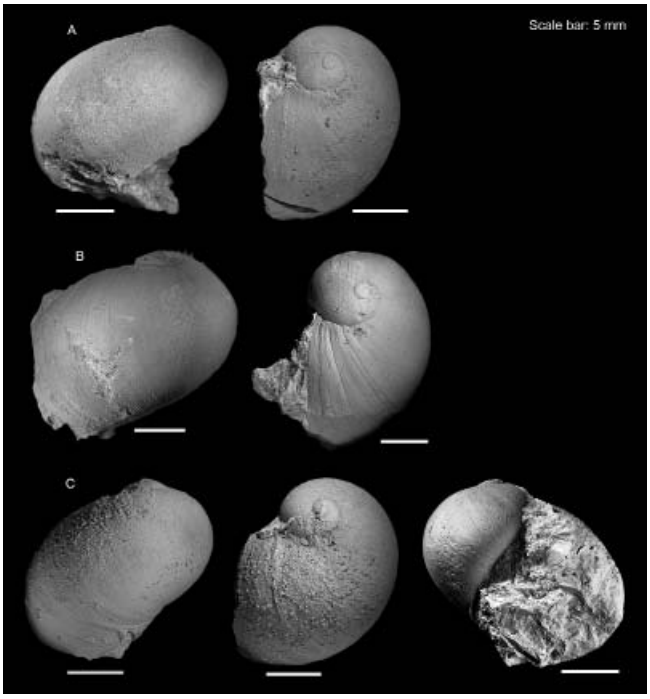

Figure 13: Gastropods from the Asselah boudler. A-C, *Naticopsis* sp.; A, PIMUZ XXXXX; B, PIMUZ XXXXX; C, PIMUZ XXXXX.

4.4 Ammonoids

Despite their abundance, only 10 ammonoid specimens from beds 1c, 1d and 3 could be prepared mechanically. They are all of rather small size (maximum 4 cm) and strongly recrystallized (Fig. 14). The small size of the specimens may suggest some sorting. Recrystallization has often destroyed the septa, so the suture lines are only occasionally and partially visible. The small sample size included here, the small size of the specimens and their strong recrystallization make identifications at the species level difficult.

We identified five species belonging to four genera *Episageceras*, *Metophiceras*, *Aldonoceras* and *Ophiceras*. Seven out of the ten specimens are from bed 3. *Metophiceras subdemissum* is the most common form. This species has been previously reported only from NE Greenland (Bjerager et al., 2006; Spath, 1930, 1935a, b), the material reported from Nepal (Waterhouse, 1994) being useless because of very poor preservation.

Most of the ammonoids occurring in the Asselah boulders belong to Permian families (*Metophiceras* and *Aldonoceras* belong to *Xenodiscidae*; *Episageceras* belongs to *Episageceratidae*) that survived the mass-extinction (Tozer, 1981).

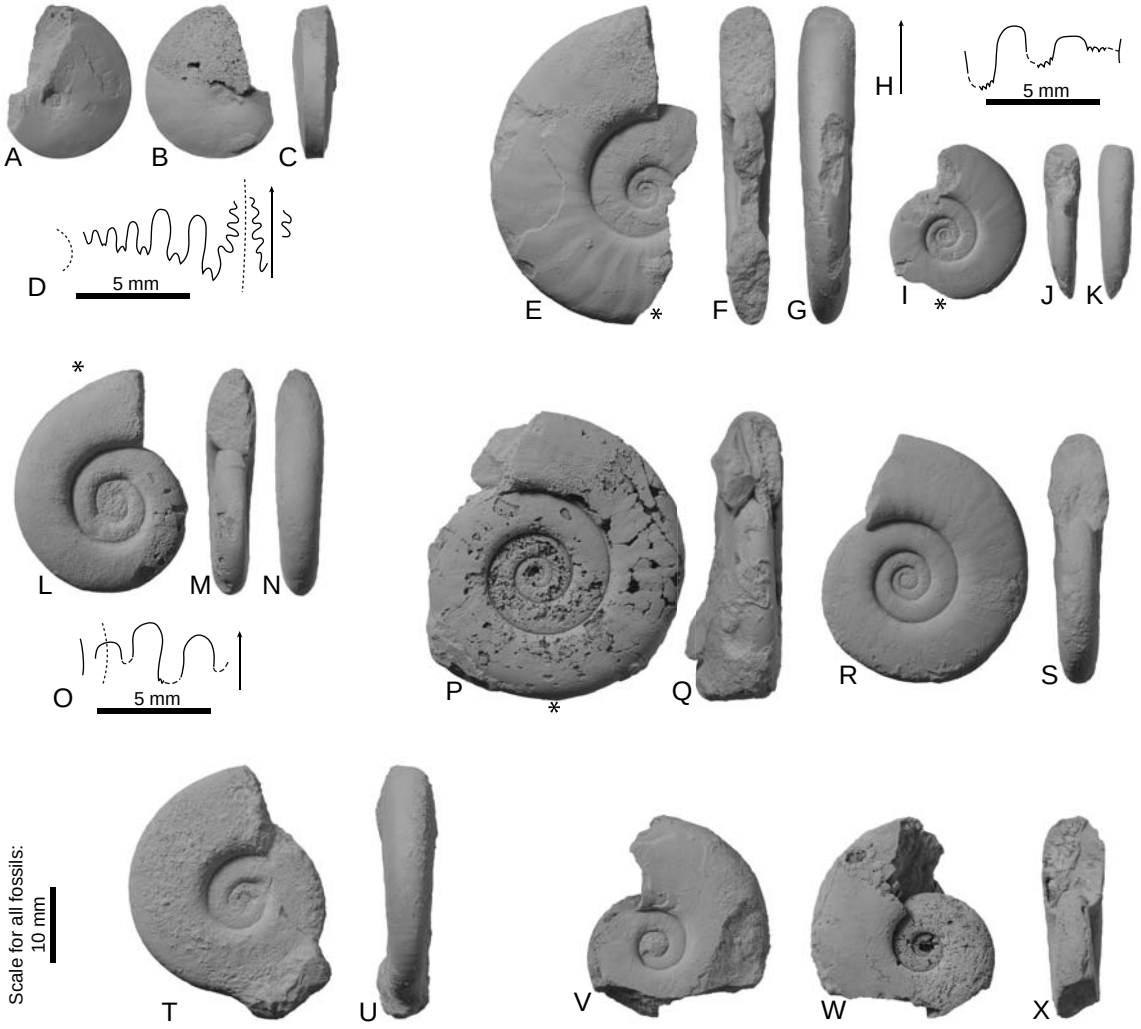

Figure 14: Ammonoids from the Asselah boulder. All figures natural size except the suture lines. Asterisks indicate position of last septum. A-D, *Episageceras* sp., bed 3, lateral (A, B) and ventral (C) views, suture line (D) at H=8.3 mm, Unit A3, PIMUZ XXXXX. E-K, *Aldonoceras* sp.; E-H, lateral (E), apertural (F) and ventral (G) views, suture line (H) at H=8.5 mm, Unit A1-D, PIMUZ XXXXX; I-K, lateral (I), apertural (J) and ventral (K) views, Unit A1-D, PIMUZ XXXXX. L-S, *Metophiceras subdemissum*; L-O, lateral (L), apertural (M) and ventral (N) views, suture line (O) at H=6 mm, Unit A3, PIMUZ XXXXX; P-Q, lateral (P), and apertural (Q) views, Unit A3, PIMUZ XXXXX; R-S, lateral (R), and apertural (S) views, Unit A3, PIMUZ XXXXX. T-U, *Ophiceras* sp. A, lateral (T) and ventral (U) views, Unit A1-C, PIMUZ XXXXX. V-U: *Ophiceras* sp. B, lateral (V, W) and ventral (X) views, Unit A3, PIMUZ XXXXX.

4.5. Crinoids

The Asselah boulder yielded numerous, poorly preserved crinoid ossicles. Sub-pentagonal proximal columnals (Fig. 15) and long cylindrical cirrals with transverse ridges on the articulation facets (Fig. 16) were recovered. The distal columnals are cylindrical with multiradiate facets (Fig. 17) and with culmina that may bifurcate as is typical for *Holocrinidae*. Columnals' facets allow assignment to *Baudicrinus krystyni* Oji and Twitchett (2015). This taxon was erected on the basis of material from the Wadi Wasit block. Contrary to the conclusion of Oji and Twitchett (2015), the sub-pentagonal proximal columnals and the bifurcated culmina suggest assignment of *Baudicrinus* to *Holocrinidae* family rather than to *Dadocrinidae*.

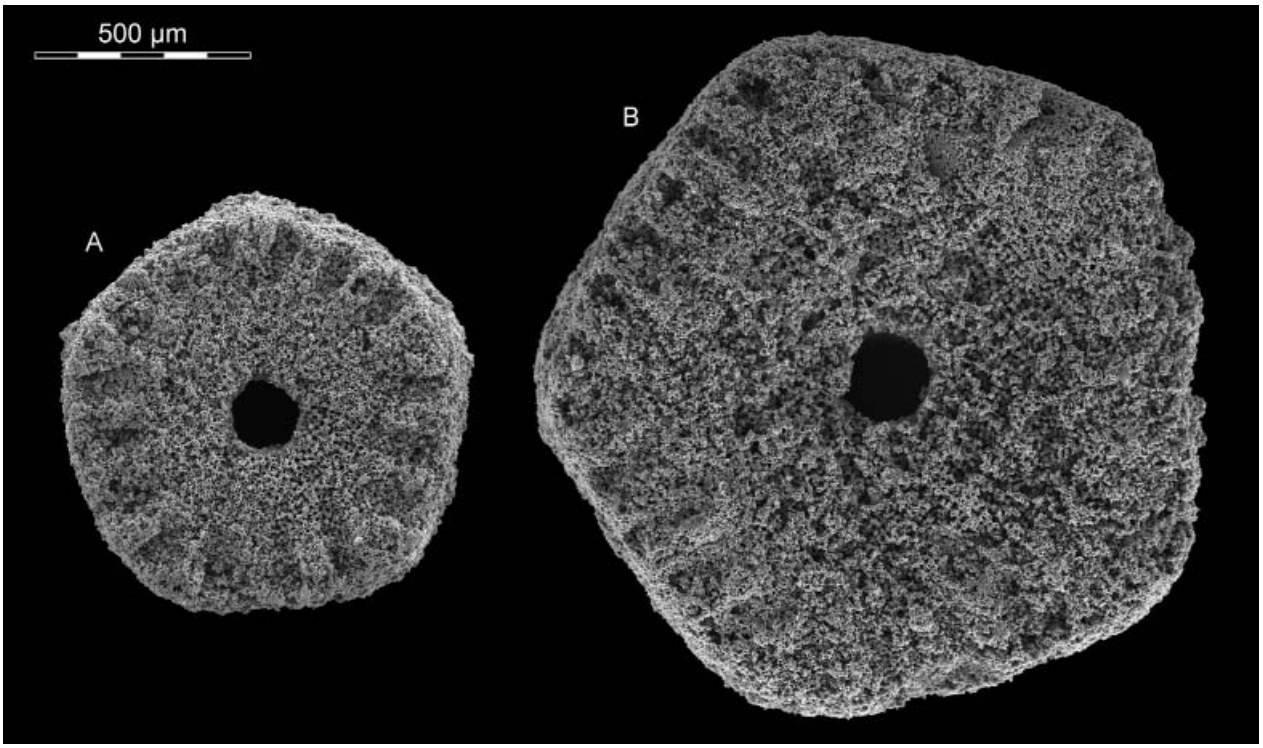

Figure 15: Crinoid ossicles from the Asselah boulder: proximal columnals, Unit A2+A3. A, PIMUZ XXXXX; B, PIMUZ XXXXX.

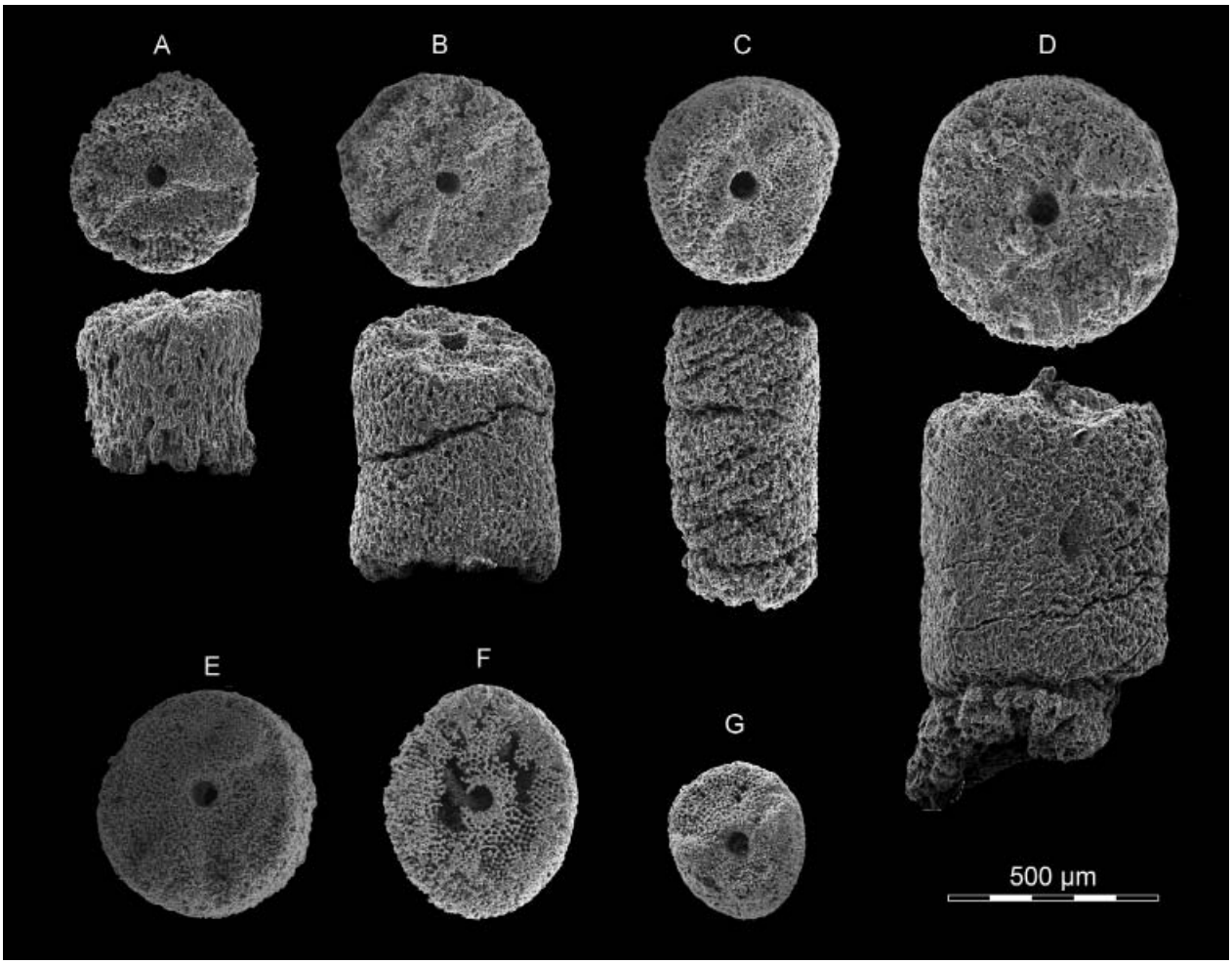

Figure 16: Crinoid ossicles from the Asselah boulder: cirrals, Unit A2+A3. A, PIMUZ XXXXX; B, PIMUZ XXXXX; C, PIMUZ XXXXX; D, PIMUZ XXXXX; E, PIMUZ XXXXX; F, PIMUZ XXXXX; G, PIMUZ XXXXX. Note the transverse ridges on the articulation facets.

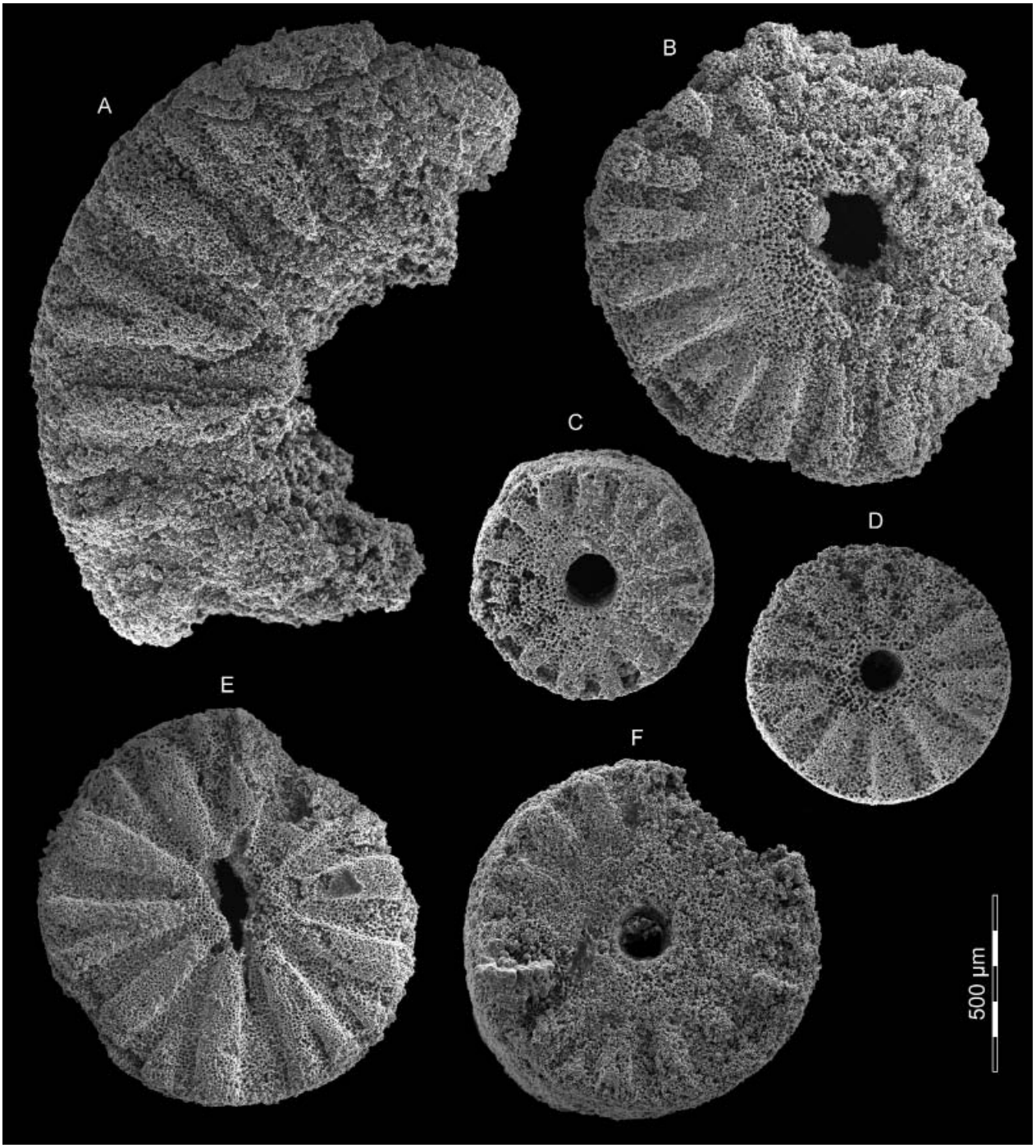

Figure 17: Crinoid ossicles from the Asselah boulder: distal columnals, Unit A2+A3. A, PIMUZ XXXXX; B, PIMUZ XXXXX; C, PIMUZ XXXXX; D, PIMUZ XXXXX; E, PIMUZ XXXXX; F, PIMUZ XXXXX. Note the bifurcated culmina in A and E.

5. Comparison with the Wadi Wasit block

The Wadi Wasit block spans a Permian to Dienerian and interval. The Dienerian age assignment rests on the occurrence of *Sweetospathodus kummeli* (=*Neospathodus kummeli* in Krystyn et al., 2003), a typical form of the base of the Dienerian within low latitudes (Orchard, 2007; Chapter III). The Asselah boulder represents a shorter time interval, entirely included within the Griesbachian (see part 4.2. Conodonts). The Asselah boulder includes 11 species of Griesbachian conodonts, whereas only six Griesbachian conodont species are recorded from Wadi Wasit.

The Griesbachian gastropods assemblage is richer in Wadi Wasit than in Asselah, the latter being only a small subset of the former. Wheeley and Twitchett (2005) listed no less than 11 genera at Wadi Wasit, which stands in marked contrast with the two genera assemblage of Asselah (*Worthenia* sp. and *Naticopsis* sp.). Rare specimens of *Bellerophon* have been discovered at Wadi Wasit (Fig. 2.F-H in Wheeley and Twitchett, 2005), none could be found in Asselah.

The size ranges of *Naticopsis* from both localities are similar, with width exceeding 20 mm (Twitchett et al., 2004; Wheeley and Twitchett, 2005). The average size of these *Naticopsis* is larger than that of other previously described Griesbachian gastropods populations (e.g. 5 mm in average; Price-Lloyd and Twitchett, 2002; Wheeley and Twitchett, 2005; Twitchett, 2007).

The main difference between Wadi Wasit and Asselah relates to the biomass represented by volumetric abundance of the benthos: while bivalves are very abundant and amount up to 95% of some beds (e.g. *Eumorphotis/ Claraia* biofacies) at Wadi Wasit, they are far less abundant and all fragmentary at Asselah, precluding identifications. Differing from to Wadi Wasit, crinoids represent the main component of the biomass in the Asselah. However, it is worth noting here that another boulder of Griesbachian age from Asselah is mostly composed of bivalves, thus confirming substantial heterogeneity in the main components of the benthos biomass. These mass abundances of bivalves or crinoids on offshore sea mounts speaks against the notion of ecological refugium as initially proposed for the Wadi Wasit assemblage (Krystyn et al., 2013).

The upper part of the *Eumorphotis* bed (upper part of the Wadi Wasit block) and the entire boulder of Asselah mainly consist in crinoid ossicles assigned to the holocrinids, to which *Baudicrinus krystyni* Oji and Twitchett (2015; see part 4.5. crinoids) is here reassigned. Holocrinids have also recently been described in Svalbard, Artic (Salamon et al., 2015) from the Vardebukta Formation (Griesbachian/ Dienerian age; Nakrem et al., 2008). Holocrinids had hitherto not been documented until the Smithian (Hagdorn, 2011) and those crinoid records re-establish them as most basal of the crown-group articulates and push back their origin into to the Griesbachian, synchronously within the Boreal and the Tethyan realms.

The Asselah boulder and Wadi Wasit outcrops have a much higher diversity than what is suggested by the traditional model of Griesbachian devastated faunas. Organisms thrived in well-oxygenated, clastic-free and in carbonate super-saturated waters. Krystyn et al. (2003) reported an increase of almost 2‰ of $\delta^{13}C_{carb}$ isotope values throughout the Wadi Wasit block that they interpreted as an increase in primary productivity. They concluded that the Wadi Wasit area was a shelter for marine organisms during the harsh environmental conditions of the Early Triassic.

6. Discussion

6.1 Griesbachian oceanic conditions

6.1.1 Anoxia

The occurrence of a diverse community thriving on a well-oxygenated sea-floor during the Griesbachian in Oman stands in sharp contrast with the interpretation of a delayed biotic recovery due to a global anoxia (Hallam, 1991; Isozaki, 1997). The anoxia hypothesis relies on geochemical evidences (Cerium anomaly, carbon/sulphur ratios, sulphur isotopes; Wignall and Hallam, 1992), low amount of trace fossils during the Early Triassic (Wignall and Twitchett, 1996; Wignall et al., 2016), and was reinforced by the frequent occurrence of pyrite framboids (Wignall et al. 2005; Liao et al., 2010; Bond and Wignall, 2010; Liao et al., 2016). However, a succession of different redox condition phases observed in Meishan (South China) indicates that the redox evolution was not due to a global anoxia (Li et al., 2015) and could be instead due to temperature fluctuations (Huang et al., 2016). Moreover, the presence of pyrite framboids themselves does not necessary implies an anoxic water column, as they can also form within anoxic sediment porewaters in otherwise oxic conditions (Wilkin et al. 1996; Roychoudhury et al., 2003). The paradoxical association of pyrite framboids and diversified shelly remains in shallow-water microbialite-bearing sections (Li et al., 2015) can also been explained by the transport of the pyrite from anoxic to oxic zones by oceanic circulation (Kershaw and Liu, 2015). Hofmann et al. (2011, 2013) also evidenced a recovery of trace fossils as soon as the Griesbachian and suggested that the low amount of trace fossils is an effect of the mass-extinction rather than of a protracted anoxia during the early Triassic (the reader is referred to Erwin (1993) and Hofmann (2016) for a more extensive discussion).

The presence of Griesbachian well-oxygenated conditions has been inferred not only in the Tethyan offshore sea-mounts (Krystyn et al. 2003; this study) but also on the northern Indian margin (Hermann et al., 2011, 2013), in the north-east Greenland rift (Sanson-Barrera et al., 2015) and in shallow water microbialite of Guangxi, South China (Kaim et al., 2010; Hautmann et al., 2015; Bagherpour et al. accepted in Gondwana Research). The local occurrence of anoxia in the Nanpanjiang Basin has been shown to be restricted to grabens (Fig. in Bagherpour et al., accepted in Gondwana Research 19) while microbialite developed in oxic conditions on neighbouring horsts. Based on trace fossils analyses, Beatty et al. (2008) described a 'colonization window' and propose the occurrence of a narrow, shallow and well-oxygenated habitable zone pinched between the edge of anoxic water of the continental shelf and the shoreline. It is clear that the basal Triassic anoxia was not ubiquitous and was influenced by palaeotopograhy and palaeogeography.

6.1.2 Climate

Sun et al. (2012) characterized the climate during the Griesbachian as 'lethally hot' followed by a cooling event during the Dienerian. The authors located the thermal maximum within *Ng. planata* Zone, interpreted as late Griesbachian. However, Sun et al. (2012) overlooked the overlying Griesbachian *Ng. discreta* Zone (Chen et al., 2015), and, at least at Meishan section, ignored the 93 m thick interval between bed 40 and bed 73, e.g. the base of the Dienerian. Hence the temperature curve from Sun et al. (2012) lacks the upper part of the Griesbachian and possibly the beginning of the Dienerian. Moreover, their curve is produced by 'stitching' the oxygen isotope records from different sections and ignoring the various environmental settings. It is also worth noting

that these extremely hot temperatures are all derived from the South Chinese record (Joachimski et al., 2012; Sun et al., 2012; Chen et al., 2016), whose equatorial position is the least climate sensitive configuration. Absence of a temperature relative maximum is also documented from the Salt Range record by Romano et al. (2013).

A recent study published by Hochuli et al. (2016) on the palynology of Kap Stosch, NE Greenland, showed that the Griesbachian was not characterized by the demise of land plants, but rather by a major turnover in the floral assemblage. They evidenced that the Griesbachian was characterized by by a gymnosperm-dominated flora, thus suggesting a cool/temperate and dry climate.

The model of Renne et al., (1995) is also supported by Baresel et al. (accepted in Science Report), who both proposed a fast cooling at the PTB triggered by atmospheric injections of sulphur-rich volatiles from the Siberian Traps. This interval was followed by a transient Griesbachian climate due to slower accumulation of CO_2, until greenhouse conditions were reached not earlier than the Dienerian, i.e. 500ky later (Baresel et al. accepted in Science Report).

6.2 'Exceptional' Griesbachian records

The exceptional biotic assemblage from Asselah and Wadi Wasit are not restricted to Oman. Calcarenitic lenses intercalated within the microbialite domes in the Nanpanjiang Basin (South China, Equatorial Realm) yielded abundant and diverse assemblages of Griesbachian age. These coquinoid lenses yielded nektonic organisms such as conodonts and ammonoids (Brühwiler et al., 2008; Brosse et al., 2015; Hautmann et al., 2015) together with benthics such as bivalves and gastropods, supplemented by echinoderm ossicles, ostracods and rare brachiopods (Kaim et al., 2010; Hautmann et al., 2015). Noteworthy, the shelly faunas from the microbialite are exceptionally well-preserved with delicate details of the shell surface (Hautmann et al., 2015). Hautmann et al. (2015) attributed this exceptional preservation to a carbonate super-saturated clastic-free water, early micritization and to a *Konzentrat-Lagerstätte* effect. Forel et al. (2013) suggested that the oxygen produced by the microbial mounts acted as a protection against the surrounding anoxia and thus they categorized the microbial limestones as refugium for Lazarus taxa (Vermeij, 1986; Erwin, 1996; Zonneveld et al., 2010). The refugium interpretation for the microbial limestones is questionable because 75% of the macroinvertebrate genera found trapped between the microbial domes at Wuzhuan section (Guangxi) are also known from other microbial-barren localities (Hautmann et al., 2015).

At Wadi Wasit, only one of Erwin's Lazarus genus (*Ananias*) was confidently identified from the silicified gastropods assemblages and over 50% of the genera could also be found in other localities (Wheeley and Twitchett, 2005), which, like in the microbialite, indicates that the Wadi Wasit block was not a refugium for Lazarus taxa.

Foster et al. (2016) describe a diverse and exquisitely preserved silicified Griesbachian benthic community in Svalbard (Boreal Realm), counting 14 species of bivalves and gastropods. Noteworthy, about 35% of the families of benthics found at Svalbard are inherited from the Permian (Fig. 14 in Foster et al., 2016).

A silicified community of Griesbachian and Dienerian crinoids has been recovered from the Vardebukta Fm. in Svalbard (Salamon et al., 2015) and shows that the recovery of crinoids was synchronous within the Tropical and the

Boreal realms.

A community of sea-urchin thriving on microbial mats was also discovered in a Griesbachian horizon of the Shangsi section, South China (Godbold et al., 2016), showing that echinoids occurred likewise in the Equatorial Realm as soon as the Griesbachian.

We can explain the diverse fossil records of the Oman sea mounts thanks to their palaeogeography: During the tectonic instability of the basal Triassic, the offshore of the Gondwana margin consisted in uplifted tilted blocks above the Calcite Compensation Depth, away from the environmental stress that may have affected continental shelves (Fig. 16 in Baud et al., 2012).

Every Griesbachian communities reported here is also characterized by a particular preservation, from early micritisation to silicification. The fossil gap observed during the Griesbachian interval seems to be strongly related to selective preservation rather than global harsh environmental conditions. The preservation bias hypothesis has been first proposed by Erwin (1996), who suggested that the low diversity and the Lazarus gastropods taxa in the Permian-Triassic interval were due to the poor quality fossil record and the absence of silicified fauna, possibly explained by the decline and offshore migration of siliceous sponges (Schubert et al., 1997).

Synchronous rich Griesbachian fossil records from the Equatorial to the Boreal Realms demonstrate that the biotic recovery was neither delayed nor faster in low latitudes. Interestingly, the fossil assemblages of bivalves, gastropods, conodonts and ammonoids discussed above contain substantial amount of Permian holdovers. The high diversity of these Griesbachian communities is hence partially due to the survival of Permian genera than to an early post-extinction diversification (Hautmann et al., 2015).

7. Conclusions

The Tethyan offshore sea mounts of Oman were located on uplifted blocks that escaped the harsh environmental conditions of the continental shelves and provided well-oxygenated clastic-free environments. We see here that diversity of the Griesbachian record is constrained by local palaeotopography (Bagherpour et al., accepted in Gondwana Research), palaeogeography (Krystyn et al., 2003; Beatty et al., 2008) and preservation (Hautmann et al., 2015; Foster et al. 2016).

The Griesbachian fossil communities recorded in Oman are not restricted to the Tethyan Tropical Realm, as comparable benthic faunas have also been described from the Equatorial Tethyan Realm (Hautmann et al. 2015, Godbold et al. 2016) and the Boreal Realm (Salamon et al. 2015; Foster et al. 2016). The hypothesis of a faster biotic recovery in the Boreal Realm due to hot climate is here discarded (see additional arguments in Hochuli et al., 2016; Baresel et al., accepted in Science Report). We propose that the diversity 'low' initially observed during the Griesbachian is due to a preservation bias rather than unusually harsh environmental conditions. We also argue that the diversity of Griesbachian assemblages is partially accountable for by surviving Permian taxa, thus favouring an interval of transition rather than of devastation.

Acknowledgments

This work is supported by the Swiss NSF project 200021_135446 (to H.B.) and a French ANR @RAction grant (project EvoDevOdonto to N.G.). Å.M.F is supported by The Swedish Research Council (Vetenskapsrådet). We are thankful to Markus Hebeisen and Rosie Roth who extracted and took photographs of the ammonoids. Matthieu Gravito (Beicip-Franlab,

Paris, France) is thanked for his insights on the microfacies analyses. We are grateful to Mohamad Al Battashi and Mohamed Alaraim in Geological Research Ministry of Commerce and Industry Sultanate of Oman for fieldwork authorization.

References

Abstract

Godbold, A. L., Henderson, C. M. and Schoepfer, S. D. The refugia concept following the end-Permian mass extinction. GSA Annual Meeting in Denver, Colorado, USA – 2016.

Book

Erwin, D. H., 1993. The great Paleozoic crisis: life and death in the Permian. Columbia University Press.

Hofmann, R., in M.G. Mángano, L.A. Buatois (eds.), The Trace-Fossil Record of Major Evolutionary Events, Topics in Geobiology 39, Chapter 7: The End-Permian Mass Extinction, 325-349.

Journal

Bagherpour, B., Bucher, H., Baud, A., Brosse, M., Vennemann, T., Martini, R., and Guodun. K. Onset, development, and cessation of basal Early Triassic microbialites (BETM) in the Nanpanjiang pull-apart Basin, South China Block. Accepted in Gondwana Research.

Baud, A., Richoz, S., Beauchamp, B., Cordey, F., Grasby, S., Henderson, C. M., ... & Nicora, A., 2012. The Buday'ah Formation, Sultanate of Oman: A Middle Permian to Early Triassic oceanic record of the Neotethys and the late Induan microsphere bloom. Journal of Asian Earth Sciences, 43(1), 130-144.

Baresel B., Bucher H., Bagherpour B., Brosse M., Guodun K. and Schaltegger U. Timing of global regression and microbial bloom marking the Permo-Triassic mass extinction. Accepted in Science Report.

Beatty, T. W., Zonneveld, J. P., and Henderson, C. M., 2008. Anomalously diverse Early Triassic ichnofossil assemblages in northwest Pangea: A case for a shallow-marine habitable zone. Geology, 36(10), 771-774.

Benton, M. J., and Twitchett, R. J., 2003, How to kill (almost) all life: the end-Permian extinction event: Trends in Ecology & Evolution, v. 18, no. 7, p. 358-365, doi:10.1016/S0169-5347(03)00093-4.

Bjerager, M., Seidler, L., Stemmerik, L., and Surlyk, F., 2006. Ammonoid stratigraphy and sedimentary evolution across the Permian-Triassic boundary in East Greenland: Geological Magazine, v. 143, no. 5, p. 635-656, doi:10.1017/S0016756806002020.

Brayard, A., Bucher, H., Escarguel, G., Fluteau, F., Bourquin, S., and Galfetti, T., 2006. The Early Triassic ammonoid recovery: paleoclimatic significance of diversity gradients. Palaeogeography, Palaeoclimatology, Palaeoecology, 239(3), 374-395.

Brayard, A., Escarguel, G., Bucher, H., & Brühwiler, T., 2009. Smithian and Spathian (Early Triassic) ammonoid assemblages from terranes: paleoceanographic and paleogeographic implications. Journal of asian earth Sciences, v. 36(6), 420-433. doi.org/10.1016/j.jseaes.2008.05.004.

Brayard, A., Escarguel, G., Bucher, H., Monnet, C., Brühwiler, T., Goudemand, N., Galfetti, T., and Guex, J., 2009, Good genes and good luck: ammonoid diversity and the end-Permian mass extinction: Science, v. 325, no. 5944, p. 1118-1121, doi:10.1126/science.1174638.

Brayard, A., Vennin, E., Olivier, N., Bylund, K. G., Jenks, J., Stephen, D. A., Bucher, H., Hofmann, R., Goudemand, N., and Escarguel, G., 2011, Transient metazoan reefs in the aftermath of the end-Permian mass extinction: Nature Geoscience, v. 4, no. 10, p. 693-697, doi:10.1038/ngeo1264.

Brühwiler, T., Brayard, A., Bucher, H., and Guodun, K., 2008. Griesbachian and Dienerian (Early Triassic) ammonoid faunas from northwestern Guangxi and southern Guizhou (south China). Palaeontology, 51(5), 1151-1180.

Chen, J., Shen, S. Z., Li, X. H., Xu, Y. G., Joachimski, M. M., Bowring, S. A., ... & Wang, Y., 2016. High-resolution SIMS oxygen isotope analysis on conodont apatite from South China and implications for the end-Permian mass extinction. Palaeogeography, Palaeoclimatology, Palaeoecology, 448, 26-38.

Erwin, D. H., 1996. Understanding biotic recoveries: extinction, survival, and preservation during the end-Permian mass extinction. Evolutionary paleobiology. University of Chicago Press, Chicago, 398-418.

Erwin, D. H., 2001, Lessons from the past: biotic recoveries from mass extinctions, Proceedings of the National Academy of Sciences, v. 98, no. 10, p. 5399-5403, doi: 10.1073/pnas.091092698.

Forel, M. B., Crasquin, S., Kershaw, S., & Collin, P. Y., 2013. In the aftermath of the end-Permian extinction: the microbialite refuge?. *Terra Nova*, *25*(2), 137-143.

Foster, W. J., Danise, S., & Twitchett, R. J, 2016. A silicified Early Triassic marine assemblage from Svalbard. Journal of Systematic Palaeontology, 1-27.

Fraiser, M. L., and Bottjer, D. J., 2004, The non-actualistic Early Triassic gastropod fauna: a case study of the Lower Triassic SinbadLimestone member:

Palaios, v. 19, no. 3, p. 259-275, doi:10.1669/0883-1351(2004)01.

Fraiser, M. L., Twitchett, R. J., and Bottjer, D. J., 2005, Unique microgastropod biofacies in the Early Triassic: indicator of long-term biotic stress and the pattern of biotic recovery after the end-Permian mass extinction: Comptes Rendus Palevol, v. 4, no. 6, p. 543-552, doi:10.1016/j.crpv.2005.04.006.

Fraiser, M. L., and Bottjer, D. J., 2009. Opportunistic behaviour of invertebrate marine tracemakers during the Early Triassic aftermath of the end-Permian mass extinction. Australian Journal of Earth Sciences, 56(6), 841-857.

Frýda, J., Racheboeuf, P. R., Frýdová, B., Ferrová, L., Mergl, M., and Berkyová, S., 2009, Platyceratid gastropods–stem group of patellogastropods, neritimorphs or something else: Bulletin of Geosciences, v. 84, no. 1, p. 107-120.

Goudemand, N., Romano, C., Brayard, A., Hochuli, P. A., Bucher, H., 2013. Comment on "Lethally hot temperatures during the Early Triassic greenhouse". Science, 339(6123).

Glennie, K. W., Boeuf, M. G. A., Clarke, M. H., Moody-Stuart, M., Pilaar, W. F. H., and Reinhardt, B. M., 1973. Late Cretaceous nappes in Oman Mountains and their geologic evolution. AAPG Bulletin, 57(1), 5-27.

Hallam, A., 1991. Why was there a delayed radiation after the end-Palaeozoic extinctions?. Historical Biology, 5(2-4), 257-262.

Hagdorn, H., 2011, Triassic: the crucial period of post-Palaeozoic crinoid diversification: Swiss Journal of Palaeontology, v. 130, no. 1, p. 91-112.

Hauser, M., Martini, R., Burns, S., Dumitrica, P., Krystyn, L., Matter, A., Peters, T., and Zaninetti, L., 2001, Triassic stratigraphic evolution of the Arabian-Greater India embayment of the southern Tethys margin: Eclogae Geologicae Helvetiae, v. 94, no. 1, p. 29-62.

Hautmann, M., Bucher, H., Brühwiler, T., Goudemand, N., Kaim, A., and Nützel, A., 2011, An unusually diverse mollusc fauna from the earliest Triassic of South China and its implications for benthic recovery after the end-Permian biotic crisis: Geobios, v. 44, no. 1, p. 71-85, doi:10.1016/j.geobios.2010.07.004.

Hautmann, M., Smith, A. B., McGowan, A. J., and Bucher, H., 2013. Bivalves from the Olenekian (Early Triassic) of south-western Utah: systematics and evolutionary significance. Journal of Systematic Palaeontology, 11(3), 263-293.

Hautmann, M., et al., 2015, Competition in slow motion: the unusual case of benthic marine communities in the wake of the end-Permian mass extinction: Palaeontology, v. 58, no. 5, p. 871-901, doi:10.1111/pala.12186.

Hermann, E., Hochuli, P. A., Bucher, H., Vigran, J. O., Weissert, H., and Bernasconi, S. M., 2010. Close-up view of the Permian Triassic boundary based on extended organic carbon isotope records from Norway (Trøndelag and Finnmark Platform). Global and Planetary Change 74(3-4), 156-167.

Hermann, E., Hochuli, P. A., Bucher, H., Brühwiler, T., Hautmann, M., Ware, D., and Roohi, G., 2011. Terrestrial ecosystems on North Gondwana following the end-Permian mass extinction. Gondwana Research 20, 630-637.

Hermann, E., Hochuli, P. A., Bucher, H., and Roohi, G., 2012. Uppermost Permian to Middle Triassic palynology of the Salt Range and Surghar Range, Pakistan. Review of Palaeobotany and Palynology, 169, 61-95.

Hochuli, P.A., Vigran, J.O., Hermann, E., and Bucher, H., 2010. Multiple climatic changes around the Permian Triassic boundary event revealed by an expanded palynological record from Mid Norway. GSA Bulletin 122, 884-896.

Hochuli, P.A., Sanson-Barrera, A., Schneebeli-Hermann, E., and Bucher, H. 2016. Severest crisis overlooked—Worst disruption of terrestrial environments postdates the Permian-Triassic mass extinction. Scientific Reports, 6, pp. 1-7.

Hofmann, R., Goudemand, N., Wasmer, M., Bucher, H., & Hautmann, M., 2011, New trace fossil evidence for an early recovery signal in the aftermath of the end-Permian mass extinction: Palaeogeography, Palaeoclimatology, Palaeoecology, 310, no. 3, p. 216-226, doi:10.1016/j.palaeo.2011.07.014.

Hofmann, R., Hautmann, M., Wasmer, M., and Bucher, H., 2013. Palaeoecology of the Spathian Virgin Formation (Utah, USA) and its implications for the Early Triassic recovery. Acta Palaeontologica Polonica, 58(1), 149-173.

Hori, R. S., Yamakita, S., Ikehara, M., Kodama, K., Aita, Y., Sakai, T., Takemura, A., Kamata, Y., Suzuki, N., Takahashi, S., Spörli, K. B. and Grant-Mackie J. A., 2011. Early Triassic (Induan) Radiolaria and carbon-isotope ratios of a deep-sea sequence from Waiheke Island, North Island, New Zealand. Palaeoworld, 20(2), 166-178.

Isozaki, Y. (1997). Permo-Triassic boundary superanoxia and stratified superocean: records from lost deep sea. Science, 276(5310), 235-238.

Jeppsson, L., and Anehus, R., 1999, A new technique to separate conodont elements from heavier minerals: Alcheringa, v. 23, no. 1, p. 57-62, doi:10.1080/03115519908619339

Jeppsson, L., Anehus, R., and Fredholm, D., 1999, The optimal acetate buffered acetic acid technique for extracting phosphatic fossils: Journal of Paleontology, v. 73, no. 5, p. 964-972, doi:http://

www.jstor.org/stable/1306854.

Joachimski, M. M., Lai, X., Shen, S., Jiang, H., Luo, G., Chen, B., Chen, J., and Sun, Y., 2012, Climate warming in the latest Permian and the Permian–Triassic mass extinction: Geology, v. 40, no. 3, p. 195-198, doi:10.1130/G32707.1.

Kaim, A., and Nützel, A., 2011. Dead bellerophontids walking-The short Mesozoic history of the Bellerophontoidea (Gastropoda). Palaeogeography, Palaeoclimatology, Palaeoecology, 308(1), 190-199.

Kaim, A., Nützel, A., Bucher, H., Brühwiler, T., and Goudemand, N., 2010, Early Triassic (Late Griesbachian) gastropods from South China (Shanggan, Guangxi): Swiss Journal of Geosciences, v. 103, no. 1, p. 121-128.

Kaim, A., Nützel, A., Hautmann, M., & Bucher, H., 2013, Early Triassic gastropods from Salt Range, Pakistan: Bulletin of Geosciences, v. 88, p. 505-516, doi:10.3140/bull.geosci.1395.

Kershaw, S., and Liu, M., 2015. Modern Black Sea oceanography applied to the end-Permian extinction

Krystyn, L., Richoz, S., Baud, A., and Twitchett, R. J., 2003, A unique Permian–Triassic boundary section from the neotethyan Hawasina basin, Central Oman Mountains: Palaeogeography, Palaeoclimatology, Palaeoecology, v. 191, no. 3, p. 329-344, doi:10.1016/S0031-0182(02)00670-3.

Li, G., Wang, Y., Shi, G. R., Liao, W., and Yu, L., 2016. Fluctuations of redox conditions across the Permian–Triassic boundary—New evidence from the GSSP section in Meishan of South China. *Palaeogeography, Palaeoclimatology, Palaeoecology*, *448*, 48-58.

Liao, W., Bond, D. P., Wang, Y., He, L., Yang, H., Weng, Z., and Li, G., 2016. An extensive anoxic event in the Triassic of the South China Block: A pyrite framboid study from Dajiang and its implications for the cause(s) of oxygen depletion. Palaeogeography, Palaeoclimatology, Palaeoecology.

Nakrem, H. A., Orchard, M. J., Weitschat, W., Hounslow, M. W., Beatty, T. W., and Mørk, A., 2008. Triassic conodonts from Svalbard and their Boreal correlations. Polar Research, 27(3), 523-539.

Neri, C., and Posenato, R., 1985. New biostratigraphical data on uppermost Werfen Formation of western Dolomites (Trento, Italy). Geologisch–Paläontologische Mitteilungen Innsbruck, 14, 83-107.

Oji, T., and Twitchett, R. J., 2015, The Oldest Post-Palaeozoic Crinoid and Permian-Triassic Origins of the Articulata (Echinodermata): Zoological science, v. 32, no. 2, p. 211-215, doi:http://dx.doi.org/10.2108/zs140240.

Orchard, M. J., 2007, Conodont diversity and evolution through the latest Permian and Early Triassic upheavals: Palaeogeography, Palaeoclimatology, Palaeoecology, v. 252, no. 1, p. 93-117, doi:10.1016/j.palaeo.2006.11.037.

Orchard, M. J., and Krystyn, L., 1998, Conodonts of the lowermost Triassic of Spiti, and new zonation based on Neogondolella successions: Rivista Italiana di Paleontologia e Stratigrafia, v. 104, no. 3, p. 341-638.

Payne, J. L., 2005, Evolutionary dynamics of gastropod size across the end-Permian extinction and through the Triassic recovery interval: Paleobiology, v. 31, no. 2, p. 269-290, doi:http://dx.doi.org/10.1666/0094-8373(2005)031[0269:EDOGSA]2.0.CO;2.

Price-Lloyd, N., and Twitchett, R. J., 2002, October. The Lilliput effect in the aftermath of the end-Permian mass extinction event. In 2002 Denver Annual Meeting.

Renne, P. R., Zichao, Z., Richards, M. A., Black, M. T., and Basu, A. R., 1995. Synchrony and causal relations between Permian-Triassic boundary crises and Siberian flood volcanism. Science, 269(5229), 1413.

Rodland, D. L., and Bottjer, D. J., 2001, Biotic recovery from the end-Permian mass extinction: behavior of the inarticulate brachiopod Lingula as a disaster taxon: Palaios, v. 16, no. 1, p. 95-101, doi:10.1669/0883-1351(2001)01.

Rollins, H. B., and Brezinski, D. K., 1988, Reinterpretation of crinoid-platyceratid interaction: Lethaia, v. 21, no. 3, p. 207-217, doi:10.1111/j.1502-3931.1988.tb02072.x

Roychoudhury, A. N., Kostka, J. E., and Van Cappellen, P., 2003. Pyritization: a palaeoenvironmental and redox proxy reevaluated. Estuarine, Coastal and Shelf Science, 57(5), 1183-1193.

Salamon, M. A., Gorzelak, P., Hanken, N., Riise, H. E., and Ferré, B., 2015. Crinoids from Svalbard in the aftermath of the end-Permian mass extinction. Polish Polar Research, 36(3), 225-238.

Sanson-Barrera, A., Hochuli, P. A., Bucher, H., Schneebeli-Hermann, E., Meier, M., Weissert, H., and Bernasconi, S. M., 2015. Late Permian-earliest Triassic high-resolution carbon isotope and palynofacies records from Kap Stosch (East Greenland). Global and Planetary Change 133, 149-166.

Schubert, J. K., and Bottjer, D. J., 1992, Early Triassic stromatolites as post-mass extinction disaster forms: Geology, v. 20, no. 10, p. p. 883-886, doi:10.1130/0091-7613(1992).

Schubert, J. K., Bottjer, D. J., and Simms, M. J., 1992, Paleobiology of the oldest known articulate crinoid. Lethaia, v. 25, no. 1, p. 97-110, doi: 10.1111/j.1502-3931.1992.tb01794.x.

Schubert, J. K., Kidder, D. L., and Erwin, D. H., 1997. Silica-replaced fossils through the Phanerozoic. Geology, 25(11), 1031-1034.

Song, H., Tong, J., and Chen, Z. Q, 2009a, Two episodes of foraminiferal extinction near the Permian–Triassic boundary at the Meishan section, South China: Australian Journal of Earth Sciences, v. 56, no. 6, p. 765-773.

Song, H., Tong, J., Chen, Z. Q., Yang, H. A. O., and Wang, Y., 2009b, End-Permian mass extinction of foraminifers in the Nanpanjiang Basin, South China: Journal of Paleontology, v. 83, no. 05, p. 718-738, doi:http://dx.doi.org/10.1666/08-175.1.

Song, H., et al., 2011, Recovery tempo and pattern of marine ecosystems after the end-Permian mass extinction: Geology, v. 39, no. 8, p. 739-742, doi:10.1130/G32191.1.

Song, H., Wignall, P. B., Chu, D., Tong, J., Sun, Y., Song, H., He, W., and Tian, L., 2014. Anoxia/high temperature double whammy during the Permian-Triassic marine crisis and its aftermath. Scientific reports, 4.

Spath, L.F., 1930. The Eotriassic Invertebrate Fauna of East Greenland: Meddelelser om Grönland, v. 83, p. 1–90.

Spath, L.F., 1935a. The Eotriassic Invertebrate Fauna of East Greenland: Meddelelser om Grönland, v. 83, p. 1–90.

Spath, L.F., 1935b. Additions to the Eotriassic Invertebrate Fauna of East Greenland: Meddelelser om Grönland, v. 98, p. 1–115.

Spörli, K. B., Aita, Y., Hori, R. S., and Takemura, A., 2007. Results of multidisciplinary studies of the Permian/Triassic ocean floor sequence (Waipapa Terrane) at Arrow Rocks, Northland, New Zealand. GNS Science Monograph, 24, 219-229.

Sun, Y., Joachimski, M. M., Wignall, P. B., Yan, C., Chen, Y., Jiang, H., Wang, L., and Lai, X., 2012. Lethally hot temperatures during the Early Triassic greenhouse. Science, 338(6105), pp. 366-370.

Tozer, E. T. (1981). Triassic Ammonoidea: classification, evolution and relationship with Permian and Jurassic forms. The ammonoidea, 18, 66-100.

Twitchett, R. J., and Barras, C. G., 2004. Trace fossils in the aftermath of mass extinction events. Geological Society, London, Special Publications, 228(1), 397-418.

Twitchett, R. J., 2007, The Lilliput effect in the aftermath of the end-Permian extinction event: Palaeogeography, Palaeoclimatology, Palaeoecology, v. 252, no. 1, p. 132-144, doi:10.1016/j.palaeo.2006.11.038.

Twitchett, R. J., Krystyn, L., Baud, A., Wheeley, J. R., and Richoz, S., 2004, Rapid marine recovery after the end-Permian mass-extinction event in the absence of marine anoxia: Geology, v. 32, no. 9, p. 805-808, doi: 10.1130/G20585.1.

Urbanek, A., 1993, Biotic crises in the history of Upper Silurian graptoloids: a palaeobiological model: Historical Biology, v. 7, no. 1, p. 29-50.

Vermeij, G. J. (1986). Survival during biotic crises: the properties and evolutionary significance of refuges. *Dynamics of extinction. Wiley, New York*, 231-246.

Ware, D., Bucher, H., Brayard, A., Schneebeli-Hermann, E., and Brühwiler, T., 2015. High-resolution biochronology and diversity dynamics of the Early Triassic ammonoid recovery: the Dienerian faunas of the Northern Indian Margin. Palaeogeography, Palaeoclimatology, Palaeoecology, 440, 363-373.

Wasmer, M., Hautmann, M., Hermann, E., Ware, D., Roohi, G., Ur-Rehman, K., Yaseen, A., and Bucher, H., 2012. Olenekian (Early Triassic) bivalves from the Salt Range and Surghar Range, Pakistan. Palaeontology, 55(5), 1043-1073.

Waterhouse, J.B., 1994, The Early and Middle Triassic ammonoid succession of the Himalayas in western and central Nepal. Part 1. Stratigraphy, classification and Early Scythian ammonoid systematics: Palaeontographica, Abteilung A, v. 232, 1–83.

Wheeley, J., and Twitchett, R., 2005, Palaeoecological significance of a new Griesbachian (Early Triassic) gastropod assemblage from Oman: Lethaia, v. 38, no. 1, p. 37-45, doi:10.1080/0024116051003150.

Wignall, P. B., Kozur, H., & Hallam, A., 1996, On the timing of palaeoenvironmental changes at the Permo-Triassic (P/TR) boundary using conodont biostratigraphy, Historical Biology, v. 12, no. 1, p. 39-62.

Wignall PB, Hallam A, 1992. Anoxia as a cause of the Permian/Triassic mass extinction: facies evidence from northern Italy and the western United States. Palaeogeogr Palaeoclimatol Palaeocol 93:21–46

Wignall, P. B., Morante, R., and Newton, R., 1998. The Permo-Triassic transition in Spitsbergen: δ 13 C org chemostratigraphy, Fe and S geochemistry, facies, fauna and trace fossils. Geological Magazine, 135(01), 47-62.

Wilkin, R. T., Barnes, H. L., and Brantley, S. L., 1996. The size distribution of framboidal pyrite in modern sediments: an indicator of redox conditions. Geochimica et Cosmochimica Acta, 60(20), 3897-3912.

Yin, H.F., Wu, S.B., Ding, M.H., Zhang, K.X., Tong, J.N., Yang, F.Q., and Lai, X.L., 1996. The Meishan section, candidate of the global stratotype section and point of Permian-Triassic boundary. The Paleozoic-Mesozoic Boundary Candidates of the Global Stratotype Section and Point of the Permian-Triassic Boundary, pp. 31-48.

Paper in a Multiauthor Volume

Baud, A., Marcoux, J., Guiraud, R., Ricou, L.E., Gaetani, M., 1993. Late Murgabian (266 to 264 Ma). In: Dercourt, J., Ricou, L.E., Vrielynck, B. (Eds.), Atlas Tethys Palaeoenvironmental Maps, Explanatory Notes. Gauthier-Villars, Paris, pp. 9-21.

Baud, A., Béchennec, F., Cordey, F., Krystyn, L., Le Métour, J., Marcoux, J., Maury, R., Richoz, S., 2001a. Permo–Triassic Deposits: from the Platform to the Basin and Seamounts. In: Conference on the Geology of Oman, Muscat, Oman, Field Guidebook A01, pp. 1–54.

Baud, A., Béchennec, F., Cordey, F., Le Métour, J., Marcoux, J., Maury, R., and Richoz, S., 2001b. Permo–Triassic deposits: from shallow water to base of slope. In: Conference on the Geology of Oman, Muscat, Oman. Field Guidebook B01, pp. 1–40.

Erwin, D.H. and Pan, Hua-Zhang., 1996. Recoveries and radiations: gastropods after the Permo-Triassic mass extinction. In Hart, M.B. (ed.): Biotic recovery from mass extinction events. Geological Society London Special Publication 102, 223–229.

Hauser, M., 2001. The stratigraphic evolution of the Batain embayment of the Southern Tethys. Excursion guide, International Conference Geology of Oman 2001.

Paul, C. R. C., 1988, Extinction and survival in the echinoderms, in Extinction and Survival in the Fossil Record, Systematics Association Special Volume (ed) Larwood G. P., Oxford, UK, v. 34, p. 155-170.

Appendix A: Measurements of the population of the *Naticopsis* sp. from the Asselah boulder.

Naticopsis sp.		
Sample	**Width (mm)**	**Height (mm)**
Assa 1d	1.1	
Assa 2	1.3	
Assa 2	1.3	
Assa 1d	1.5	
Assa 1c	2.0	
Assa 1d	2.3	
Assa 1c	2.3	
Assa 2	2.4	
Assa 1d	2.5	
?	2.5	2.3
Assa 2	2.7	2.0
Assa 1c	2.8	
Assa 2	3.1	
Assa 1c	3.1	
Assa 2	3.2	
Assa 1d	3.2	
Assa 1c	3.2	
Assa 1c	3.3	
Assa 1b	3.6	
Assa 3	3.8	
Assa 1c	3.8	
Assa 1d	3.9	2.6
Assa 1d	4.0	
Assa 1c	4.0	
Assa 1c	4.0	
Assa 1c	4.2	
Assa 3	4.3	2.6
Assa 1c	4.3	
Assa 2	4.5	
Assa 1c	4.6	
Assa 2	4.8	
Assa 2	4.8	
Assa 1c	4.8	
Assa 1c	5.0	
Assa 2	5.1	
Assa 1d	5.1	
Assa 1c	5.1	
Assa 1c	5.2	
Assa 1c	5.4	4.0
Assa 1	5.4	
Assa 2	5.5	
Assa 1c	5.7	
Assa 2	5.8	
Assa 2	6.1	
Assa 1d	6.2	4.4
Assa 1b	6.2	
Assa 1b	6.3	
Assa 3	6.5	
Assa 1d	6.6	
Assa 1c	6.6	
Assa 3	6.7	
Assa 2	6.7	
Assa 1d	6.7	
Assa 1c	6.8	

Naticopsis sp.		
Sample	**Width (mm)**	**Height (mm)**
Assa 2	7.1	
Assa 1c	7.1	6.3
Assa 1c	7.3	
Assa 1c	7.3	
Assa 2	7.5	
Assa 1c	7.5	
Assa 2	7.6	
Assa 2	7.7	
Assa 2	7.8	
Assa 1c	7.8	6.8
Assa 1b	7.9	
Assa 4	8.0	
Assa 1c	8.1	
Assa 1c	8.4	6.5
Assa 3	8.5	5.0
Assa 1d	8.5	
Assa 1c	8.6	
Assa 1c	8.7	
Assa 1d	8.8	
Assa 1b	9.3	
Assa 2	9.5	
Assa 1c	9.5	
Assa 1b	9.5	
Assa 3	9.6	6.1
Assa 1c	9.6	
Assa 2	10.1	
Assa 2	10.2	
Assa 1c	10.3	
Assa 3	10.4	7.5
Assa 1d	10.4	
Assa 1	10.4	
Assa 2	10.5	
Assa 1d	10.5	
Assa 1c	10.5	
Assa 1c	10.6	7.7
Assa 1c	10.6	
Assa 1c	10.7	
Assa 1c	10.7	
Assa 1c	10.8	
Assa 1c	11.0	
Assa 1c	11.0	
Assa 2	11.1	9.8
Assa 1c	11.1	
Assa 4	11.2	
?	11.2	9.8
Assa 1d	11.4	8.7
Assa 3	11.5	7.0
Assa 1c	11.5	11.1
Assa 1b	12.1	
Assa 1d	12.2	7.7
?	12.2	
Assa 1d	12.5	
Assa 1c	12.7	12.1
Assa 1c	12.7	

Naticopsis sp.		
Sample	**Width (mm)**	**Height (mm)**
Assa 2	13.2	11.9
Assa 1	13.5	
Assa 1d	13.9	
Assa 1d	14.0	
Assa 1c	14.2	10.9
Assa 3	14.3	
Assa 3	14.3	
Assa 1c	14.3	
Assa 1c	14.5	8.6
Assa 1c	14.6	
Assa 1c	14.6	
Assa 3	14.8	8.7
Assa 1c	14.9	13.8
Assa 1c	15.0	
Assa 3	15.2	10.6
Assa 2	15.2	14.4
Assa 1d	15.2	
Assa 1c	15.2	13.2
Assa 1c	15.6	
Assa 1d	15.7	13.0
Assa 1d	15.8	
Assa 3	16.1	
Assa 2	16.1	
Assa 1c	16.1	
?	16.1	
Assa 3	16.3	12.0
Assa 1c	16.3	
Assa 1c	16.3	
Assa 1c	16.3	
Assa 1c	16.4	13.3
Assa 1d	16.5	
Assa 2	16.7	
Assa 1c	16.7	
Assa 1c	17.0	15.0
Assa 2	17.4	15.4
Assa 2	17.7	
Assa 1c	17.8	
Assa 1c	18.0	
Assa 1d	18.2	10.3
Assa 1d	18.4	14.4
Assa 2	18.5	13.8
Assa 1c	18.6	
Assa 1c	18.7	
Assa 1c	19.0	
Assa 1c	19.2	
Assa 1b	19.3	13.4
Assa 3	20.2	13.5
Assa 1a	20.3	13.9
Assa 1c	20.8	
Assa 3	21.1	13.5
Assa 1c	21.1	
Assa 1c	22.1	

APPENDIX A

COLLABORATION WITH OTHER PROJECTS (ABSTRACTS)

Competition in slow motion: The unusual case of benthic marine communities in the wake of the end-Permian mass extinction

Michael Hautmann, Borhan Bagherpour, Morgane Brosse, Åsa Frisk, Richard Hofmann, Aymon Baud, Alexander Nützel, Nicolas Goudemand and Hugo Bucher

Changes of community structure in response to competition usually take place on timescales that are much too short to be visible in the geological record. Here we report the notable exception of a benthic marine community in the wake of the end-Permian mass extinction, which is associated with the microbial limestone facies of the earliest Triassic of South China. The newly reported fauna is well preserved and extraordinarily rich (30 benthic macroinvertebrate species, including the new species *Astartella? Stefaniae* (Bivalvia) and *Eucochlis obliquecostata* (Gastropoda)) and stems from an environmentally stable setting providing favourable conditions for benthic organisms. Whereas changes in the taxonomic composition are negligible over the observed time interval of 10–100 ka, three ecological stages are identified, in which relative abundances of initially rare species continuously increased at the cost of previously dominant species. Concomitant with the changes of dominant species is an increase in faunal evenness and heterogeneity. In the absence of both environmental and taxonomic changes, we attribute this pattern to the longterm effects of interspecific competition, which acted at an unusually slow pace because the number of competing species and potential immigrants was dramatically reduced by the end-Permian mass extinction. We suggest that these non-actualistic conditions led to decreased rates of niche differentiation and hence to the delayed rediversification of benthos that characterizes the aftermath of the greatest Phanerozoic mass extinction event. A hyperbolic diversification model is proposed, which accounts for the positive relationship between the intensity of interspecific competition and the rate of niche differentiation and resolves the conundrum of delayed rediversification at a time when niche space was largely vacated.

Palaeontology, *58*(5), 871-901. DOI: 10.1111/pala.12186.

Precise age for the Permian-Triassic boundary in South China from high precision U-Pb geochronology and Bayesian age-depth modelling

Björn Baresel, Hugo Bucher, Morgane Brosse, Fabrice Cordey, Kuang Guodun, and Urs Schaltegger

This study is based on zircon U-Pb ages of 12 volcanic ash layers and volcanogenic sandstones from two marine sections with conformable formational Permian-Triassic boundaries (PTB) in the Nanpanjiang Basin (South China). Our dates of single, thermally annealed and chemically abraded zircons bracket the PTB in Dongpan and Penglaitan and provide the basis for a first proof-of-concept study utilizing a Bayesian chronology model comparing the three sections of Dongpan, Penglaitan and the Global Stratotype Section and Point (GSSP) Meishan. Our Bayesian modeling demonstrates that the formational boundaries in Dongpan (251.938 ± 0.029 Ma), Penglaitan (251.982 ± 0.031 Ma) and Meishan (251.956 ± 0.033 Ma) are synchronous within analytical uncertainty of ca. 30 ka. It also provides quantitative evidence that the ages of the paleontologically defined boundaries, based on conodont Unitary Associations zones in Meishan and on macrofaunas in Dongpan, are identical and coincide with the age of the formational boundaries. The age model also confirms the extreme condensation around the PTB in Meishan, which distorts the projection of any stratigraphic points or intervals onto other more expanded sections by means of Bayesian age-depth models. Dongpan and Penglaitan possess significantly higher sedimentation rates and thus offer a greater potential for high resolution studies of environmental proxies and correlations around the PTB than Meishan. This study highlights the power of high-resolution radio-isotopic ages that allow a robust intercalibration of patterns of biotic changes and fluctuating environmental proxies and will help recognizing their global, regional or local significance.

Solid Earth Discuss., doi:10.5194/se-2016-145, in review, 2016.

Onset, development, and cessation of basal Early Triassic microbialites (BETM) in the Nanpanjiang pull-apart Basin, South China Block

Borhan Bagherpour, Hugo Bucher, Aymon Baud, Morgane Brosse, Torsten Vennemann, Rossana Martini, Kuang Guodun

New investigations in the Nanpanjiang Basin indicate that the onset of the iconic microbialites associated with the Paleozoic-Mesozoic boundary was Early Triassic in age. Bathymetry (water agitation, oxygenation, light penetration) and clastic load are shown to have exerted a direct control on the growth of microbialites. Carbonate supersaturation is also required for the deposition of the microbialites. Bathymetric control is further corroborated by the topographic inheritance of a latest Permian pull-apart basin into Early Triassic times, with a distribution of basal Early Triassic microbialites (BETM) restricted to uplifted blocks. This control is also reflected by the accumulation of carbonaceous black shales in adjacent troughs. The geographically most extensive Nanpanjiang BETM bloomed on a large NW-SE trending uplifted block exceeding 12000 km^2 (Luolou Platform) centered on northwestern Guangxi. Post-Triassic displacements along the Youjiang Fault obscure the paleogeographic relation of BETM exposed west of this fault.

Triassic foraminifers occur in the basal most BETM episode, which is locally bracketed by high-energy grainstones made of reworked Permian foraminifers. Therefore, the Permian-Triassic boundary (PTB) is within the unconformity that separates the Late Permian Heshan Fm. from the basal most BETM. Where accommodation space was sufficient, up to five event surfaces are associated with the unconformity. Microfacies analysis supports chemical dissolution but did not reveal evidence for subaerial erosion, although intercalated grainstone made of Permian foraminifers indicate reworking. Chemical dissolution and mechanical erosion both conceivably contributed to the genesis of the unconformity. The upward shift from tabulated to domical microbial build-ups is accompanied by accumulation of coquinoid lenses between domes, which indicates deepening of the Luolou Platform BETM. The main drowning resulting from both regional tectonic subsidence and a global sea-level rise led to the cessation of the BETM that were buried under predominant fine siliciclastics. Any concomitant change in sea water chemistry appears unlikely.

Accepted in *Gondwana Research*. DOI: 10.1016/j.gr.2016.11.013

Smithian ammonoid faunas from northeastern Nevada: implications for Early Triassic biostratigraphy and correlation within the western USA basin.

Romain Jattiot, Hugo Bucher, Arnaud Brayard, Morgane Brosse, James F. Jenks and Kevin G. Bylund

Intensive sampling of the lower portion of the Thaynes Group within the Palomino Ridge area (northeastern Nevada) yielded abundant and well-preserved Smithian (Early Triassic) ammonoid faunas. Ammonoid taxonomy and a detailed biostratigraphy for this locality are reported herein. One new genus (*Palominoceras*) and one new species (?*Pseudosageceras bullatum*) are described.

Additionally, based on new data from Palomino Ridge and previous data from neighboring localities in Utah, we provide here the first quantitative Smithian ammonoid biochronological scheme for the western USA basin. This new zonation is based on the Unitary Associations (UA) method. The biochronological sequence comprises five unitary association zones that can be correlated with other localities from the Northern Indian Margin (Salt Range, Pakistan; Spiti northern India; and Tulong, South Tibet). Three unitary association zones (UAZ_1, UAZ_2 and UAZ_3) are defined for the early Smithian, one (UAZ_4) spans the entire middle Smithian and one (UAZ_5) comes into the first part of the late Smithian. Finally, a provisional UAZ_6 would represent the second part of the late Smithian.

Accepted in *Palaeontographica Abteilung A*.

From icehouse to hothouse: Timing of the global regression marking the Permian-Triassic boundary crisis and of the following microbial bloom

Björn Baresel, Hugo Bucher, Borhan Bagherpour, Morgane Brosse, Kuang Guodun, Urs Schaltegger

New high-resolution U-Pb dates lead to a minimal duration of 68 ka for the Permian part of the hiatus straddling the Permian-Triassic boundary (PTB) in shallow water settings of the Nanpanjiang Basin (South China) and give a duration of 37 ± 61 ka for the next overlying microbial limestone. The timing of the hiatus is similar to that of the extinction interval in the Meishan Global Stratotype Section and Point. Sedimentation rates below and above the PTB hiatus indicate a seven-fold decrease compatible with a cool and dry climate during the Griesbachian and the glacio-eustatic low stand needed for the genesis of the worldwide hiatus straddling the PTB in shallow water sections. The timing of the hiatus is synchronous with the initial explosive phase of the Siberian Traps that likely released sulfur volatiles into the stratosphere, thus eliciting a short-lived ice age, a global low-stand, and acidified sea water. In a second step, the protracted build-up of volcanogenic CO2 induced a transient cool climate until greenhouse conditions were reached not earlier than 500 ka after the main extinction episode, as indicated by terrestrial plants.

Under review in *Nature Scientific Reports*.

APPENDIX B

PARTICIPATION TO CONFERENCES

(FIRST AUTHOR PRESENTATIONS ONLY)

Brosse M., Baud A., Bucher H., Goudemand N., Nützel A., Ware D., Frisk, Å. M., & Hagdorn H. *Basal triassic exotic blocks from oman: the promised land, no raft of the medusa*. 14th Swiss Geoscience Meeting, Geneva, 11/2016.

Brosse M., Baud A., Bucher H., Goudemand N., Nützel A., Ware D., Frisk, Å. M., & Hagdorn H. *Basal Triassic Oman oases: Griesbachian crinoidal limestone from the Batain Plain, eastern Oman.* GSA, Denver Co., US, 25-28/09/2016.

Brosse M., Bucher H., & Goudemand N. Conodont-based, high-resolution, quantitative biochronology of the end-Permian mass extinction in South China. 59th Annual Meeting of the Palaeontological Association, Cardiff, 12/2015.

Brosse M., Goudemand N., Frisk Å. M., Baud A., Bagherpour B., Guodun K., Bucher H., 2014. *Basal Triassic (Griesbachian) conodonts from the microbial limestone in the Nanpanjiang Basin, South China*. GSA Joint Annual Meeting, Vancouver, BC, 10/2014.

Brosse M., Goudemand N., Frisk A., Baud A., Bagherpour B., Bucher H., 2013. *New conodonts from the Griesbachian microbialite in South China: implications for an improved definition of the base of the Triassic.* 57th Annual Meeting of the Palaeontological Association, Zurich, 12/2013.

Brosse M., Goudemand N., Frisk A., Baud A., Bagherpour B., Bucher H., 2013. *New conodonts from the Griesbachian microbialite in South China: implications for an improved definition of the base of the Triassic.* 11th Swiss Geoscience Meeting, Lausanne, 11/2013.

Brosse M., Goudemand N., Baud A., Meier M., Bucher H., 2013. *Earliest Triassic conodont faunas from Guryul Ravine, Kashmir*. 3rd ICOS, Mendoza, Argentina, 07/2013.

APPENDIX C

COMMENT ON QUANTITATIVE BIOCHRONOLOGY OF THE PERMIAN-TRIASSIC BOUNDARY IN SOUTH CHINA BASED ON CONODONT UNITARY ASSOCIATIONS

Jiang et al. 2016

in press in Earth-Science Reviews

ARTICLE IN PRESS

EARTH-02290; No of Pages 2

Earth-Science Reviews xxx (2016) xxx–xxx

Contents lists available at ScienceDirect

Earth-Science Reviews

journal homepage: www.elsevier.com/locate/earscirev

Discussion

Comment on "Quantitative biochronology of the Permian–Triassic boundary in South China based on conodont unitary associations" by Brosse et al. (2016)

Haishui Jiang [a,b,*], Paul B. Wignall [c], Zhong-Qiang Chen [a], Shucheng Xie [a,b], Xulong Lai [a,b], Haijun Song [a,b], Lina Wang [a,b]

[a] State Key Laboratory of Biogeology and Environment Geology, China University of Geosciences, Wuhan 430074, China
[b] School of Earth Sciences, China University of Geosciences, Wuhan 430074, China
[c] School of Earth and Environment, University of Leeds, Leeds LS2 9JT, UK

ARTICLE INFO

Article history:
Received 6 May 2016
Received in revised form 16 July 2016
Accepted 21 July 2016
Available online xxxx

Keywords:
Permian–Triassic boundary
Unitary associations
Conodonts
South China

ABSTRACT

Recently, Brosse et al. (2016) have proposed the use of conodont Unitary Associations Zones (UAZs) to substantially modify the biostratigraphy of the Permian–Triassic transition and to redefine the Permian–Triassic boundary (PTB). However, in our opinion, the UAZ analysis presented by Brosse et al. (2016) is based on unreliable taxonomic data sets with unjustified taxonomic re-assessments. No evidence shows that the UAZ approach improves the biozone biostratigraphy currently used to date the PTB.

Brosse et al. (2016) have proposed the use of conodont Unitary Associations Zones (UAZs) to substantially modify the biostratigraphy of the Permian–Triassic transition and to redefine the chosen level of the Permian–Triassic boundary (PTB), because of a perceived weakness of conventional interval zones. They state that these zones have diachronous boundaries caused by the first occurrences (FOs) of conodont species being subject to 'local ecological conditions, sampling effort and selective preservation'. However, conodont distributions also define the UAZs, and the latter therefore suffer from the same problems. As reintroduced in Guex et al. (2015), the Unitary Association Method mainly provides biochronological time scales of discrete UAZs defined by characteristic species. Strata lacking these characteristic species cannot be assigned to any zones but are, instead, termed "intervals of separation", which vary greatly in duration among sections.

The UAZ approach provides a much lower-resolution biostratigraphy than the existing conodont zones that are defined by the first appearance datum (FAD) of zonal species. For example, Brosse et al. (2016) established six UAZs over the Permian—Triassic transition. Among them, five UAZs were recognized from the Meishan section, South China. In contrast, seven conodont zones have been established from the same stratal interval of the same section by means of conventional biostratigraphical approaches (Jiang et al., 2007, 2011; Zhang et al., 2009; Chen et al., 2015). Moreover, an even worse scenario appears in another well-studied PTB section in Shangsi, northern Sichuan Province, South China. Therein, three UAZs are established by Brosse et al. (2016) in an interval with six conodont interval zones (Jiang et al., 2011). Thus, the UAZ approach generates a lower-resolution correlation scheme and leaves many strata undated. However, the key feature of the UAZs, according to Brosse et al. (2016), is their improved "accuracy". However, the so-called improvement is not due to the UAZ method itself, but to substantial taxonomic re-assessment of published conodont occurrences by Brosse et al. (2016). We interpret the discrepancy between the newly proposed UAZ correlations (Brosse et al., 2016) and current biozones to be due to the failure to use the most recent published conodont ranges from some key Chinese sections (i.e., Jiang et al., 2011; Chen et al., 2015).

To establish conodont UAZs, Brosse et al. (2016) studied six PTB sites, namely Meishan, Shangsi, Yangou, Dawen, Dajiang, and Wuzhuan, in South China with well-established conodont records. Surprisingly, stratigraphical ranges of some key conodont elements/zones in the Meishan, Dawen, and Bianyang sections were incorrectly placed when Brosse et al. (2016) undertook their UAZ analysis. In Meishan, these authors placed the base of the *Hindeodus changxingensis* Zone at the base of Bed 27 and the base of the *Isarcicella staeschi* Zone at the base of Bed 27d, but these have been placed at the bases of Bed 26 and Bed 28, respectively in the latest literatures (see Zhang et al., 2009; Jiang et al., 2011). The Dawen biostratigraphy uses the findings of Chen et al. (2009), but these authors failed to note the earliest studies of Liu

* Corresponding author at: State Key Laboratory of Biogeology and Environment Geology, China University of Geosciences, Wuhan 430074, China.
E-mail address: jiangliuis@163.com (H. Jiang).

et al. (2007), which has a significant impact on the chosen zonal boundaries (see discussion in Jiang et al., 2014). Jiang et al. (2015) also provided an updated conodont ranges for the Permian–Triassic transition from the neighboring Bianyang section, ~13 km from Dawen. These updated conodont range data were not cited in Brosse et al.'s (2016) analysis.

The Wuzhuan section records a microbialite succession across the PTB. Brosse et al. (2015) found *Hindeodus parvus* in the upper part of the microbialite, and thus suggested that the first occurrence of *H. parvus* in Wuzhuan is later than that in the GSSP Meishan. *H. parvus* is also know form the upper part of the PTB microbialite beds in other sections (i.e., Wuzhuan), but it has also been detected in association with *Clarkina changxingensis* and other Permian species from the base of the microbialite deposits in other sections [i.e., Dawen (Liu et al., 2007), Dajiang (Jiang et al., 2014), and Cili (Wang et al., 2016)]. This is likely because the Permian conodonts have been concentrated as insoluble residues at karstification surfaces seen at the base of some microbialite beds and subsequently co-sampled with Triassic conodonts (Chen et al., 2009; Jiang et al., 2014). Such effects, and the rarity of conodonts in microbialite facies, suggests caution must be exercised when assessing conodont ranges in microbialite beds.

Brosse et al. (2016) changed the identification of many conodont species reported from South China in earlier publications without discussions. Thus, the authors downgraded the status of many species to "indeterminate" but failed to explain the reasoning for the revisions. Furthermore, Brosse et al. (2016) also illustrated holotypes of several key PTB conodont species. Of these, the illustrated specimen of *Isarcicella lobata* is not the true holotype proposed by Perri and Farabegoli (2003, plate 3, Figs. 21–23). This misallocation of holotypes and lack of explanation of some taxonomic data brings into question the reliability of their UAZ analysis.

The most important advantage of the UAZ study, as suggested by Brosse et al. (2016), is to improve the stratigraphical correlation and define precisely the PTB at the Meishan GSSP. These authors therefore placed the PTB 'within the interval of separation bracketed by UAZ_2 and UAZ_3'. However, UAZ_3 was only identified at the Meishan section, and was not located in the other five sections studied by Brosse et al. (2016). In fact, UAZ_2 is only defined in the Dawen and Meishan sections (see Fig. 10 in Brosse et al., 2016). This means that the PTB cannot be determined by UAZs in five of the six studied sections. Even in Meishan, the PTB could not be located precisely, but was placed at some uncertain levels within Bed 26. As a result, the PTB cannot be precisely located using the UAZ approach. It is also worth noting that Brosse et al. (2016) incorrectly placed the boundary between the Changxing and Yinkeng formations at the contact between Bed 26 and Bed 27. Instead, the boundary of these two formations has been traditionally located at the contact between Bed 24 and Bed 25 (Yin et al., 2001).

Brosse et al. (2016) argued that the FOs of some conodont species may contradict one another in various sections, especially the FOs of *H. parvus* and *H. praeparvus*, and concluded that there were contradictory correlations by interval zones, which usually heavily rely on the sampling effort. In fact, the FOs and ranges of conodont species used in the UAZ analysis suffer the same bias, such as, conodont range data from the Wuzhuan section used by Brosse et al. (2015) discussed above. Henderson (2006) differentiated the FO and the FAD, and pointed out that the FO of *H. parvus* merely indicates that they are within the range or biozone of *H. parvus*. It is true that the FO of *H. parvus* may be diachronous in various sections if the sampling effort was not sufficient. Obviously, this is not the case for the PTB sections in South China, in which the FO of *H. parvus* is likely synchronous (i.e., Jiang et al., 2015, Fig. 3) because most of the PTB sections have been densely sampled and studied in the past decades. In contrast, the mass extinction losses are more complicated because clades died out diachronously in different habitats (Song et al., 2013).

In summary, the effort by Brosse et al. (2016) to improve the biochronostratigraphical subdivision and correlation is encouraged, but currently the UAZ approach does not provide an improvement on the use of conventional interval zones in the PTB interval. Instead, the UAZ analysis presented by Brosse et al. (2016) is based on unreliable taxonomic data sets with unjustified taxonomic re-assessments.

Acknowledgements

We thank Editor A. Strasser for his professional editorial work. We are very grateful to Hongfu Yin, Jinnan Tong and Yongbiao Wang for their suggestions and discussion.

References

Brosse, M., Bucher, H., Bagherpour, B., Baud, A., Frisk, Å.M., Guodun, K., Goudemand, N., 2015. Conodonts from the early Triassic microbialite of Guangxi (South China): implications for the definition of the base of the Triassic system. Palaeontology 58, 563–584.

Brosse, M., Bucher, H., Goudemand, N., 2016. Quantitative biochronology of the Permian–Triassic boundary in South China based on conodont unitary associations. Earth-Sci. Rev. 155, 153–171.

Chen, J., Beatty, T.W., Henderson, C.M., Rowe, H., 2009. Conodont biostratigraphy across the Permian–Triassic boundary at the Dawen section, Great Bank of Guizhou, Guizhou Province, South China: implications for the late Permian extinction and correlation with Meishan. J. Asian Earth Sci. 36, 442–458.

Chen, Z.Q., Yang, H., Luo, M., Benton, M.J., Kaiho, H., Zhao, L.S., Huang, Y.G., Zhang, K.X., Fang, Y.H., Jiang, H.S., Qiu, H., Li, Y., Tu, C.Y., Shi, L., Zhang, L., Feng, X.Q., Chen, L., 2015. Complete biotic and sedimentary records of the Permian–Triassic transition from Meishan section, South China: ecologically assessing mass extinction and its aftermath. Earth-Sci. Rev. 149, 63–103.

Guex, J., Galster, F., Hammer, Ø., 2015. Discrete Biochronological Time Scales. Springer (160 pp.).

Henderson, C.M., 2006. Beware of your FO and beware of FAD. Permophiles 47, 8–9.

Jiang, H.S., Lai, X.L., Luo, G.M., Aldridge, R., Zhang, K.X., Wignall, P.B., 2007. Restudy of conodont zonation and evolution across the P/T boundary at Meishan section, Changxing, Zhejiang, China. Glob. Planet. Chang. 55, 39–55.

Jiang, H., Lai, X., Yan, C., Aldridge, R.J., Wignall, P., Sun, Y., 2011. Revised conodont zonation and conodont evolution across the Permian–Triassic boundary at the Shangsi section, Guangyuan, Sichuan, South China. Glob. Planet. Chang. 77, 103–115.

Jiang, H., Lai, X., Sun, Y., Wignall, P.B., Liu, J., Yan, C., 2014. Permian–Triassic conodonts from Dajiang (Guizhou, South China) and their implication for the age of microbialite deposition in the aftermath of the end-Permian mass extinction. J. Earth Sci. 25, 413–430.

Jiang, H.S., Joachimski, M.M., Wignall, P.B., Zhang, M.H., Lai, X.L., 2015. A delayed end-Permian extinction in deepwater locations and its relationship to temperature trends (Bianyang, Guizhou Province, South China). Palaeogeogr. Palaeoclimatol. Palaeoecol. 440, 690–695.

Liu, J.B., Ezaki, Y., Yang, S.R., Wang, H.F., Adachi, N., 2007. Age and sedimentology of microbialites after the end-Permian mass extinction in Luodian, Guizhou Province. J. Palaeogeogr. 9, 473–486 (in Chinese with English abstract).

Perri, M.C., Farabegoli, E., 2003. Conodonts Across the Permian–Triassic Boundary in the Southern Alps. Vol. 245. Courier Forschung Institute of Senckenberg, pp. 281–313.

Song, H., Wignall, P.B., Tong, J., Yin, H., 2013. Two pulses of extinction during the Permian–Triassic crisis. Nat. Geosci. 6, 52–56.

Wang, L.N., Wignall, P.B., Wang, Y.B., Jiang, H.S., Sun, Y.D., Li, G.S., Yuan, J.L., Lai, X.L., 2016. Depositional Conditions and Revised Age of the Permo–Triassic Microbialites at Gaohua Section, Cili County (Hunan Province, South China). http://dx.doi.org/10.1016/j.palaeo.2015.11.032 (in press).

Yin, H.F., Zhang, K.X., Tong, J.N., Yang, Z.Y., Wu, S.B., 2001. The global stratotype section and point (GSSP) of the Permian–Triassic boundary. Episodes 24, 102–114.

Zhang, K., Tong, J., Lai, X., Jiang, H., 2009. Progress on study of conodont sequence for the GSSP section at Meishan, Changxing, Zhejiang Province, South China. Acta Palaeontol. Sin. 48, 474–486 (in Chinese with English abstract).

Acknowledgments

This dissertation would not have been possible without the guidance of my advisors Prof. Dr. Hugo Bucher (Paleontological Institute and Museum, University of Zurich) and Dr. Nicolas Goudemand (IGFL, ENS Lyon, France). Their scientific advises and enthusiasm for the Permian-Triassic boundary and conodonts were the cornerstones of the success of this work.

Pr. Dr. Marcelo Sánchez (Paleontological Institute and Museum, University of Zurich) and Pr. Dr. Christoph Zollikofer (Department of Anthropology, University of Zurich) are thanked for agreeing to be part of my dissertation committee.

I am very thankful to our collaborators for their precious help (alphabetical order):

- Borhan Bagherpour (Paleontological Institute and Museum, University of Zurich) helped on the field in China and brought expertize on the microbialite.
- Dr. Aymon Baud (Geological Museum, Lausanne University) helped on the field in China and Kashmir and brought expertize on the Permian-Triassic boundary.
- Prof. Dr. Ghulam M. Bhat (Department of Geology, University of Jammu, Kashmir) helped on the field in Kashmir.
- Dr. Åsa M. Frisk (Department of Earth Sciences, Uppsala University, Sweden) helped on the field in China and in Oman.
- Dr. Kuang Guodun (Guangxi Bureau of Geology and Mineral Resources) helped on the field in China.
- Prof. Dr. Hans Hagdorn (Muschelkalkmuseum, Ingelfingen, Germany) brought expertize on echinoderms.
- Marc Leu (Paleontological Institute and Museum, University of Zurich) helped on the field in Kashmir.
- Prof. Dr. Alexander Nützel (Bayerische Staatssammlung für Paläontologie und Geologie, Munich, Germany) brought expertize on gastropods.
- Louise Souquet (IGFL, ENS Lyon, France) conducted many analyses on the R software.
- Prof. Dr. Torsten Vennemann (UNIL, Lausanne) processed the carbon isotope samples of Guryul Ravine, Kashmir.
- Dr. David Ware (Naturkundemuseum Berlin) brought expertize on ammonoids.

I am indebted to the persons who kindly provided impeccable technical support during my PhD project:

- Lorena Tessitore (Lilles University, France) and Marc Leu (Paleontological Institute and Museum, University of Zurich) helped me preparing a considerable amount of samples.
- Thomas Brühwiler (Paleontological Institute and Museum, University of Zurich) and Vivien Jaquier (Winterthur) temporary helped in the conodont lab.
- Rossana Martini (Department of Earth Sciences, University of Geneva) granted me access to the SEM in Geneva.
- Agathe Martignier (Department of Earth Sciences, University of Geneva) and Andres Käch (Center for Microscopy and Image Analysis, University of Zurich) provided technical support with the SEMs.
- Maximiliano Meier (Bulles) helped on the field in Kashmir.

Many thanks as well to Marc Leu and and PD Dr. Torsten Scheyer for helping me with the German abstract.

Heartfelt thanks to my family, for their constant and unshakable support.

And finally, my special thanks to my colleagues (and ex-colleagues) from the Paleontological Institute and Museum, who eventually became some of my closest friends. I owe more to them than could be listed here.

CURRICULUM VITAE

BROSSE Morgane

Date of birth: 15.08.1988
Place of birth: Sens (France)
Nationality: French

Education

2011-2016 PhD student, Paleontological Institute and Museum, University of Zurich, Switzerland.
Dissertation: Palaeoecology and Conodont-based Biochronology Of basal Triassic within the Tethyan Realm.
Supervisors: Prof. Dr. H. Bucher (University of Zurich, Switzerland) and Dr. N. Goudemand (IGFL, ENS lyon, France).

2011 MSc 'Géobiosphère', minor Palaeontology/Sedimentology, University of Burgundy, France.
Dissertation: Ammonoids recovery after the Permian-Triassic extinction: morphological and phylogenetical patterns.
Supervisors: Dr. A. Brayard and Dr. E. Fara (University of Burgundy, France).

2010 First year of the MCs degree, Physical Geography and Quaternary Geology department, University of Stockholm, Sweden.
Dissertation: Glacial processes and landscape evolution in the vicinity of Mariannelund (Småland, South of Sweden).
Supervisors: Pr. I. Borgström and Dr. E. Lind Mettävainio (Stockholm University, Sweden).

2009 BSc 'Earth Science and Environment', University of Burgundy, France.

2006 Scientific Baccalauréat (equivalent of Matura), minor Mathematics, option Latin, Sens, France.

Scholarship during the doctoral studies

2013 Candoc Forschungskredit der Universität Zürich (55'200 CHF).

The Road goes ever on and on,
Down from the door where it began.
Now far ahead the Road has gone,
And I must follow, if I can,
Pursuing it with eager feet,
Until it joins some larger way
Where many paths and errands meet.
And whither then? I cannot say.

J.R.R Tolkien, The fellowship of the Ring